

# ‘Strategies to identify and further characterize novel and known genes involved in regulation of skeletogenesis’

Ph.D. Thesis  
to accomplish

Doctorate Degree in Science

at the Faculty of Biology

Johannes Gutenberg-University of Mainz  
in Mainz , Germany

**Silke Schlaubitz**

born in Düsseldorf, Germany

Mainz, Germany, 2007

Dean:

1. Correspondent:

2. Correspondent:

Oral examination: December 04<sup>th</sup>, 2007

## Index of figures

## Index of tables

1. <i>Introduction</i> .....	1
1.1. Endochondral and intramembranous bone formation.....	2
1.2. Patterning during vertebrate limb bud development.....	8
1.2.1. D/V patterning of the apical ectodermal ridge (AER) and the progressive zone model.....	12
1.3. <i>Lmx1b</i> .....	14
1.3.1. Discovery of <i>Lmx1b</i> .....	14
1.3.2. <i>Lmx1b</i> expression and knockout model.....	15
1.3.3. Downstream targets of <i>Lmx1b</i> .....	17
1.3.4. <i>LMX1B</i> and Nail-Patella-Syndrome.....	18
1.4. Genitopatellar Syndrome.....	19
1.5. Specific Aims.....	20
2. <i>Methods</i> .....	22
2.1. DNA Isolation.....	22
2.1.1. Isolation of genomic DNA from blood.....	22
2.1.2. Isolation of plasmid DNA.....	22
2.1.3. Isolation of genomic DNA from mouse tissues for genotyping PCR.....	22
2.2. RNA Isolation.....	23
2.2.1. Isolation of total RNA from tissues or cells.....	23
2.2.2. mRNA isolation from total RNA.....	24
2.2.3. RNA preparation from prenatal limb buds for microarray experiments.....	24
2.2.4. RNA preparation from differentiated and dedifferentiated chondrocytes.....	24
2.2.5. Laser Capture Microscopy and RNA preparation from captured cells.....	25
2.3. DNA and RNA standard methods.....	26
2.3.1. Determination of DNA, cDNA and RNA concentrations.....	26
2.3.2. Agarose gel electrophoresis of DNA and RNA.....	26
2.3.3. Blotting of RNA .....	27
2.3.4. DNaseI digestion of total RNA.....	28
2.3.5. Reverse Transcription of RNA.....	28
2.3.6. Polymerase Chain Reaction and Reverse Transcription Polymerase Chain Reaction (PCR and RT-PCR).....	28
2.3.7. Quantitative RT-PCR (qRT-PCR).....	29
2.3.8. Cloning of PCR products in T-vectors.....	30
2.3.9. Sequencing.....	31
2.3.10. Digestion.....	31

2.3.11. Gel extraction and purification of DNA.....	31
2.3.12. DNA purification by phenol/ chloroform extraction..	32
2.3.13. Ligation.....	32
2.4. DNA and RNA labeling method.....	32
2.4.1. Random primed oligo labeling of cDNA.....	32
2.4.2. RNA labeling methods.....	33
2.4.2.1. Generation of a template.....	33
2.4.2.2. Radioactive RNA labeling with <sup>35</sup> S through in vitro transcription.....	34
2.4.2.3. Non radioactive RNA labeling with DIG through in vitro transcription.....	34
2.5. Hybridization methods.....	34
2.5.1. Radioactive Hybridization Methods.....	34
2.5.1.1. Northern Blot.....	34
2.5.1.2. Hybridization of cDNA filter.....	35
2.5.1.3. In situ hybridization (ISH).....	35
2.5.2. Non-radio active hybridization methods.....	37
2.5.2.1. Affymetrix.....	37
2.5.2.2. Fluorescent in Situ Hybridization (FISH).....	37
2.5.2.3. Array based comparative genome hybridization (array CGH).....	38
2.5.2.4. Whole mount in situ hybridizat on (WISH)....	39
2.6. Protein isolation, electrophoresis, and mass spectroscopy....	41
2.7. Histological methods.....	41
2.7.1. Paraffin embedding.....	41
2.7.2. Embedding for cryo sections.....	42
2.7.3. Sectioning of paraffin embedded specimens.....	42
2.7.4. Cryo sectioning.....	42
2.7.5. Vital staining of paraffin sections with Hematoxylin & Eosin.....	42
2.7.6. Vital staining of frozen sections with Hematoxylin & Eosin.....	43
2.8. Working with Bacteria culture.....	43
2.8.1. Competent Cells.....	43
2.8.2. Transformation.....	44
2.9. Working with cell culture.....	44
2.9.1. Standard cell culture.....	44
2.9.2. Transfection of adherent cells.....	44
2.9.3. Cell lines.....	45
2.9.4. EBV transformation.....	45
2.10. Working with a Phage Library.....	46
2.10.1. Human fetal cartilage cDNA library.....	46
2.10.2. Plate a phage library.....	46
2.10.3. Processing of a large number of phage clones for sequencing .....	47
2.11. Working with Mice.....	47

2.11.1. Housing mice.....	47
2.11.2. <i>Lmx1b</i> knockout mice.....	48
2.11.3. Dissection of limb buds for RNA preparation.....	48
2.12. Immunohistochemistry.....	48
2.13. Bioinformatic.....	50
2.13.1. Batched Sequence Analysis of EST sequences.....	50
2.13.2. Analysis of single sequences.....	51
2.13.3. Affimetrix normalization and analysis.....	52
2.14. Material.....	53
2.14.1. Solutions.....	53
2.14.2. Chemicals.....	57
2.14.3. Miscellaneous materials.....	59
2.14.4. Kits.....	60
2.14.5. Equipment.....	61
2.14.6. Plasmids.....	62
2.14.7. Oligos .....	62
2.14.7.1. Common oligos.....	62
2.14.7.2. <i>Lmx1b</i> genotyping oligos.....	63
2.14.7.3. Oligos to amplify inserts in pcDNA 3.1 and pcDNA 3.1/V5-HisA.....	63
2.14.7.4. Oligos used for qRT-PCR.....	63
2.14.7.5. Oligos used for EST clone ch11g10/ <i>LRRC59</i> .....	66
2.14.7.6. Screening oligos for <i>LMX1B</i> , <i>TBX4</i> , <i>WNT4</i> , <i>WNT7A</i> .....	66
2.14.7.7. Oligos used to generate ISH/WISH probes..	68
2.14.8. Molecular weight marker.....	68
3. Results.....	69
3.1. EST project.....	69
3.1.1. Results from database searches.....	69
3.1.2. Statistical annotation of EST sequences.....	71
3.1.3. Characterization of selected EST clones.....	78
3.1.3.1. Characterization of clone B-C12.....	78
3.1.3.2. Characterization of clone ch11g10.....	79
3.1.3.2.1. Knock-out model for <i>Lrrc59</i> .....	85
3.1.3.3. Characterization of clone ch32F03.....	87
3.1.4. Microarray experiment.....	91
3.1.4.1. Normalization and evaluation of microarray data.....	91
3.1.4.2. Evaluation of microarray data using qRT- PCR.....	92
3.2. <i>Lmx1b</i> .....	94
3.2.1. Finding a downstream target of <i>Lmx1b</i> .....	95

3.2.1.1. Differentially expressed genes in fore limb buds.....	97
3.2.1.2. Evaluation of micro array experiment using qRT-PCR.....	99
3.2.2. Evaluation of microarray experiment using WISH.....	101
3.2.2.1 Whole mount in situ hybridization for <i>Lmx1b</i> ..	101
3.2.2.2. Whole mount in situ hybridization for putative <i>Lmx1b</i> downstream targets.....	101
3.2.3. Neuropilin 2 ( <i>Nrp2</i> ).....	102
3.3. Genitopatellar syndrome.....	103
3.3.1. Patient # 152-01-01.....	103
3.3.2. Mutation screening.....	107
3.3.3. Array-based comparative genomic hybridization.....	108
3.3.4. Determination of the breakpoints.....	110
3.3.5. Quantitative RT-PCR for genes within the micro deletion.....	111
4. Discussion.....	113
4.1. EST project.....	114
4.1.1. Comparison of the present library with previously published studies.....	116
4.1.2. Advances in skeletogenesis research.....	121
4.1.3. Limb bud microarray.....	123
4.1.4. EST clones B-C12 and ch32F03.....	126
4.1.5. EST clone ch11g10 ( <i>LRRC59</i> ).....	127
4.2. <i>Lmx1b</i> downstream targets.....	133
4.2.1. Potential <i>Lmx1b</i> downstream target Agrin ( <i>Agrn</i> ).....	136
4.2.2. Potential <i>Lmx1b</i> downstream target carbonic anhydrase 2 ( <i>Car2</i> ).....	136
4.2.3. Potential <i>Lmx1b</i> downstream target Neuropilin 2 ( <i>Nrp2</i> ).....	137
4.3. Genitopatellar Syndrome.....	142
4.4. Conclusions and further directions.....	147
5. Summary.....	150
6. References.....	152
7. Acknowledgement.....	174
8. Appendix.....	175
8.1 Abbreviation.....	175
8.2. Additional results.....	178
8.3. Curriculum vitae.....	181
8.4. Publications.....	182
8.5. Poster presentations.....	183
8.6. Oral presentations.....	185

## Index of figures

<b>Figure 1:</b>	Steps of endochondral bone formation.....	3
<b>Figure 2:</b>	Signaling in the zones of proliferating and hypertrophic chondrocytes within the growth plate.....	5
<b>Figure 3:</b>	Osteoblast differentiation.....	6
<b>Figure 4:</b>	Basic structures of vertebrate limbs.....	9
<b>Figure 5:</b>	View through the D/V axis of the hind limb field in a chick embryo at stage 13.....	10
<b>Figure 6:</b>	View through the D/V axis of the hind limb field in a chick embryo at stage 16.....	11
<b>Figure 7:</b>	Graphical comparison of the Progressive zone model with the model suggested by Dudley.....	12
<b>Figure 8:</b>	View through the D/V axis of the hind limb field in a chick embryo at stage 22.....	13
<b>Figure 9:</b>	Protein structure of the murine <i>Lmx1b</i> .....	15
<b>Figure 10:</b>	Comparison between newborn B6/129 wild type and <i>Lmx1b</i> knockout mice.....	16
<b>Figure 11:</b>	Northern blot assembling.....	27
<b>Figure 12:</b>	Vector map of pGEM-T® Vector.....	33
<b>Figure 13:</b>	Vector map of pcDNA3.1/V5-His A, B, C.....	49
<b>Figure 14:</b>	Chartflow of EST-annotation.....	50
<b>Figure 15:</b>	Example for an ESTsweep result file.....	51
<b>Figure 16:</b>	Partial EST annotation sheet.....	70
<b>Figure 17:</b>	Percentage functional distribution of analyzed EST sequences	71
<b>Figure 18:</b>	Genes with the highest frequencies within the 5000 ESTs.....	72
<b>Figure 19:</b>	Frequencies of collagen genes.....	73
<b>Figure 20:</b>	Frequencies of proteoglycan constituents of the ECM.....	73
<b>Figure 21:</b>	Frequencies of non-collagen/ non-proteoglycan ECM constituents.....	74
<b>Figure 22:</b>	Exon-intron structure of the human <i>ZNF577</i> .....	79
<b>Figure 23:</b>	Exon-intron organization of the human <i>LRRC59</i> and its murine orthologue.....	80
<b>Figure 24:</b>	Alignment of the protein sequence of LRRC59 of 7 different species.....	80
<b>Figure 25:</b>	Quantitative RT-PCR for <i>Lrrc59</i> on a variety of tissues.....	81
<b>Figure 26:</b>	Northern blot hybridization of rat/ murine and human RNA samples using a <i>Lrrc59</i> / <i>LRRC59</i> specific probe.....	82
<b>Figure 27:</b>	In situ hybridization of <i>Lrrc59</i> on sagittal sections.....	83
<b>Figure 28:</b>	WISH with <i>Lrrc59</i> specific probe.....	83
<b>Figure 29:</b>	Alignment of 5 small leucine-rich proteoglycans (SLRP) with <i>LRRC59</i> .....	84
<b>Figure 30:</b>	Co-localization of murine <i>Lrrc59</i> with Vinculin.....	85
<b>Figure 31:</b>	Composition of clone MHPN88m09.....	86
<b>Figure 32:</b>	Exon-intron organization of the human <i>CRELD2</i> and its	

	murine orthologue.....	87
<b>Figure 33:</b>	Northern Blot hybridization for <i>Creld2/ CRELD2</i> .....	88
<b>Figure 34:</b>	Alignment of the protein sequence of the human CRELD2 and the murine Creld2.....	89
<b>Figure 35:</b>	RT-PCR for <i>CRELD2/ Creld2</i> .....	90
<b>Figure 36:</b>	Distribution of the biological function of the 98 individual genes	92
<b>Figure 37:</b>	Microarray data vs. qRT-PCR.....	93
<b>Figure 38:</b>	Relative expression of genes involved in skeletogenesis vs. housekeeping gene <i>Hprt I</i> .....	99
<b>Figure 39:</b>	Relative expression of genes involved in skeletogenesis vs. housekeeping gene <i>Hprt II</i> .....	100
<b>Figure 40:</b>	Relative expression of potential <i>Lmx1b</i> downstream targets versus housekeeping gene <i>Hprt</i> .....	100
<b>Figure 41:</b>	WISH with <i>Lmx1b</i> specific probe on E11.5 embryos.....	101
<b>Figure 42:</b>	WISH with <i>Shox2</i> specific sense probe on E12.5 embryo.....	102
<b>Figure 43:</b>	WISH with <i>Nrp2</i> specific probe on E11.5 embryos.....	102
<b>Figure 44:</b>	Patient # 152-01-01.....	105
<b>Figure 45:</b>	Pathology of ovotestes and associated structures.....	105
<b>Figure 46:</b>	Karyotype of patient # 152-01-01.....	106
<b>Figure 47:</b>	FISH analysis for a <i>SRY</i> specific probe and a chromosome X centromere specific probe .....	106
<b>Figure 48:</b>	Array CGH profiles of chromosome 9 of patient # 152-01-01...	109
<b>Figure 49:</b>	FISH for <i>LMX1B</i> and telomere control probe.....	109
<b>Figure 50:</b>	FISH for G248P85560F9 and control centromere probe.....	111
<b>Figure 51:</b>	Leucine-rich repeats within <i>LRRC59</i> .....	129
<b>Figure 52:</b>	Phylogenetic analysis of known SLRP.....	129
<b>Figure 53:</b>	3D models of <i>LRRC59</i> and decorin.....	130
<b>Figure 54:</b>	Possible model for <i>LRRC59</i> .....	132
<b>Figure 55:</b>	Ligand/ receptor pairs that are involved in axon guidance and blood vessel development.....	138



**Index of tables**

<b>Table 1:</b>	Expected range of separation depending on agarose concentration.....	26
<b>Table 2:</b>	Summary of cell lines used for analysis.....	45
<b>Table 3:</b>	Composition of clones in present and previous cartilage EST sequencing projects.....	75
<b>Table 4:</b>	Distribution of matrix components in present and previous cartilage EST sequencing projects.....	76
<b>Table 5:</b>	Distribution of ribosomal and other proteins in present and previous cartilage EST sequencing projects.....	77
<b>Table 6:</b>	Results from mass spectrometry analysis.....	95
<b>Table 7:</b>	20 most down regulated genes in microarray experiment performed with E11.5 wild type vs. knock-out fore limb buds...	98
<b>Table 8:</b>	Phenotypic comparison among Genitopatellar Syndrome patients.....	104
<b>Table 9:</b>	Summary of analysis defining breakpoints on chromosome 9q33.3-q34.11 for patient # 152-01-01.....	110
<b>Table 10:</b>	21 out of 98 differentially expressed genes, whose orthologue genes were found in the cartilage EST project.....	124
<b>Table 11:</b>	List of 98 individual genes that were found differentially expressed.....	178

## 1. Introduction

Skeletogenesis consists of chondrogenetic and osteogenetic events resulting in cartilaginous and bony tissues that establish all parts of the skeleton. Osteochondrodysplasias describe malformations of parts of the skeleton [Cohen, 2006; Cohn, 2001; Kornak and Mundlos, 2003; Superti-Furga and Unger, 2007], that are often genetically based. Many of these have been described and the underlying complexity of their molecular and pathogenetic mechanisms has emerged. It is therefore important to understand development, growth and homeostasis of skeletal elements and the genetic programs that lie behind these processes. There are more than 300 bony and cartilaginous parts of the skeleton at birth that partially adhere, elongate and strengthen during development to provide the body with stability, mobility, flexibility and protection of its inner organs. Although the Greek word 'skeleton' means 'desiccated', the skeleton is a living organ, that, in addition to its structural functions, also provides the anatomical niche for bone marrow haematopoiesis and stores minerals like calcium and phosphorus. It is formed by two tissues (cartilage and bone) and three cell types of mesodermal origin (chondrocytes, osteoblasts and osteoclasts). Chondrocytes and osteoblasts arise from mesenchymal cells, whereas the bone-resorbing osteoclasts derive from the macrophage/monocyte cell lineage. Importantly, the interaction between osteoblasts and osteoclasts insures the proper balance between bone formation and bone resorption [Shimizu et al., 2007; Zaidi, 2007].

The skeleton is divided into three parts, the craniofacial skeleton, the axial skeleton and the appendicular skeleton (extremities). Both neural crest- and mesoderm-derived cells contribute to the formation of the cartilaginous and bony elements of the craniofacial skeleton; the extremities develop from the lateral plate mesoderm, while ribs and vertebrae of the axial skeleton derive from the sclerotome of the somites. Two distinct types of bones are present in the skeleton: cortical bones in long bone shafts that consist of mineralized hardened

collagen, resistant to bending and torsion, to provide strength, and spongy cancellous bones of the axial skeleton that shows a higher flexibility [Zaidi, 2007]. All skeletal elements are formed during two major processes: a) a patterning process that regulates shape, size, and number of the skeletal elements and b) a differentiation process that controls cellular maturation and maintenance pathways [Cohen, 2006; Goldring et al., 2006; Karsenty, 2003; Kronenberg, 2003; Niswander, 2003]. All skeletal elements result either from endochondral or intramembranous bone formation, depending on shape, location and hence function of the developing bone.

### **1.1. Endochondral and intramembranous bone formation**

The vast majority of short and long bones are formed through a process called endochondral bone formation (figure 1) during which an initial bone template made of cartilage is progressively and almost entirely replaced by bone [Colnot, 2005; Olsen et al., 2000].

Instead, a few flat bones of the skull and the jaw are formed by intramembranous bone formation, a process during which bone-forming osteoblasts directly replace the condensed mesenchymal cells, without intervening formation of cartilage. A fibrous connective tissue, the periosteum, develops on the surface of the newly formed bone, and migrating osteoblasts continue the process of bone formation. Articular cartilage, which covers the joint regions at the extremities of many bones, and cartilaginous tissues in the ears, the nose and the throat stays as permanent cartilage and never gets converted into bony tissue [Carter et al., 2004; Karsenty, 2003; Kronenberg, 2003].

Four primary phases of skeletogenesis initiate endochondral bone formation [Colnot, 2005]: 1) cells migrate to the site of future skeletogenesis, 2) epithelial and mesenchymal tissues interact with each other and result in condensation. 3) mesenchymal cells condensate into tissue elements outlining the future skeletal structure (figures 1a and 4). The condensed cells differentiate into chondrocytes (figure 1b) and therefore become primary cartilage cells [Hall and Miyake, 2000].

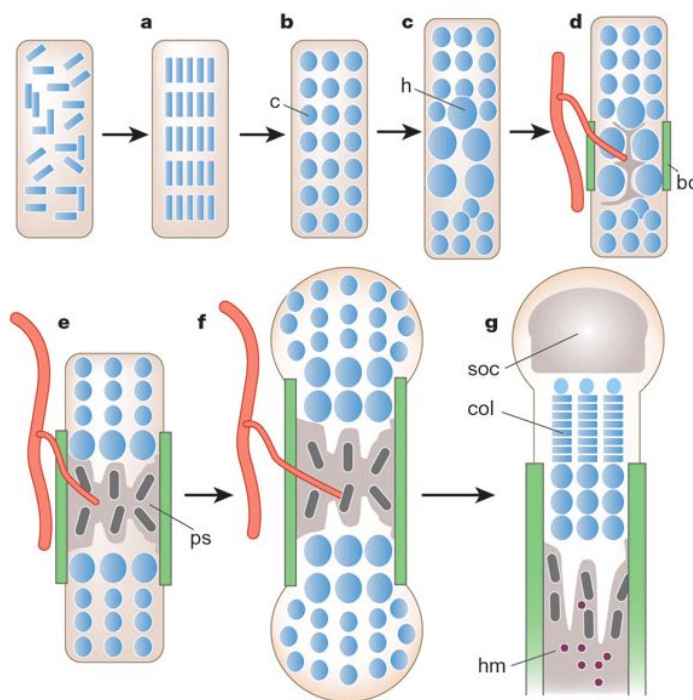


**Figure 1: Steps of endochondral bone formation.** a: Condensation of mesenchymal cells; b: condensed cells become chondrocytes (c) and start proliferating; c: chondrocytes stop proliferation, differentiate into hypertrophic (h) chondrocytes; d: cells adjacent to hypertrophic chondrocytes (perichondrial cells) become osteoblasts and form the initial bone collar (bc), hypertrophic chondrocytes initiate formation of mineralized matrix, migration of blood vessels; e: osteoblasts accompany vascular invasion, forming primary spongiosa (ps); f: ongoing chondrocytes proliferation, lengthening the bone, osteoblasts of bone collar become cortical bone; g: secondary ossification center (soc) forms through cycles of chondrocyte hypertrophy, vascular invasion and osteoblast activity, growth plate below the second center of ossification forms orderly columns of proliferating chondrocytes (col), haematopoietic marrow (hm) expands in marrow space along with stromal cells (adapted from Kronenberg, 2003).

These primary chondrocytes start proliferating and synthesize the cartilage specific extracellular matrix (ECM) enriched with type II, IX, and XI collagen and aggrecan. The outer layer forms the protecting perichondrium, a dense membrane composed of an outer fibrous layer and an inner chondrogenic layer. Once vascularized, the perichondrium becomes the periosteum containing a layer of undifferentiated cells that later become osteoblasts. Stimulated by the bone morphogenic proteins *BMP2* and *BMP4* and the secreted protein Sonic hedgehog (*SHH*), the transcription factor *Sox9*, in cooperation with its other family members *L-Sox5* and *Sox6*, mainly drives these processes [Kawakami et al., 2006]. *Sox9* is up regulated in chondrogenic and osteogenic mesenchymal cells prior to condensation, remains highly expressed in primary chondrocytes

and chondrocyte forming chondroblasts. No expression of *Sox9* can be detected when the cells undergo hypertrophy. In *Sox9* mutant mice, no chondrogenic mesenchymal condensation was observed and expression of *Col2a1*, *Col9a1*, *Col11a2* and aggrecan was absent, indicating the importance of *Sox9* for chondrogenic mesenchymal condensation [Bi et al., 2001].

After mesenchymal condensation, chondrocytes continue to proliferate along the longitudinal axis of the future bone. When they stop, they become prehypertrophic, then hypertrophic (figure 1c) and start to secrete type X collagen. Proliferating prehypertrophic chondrocytes also express *Indian hedgehog (Ihh)* [Ehlen et al., 2006], an important morphogen that signals through its receptors, *Patched* and *Smoothened* [McMahon, 2000]. *Ihh* creates a negative feedback loop (figure 2) with parathyroid hormone-related protein (*PTHrP*) that delays hypertrophy by acting on proliferating chondrocytes: it keeps them proliferating, until *PTHrP* insufficiently stimulates them [Kronenberg and Chung, 2001]. When *PTHrP* action ceases, *Ihh* expression begins to support chondrocyte differentiation towards hypertrophy, but also stimulates the expression of *PTHrP* through the loop and thereby delays hypertrophy [Minina et al., 2001; Vortkamp et al., 1996]. The interaction of *Ihh* and *PTHrP* finely tunes the ability of chondrocytes to undergo hypertrophy [Kronenberg and Chung, 2001] and determines the lengths of the proliferative columns.

Signaling of *BMP2* - *BMP5* and *BMP7* in the perichondrium and *BMP6* in hypertrophic chondrocytes increases the domain of *Ihh* expression and therefore supports chondrocytes hypertrophy, while signaling of fibroblast growth factors (FGFs) has opposite effects and FGFs can be considered as BMP antagonist (figure 2) [Yoon et al., 2006]. BMPs are members of the *TGF- $\beta$*  superfamily that also includes Anti-müllerian hormone, Smads, Activin, Nodal and *TGF- $\beta$* 's [Li and Cao, 2006; Pogue and Lyons, 2006; Wozney and Rosen, 1998].

Hypertrophic chondrocytes direct perichondrial cells to form the bone collar (figure 1d). On either side of the ossification centers, chondrocytes start assuming a flattened shape and organize into longitudinal columns to establish

cartilage growth columns [Mundlos and Olsen, 1997]. They proliferate at a high rate, then exit the cell cycle and start to increase in size.

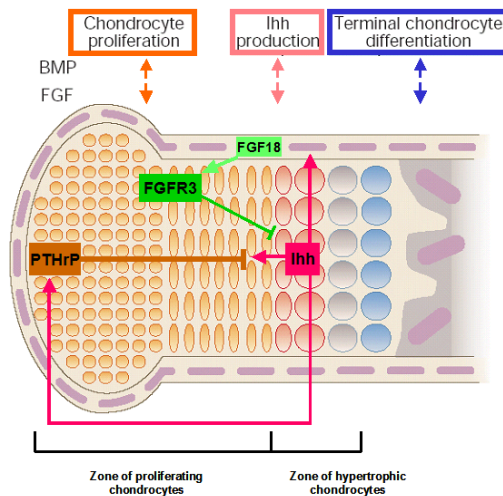


**Figure 2: Signaling in the zones of proliferating and hypertrophic chondrocytes within the growth plate** indicating Indian hedgehog (*Ihh*)/ parathyroid hormone-related protein (*PTHrP*) negative feedback loop and its interaction with *FGF18* and *FGFR3*, opposite effects of BMP and FGF signaling in chondrocyte differentiation (orange box and arrows), *Ihh* induction (pink box and arrows), and terminal chondrocyte differentiation (blue box and arrows); (adapted from Kronenberg, 2003).

Hypertrophic chondrocytes finally undergo apoptosis and get replaced by woven bone in the so-called primary spongiosa. Cartilage matrix, blood vessels and invading osteoblasts and osteoclasts are present in this area (figure 1e); osteoblasts of the bone collar start becoming cortical bone (figure 1f), the hard bone structure that contributes mainly to the weight of the skeleton. Cells at the epiphyses of each long bone develop secondary ossification centers (figure 1g), so that the cartilage between the primary and the secondary ossification centers defines the metaphyseal growth plate. This is the zone that through the process of endochondral bone formation is ultimately responsible for the longitudinal growth of the long bones. Joints start to form when Growth and differentiation factors (*GDFs*) are expressed at both ends of the developing long bone: mesenchymal cells located in presumptive joint areas differentiate up to a prechondrocytic stage and then undergo apoptosis to create joint cavities [Lefebvre and Smits, 2005].

Just as during chondrocyte development, *Ihh* and *BMP2* cooperate again during osteoblast differentiation, when *runx related transcription factor 2* (*Runx2*), the essential transcription factor during bone formation and osteoblasts differentiation expressed in hypertrophic chondrocytes, functions downstream of

*BMP2* during osteoblastogenesis resulting in preosteoblasts differentiated from multipotent mesenchymal cells (figure 3) [Nishimura et al., 2002].

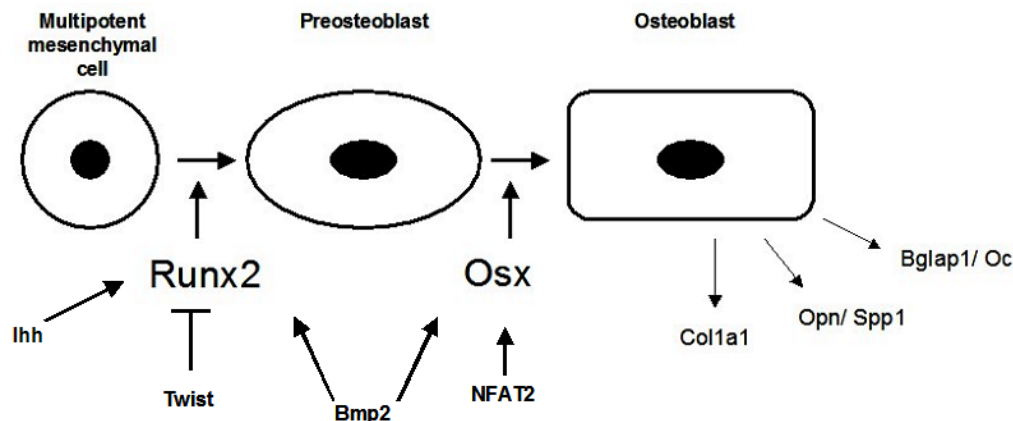


**Figure 3: Osteoblast differentiation.** Under the control of *Runx2*, multipotent mesenchymal cells differentiate into preosteoblasts that further differentiate into osteoblasts. To establish functional osteoblasts, that express the osteoblasts gene markers type 1 collagen, osteopontin, and osteocalcin, *Osx* is needed. The influence of *Ihh*, *Twist*, *Bmp2* and *NFAT2* is further explained in the text (adapted from Murakami et al., 2004).

As no *Runx2* expression was seen in the perichondrium of *Ihh*<sup>-/-</sup> mouse embryos [Enomoto et al., 2004; St-Jacques et al., 1999; Yoshida et al., 2004], *Ihh* was found to regulate *Runx2* during osteoblast differentiation of mesenchymal cells [Murakami et al., 2004; Regl et al., 2002; Shimoyama et al., 2007]. Additionally, *Runx2* is negatively regulated by the transcription factor *Twist* (figure 3). *Twist-1* and *-2* are expressed in *Runx2*-expressing cells during development, and osteoblast-specific gene expression occurs only after their expression decreases. *Twist-1* over expression inhibits osteoblast differentiation without affecting *Runx2* expression [Bialek et al., 2004]. As *Runx2* is the master transcription factor in osteoblasts differentiation and heterozygous loss causes the severe Cleidocranial Dysplasia (CCD, OMIM 119600) in humans [Mundlos et al., 1997], it regulates the expression of a lot of other genes. To identify new transcripts potentially involved in cartilage and bone development, the expression profiles of E14.5 wild type and *Runx2*-null humeri were recently compared and 21 known genes were found differentially expressed that have not been described in skeletogenesis yet [Hecht et al., 2007].

A second transcription factor called *Osterix* (*Osx*) that is specifically expressed in osteoblasts is required for their differentiation. It is also regulated by *Bmp2*, activates the expression of *osteocalcin* and *type I collagen* and was shown to require *Runx2* in gene-targeting experiments, revealing that *Osx* acts downstream of *Runx2* (figure 3). As in *Runx2*-null mice [Komori et al., 1997; Otto et al., 1997], there is also no endochondral and intramembranous bone formation in *Osx*-null mice, although osteoblast differentiation stops at a later stage than in *Runx2* mutant mice [Nakashima et al., 2002]. *Osx* interacts with the activated form of nuclear factor of activated T cells 2 (NFAT2) that impairs bone formation when deleted [Koga et al., 2005].

The canonical *Wnt*- $\beta$ -catenin signaling pathway is another critical factor for osteoblasts differentiation [Zaidi, 2007], leading to enhanced ossification and suppression of chondrocyte formation. The key event is the regulation of  $\beta$ -catenin stability through its phosphorylation.  $\beta$ -catenin is phosphorylated through glycogen synthetase kinase-3 $\beta$  (GSK-3 $\beta$ ) in the absence of Wnt proteins and phosphorylated  $\beta$ -catenin is targeted for degradation. But when Wnt ligands bind to their receptors Frizzled and LDL receptor related proteins 5 and 6, GSK-3 $\beta$  activity is suppressed and  $\beta$ -catenin therefore not phosphorylated. Accumulated  $\beta$ -catenin is able to enter the nucleus and interact with TCF/LEF family transcription factors to promote specific gene expression [Yang, 2003]. Mutations in Wnt members, excision of Wnt co-receptors, or exposure to Wnt inhibitors result in reduced osteoblasts differentiation and bone formation [Bodine et al., 2004; Li et al., 2005]. Inactivation of  $\beta$ -catenin in mesenchymal progenitor cells *in vitro* was found to cause chondrocyte differentiation under conditions allowing only osteoblasts to form, demonstrating that beta-catenin is also essential in determining whether mesenchymal progenitors will become osteoblasts or chondrocytes [Day et al., 2005].

At the end of skeletal patterning, development and growth, bone homeostasis is maintained by the highly regulated balance between osteoblasts activity, forming new bone, and osteoclasts activity to resorb it [Hadjidakis and Androulakis, 2006]. The constant remodeling of bone is partly regulated by feedback loops of



multiple hormones suggesting a certain endocrine function of bone cells. The adipocyte-derived hormone leptin affects bone formation and resorption through multiple pathways. It inhibits bone formation via CREB (camp response element-binding protein), transcription factor AP-1 and the clock genes, and stimulates bone resorption via the CREB related transcription factor *ATF4* [Elefteriou et al., 2005; Fu et al., 2005]. It also acts on osteoblasts to regulate bone mass through a neuronal pathway by CART [Karsenty, 2006].

By investigating the phenotypes of mice deficient for the protein tyrosine phosphatase OST-PTP and mice lacking osteocalcin that are both specifically expressed in osteoblasts, an endocrine regulation of sugar homeostasis by the skeleton was revealed, also indicating an involvement of skeleton specific genes in energy metabolism [Lee et al., 2007].

Overall, patterning processes involve the most important events during skeletogenesis and are to date best described during limb bud development.

## **1.2. Patterning during vertebrate limb bud development**

The extremities are first visible as small limb buds that grow and develop along the three axes (figures 4A and B). During development, they extend along the proximal-distal (P/D) axis (figure 4B) –from the shoulder to the fingertips – and establish three major elements, the proximal stylopod, the intermediate zeugopod and the distal autopod (figure 4C). The anterior-posterior (A/P) axis runs from the thumb to the little finger (figure 4B), while the dorsal-ventral (D/V) axis is defined from the back of the hand to the palm (figure 4B).

The first step in vertebrate limb development is the determination of a group of cells in the lateral plate mesoderm (LPM, figure 5), covered by ectoderm, that will give rise to the limb bud [Capdevila and Izpisua Belmonte, 2001; Mariani and Martin, 2003; Niswander, 2003]. These mesodermal cells provide the progenitors of the chondrocytes and connective tissues such as tendons and muscle sheets, while muscles and blood vessels develop from cells that migrate into the early limb bud [Kardon et al., 2002].

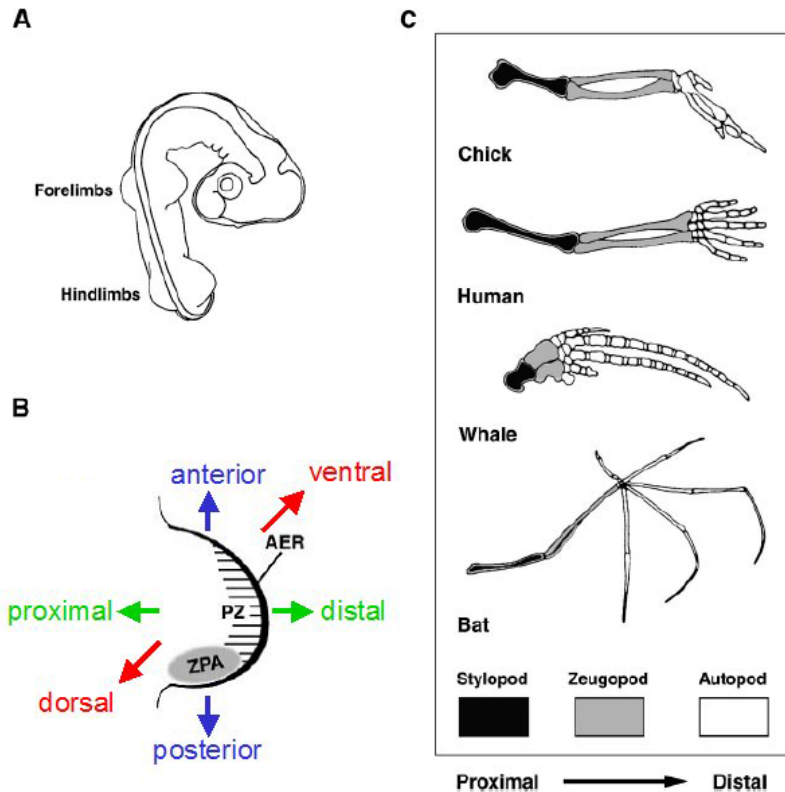


**Figure 4: Basic structures of vertebrate limbs;** A: Chick embryo with two pairs of limb buds (fore and hind limbs) located in the embryonic flank; B: Dorsal view of the limb bud indicating the localization of the progressive zone (PZ), the apical ectodermal ridge (AER), and the zone of polarizing activity (ZPA), as well as the three body axis anterior-posterior (A/P, blue arrows), dorsal-ventral (D/V, red arrows), and proximal-distal (P/D, green arrows); C: Schematic comparison of skeletal structures of forelimbs from four different vertebrates. High conservation of structural elements is obvious in the basic skeletal structures (stylopod in black, zeugopod in gray, and autopod in white) among the tetrapods; (adapted from Capdevila and Izpisua Belmonte, 2001).

To develop limbs in a vertebrate with a tetrapod body plan, four limb fields in the flank of each embryo must be determined that is partly ensured by a specific combined expression of *Hox* genes. These are expressed at different levels along the A/P axis of the embryonic trunk and, more in general, are organized in four *Hox* gene clusters (*Hox A-D*). For proper limb development, especially vertebrate *HoxA* and *HoxD* cluster genes are required [Kmita et al., 2005]. In coordination with *Tbx4* and *Tbx5*, *Hox genes* determine whether a fore or a hind limb will be developed [King et al., 2006]. Although the two T-box transcription factors *Tbx4* and *Tbx5* are specifically expressed in the LPM, *Tbx5* in the prospective fore, and *Tbx4* in the prospective hind limb region, they are not sufficient to determine limb-specific morphologies. Such mechanisms might be

furthermore dictated by positional codes like *Pitx1* and *Hox* genes in the lateral plate mesoderm [Minguillon et al., 2005]. The *paired-related homeodomain factor* (*Pitx1*) is only expressed in the prospective hind limb region and was found to be controlled by *Shh* expression [Capellini et al., 2006].

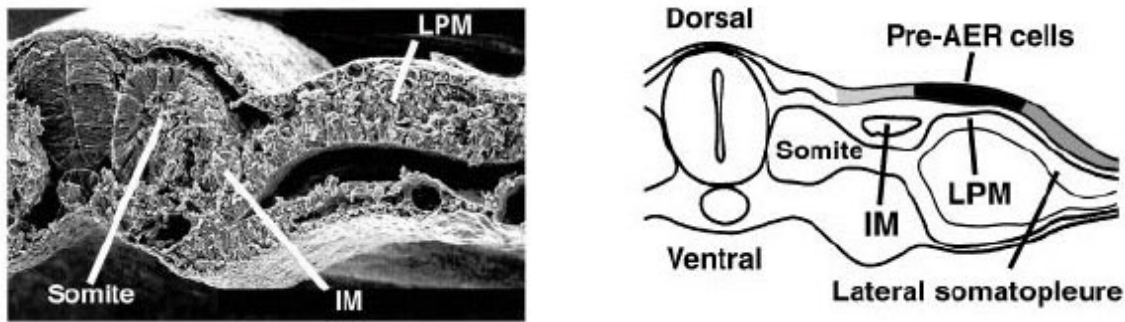


**Figure 5: View through the D/V axis of the hind limb field in a chick embryo at stage 13**, left panel shows a scanning electron micrograph of a traverse section, right panel shows a scheme indicating the positions of intermediate mesoderm cells (IM), lateral plate mesoderm cells (LPM), somite, cells becoming dorsal limb ectoderm (light gray), cells becoming AER (black), cells becoming ventral limb ectoderm (dark gray), (adapted from Capdevila and Izpisua Belmonte, 2001).

Little is known about how the size of the limb bud is determined, but inactivating a key player like *fibroblast growth factor 8* (*Fgf8*) in early limb induction causes a substantial reduction in limb bud size [Lewandoski et al., 2000] and alters expression of other *Fgf* genes, as well as *Shh* and *Bmp2* [Moon and Capecchi, 2000]. Beside *Fgf8*, additional FGFs and FGF receptors (FGFRs) have been described with different functions in early stages of skeletal formation [Chen and Deng, 2005; Ornitz and Marie, 2002].

For instance, *Fgf18* is expressed in the perichondrium and is regulated by *Ihh* and BMPs [Haque et al., 2007] when it signals through *FGFR3* to promote chondrogenesis (figure 2) [Davidson et al., 2005; Haque et al., 2007; Ohbayashi et al., 2002]. *Fgfr3* is an important member of the FGFR gene family. It is expressed shortly after the mesenchymal condensation in the proliferating chondrocytes and later in the reserve and proliferating zones, suggesting its role in regulating chondrocytes proliferation and differentiation.

Importantly, FGF and FGFR signaling is closely associated with other important signaling pathways, including *lhh* [Minina et al., 2001], and *Sox9* [Murakami et al., 2000].

*Fgf8* is clearly one of the key inducers of limb bud formation. It is expressed in the intermediate mesoderm (IM, figure 5) in both fore and hind limbs and before and during limb induction [Boulet et al., 2004]. It signals towards the LPM through *Fgf10* [Yonei-Tamura et al., 1999], and placing a barrier between the LPM and the IM of a chick embryo resulted in limb reduction [Stephens and McNulty, 1981; Tickle, 2004]. *FGF10* expressed in the mesoderm signals towards the overlying ectoderm to activate BMP and Wnt family members, as well as *FGFR2b*. This signaling maintains the apical ectodermal ridge (AER, see 1.2.1.). *FGF8*, that is subsequently expressed in the AER, signals back through *FGFR1c* to the limb mesoderm to close the FGF8/FGF10 loop [Martin, 1998; Tickle and Munsterberg, 2001].

During limb outgrowth, ectodermal cells above the somites start growing along the dorsal axis (light gray areas in figures 5, 6), while ectodermal cells above the lateral somatopleural mesoderm start growing along the ventral axis (dark gray areas in figures 5, 6). The ectodermal cells migrate laterally to cover the underlying mesoderm [Altabef et al., 1997; Michaud et al., 1997] and the AER remains at the border of dorsal and ventral ectoderm ( see also figure 8).

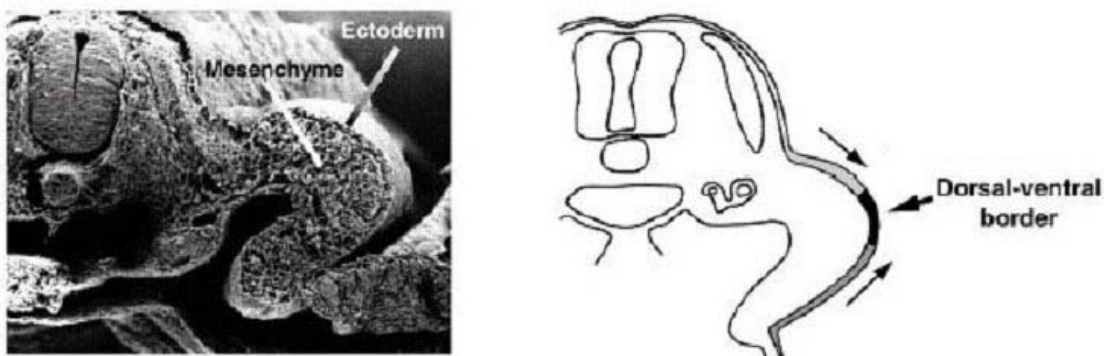


**Figure 6: View through the D/V axis of the hind limb field in a chick embryo at stage 16**, left panel shows scanning electron micrograph of traverse section, right panel shows a cartoon indicating the direction of ectodermal cell migration (thin arrows) and the position of the border between D/V compartments (thick arrows), cells becoming dorsal limb ectoderm (light gray), cells becoming AER (black), cells becoming ventral limb ectoderm (dark gray), (adapted from Capdevila and Izpisua Belmonte, 2001).

### 1.2.1. D/V patterning, the apical ectodermal ridge (AER) and the progressive zone model

The AER is an ectodermal thickening along the A/P axis of the limb bud that separates the dorsal from the ventral side of the limb (figures 4, 8) [Guo et al., 2003]. The induction of the AER starts after *Fgf10* is expressed in the prospective fore and hind limb areas. Surgical removal of the AER from the chick embryonic limb at progressive stages results in limb truncation and the later the AER removal is performed, the more distal truncations will be observed [Saunders, 1948; Summerbell, 1974]. To explain the evidence that cells undergo progressive changes in specification from proximal to distal fate, the progressive zone (PZ) model was established in the 1970s (figure 7) [Summerbell et al., 1973].

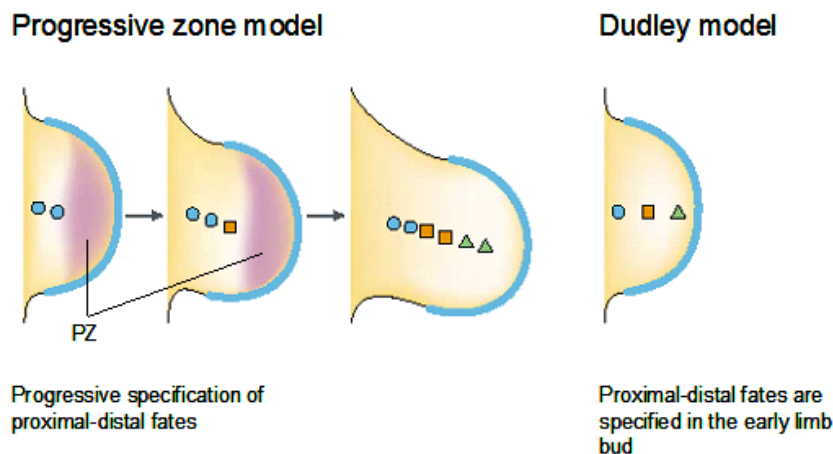


**Figure 7: Graphical comparison of the Progressive zone model (left panel) with the model suggested by Dudley et al. 2002 (right panel).** In the progressive zone model, proximal-distal specification depends on the AER, in which proximal fate is specified first, followed by more distal specification. In the right model, proximal-distal fates are specified within the early limb bud; stylopod precursors are indicated as blue circles, zeugopod precursors as orange squares, autopod precursors as green triangles, PZ: progressive zone (adapted from Niswander, 2003).

The PZ was defined as the mesenchyme underlying and being influenced by the AER. When the AER is removed, cells at the distal tip cease progressing and do not acquire more distal fates. Therefore, more distal structures get lost with later AER removal.

In 2002, proximodistal patterning has been re-examined and new data suggested that the various limb segments are 'specified' early in limb development as distinct domains, with subsequent development involving expansion of these progenitor populations before differentiation (figure 7) [Dudley et al., 2002]. It was shown that removal of the AER at early stages results in a zone of cell death, while AER removal after stage 24 does not effect cell survival. Cells that will distribute to all proximal-distal structures exist in layered domains within the early limb bud: the extent of the limb elements formed is a reflection of the population of proximal-distal progenitors that are located outside the zone of cell loss and that differentiated according to their proximal-distal fate, as specified early in limb bud development [Niswander, 2003].

The location of the AER is determined by the expression of *Radical fringe* (*Rfng*) and the homeobox-containing transcription factor *Engrailed-1* (*En-1*). In fact, the AER forms at the boundary between cells that do or do not express *Rfng* (figure 8) and *Rfng* expression in dorsal ectoderm is partly established through its repression by *En-1* in the ventral ectoderm [Laufer et al., 1997; Moran et al., 1999].

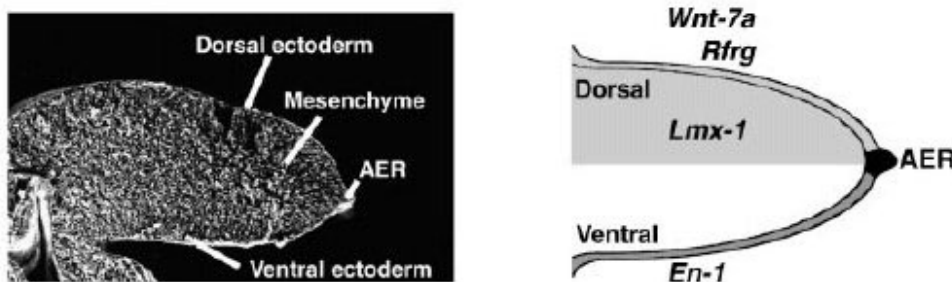


**Figure 8: View through the D/V axis of the hind limb field in a chick embryo at stage 22**, left panel: scanning electron micrograph of traverse section, right panel: cartoon indicates the position of the AER (black) and the restricted expression of *Wnt-7a* and *Rfng* in the dorsal (light gray) and *En-1* in the ventral ectoderm (dark gray). Chick *Lmx-1* expression is restricted to the dorsal mesoderm (gray), (adapted from Capdevila and Izpisua Belmonte, 2001).

The AER is therefore established at the boundary of dorsal and ventral limb territories. Its formation is one event during D/V patterning that leads to the dorsoventral asymmetry of the limb as seen in most vertebrates. After the appearance of the AER, two more genes play critical roles in D/V patterning,

*Wnt7a* and *Lmx1b*. The secreted glycoprotein *Wnt7a*, like *Rfng*, is expressed in the dorsal ectoderm, while the LIM-homeodomain containing protein *Lmx1b* is expressed in the dorsal mesenchyme of the developing limb bud (Lmx-1 in figure 8). According to current models, *En-1* represses *Wnt7a* transcription in the ventral ectoderm; as a consequence *Wnt7a* expression is restricted to the dorsal ectoderm, from where it induces *Lmx1b* expression in the dorsal mesenchyme.

The importance of *Wnt7a* and *Lmx1b* in establishing the dorsoventral axis appears in animal models that lack expression of these genes. *Wnt7a*-null mice show dorsal-to-ventral transformations of the limb mesoderm, indicating *Wnt7a* as a dorsalizing signal. In addition, these mutant mice partly lack posterior digits, demonstrating that *Wnt7a* is also required for anterior-posterior patterning by interaction with *Shh*. *Shh* is specifically expressed in the Zone of Polarizing Activity (ZPA, figure 4), located at the posterior margin of the developing limb bud. It is supported by FGF signaling from the apical ectodermal ridge, as well as by *Wnt7a* secretion from the dorsal ectoderm [Adamska et al., 2005; Nusse, 2003; Robert and Lallemand, 2006]. Although *Shh* is not involved in AER induction, it controls its FGF signaling and therefore is required for its maintenance. Hence, normal limb development requires interactions between the D/V and the A/P signaling systems [Parr and McMahon, 1995].

The best studied model for signaling along the A/P and D/V axes is e.g., LMX1B. Limbs in *Lmx1b*-null mice have bi-ventral features extending along the entire A/P axis [Chen et al., 1998a].

### **1.3. *Lmx1b* (LIM homeobox transcription factor 1 beta)**

#### **1.3.1. Discovery of *Lmx1b***

Hamster *Lmx1* was first isolated while searching for proteins that bind to the Far-FLAT elements of the rat mini-insulin gene [German et al., 1992b]. As of today, two hamster homologues of the Lmx gene, *Lmx1.1* and *Lmx1.2* [German et al., 1992a, 1992b; Johnson et al., 1997], corresponding to the murine *Lmx1a* and

*Lmx1b* [Chen et al., 1998a; Millonig et al., 2000] and the human *LMX1A* and *LMX1B* genes [Dreyer et al., 1998; Thameem et al., 2002; Vollrath et al., 1998] have been described in the literature. In chick, only the *C-Lmx1* gene has been isolated [Riddle et al., 1995; Vogel et al., 1995].

### 1.3.2. *Lmx1b* expression and knockout model

The murine *Lmx1b* gene is located on chromosome 2qB and spans over a length of ~80 kb. The transcript of 1119 bp consists of 8 exons (The Jackson Laboratory, Bar Harbor/ Maine, USA; <http://www.informatics.jax.org>). The open reading frame encodes 372 amino acids and the following domains can be identified: two protein-protein interaction cysteine- and histidine-rich zinc finger motifs at the amino terminus, - LIM-A and LIM-B - [Dawid et al., 1998; Sanchez-Garcia and Rabbitts, 1994], a DNA binding homeodomain, and a glutamine rich and serine-rich domain [Curtiss and Heilig, 1998; German et al., 1994] (figure 9).

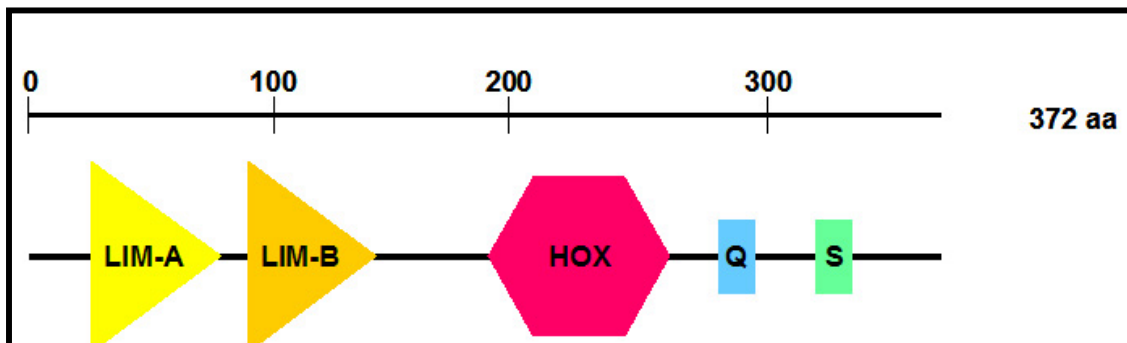


**Figure 9: Protein structure of the murine *Lmx1b*** that is 372 amino acids long. The protein contains two LIM domains - LIM-A (yellow box) and LIM-B (orange box), a homeodomain (pink box), a glutamine rich domain (blue box), as well as a serine-rich domain (green box).

Therefore, *Lmx1b* is a homeodomain transcription factor and belongs to the subfamily of LHX (lim-homeodomain) transcription factors [Hobert and Westphal, 2000]. This family of genes controls important aspects of embryonic development including pattern formation, cell fate specification, cell differentiation, and promotion of cell survival. LHX transcription factors are divided into six subgroups based on the similarities within their homeodomains [Hobert and



Westphal, 2000]. The nomenclature 'LIM' derives from three proteins containing LIM domains: *Lin-11* (*C. elegans*), *Is1-1* (rat), and *Mec-3* (*C. elegans*).

*Lmx1b* is expressed early during development and can be detected in the lateral plate mesoderm of presumptive limb buds as early as E8.5, followed by expression in the dorsal mesenchyme of the outgrowing limbs (*Lmx-1* in figure 8) at E11.5 [Cygan et al., 1997]. Later studies observed a maximal expression at E14.5 that was significantly diminished by E16.5, and effectively abolished by E18.5 [Dreyer et al., 2000]. The latest expression was seen in the most distal dorsal tissues, including nail mesenchymal precursor cells, suggesting its role in initializing the specification of dorsal limb cell differentiation.

*Lmx1b* is also expressed in the mesenchyme that contributes to portions of the cranial vault suggesting a role in cell proliferation and morphogenesis [Chen et al., 1998b] that was not further investigated.

Furthermore, *Lmx1b* is expressed in kidneys at all levels of glomerular differentiation and was detected in immature S-shaped bodies, as well as in mature glomeruli by *in situ* hybridization [Morello et al., 2001]. Within the glomeruli, *Lmx1b* expression is restricted to podocytes, specialized cells with epithelial and mesenchymal characteristics that are essential for glomerular filtration.

*Lmx1b* expression was also detected in mesencephalic dopaminergic neurons of distinct brain areas in E7.5 mice and in adult humans [Smidt et al., 2000], as well as in mammary glands [Schweizer, 2003].



**Figure 10: Comparison between newborn B6/129 wild type (left) and *Lmx1b* knockout mice (right); note the overall shortening of the embryo, the dumpy skull and the lost pattern of the limb.**

Targeted disruption of exons 3-7 of the *Lmx1b* gene on a B6/129 genetic background leads to a null allele and to death within the first hours after birth due to multiple defects in homozygous null pups [Chen et al., 1998a; Chen et al., 1998b]. The most obvious malformations affect the skull and the extremities (figure 10). The skull appears dumpy while fore and hind limbs equally show a loss of dorsal features, and absent patellae and nails.

The skull of *Lmx1b* mutant mice does not show the usual division between calvarial bones that were abnormally fused, underdeveloped or completely absent. The fontanel was absent and overall, the optic and parietal cartilage as well as the occipital arch appeared reduced in their dorsal aspects [Chen et al., 1998b].

Further characterization of *Lmx1b* mutant limbs revealed a complete ventralization of the dorsal tissues in zeugopod and autopod [Chen et al., 1998a]. This was somehow expected, since ectopic expression of *Lmx1b* in chick embryos resulted in ventral-to-dorsal conversions of distal limb tissues [Riddle et al., 1995; Vogel et al., 1995].

The mutant pups are unable to suckle and have breathing problems. Heterozygous mice did not show any of the limb or skull defects, but a significant reduction in compensatory renal growth and increased glomerulosclerosis after unilateral nephrectomy were investigated, indicating a possible pathogenic effect on the glomeruli [Endele et al., 2007]. Although this differs from the human situation, it may reflect a difference in gene-dosage sensitivity in glomeruli development and in the establishment of the dorsal-ventral aspect of the limb and the skull in mice versus humans.

### **1.3.3. Downstream targets of *Lmx1b***

*Lmx1b* functions as a transcription factor, but little is known about its targets. Kidneys from *Lmx1b* mutant pups appeared to be smaller than from their wild type littermates and biopsy material from patients with *LMX1B* mutations showed abnormal development of the glomerular basement membrane (GBM). Therefore, the expression of different extracellular matrix components was

investigated and *Col4a4* and *Col4a3* were strongly diminished in the GBM of *Lmx1b*-null mice [Morello et al., 2001], as *Lmx1b* can bind to an enhancer-like element in intron1 of *Col4a4* [German et al., 1992b].

Additionally, *Lmx1b*-null podocytes were dysplastic with a reduced number of foot processes, and lacking the typical slit diaphragms. To indicate whether this arrest in podocyte development is due to *Lmx1b* inactivation, the expression of marker genes important for slit diaphragm assembly was investigated. Podocin (*Nphs2*) as well as *Cd2ap* that have important functions in foot process effacement [Boute et al., 2000; Shih et al., 1999], contain *Lmx1b* binding sites flanking their first exons, and were found to be down regulated in *Lmx1b*-null podocytes [Miner et al., 2002; Rohr et al., 2002]. These findings suggests that the kidney phenotype as seen in *Lmx1b*-null mice is at least partly due to reduced levels of the *Lmx1b* downstream targets *Col4a4*, *Col4a3*, *Cd2ap* and *Nph2p*.

In the limbs, *Lmx1b* expression has been examined during early joint, tendon and muscle formation, as well as a few genes spatially restricted to these tissues. While growth differentiation factor 5 (*Gdf5*) and *secreted frizzled-related sequence protein 3* (*sFrp3*) were symmetrical expressed along the dorsoventral axis in normal and *Lmx1b*-null mice, *sFrp2* and the homeobox genes *Six1* and *Six2* exhibited a dorsoventral expression asymmetry that was not seen in the mutant mice [Dreyer et al., 2004]. However, they were not solely restricted to or excluded from dorsal *Lmx1b* expressing tissues, and *Six1* was found to be mainly depending on *Shh* expression [Bonnin et al., 2005].

#### 1.3.4. **LMX1B and Nail-Patella-Syndrome**

The *LMX1B* mRNA was isolated from a human chondrosarcoma cell line (ATCC HTB94) and EBV-transformed lymphoblastoid RNA [Dreyer et al., 1998]. The mouse and human mRNA sequences are 99% identical. The cDNA contained an open reading frame of 372 amino acids, and Northern blot analysis of RNA from human fetal and adult tissues revealed a 7 kb transcript in fetal and adult kidney. An upstream start codon in the *LMX1B* gene, in-frame with the previously

determined open reading frame, extended the protein sequence to 395 or 402 amino acids respectively, depending on exon 7 splice-site selection. More recently, upstream of this start codon two additional short open reading frames of unclear function were identified [Dunston et al., 2004].

Loss-of-function mutations in *LMX1B* cause Nail-Patella syndrome (NPS, OMIM 161200) [Dreyer et al., 1998; Lee and Morello, 2004]. NPS is an autosomal dominant inherited skeletal malformation syndrome affecting a variety of organs. The main clinical features are dysplasia of the nails and abnormal skeletal features, including aplastic or hypoplastic patellae, impaired pronation and supination of the elbows, and the presence of iliac horns [Jones and Smith, 1997; Sweeney et al., 2003]. Importantly, a significant percentage of NPS patients will develop nephropathy [Bennett et al., 1973] and open-angle glaucoma [Beals and Eckhardt, 1969]. Additionally, muscle aplasia, vasomotor and neurological problems are also associated with the disease [Sweeney et al., 2003].

Over 90 different mutations in more than 150 unrelated families have been identified, including missense, nonsense, and splice site mutations, as well as microinsertions and deletions [Bongers et al., 2005a; Dreyer et al., 1998; McIntosh et al., 2005; Seri et al., 1999; Vollrath et al., 1998]. Most of the mutations affect the LIM domains or the homeodomain and are therefore localized in exons 2-5, while none have been found in exons 1, or 6-8.

In contrast to heterozygous mice, that do not display an obvious phenotype, heterozygosity at the human *LMX1B* locus leads to NPS.

While there are a lot of studies regarding the phenotype of human *LMX1B* mutations and the molecular mechanisms behind this disease, similar syndromes -like genitopatellar syndrome- receive less attention

#### **1.4. Genitopatellar Syndrome**

Genitopatellar syndrome (GPS; OMIM 606170) is considered a distinct entity from Nail-Patella syndrome. GPS is a rare multi-systemic disorder characterized by genital and renal abnormalities and absent or displaced and rudimentary patellae

–similar as in NPS–, skeletal and minor facial anomalies, and mental retardation [Schlaubitz et al., 2007]. Associated skeletal malformations include joint contractures and flexion deformities of hip, knees, elbows and talipes, pelvic hypoplasia and brachydactyly of the fingers in one third to one fifth of the reported individuals. Genital anomalies range from scrotal hypoplasia in males to cryptorchidism. Hydronephrosis and multicystic kidneys were found in most patients and ureterohydronephrosis and oligohydramnios were seen sporadically. Microcephaly, agenesis of corpus callosum and hypotonia appeared to be common, while only two patients had hearing defects [Abdul-Rahman et al., 2006]. Four patients were also described with heart anomalies and respiratory problems, leading to death in at least two cases by apnea [Cormier-Daire et al., 2000]. All previously reported patients had apparently normal chromosomes.

### **1.5. Specific Aims**

Cartilage is a rare and difficult to extract tissue. Therefore, the identification of novel genes involved in skeletogenesis is difficult. Although an association with at least one gene can be stated for over 200 osteochondrodysplasias and dysostoses, the molecular changes behind a lot of cartilage disorders remain illusive to date.

In the following thesis, novel genes involved in skeletogenesis will be identified in an EST sequencing project using a phage library that was previously generated from human fetal cartilage RNA. A statistically relevant number of 5000 ESTs will be sequenced, bioinformatically analyzed and rated regarding their importance in skeletogenesis. Genes that appear to be required for cartilage development, will be further characterized regarding their expression and function. Due to the mentioned rare occurrence of human cartilage tissue and the high sequence homologies between human and mouse genes, part of the analysis will be carried out with the help of the mouse as a model system. Beside expression studies performed with murine tissues, an additional project will be started to identify potential murine candidate genes. Mouse limb buds at E11.5, E12.5 and

E13.5 stage of embryonic development will be dissected for RNA isolation to be further evaluated in microarray expression studies. The chosen time points cover the timeframe just before the occurrence of precartilaginous mesenchymal condensation, that starts at E12.0, and afterwards. Genes that show statistically relevance expression over time that will also be validated by quantitative RT-PCR are therefore thought to be of further interest for limb bud development and will help to decrease the number of unknown genes in endochondral ossification. To find candidate genes for cartilage disorders also through a disease driven approach, the second part of this thesis will be related to a key-player in dorsal-ventral patterning, the transcription factor *Lmx1b*. After establishing the limb bud dissection experiment, the same technique will be used to identify downstream targets of *Lmx1b*. With this approach a better understanding of the dorsal-ventral patterning processes during limb development will be elucidated. Therefore, E11.5 limb buds from wild type and mutant embryos will be excised and used for microarray expression studies as described before. A small number of genes that are differentially expressed in the microarray experiment, will be selected for further analysis including quantitative RT-PCR and whole mount *in situ* hybridization. Because of the important role of *Lmx1b*, potential downstream targets are expected to have unique functions in skeletogenesis as well.

To investigate potential rearrangements in regulatory elements affecting the function of *LMX1B* and potential candidate genes for syndromes similar to Nail-Patella syndrome (NPS, caused by mutations in *LMX1B*), six patients with clinical Genitopatellar syndrome (GPS), a distinct entity from NPS, will be involved into an extensive study. The molecular pathogenesis of GPS remains illusive to date, and all described patients suffer from severe genital anomalies that are not seen in NPS patients. Therefore, genes that are involved in D/V patterning or genital development will be screened for mutations, array based comparative genome hybridization (CGH) and fluorescence *in situ* hybridization will be performed to find chromosomal abnormalities, and quantitative RT-PCR will be used to investigate dosage dependent abnormalities in this rare disease.

## **2. Methods**

### **2.1. DNA Isolation**

#### **2.1.1. Isolation of genomic DNA from blood**

DNA from 3-5 ml of human EDTA blood was prepared with the Genomic DNA Purification kit (Gentra, Minneapolis, MN, USA) following the manufacturer's instructions. The DNA was usually dissolved in 200  $\mu$ l of  $\frac{1}{4}$  x TE and stored at 4°C.

#### **2.1.2. Isolation of plasmid DNA**

Extraction of plasmid DNA was adapted from a BAC DNA isolation protocol [Sheng et al., 1995] and was based on the alkaline lysis procedure described by Birnboim and Doly [Birnboim and Doly, 1979].

A single bacteria colony was incubated in 5 ml of LB medium supplement with antibiotic at 200-250 rpm ON at 37°C. 1 ml of ON culture was mixed with 1 ml of 2x FM to be frozen as a stock at -80°C, while the remaining 4 ml were collected in a single tube by two rounds of centrifugation, spinning at 14,000 rpm for 10 seconds in a bench top centrifuge. Each pellet was resuspended in 100  $\mu$ l of solution 1. 200  $\mu$ l of freshly prepared solution 2 were added and mixed by inverting several times. 150  $\mu$ l of ice-cold solution 3 were added and incubated on ice for 10 min. After 6 min of centrifugation at top speed, the supernatant was transferred to a new tube containing 1 ml EtOH 100%. A short mixture was followed by 30 min of centrifugation and the pellets were washed for 5 min with 500  $\mu$ l EtOH 70%, then air-dried and dissolved in 30  $\mu$ l  $\frac{1}{4}$  x TE pH 8.0. The DNA was stored at 4°C.

#### **2.1.3. Isolation of genomic DNA from mouse tissues for genotyping PCR**

DNA from mice tails of newborn and older mice was extracted with saturated sodium chloride solution. At least 0.4 cm of mouse tail was digested ON in 700  $\mu$ l NTES solution containing 0.5 U proteinase K (Roche, Indianapolis, IN, USA) in a water bath or a hybridization oven set to 57°C. The digested tissue was centrifuged in a bench top centrifuge at maximum speed (~14000 rpm)

for 5 min at RT. The supernatant was transferred to a new tube containing 200 µl of 4 M NaCl. The mixture was vortexed for 20 sec and centrifuged for 10 min at maximum speed. The supernatant was transferred to a tube containing 1 ml of EtOH 100% and carefully inverted about 10 times until the DNA became visible as a fibric precipitate. The DNA was spooled out using a heat-sealed Pasteur pipette, washed with EtOH 70% and air-dried for 5 min. The DNA was resuspended in 50-200 µl DI water and concentration was determined as described in 2.3.1. About 100 ng of DNA was used for genotyping PCR.

DNA from prenatal mice was extracted with the DNeasy kit (Qiagen, Hilden, Germany) following the manufacturer's instructions. Alternatively, a piece of skin as small as  $\sim 4 \text{ mm}^2$  was dissected from the embryo and boiled in 500 µl of 50 mM NaOH for 45-60 min. After cooling the tubes on ice for 5 min, 50 µl of 1M Tris pH 8.0 were added. About 10 µl of the mixture were used in a PCR reaction of 50 µl total volume.

## **2.2. RNA Isolation**

### **2.2.1. Isolation of total RNA from tissues or cells**

Isolation of RNA from tissues or cells was performed with Trizol reagent<sup>®</sup> (Invitrogen, Carlsbad, CA, USA), based on previous publications [Chomczynski, 1993; Chomczynski and Sacchi, 1987; Wilfinger et al., 1997]. 50-100 mg of fresh or frozen tissue or  $5-10 \times 10^6$  of pelleted cells were homogenized in 1 ml of Trizol reagent<sup>®</sup> (Invitrogen, Carlsbad, CA, USA) using a Ultra-Turrax<sup>®</sup> T25 Basic homogenizer and incubated at RT for 5 min. Phase separation was initiated by adding 0.2 vol. of chloroform with isoamyl alcohol (24:1), vortexing for 15 sec and incubation for 3 min at RT. After centrifugation for 15 min at 4°C and top speed, the RNA remained exclusively in the aqueous phase, which was transferred to a new tube and again mixed with 0.2 vol. of chloroform with isoamyl alcohol, vortexed, incubated for 3 min at RT and centrifuged for 15 min at 4°C. The aqueous phase was transferred to a new tube and the precipitation of the RNA was performed by adding 0.5 vol.



ice-cold isopropanol. After 10 min of incubation at RT, centrifugation was performed at 14,000 rpm and 4°C for 10 min. The pellet was washed with 500 µl of ice-cold EtOH 75% for 5 min at 9,500 rpm and 4°C. The pellet was air-dried for 10 min and resolved in a mixture of solutions for DNaseI digestion, as described in 2.3.4. Alternatively, the GenElute Mammalian RNA Purification Kit (Sigma-Aldrich Corp., St. Louis, MO, USA) was used for faster RNA extraction.

#### **2.2.2. mRNA isolation from total RNA**

mRNA was isolated from total RNA by hybridizing beads containing oligo-dT to the polyA tail of the mRNAs. Procedure was performed with the Dynabeads® mRNA Purification Kit (Dyna/ Invitrogen, Carlsbad, CA, USA) following the manufacturer's instructions.

#### **2.2.3. RNA preparation from prenatal limb buds for microarray experiments**

RNA from prenatal limb buds (E11.5-13.5), further used for microarray studies (2.5.2.1.), was isolated with the Versagene™ RNA isolation kit (Gentra, Minneapolis, MN, USA) including the DNaseI digestion step following the manufacturer's instructions. Homogenization was performed using insulin syringes and the final elution was performed with 15 µl/ 4 pairs of forelimb buds. Concentration was measured with a Nanodrop spectrometer (2.3.1.) and the 260/280, 260/230 OD ratios were calculated as a quality check.

#### **2.2.4. RNA preparation from differentiated and dedifferentiated chondrocytes**

Long bones from two E16.5 or E18.5 limbs of C57Bl/6 embryos were dissected and disrupted using fine sterile forceps (Fine Science Tools, Foster City, CA, USA). The resulting pieces of bone were incubated in 6 ml DMEM complete (2.9.1.) containing 0,05 % collagenase type II (Gibco BRL/ Invitrogen, Carlsbad, CA, USA) in a 25 cm<sup>2</sup> cell culture dish (Nunc, Rochester, NY, USA) for two days at 37°C [Dietz and Sandell, 1996]. Differentiated chondrocytes were harvested directly, while chondrocytes that were

designated for dedifferentiation were further cultured with 5 ml DMEM complete containing  $3 \times 10^{-6}$  M all-trans retinoic acid (Sigma-Aldrich Corp., St. Louis, MO, USA) for one week, with media changes every other day. After harvest, the chondrocytes were processed for RNA preparation as described in 2.2.1. Retinoic acid treated chondrocytes can be used as a model system to investigate the mechanisms of chondrocyte 'dedifferentiation', where expression of type II collagen is repressed [Dietz and Sandell, 1996].

### **2.2.5. Laser Capture Microscopy and RNA preparation from captured cells**

P1 glomeruli were laser captured from frozen H & E stained frozen kidney sections (2.7.6.) using CapSure<sup>®</sup> Macro LCM Caps (Arcturus/ Molecular Devices, Mountain View, CA, USA) on a PixCell<sup>®</sup> Ile LCM Instrument with PixCell II Image Archiving Workstation (110 volts) (Arcturus/ Molecular Devices, Mountain View, CA, USA). At 20x magnification, about 40-60 glomeruli were captured per kidney. Per session, 30 kidney sections were processed. Caps were frozen in liquid nitrogen and stored at  $-70^{\circ}\text{C}$  until RNA preparation. RNA was isolated using the PicoPure<sup>®</sup> RNA Isolation Kit (Arcturus/ Molecular Devices, Mountain View, CA, USA). Therefore, 50  $\mu\text{l}$  extraction buffer were added into 0.5 ml tubes and closed with a cap carrying captured cells. The tubes were inverted and incubated at  $42^{\circ}\text{C}$  for 30 min. After preparation of the purification column filter membrane, the tubes were centrifugated at  $800 \times g$  for 2 min, and 10  $\mu\text{l}$  of 70% EtOH each were added into the cell extract, mixed and pipetted into the purification column. At this step, all the cell extracts from one specimen were pooled on one column. The remaining procedure followed the protocol including the recommended DNase treatment step. Elution was done with 11  $\mu\text{l}$  buffer per column. One  $\mu\text{l}$  was used for quality check using the RNA 6000 Pico LabChip<sup>®</sup> Kit on a Bioanalyser 2100 (both Agilent Technologies, Palo Alto, CA, USA). Per specimen, about 100 ng of RNA were extracted that needed to be amplified for microarray experiment (2.5.2.1.) using RiboAmp<sup>™</sup> HS RNA Amplification Kit (Arcturus/ Molecular Devices, Mountain View, CA, USA).

## 2.3. DNA and RNA standard methods

### 2.3.1. Determination of DNA, cDNA and RNA concentrations

The concentration of DNA, cDNA and RNA samples was determined by measuring the absorbance of nucleic acids at 260nm with the PicoGreen<sup>®</sup> dsDNA or RiboGreen RNA/ cDNA Quantification Kit (Molecular Probes/ Invitrogen, Carlsbad, CA, USA) in a FLUOstar OPTIMA plate reader (BMG LABTECH GmbH, Offenburg, Germany) or with a ND-1000 Spectrophotometer (NanoDrop Technologies, Wilmington, DE, USA).

The quality was calculated from the OD at 230, 260, and 280 nm. Good quality RNA has ratios of 1.8 to 2 (OD 260/ 280) and 1.8 or greater (OD 260/ 230). This is because nucleic acid is detected at 260 nm, whereas protein, salt and solvents are detected at 230 and 280 nm. A high OD 260/ 280 and OD 260/ 230 ratio therefore indicates that the extracted RNA devoid of any of these contaminants.

### 2.3.2. Agarose gel electrophoresis of DNA and RNA

Separation of DNA was performed with horizontal agarose gels in 1x TBE buffer. Depending on the range of estimated fragments, concentration of agarose was adapted as shown below.

Agarose concentration (%)	Separation (kb)
0.7	0.8-10
0.9	0.5-7
1.2	0.4-6
1.5	0.2-4
2.0	0.1-3

Table 1: Expected range of separation depending on agarose concentration.

DNA samples were diluted in ½ - ¼ vol. of Orange G dye before loading in the slots of an agarose gel containing 100 µg/ ml ethidium bromide. Electrophoresis was performed at 110V (~25mA). Visualization at 356 nm and documentation of the results were done with the gel image system Eagle

sight (Stratagene, La Jolla, CA, USA).  $\lambda$  Hind III fragments (2.027 – 23.130 kb), 1 kb plus ladder (100bp - 12 kb), and 100 bp ladder (100 bp – 2.072 kb; all Invitrogen, Carlsbad, CA, USA) were used as DNA ladders.

Separation of RNA was performed with horizontal 1.2 % agarose gels in 10 mM NaPO<sub>4</sub> pH 6.8 with 0.5  $\mu$ g/ ml ethidium bromide, as published by Kevil et al. [Kevil et al., 1997]. RNA samples were incubated for 1 h at 50°C in a buffer containing 1.0 M DI glyoxal pH 7.0, 50% DMSO, and 10 mM NaPO<sub>4</sub> pH 6.8 at a final vol. of 32  $\mu$ l.  $\frac{1}{8}$  vol. of RNA loading dye containing 0.15% bromphenol blue and 0.15% xylene cyanol in 15% glycerol were added before loading the probes in the slots of the agarose gel. Electrophoresis was performed at 70-80V with a pump helping the buffer circulation. Visualization and documentation were done with the gel image system Eagle sight (Stratagene, La Jolla, CA, USA). 0.24-9.5 Kb RNA ladder (Invitrogen, Carlsbad, CA, USA) was used to identify the 28S RNA band at 4718 bp and the 18S band at 1814 bp. The RNA within the agarose gel was transferred to nylon membrane as described in 2.3.3.

### 2.3.3. Blotting of RNA

15 – 20  $\mu$ g of total RNA that have been separated in a 1.2 % agarose gel (), were transferred to a charged nylon Hybond™ XL membrane (Amersham Bioscience, GE Healthcare Life Science, Pittsburgh, PA, USA) by blotting the gel ON in 0.02 N NaOH transfer buffer as shown in figure 11 and described by Kevil et al. [Kevil et al., 1997]. To form covalent linkages between the RNA and amine groups on the surface of the membrane, the damp membrane was cross-linked at ~120 millijoules/ cm<sup>2</sup> with a Stratalinker® 1800 UV Crosslinker (Stratagene, La Jolla, CA, USA).

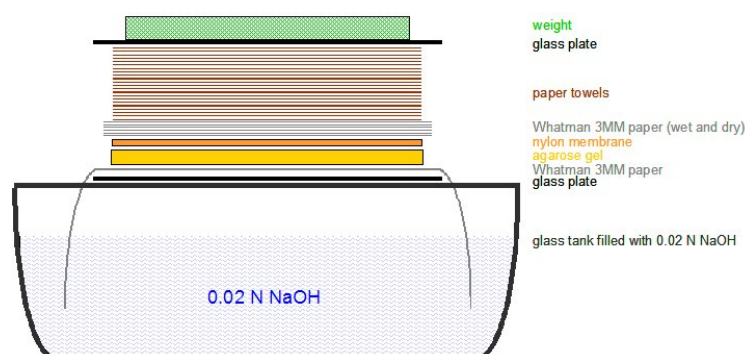


**Figure 11: Northern blot assembling**

#### **2.3.4. DNaseI digestion of total RNA**

After isolation of total RNA from tissues or cells (2.2.1.), RNA pellets were dissolved in a mixture containing 10-20 U of RNase free DNaseI enzyme (Roche, Indianapolis, IN, USA), 80 U RNase-Inhibitor (Promega, Madison, WI, USA), 10 mM DTT, 10 mM MgCl<sub>2</sub>, 1x TE and incubated for 2 hours in a water bath set to 25°C. To clean up the RNA from remaining proteins and contents of the buffer after the enzymatic digest, the Mammalian RNA purification kit (Sigma-Aldrich Corp., St. Louis, MO, USA) was used, following the manufacturer's instructions.

#### **2.3.5. Reverse Transcription of RNA**

To transcribe total RNA into double stranded complementary DNA (cDNA), 2-4 µg of total RNA were incubated at 70°C for 10 min using a thermal cycler (Applied Biosystems, Foster City, CA, USA). Within the following incubation at 4°C for 5 min, a mixture of 0.25 µg oligo dT<sub>12-18</sub> primer (Invitrogen, Carlsbad, CA, USA), 1.5 µg Random hexamers (Promega, Madison, WI, USA), 0.875 mM dNTP's, 40 U RNase-Inhibitor (Promega, Madison, WI, USA), 1x 1<sup>st</sup> strand and 10 mM DTT were added and reverse transcription was performed at 37°C for 100 min under the control of 200 U MMLV-RT (Invitrogen, Carlsbad, CA, USA) as described previously [Gerard et al., 1997]. Success of the procedure was verified by using 1 µl of the double stranded cDNA in a control RT-PCR (2.3.6.) with intron over spanning primers from a ubiquitously expressed gene like human hypoxanthine guanine phosphoribosyltransferase 1 (*HPRT*) or mouse β-actin.

#### **2.3.6. Polymerase Chain Reaction and Reverse Transcription Polymerase Chain Reaction (PCR and RT-PCR)**

With the Polymerase Chain Reaction, small amounts of DNA can quickly and repeatedly be copied to produce sufficient quantities of DNA to be further used for conventional laboratory methods, like sequencing or cloning. Therefore, about 200 ng of DNA were mixed with 0.8 µM of short ssDNA oligonucleotide primers - base-complementary to opposite ends of either strand of DNA region of interest-, 0.1 mM of each of the four dNTP's, 1 x PCR

buffer, and a heat-resistant *Taq* DNA polymerase with a 5'→ 3' polymerase and a 5'→ 3' exonuclease activity.

The mixture was transferred to a thermal cycler (Applied Biosystems, Foster City, CA, USA), and first heated to 95°C to denature the double stranded DNA. The mixture was then cooled to 45-70°C, depending on the melting temperature of the primers, and the primers annealed to their base-complementary regions in the single stranded DNA. The final step at 72°C, when the *Taq* enzyme replicated the primed single stranded DNA, is called extension. At the end of the first cycle, the region between the two primers has been copied once, producing two copies of the region of interest. Since a heat-resistant *Taq* DNA polymerase was used, the three steps including denaturing, annealing and extension were repeated continuously with doubling the amount of template in each cycle. Usually, 30 cycles were performed, resulting in a  $10^9$ -fold amplification of the starting material ( $2^{30}$ ). A final expanded extension step of ~7-10 min at 72°C was performed to align all single stranded fragments and the sample was cooled down.

Double stranded cDNA was also used as a template in so-called reverse transcription polymerase chain reaction (RT-PCR) reactions. The double stranded cDNA was a product of reverse transcription of RNA as described in 2.3.5. Oligos for RT-PCR reactions needed to be designed from messenger-RNA (mRNA) sequences, because cDNA contains only the coding parts of a gene and therefore no intronic regions.

### **2.3.7. Quantitative RT-PCR (qRT-PCR)**

Quantitative RT-PCR was used as an alternative to Northern blot hybridization to verify expression in a variety of tissues, to survey microarray experiments and to yield the fold change in expression difference for genes that were found deleted by FISH (2.5.2.2,) or array CGH (2.5.2.3.). The qRT-PCR monitored the progress of amplification during a RT-PCR in 'real time' by measuring fluorescent dyes that were released during the amplification [Bustin and Mueller, 2005; Gibson et al., 1996; Wittwer et al., 1997]. Most of the experiments were done with LightCycler FastStart DNA MasterPLUS SYBR Green I (Roche, Indianapolis, IN, USA) in a hot start reaction mix for

PCR applications in glass capillaries using the LightCycler® 2.0 (Roche, Indianapolis, IN, USA) instrument. A reaction mix of 20 µl total was used, containing 160 ng cDNA, 5µM of each primer, 3-5 mM MgCl<sub>2</sub>, and 2 µl SYBR Green. Annealing temperature was tested by gradient RT-PCR prior to the actual experiment and was chosen between 60-65 °C. For normalization purposes, the same reaction was done simultaneously with the ubiquitously expressed mouse or human hypoxanthine guanine phosphoribosyltransferase 1 (*Hprt1/ HPRT*) in each lightcycler run. The chemically modified *Taq* DNA polymerase, FastStart *Taq* DNA Polymerase, stayed inactive at room temperature and became activated at high temperatures during the initial denaturation step. SYBR Green I dye bound specifically to double-stranded DNA and therefore bound to the amplified PCR product during each PCR cycle. With each cycle, fluorescence increased due to the ongoing amplification and was monitored. Combining amplification with melting curve analysis provided specificity and sensitivity.

To perform a one step RT-PCR reaction for expression analysis of GC-rich amplicons, LightCycler® RNA Amplification Kit SYBR Green I (Roche, Indianapolis, IN, USA) was used. Instead of using cDNA as a template, 400 ng of RNA and gene specific primers were used for the reverse transcription reaction that was directly followed by amplification during RT-PCR. This results in a more specific amplification of the gene of interest and overcomes the problem of a high CG content.

### **2.3.8. Cloning of PCR products in T-vectors**

Because of the missing proofreading activity (3'→ 5' exonuclease activity) of the *Taq* DNA polymerase used in (RT-)PCR reactions (2.3.6.), an adenosine was usually incorporated on the 3' end of the new DNA strand during a PCR cycle. Therefore, cloning of the resulting PCR products in so-called T-vectors, like pGEM®-T vector (Promega, Madison, WI, USA) or pCR®II-TOPO® (Invitrogen, Carlsbad, CA, USA) that provide a single 3'-T overhang at the insertion side, was simplified.

The cloning was performed following the manufacturer's instructions and completed plasmids were used for transformation as described in 2.8.2.

### **2.3.9. Sequencing**

Sequencing of DNA fragments was performed based on techniques established by others in the 1970s [Maxam and Gilbert, 1977; Salser, 1974; Sanger et al., 1977] that were later improved by the usage of dye-labeled terminators [Lee et al., 1992].

Based on this method, DNA sequencing was fully performed by the company Seqwright ([www.seqwright.com](http://www.seqwright.com); Houston, TX, USA) that used the 3100 or 3730XL fluorescence-based DNA analysis systems with 16 or 48 capillaries (Applied Biosystems, Foster City, CA, USA).

Sequencing for the EST project was performed by GENTERprise (Mainz, Germany) on MegaBACE 1000 (Amersham Bioscience, Pittsburgh, PA, USA) and ABI 3730 (Applied Biosystems, Foster City, CA, USA) capillary sequencer platforms.

### **2.3.10. Digestion**

To cut DNA into fragments of reproducible and defined size, ~10 U of enzyme (NEB, Ipswich, MA, USA or Roche, Indianapolis, IN, USA) were added to 1 µg of purified DNA in a final volume of 30 µl with the appropriate 1x buffer, and 1x BSA if recommended, followed by incubation for at least 3 hours or ON at the optimal temperature (mostly 37°C). Adding one of the following stop solutions was used to terminate the reaction: 50% glycerol, 50 mM EDTA pH 8.0, or 0.05% bromophenol blue. If further manipulations of the digested DNA were required, raising the temperature to 65 or 80°C for 20 minutes was performed to heat inactivate the enzyme.

### **2.3.11. Gel extraction and purification of DNA**

DNA fragments of interest were cut out of an agarose gel after DNA digestion (2.3.10.) and electrophoresis (2.3.2.) using a clean razor blade and extracted with the Wizard® SV Gel and PCR Clean-Up System (Promega, Madison, WI, USA). The same procedure was performed for PCR products. This kit was used for fragments smaller than 8 kb following the manufacturer's instructions, while QIAEX II Gel Extraction Kit (Qiagen, Hilden, Germany) was used for larger fragments.



### **2.3.12. DNA purification by phenol/ chloroform extraction**

An equal volume of buffer-saturated phenol was added to DNA in solution and mixed by vortexing. Centrifugation was performed for 3 min at 14,000 rpm and RT. The aqueous layer was carefully transferred to a new tube and an equal volume of buffer-saturated phenol/ chloroform (1:1) was added. The mixture was vortexed and centrifuged as before. The aqueous layer was again transferred to a new tube and phenol/ chloroform extraction was repeated until an interface was no longer visible. To remove traces of phenol, an equal volume of chloroform was added to the aqueous layer, mixed and centrifuged for 3 min. The aqueous layer was transferred to new tube and the DNA was precipitated with EtOH 100%.

### **2.3.13. Ligation**

Ligations were performed using T4 DNA ligase (Invitrogen, Carlsbad, CA, USA) that catalyzes the formation of phosphodiester bonds between adjacent 3'-OH and 5'-PO<sub>4</sub> termini of both, cohesive and blunt-ended DNA fragments [Pheiffer and Zimmerman, 1983].

5 U of enzyme were used in a 20 µl reaction containing 1 x ligation buffer to perform a “sticky ends” ligation with about 1.5 pmol vector ends and 4.5 pmol insert ends ON at 14°C.

For blunt end ligations, a final concentration of 2 mM ATP was added.

## **2.4. DNA and RNA labeling method**

### **2.4.1. Random primed oligo labeling of cDNA**

The product of a RT-PCR was purified by gel extraction (2.3.11.) and further used for radioactive dCTP labeling with Ready-To-Go™ DNA Labeling Beads (Amersham Bioscience/ GE Healthcare Life Science, Pittsburgh, PA, USA) or High Prime (Roche, Indianapolis, IN, USA) following the manufacturer's instructions. As recommended, the labeled probe was purified over Sephadex™ G-50 columns (Amersham Bioscience/ GE Healthcare Life Science, Pittsburgh, PA, USA).

## 2.4.2. RNA labeling methods

### 2.4.2.1. Generation of a template

RNA probes for ISH or WISH were generated by *in vitro* transcription from a linearized template. Therefore, promoter for RNA polymerases must be available in the vector containing the DNA template. A 300-600 bp fragment of the 3'UTR of a gene of interest was amplified by PCR and cloned (2.3.8.) into the pGEM<sup>®</sup>-T vector containing T7 and Sp6 RNA polymerase sites (figure 12; Promega, Madison, WI, USA) and transformed in DH5 $\alpha$  bacteria cells (2.8.2.).

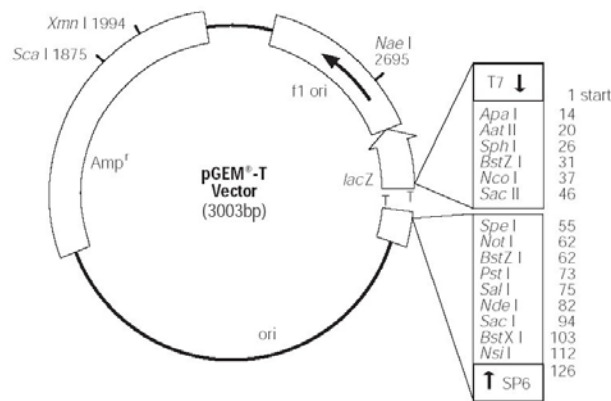


**Figure 12: Vector map of pGEM-T<sup>®</sup> Vector** showing the position of the T7-/ Sp6-promoter sequences and single cutter restriction sites in the multiple cloning site (source: [http://www.promega.com/vectors/t\\_vectors.htm](http://www.promega.com/vectors/t_vectors.htm))

After plasmid DNA preparation and linearization with a restriction enzyme located downstream of the DNA insert (mostly *SpeI*; figure 12), T7 RNA polymerase, was used to generate the sense probe that was not able to bind to the mRNA during hybridization and was therefore used as a negative control. Analogously, the so-called anti-sense probe was generated with a restriction enzyme upstream of the insert (mostly *SacII*; figure 12) and Sp6 as a RNA polymerase.

In detail, 40  $\mu$ g of DNA were needed from each plasmid for linearization by digestion. For each probe, 20  $\mu$ g of plasmid DNA were digested ON with a sufficient amount of restriction enzyme and treated with 40  $\mu$ g proteinase K (Roche, Indianapolis, IN, USA) in the presence of 0.5% SDS. The DNA was purified by phenol/ chloroform extraction (2.3.12.), precipitated with EtOH and further used for labeling.

**2.4.2.2. Radioactive RNA labeling with  $^{35}\text{S}$  through *in vitro* transcription**

0.5-1  $\mu\text{g}$  of linearized probe was mixed with 25 mM DTT, 20 U RNase-Inhibitor, 2  $\mu\text{M}$  of each RNTP, 0.02 mCi [ $\alpha$ - $^{35}\text{S}$ ] dUTP (Amersham Bioscience/GE Healthcare Life Science, Pittsburgh, PA, USA), 20 U T7 or Sp6 RNA polymerase (Roche, Indianapolis, IN, USA) and incubated at 37°C for 2.5 hours. 2 U of RNase-free DNaseI (Roche, Indianapolis, IN, USA) were added and the mixture of 50  $\mu\text{l}$  total was incubated for another 15 min and afterwards precipitated with 100  $\mu\text{g}$  tRNA, 250  $\mu\text{l}$  4M ammonium acetate and 1 ml EtOH 100% for 30 min at 4°C. After washing the pellets with EtOH 70%, they were air-dried, resuspended in hybridization buffer, and stored at -80°C.

**2.4.2.3. Non radioactive RNA labeling with DIG through *in vitro* transcription**

1  $\mu\text{g}$  of linearized probe was transcribed using the Digoxigenin (DIG) RNA labeling kit (Roche, Indianapolis, IN, USA) following the manufacturer's instructions. The RNA probe was precipitated by adding 10  $\mu\text{g}$  tRNA, 33  $\mu\text{l}$  7.5 M ammonium acetate and 300  $\mu\text{l}$  EtOH 100%. The mixture was stored ON at 80°C. Centrifugation was performed at 4°C and 14,000 rpm for 1 h. Pellets were washed with EtOH 70%, air-dried, resuspended in DI water and stored at -20°C.

**2.5. Hybridization methods****2.5.1. Radioactive hybridization methods****2.5.1.1. Northern blot**

Hybond<sup>TM</sup> XL nylon membrane with the blotted RNA was prehybridized in ExpressHyb<sup>TM</sup> Hybridization Solution (Clontech, Mountain View, CA, USA) for 1.5 hours at 68°C. Denatured cDNA probe (2.4.1.) was used for hybridization at approximately  $1\text{-}2 \times 10^6$  cpm/ ml ExpressHyb<sup>TM</sup> Hybridization Solution (Clontech, Mountain View, CA, USA) for 2.5 hours at 68°C. Washing was

performed for 40 min to one hour with 2 x SSC, 0.05% SDS at RT and 10 min with 0.1 x SSC, 0.1% SDS at 50°C. The membrane was wrapped in cling film, covered with a Kodak BioMax X-ray film (Eastman Kodak Company, New Haven, CT, USA) and stored for 2 hours to ON in an exposure cassette with intensifying screens at -80°C.

#### **2.5.1.2. Hybridization of cDNA filter**

Oligo dT-primed, directionally cloned plasmid cDNAs of different human and mouse tissues from the I.M.A.G.E. Consortium (Integrated Molecular Analysis of Genomes and their Expression, Lawrence Livermore National Laboratory, Livermore, CA, USA; <http://image.llnl.gov>) were spotted in duplicate on nylon membranes by the RZPD (German Resource Center for Genome Research, Berlin, Germany) as high-quality, arrayed filter libraries. These filters were ready for immediate use and were directly prehybridized with Church medium at 65°C for at least 30 min. Denatured cDNA probe (2.4.1.) was used for hybridization at approximately  $10^6$  cpm/ ml Church medium ON at 65°C. Stringent washing was carried out in 40 mM sodium phosphate pH 7.2, 0.1% SDS at 65°C for at least 20 min, until activity was about 50-100 decompositions/ sec when measured with a Geiger Müller counter. The filters were wrapped in cling film, covered with a Kodak BioMax X-ray film (Eastman Kodak Company, New Haven, CT, USA) and stored ON in an exposure cassette with intensifying screens at -80°C. After development of the film, the positions of signals needed to be determined to distinguish positive signals from false positive ones. RZPD offered their investigators a grid and an online service to determine and order positive clones from their libraries (<http://www.rzpd.de>).

#### **2.5.1.3. *In situ* hybridization**

Paraffin sections on glass slides (2.7.3.) underwent a series of pre-hybridization washes. Deparaffinization was done twice in Histoclear for 10 min. Hydration was performed by two washes in EtOH 100% for 2 min, followed by washes in EtOH 95%, EtOH 80%, EtOH 70%, EtOH 50%, EtOH 30% for 20 sec each, as well as 5 min each in 0.9 % NaCl and 1x PBS.

Tissue sections were fixed in 4% PFA/ 1x PBS for 20 min and again washes in 1x PBS for 5 min. Proteins were digested in proteinase K for 5 min, followed by 5 min in 1x PBS. Tissue sections were again fixed in 4% PFA/ 1x PBS for 20 min, followed by acetylation with acetic anhydride for 3 and 7 min. Sections were then washed with 1x PBS for 5 min and dehydration was performed through a series of 0.9 % NaCl for 5 min and EtOH 30% and EtOH 50% for 20 sec, followed by 5 min in EtOH 70% and 20 sec each in EtOH 80%, EtOH 95% and twice EtOH 100%. Slides were air-dried in a dust- and RNase free area and further proceeded for prehybridization with hybridization buffer for 3 hours at 58°C in a chamber moisturized with 2x SSC/ 50% formamide. Prehybridization solution was replaced by 60 µl hybridization solution containing  $3 \times 10^6$  counts/ slide of  $^{35}\text{S}$  labeled probe (2.4.2.2.) and hybridization was performed ON at 58°C. The following day, the slides underwent a serie of post-hybridization washes. First, they were incubated for 30 min at 65°C in 200 ml 5x SSC containing 355 µl β-Mercaptoethanol, followed by 30 min at 65°C in 2X SSC/ 50% formamide containing 700 µl β-Mercaptoethanol and three washes for 10 min in NTE at 37°C. 400 µl RNase A and 3 µl RNase T were added to 200 ml NTE and incubation was done for 30 min at 37°C, followed by 15 min in NTE at 37°C and 30 min at 65°C in 200 ml 2X SSC/ 50% formamide containing 700 µl β-Mercaptoethanol-30 min. Finally, slides were incubated in a series of solution at RT. 15 min in 2x SSC were followed by 15 min in 0.1x SSC and 30 sec each in EtOH 30% in 0.3 M ammonium acetate, EtOH 50% in 0.3 M ammonium acetate, EtOH 70% in 0.3 M ammonium acetate, EtOH 95% and EtOH 100%. Slides were air-dried and placed in an exposure cassette, covered with a Kodak BioMax X-ray film (Eastman Kodak Company, New Haven, CT, USA) and stored for 3 days at RT. After developing the film, slides were covered with prewarmed emulsion (42°C) in a darkroom and dried ON with a fan in the dark. The following day, slides were placed into a foil lined slide box and exposed for 4-6 days at 4°C. Slides were developed in the darkroom by incubation in developer for 2 min, some dippings in DI water, 5 min in fixer and 10 min in DI water. 40 µl Hoersch dye were added to 200 ml DI water and the slides were washed for 2

min in this solution and air-dried afterwards. Each slide was mounted with 45 µl Canada Balsam, covered with a cover slip and stored in a slide holder.

## **2.5.2. Non-radio active hybridization methods**

### **2.5.2.1. Affymetrix**

Samples were labeled using the standard Affymetrix T7 oligo(dT) primer protocol. Total RNA was reverse transcribed to produce double stranded cDNA. The cDNA product was used as a template for *in vitro* transcription reaction, producing biotin-labeled cRNA. The labeled cRNA was quantified using a ND-1000 Spectrophotometer (NanoDrop Technologies, Wilmington, DE, USA).

15 µg of the labeled cRNA was fragmented and re-checked for concentration. A hybridization cocktail containing Affymetrix spike-in controls and fragmented labeled cRNA was loaded onto a Mouse 430 2.0 GeneChip® array (Affymetrix, Santa Clara, CA, USA). The array was hybridized overnight at 45°C with rotation at 60 rpm then washed and stained with a streptavidin, R-phycoerythrin conjugate stain. Signal amplification was done using biotinylated anti-streptavidin. The stained array was scanned on the Affymetrix GeneChip® Scanner 3000 (Affymetrix, Santa Clara, CA, USA). The images were analyzed and quality control metrics recorded using Affymetrix GCOS software version 1.1.2. Labeling and hybridization was performed at the Microarray Core Lab at Baylor College of Medicine in Houston, TX, USA.

### **2.5.2.2. Fluorescent *In Situ* hybridization (FISH)**

Fluorescent *in Situ* hybridization (FISH) was performed by the FISH Core lab at Baylor College of Medicine in Houston, TX, USA following routine procedures using GTG-banded metaphase chromosomes from peripheral blood leukocytes at a 550-600-band resolution according to a standard protocol [Shaffer et al., 1997]. BAC and fosmid clones spanning the region of interest were selected from UCSC genome browser (<http://genome.ucsc.edu>, Freeze 2004). BAC or fosmid DNA was isolated using the PSYClone BAC DNA Kit (Princeton Separations, Inc., Adelphia, NJ, USA). Briefly, 200 ng of

probe DNA were directly labeled by nick translation with either Spectrum Orange-dUTP or Spectrum Green-dUTP using a commercially available kit (Vysis, Downers Grove, IL, USA) precipitated with 6 µg of salmon sperm DNA, 500 ng Cot-1 DNA, 1/10 vol. 3 M sodium acetate and 2.5 vol. EtOH 100%. Pellets were resuspended in 5 µl formamide, mixed with 1 vol. of master mix containing 20% dextran sulphate and 2 x SSC and incubated for 30 min at 37°C and for 10 min at 70°C to denature the probe that was used for ON hybridization of metaphase chromosomes on glass slides. Hybridization was performed at 37°C in a humidified chamber. Slides were washed with 50% formamide in 2x SSC pH 7.0 for 30 min total with several changes of the solution. Slides were counterstained with 0.2 µg/ ml DAPI in Vectashield (Vector Laboratories, Burlingame, CA, USA), sealed and stored at 4°C.

#### **2.5.2.3. Array based comparative genomic hybridization (array CGH)**

Array based comparative genomic hybridization (array CGH) was used to determine DNA copy number changes across the entire genome [Pinkel et al., 1998]. Therefore whole bacterial artificial chromosomes (BAC) DNA, representing the whole human genome, were spotted on chips in Dr. Cai's lab at Baylor College of Medicine (Houston, TX, USA) and hybridized with fluorescent labeled DNA [Cai et al., 2002; Yu et al., 2003].

200 ng genomic patient or control DNA in 40 µl vol. and 40 µl of 2.5x RadPrime Buffer (Invitrogen, Carlsbad, CA, USA) were denatured in a thermal cycler for 5 min at 100°C and cooled down on ice for 5 min. 20 µl 5x AAdUTP-dNTP(+TTP) and 2 µl Klenow (40 U/ µl) were added and the mix was incubated in a thermal cycler at 37°C for at least 3 hours. To cut the DNA in pieces of 100 bp to 1 kb length, 100 µl of 1M NaOH was added and the mixture was incubated in a heat block for 17 min at 100°C. After cooling the samples to RT in ice-cold water, the DNA was precipitated by adding 22 µl 5M NaCl and 240 µl isopropanol and freezing at -80°C for at least 10 min. Centrifugation was performed at 4°C and 14,000 rpm for 20 min, the pellets were washed with 300 µl 80% EtOH. Pellets were ON dissolved in 0.1 M

NaHCO<sub>3</sub> at RT to reach a concentration of 100 ng/  $\mu$ l. 10  $\mu$ l each were labeled with 2  $\mu$ l Cy3-dUTP or Cy5-dUTP (Amersham Bioscience, GE Healthcare Life Science, Pittsburgh, PA, USA) and incubated ON at RT in the dark. The labeled DNA was precipitated by adding 22  $\mu$ g of ssT-DNA and isopropanol. Centrifugation was performed for 20 min at 14,000 rpm and 4°C. Pellets were washed with EtOH 80%, dried and resolved in 3  $\mu$ l 0.1 M  $\beta$ -mercaptoethanol for 1 hour at RT. Patient DNA labeled with Cy3-dUTP was mixed with control DNA labeled with Cy5-dUTP and the other way around, while control DNA was taken from an individual with another karyotype to have an internal control of the experiment. Therefore, control DNA from the female pool was used for a 46,XY female with sex reversal. 500 ng Cot1 DNA were added to each mixture, as well as hybridization buffer to a final vol. of 60  $\mu$ l. Samples were incubated for 2 min 10 sec at 100°C and afterwards at 37°C for 40 min. Arrays were proceeded in humidified chambers, blocked ON at 37°C using 50 ng of Cot1 DNA (Invitrogen, Carlsbad, CA, USA) and hybridized ON at 37°C. Washing was done in 0.5x SSC, 0.25% SDS, 0.5% Triton X-100, and 0.03 M  $\beta$ -mercaptoethanol at 65°C. The arrays were air dried and scanned with a Scan Array 5000 (Packard BioChip Technology, Billerica, MA, USA). Fluorescence intensities were analyzed using ImaGene 5.6 software (BioDiscovery, El Segundo, CA, USA) and normalized as described previously [Zhang et al., 2003b].

A second analysis was performed using a higher density BAC array consisting of 32,447 clones [de Vries et al., 2005; Ishkanian et al., 2004; Krzywinski et al., 2004] as described previously [Vissers et al., 2003].

#### **2.5.2.4. Whole mount *in situ* hybridization (WISH)**

The following protocol was adapted from a previous publication [Harland, 1991].

Embryos of E9.5 – E13.5 were hydrated on ice through 75%, 50%, 25% EtOH/ PBS for 10 min each and washed twice with PBT. The “bleaching” of the embryos was performed with 6% H<sub>2</sub>O<sub>2</sub> in PBT for 1 h on ice and followed by three washes with PBT for 10 min at RT. Proteinase K treatment was done at RT with 0.02  $\mu$ g/ ml proteinase K in proteinase K buffer for 3-5 min,



depending on the size of the embryo. Remaining proteinase K was washed away using twice freshly prepared 2 µg/ ml glycine in PBT buffer for 5 min and two washes with PBT for 5 min, 3 washes with RIPA buffer at RT. The embryos were fixed for 20 min in 4% PFA/ 0,2 % glutaraldehyde and afterwards washed three times with PBT for 5 min. The embryos were transferred to 1.2 ml CryoTube™ Vials (Nunc, Rochester, NY, USA) in which prehybridization was performed in hybridization-buffer/ PBT (1:1) at 65°C for 3 h by rotation. The DIG-labeled probes were denatured at 80°C for 3 min in a thermal cycler and cooled down on ice for a couple of minutes. The prehybridization solution was replaced by 1 ml of hybridisation-buffer containing 1 µg DIG-labeled probe and hybridisation was performed at 65°C ON.

Embryos were washed twice with hybridisation buffer for 30 min at 65°C and cooled down to RT. After a 5 min wash with hybridisation-buffer/ RNase buffer (1:1) at RT, the embryos were incubated for 60 min at 37°C with RNase buffer containing 100 µg/ ml RNase A. Afterwards, the embryos were incubated at RT in 1:1 RNase buffer / SSC/FA/Tween20 for 5 min and then twice for 10 min and 4 times for 30 min at 65°C with SSC/FA/Tween20. The embryos were cooled down to RT and washed briefly with SSC/FA/Tween20/ 1x TBST (1:1) and twice in 1x TBST for 10 min at RT. For the antibody reaction, the embryos were first incubated for 2 h at RT in blocking solution and afterwards ON with blocking solution containing a 1:5000 dilution of DIG-Ab coupled to alkaline phosphatase at 4°C while shaking. To remove unbound antibody, the embryos were washed with 1 x TBST for 48 hours while shaking. The staining was initiated with washing the embryos with fresh alkaline phosphatase buffer that was exchanged against staining solution and shaken at 4°C until a blue staining was visible. Embryos were then washed three times for 10 min with freshly prepared alkaline phosphatase buffer and the staining was fixed in 4% PFA/ PBS ON at 4°C. Pictures were taken with a SMZ1500 Zoom Stereomicroscope (Nikon, Kanagawa, Japan).

## 2.6. Protein isolation, electrophoresis, and mass spectroscopy

Protein was extracted from kidneys of newborn mice and E13.5 forelimbs following protocols and recommendations from Kendrick laboratories (Madison, WI, USA). Briefly, frozen tissue was crushed with mortar and pestle on ice and 0.25 ml of osmotic lysis buffer containing the recommended proteinase inhibitors were added per 100 mg of tissue. The mixture was then frozen and thawed twice, and incubated on ice for 10-15 min. An equal amount of boiling buffer containing SDS was added and the mixture was boiled for 30 min in a water bath. After cooling down on ice, and a short centrifugation step to pellet the solids, protein concentration was determined using the BCA<sup>TM</sup> Protein Assay kit or the Micro BCA<sup>TM</sup> Protein Assay kit (both Pierce, Rockford, IL, USA) in a FLUOstar OPTIMA plate reader (BMG LABTECH GmbH, Offenburg, Germany). Until further use, the protein was stored at -70°C. 50 µg protein each of the *Lmx1b* wildtype and mutant fore limbs, respectively 200 µg each from the wildtype and mutant kidneys were run as a 2D-gel electrophoresis by Kendrick laboratories. Silver stained polyacrylamide gels were analyzed by computerized comparison of the 2D patterns. Potentially interesting spots each were cut out from the coomassie blue stained gels and sent off for protein identification to Dr. Arnie Falick from HHMI Mass Spec. Laboratory (Berkeley, CA, USA).

## 2.7. Histological methods

### 2.7.1. Paraffin embedding

Embryos and tissues were harvested at the necessary time points, rinsed with 1 x PBS and fixed ON in 4% PFA/ PBS. The specimens were dehydrated in ascending EtOH series (EtOH 30%/ PBS; EtOH 50%/ PBS; EtOH 70%/ PBS; EtOH 80%/ PBS; EtOH 90%/ PBS; twice EtOH 100%) and either stored in fresh EtOH 100% for at most six months at -20°C or directly proceeded for embedding. For embedding, EtOH 100% was replaced by xylene/ EtOH 100% and the specimens were incubated on a rocking platform for 30 min at RT,

followed by 15 min in xylene, 30 min in xylene/ paraffin wax at 58°C and three exchanges of paraffin wax for one hour at 58°C. The specimens were orientated in Tissue-Tek® embedding cassettes (Electron Microscopy Sciences, Hatfield, PA, USA) and covered with fresh paraffin wax. After polymerization of the paraffin, the blocks were stored at 4°C until sectioning.

### **2.7.2. Embedding for cryo-sections**

Tissues further proceeded for cryo-sections were dissected on ice, rinsed with cold 1x PBS, orientated in a labeled Tissue-Tek® embedding cassette (Electron Microscopy Sciences, Hatfield, PA, USA) that is placed in 2-Methylbutene on dry ice, and covered with Tissue-Tek® O.C.T. compound (Sakura, Torrance, CA, USA). After the specimen is completely frozen, it is stored at -70°C.

### **2.7.3. Sectioning of paraffin embedded specimens**

Embedded specimens (2.7.1.) were fixed on a microtome and serial sections of 5 µm thickness were cut, transferred to the surface of a water bath set to 42°C to spread the section that was afterwards mounted on a microscope slide. The slides were dried ON at 37°C in a dust-free environment and stored in slide holder at RT.

### **2.7.4. Cryo-sectioning**

O.C.T. embedded tissues (2.7.2.) were cryo-sliced into 5 µm thick sections, placed onto plain glass slides (Fisher Scientific, Fair Lawn, NJ, USA) and fixed with 70% EtOH for 30 sec in a RNase free environment.

### **2.7.5. Vital staining of paraffin sections with Hematoxylin & Eosin**

Hematoxylin is a basic dye with an affinity for the nucleic acids of the cell nucleus, while eosin is an acidic dye that binds to the cytoplasmic components of the cell.

Every 7<sup>th</sup> slide, sectioned from paraffin embedded specimens (2.7.3.), was stained with hematoxylin and eosin to facilitate the orientation within a tissue

section. These stained sections were used as reference sections for ISH (2.5.1.3.).

Deparaffinization was performed in three xylene washes for 3 min. Hydration was performed through a descending serie of EtOH washes for 1 min each (100%, 95%, 80%), followed by 1 min in DI water, 20 sec in Harris Hematoxylin Solution (Sigma-Aldrich Corp., St. Louis, MO, USA), a rinse with DI water, 1 min in fresh 1% NaHCO<sub>3</sub>, 1 min with running DI water, 10 dips in EtOH 80% and 45 sec in Eosin Y Solution Alcoholic (Sigma-Aldrich Corp., St. Louis, MO, USA). Dehydration was performed through EtOH 80%, EtOH 95%, 4x EtOH 100% for 1 min each and three final washings with xylene for 2 min. The slides were mounted with xylene based Cytoseal XYL (Richard Allan Scientific, Kalamazoo, MI, USA) and covered with micro cover slides (VWR, West Chester, PA, USA).

#### **2.7.6. Vital staining of frozen sections with Hematoxylin & Eosin**

Fixed sections were washed with DEPC-treated MilliQ water, stained with Artisan™ Mayer's Hematoxylin (DAKO, Glostrup, Denmark), and washed again with DEPC-treated MilliQ water. Slides were then incubated in Bluing reagent (1x Scott's tap water; Sigma-Aldrich Corp., St. Louis, MO, USA) and dehydrated with 70% EtOH and 95% EtOH for 30 sec each. Staining with Eosin (Sigma-Aldrich Corp., St. Louis, MO, USA) was followed by washes in 75% EtOH, 95% EtOH and 100% EtOH. All steps were done for 30 sec each, followed by a final incubation in xylene for 5 min. Slides were air dried and processed for Laser Capture Microscopy (2.2.5.).

### **2.8. Working with Bacteria culture**

#### **2.8.1. Competent Cells**

A single colony of DH5 $\alpha$  cells was picked from a LB plate and incubated in 5 ml LB medium at 37°C ON in a bacteria shaker at 220-220 rpm. An aliquot of the the ON culture was added to 100 ml SOB-medium to a final OD<sub>550</sub> of 0.05, further cultured for 1.5-2.5 hours until an OD<sub>550</sub> of 0.4 – 0.5 was reached. The

cells were pelleted for 10 min at 2,500 rpm and 4°C, resuspended in 20-40 ml of ice-cold TFB I buffer, gently vortexed and incubated on ice for 30 min. After centrifugation at 2,100 rpm and 4°C for 6 min, the pellet was resuspended in 4 ml of cold TFB II, gently vortexed and aliquots of 50-100 µl were directly frozen at -80°C.

### **2.8.2. Transformation**

200 ng - 1 µg of plasmid DNA were added to an aliquot of DH5α cells (2.8.1.), gently mixed with the cells and incubated for 30 min on ice. To permeabilize the cells and allow a transfer of the DNA into the cells, a heat shock treatment at 42°C was performed for 55 sec. 1 ml of LB medium was added and after 1 hour of incubation in a bacteria shaker at 37°C and 220-220 rpm, the cells were plated on LB plates supplement with antibiotic and incubated ON at 37°C.

## **2.9. Working with cell culture**

### **2.9.1. Standard cell culture**

Cell lines described in 2.9.3. were cultured in DMEM medium containing 4 mM L-glutamine, 10% FCS and 100 U/ ml penicillin/ streptomycin (all Invitrogen, Carlsbad, CA, USA) at 32 or 37°C in a 5-10% CO<sub>2</sub> atmosphere.

### **2.9.2. Transfection of adherent cells**

1.5 µg of plasmid DNA were incubated with 100 µl Opti-MEM<sup>®</sup> Reduced Serum Medium and 8 µl Plus<sup>™</sup> Reagent (both Gibco BRL/ Invitrogen, Carlsbad, CA, USA) for 15 min at RT. 100 µl Opti-MEM<sup>®</sup> Reduced Serum Medium and 8 µl Lipofectamine<sup>™</sup> 2000 (Invitrogen, Carlsbad, CA, USA) were added and incubated for another 15 min at RT. ~0.4 x 10<sup>6</sup> cells grown in each well of a 2-well Lab-Tek<sup>™</sup> II Chamber Slide<sup>™</sup> System (Nunc, Rochester, NY, USA) were washed with 1 x PBS and twice with Opti-MEM<sup>®</sup> Reduced Serum Medium. 800 µl of Opti-MEM<sup>®</sup> Reduced Serum Medium and 200 µl of the

transfection mix were added to each well and incubated for 5 hours at 37°C. 1 ml of complete DMEM medium (2.9.1.) was added to each well.

### 2.9.3. Cell lines

Cell type	Name	Publication	Description
Mouse fibroblast cells	NIH3T3	[Jainchill et al., 1969]	Developed from NIH Swiss mouse embryo cultures.
Mouse fibroblast cells	C3H10T½	[Herschman et al., 1978]	Evaluated on four murine embryo cell lines (Swiss 3T3, Balb 3T3, M2, and C3H10T 1/2)
Human embryonic kidney cells	HEK 293	[Graham et al., 1977]	Human embryonic kidney cells transformed by exposition to adenovirus type 5 DNA
African Green Monkey kidney fibroblast cells	COS7	[Gluzman, 1981]	Simian virus 40 large tumor-antigen-producing monkey kidney cell line
Mouse chondrocyte cells	MCT	[Lefebvre et al., 1995]	Immortalized with a temperature-sensitive mutant of SV40 large T antigen; proliferated at a temperature of 32°C, but differentiated and became hypertrophic and express type X collagen and other hypertrophic chondrocyte markers when grown at 37-39°C
Rat chondrosarcoma cells	RCS	[Mukhopadhyay et al., 1995]	Derived from a Swarm tumor culture and showed a stable differentiated chondrocyte-like phenotype
Rat osteoblastic cell	ROS17/2.8	[Majeska et al., 1980]	Selected from several clonal cell lines from a transplantable rat osteosarcoma to study parathyroid hormone action
Human chondrosarcoma cells	HCS-2/8	[Zhu et al., 1994]	Reflected the processes of both proliferation and differentiation of human chondrocytes in vivo by expressing cartilage specific proteoglycan and type II collagen
Conditionally immortalized mouse podocytes	MPC	[Mundel et al., 1997; Shankland et al., 2007]	Highly proliferative when cultured under permissive conditions, differentiate into differentiated podocytes within 6 days under nonpermissive conditions

**Table 2: Summary of cell lines used for analysis**

### 2.9.4. EBV transformation

Epstein Barr Virus (EBV) transformation is a reliable method to immortalize mammalian cells and was used to obtain cell lines from human lymphocytes that served as a permanent source for DNA and RNA isolation.

EBV is a herpes virus and infects only certain mammalian epithelial cells and B lymphocytes. *In vitro* EBV immortalizes B-cells by activating a number of cell cycle regulating genes as well as B-cell specific genes including immunoglobulin genes. EBV DNA is replicated as an episomal ring and 10-20 copies per cell are typical.

The Cell Culture Core lab at Baylor College of Medicine performed the EBV transformation, following standard protocols [Miller et al., 1972]. EBV-transformed human lymphocytes were cultured in RPMI media containing 4 mM L-glutamine, 10% FCS and 100 U/ ml penicillin streptomycin (all Invitrogen, Carlsbad, CA, USA) at 37°C in a 10% CO<sub>2</sub> atmosphere. RNA from EBV-transformed human lymphocytes was isolated as described previously (2.2.1.).

## **2.10. Working with a phage library**

### **2.10.1. Human fetal cartilage cDNA library**

Brendan Lee et al. at Baylor College of Medicine in Houston, TX, USA, generated the human fetal cartilage cDNA library from pooled growth plates of fetuses of the 20<sup>th</sup> week of pregnancy to 2<sup>nd</sup> year of childhood [Ahn et al., 1995]. First strand synthesis was performed using a modified oligo-dT primer to enable directed cloning of the library in the Lambda ZAP® II vector of the 'Zap-cDNA Synthesis Kit' (Stratagene, La Jolla, CA, USA).

Evaluation of this cDNA library was described previously [Stelzer, 2000; Tagariello et al., 2005] and was part of this dissertation.

This library was used to isolate the putative tumor suppressor gene *EXT1* that was found responsible for hereditary multiple exostoses [Ahn et al., 1995], as well as *SPOC1*, a PHD-finger protein highly expressed in epithelial ovarian cancer [Mohrmann et al., 2005].

### **2.10.2. Plate a phage library**

10 ml ON culture of an appropriate *E. coli* strain - for this phage library XL1-Blue MRA (Stratagene, La Jolla, CA, USA)- were grown in LB medium with 0.2 % Maltose and 10mM MgSO<sub>4</sub> at 37°C. The culture was centrifuged and the bacteria pellet was resuspended in 10mM MgSO<sub>4</sub> and OD<sub>600</sub> was adjusted to 1. To arrest the cell growth, the culture was kept on ice. 10-fold serial dilutions of the phage library were prepared in SM medium and 10-50 µl of each dilution were added to 300 µl bacteria culture, incubated for 15 min in a water

bath set to 37°C and added to 6 ml of 50°C warm NZY top agar containing 0.7 % agarose, 3 mM IPTG and 5mg/ ml X-Gal. The mixture was then purred as a second layer on prewarmed NZY plates (Ø 15 cm) containing 0.7 % of agarose. After polymerization of the top agar layer, plates were incubated ON at 37°C.

### **2.10.3. Processing of a large number of phage clones for sequencing**

Since the top agar contains X-Gal (2.9.2.), a blue-white selection of clones, as described by Ullmann [Ullmann et al., 1967], was possible. Recombinant phage plaques clones were picked and dipped in a PCR master mix and transferred to 500 µl SM medium plus 10 µl chloroform for storage at 4°C in 96-well plates.

To determine the size of the inserts, PCR with T<sub>3</sub>A/T<sub>7</sub>A-oligos was performed in 96-well plates. After agarose gel electrophoresis, only clones with inserts larger than 400 bp were used for further sequencing (about 35%). The PCR products of these clones were pooled in new 96-well plates, and precipitation was performed with 1 vol. 4 M ammonium acetate and 2 vol. isopropanol. Centrifugation was done for 30 min at RT and 14000 rpm. Pellets were washed with EtOH 70% and resolved in 2 µl DI water for sequencing (2.3.9.) with the T<sub>7</sub>A -oligo. Sequences were analyzed with a variety of databases, as described in 2.13.1. and 2.13.2.

## **2.11. Working with mice**

### **2.11.1. Housing mice**

Mice were kept under standard conditions at 22°C, 55 ± 10 % humidity, and a 12 hours artificial light-dark cycle in the transgenic mouse facility of Baylor College of Medicine in Houston (TX, USA). Females of 3 to 6 weeks of age were treated with each 5 IU of two gonadotropins per animal to cause superovulation. To guarantee optimal results, a 42- to 48-hour interval was restrained between the subcutaneous injections of the two hormones. Therefore, the first gonadotropin, pregnant mare's serum (PMS, Sigma-



Aldrich Corp., St. Louis, MO, USA), was injected around 1 p.m. and the second hormone, human chorionic gonadotropin (hCG, Sigma-Aldrich Corp., St. Louis, MO, USA), was injected around noon, 47 hours after the first injection. 2-3 hours later, luteinizing hormone was released and mice were mated ON. Females were checked for vaginal plugs at 7:30-9:00 a.m. the following morning. This time point was considered as embryonic day E0.5 *post coitum*.

### **2.11.2. *Lmx1b* knockout mice**

Mixed B6/129 mice with a targeted disruption of *Lmx1b* by removing exons 3-7 were accomplished by Haixu Chen and Randy L. Johnson at MD Anderson in Houston, TX, USA [Chen et al., 1998a; Chen et al., 1998b]. The caused deletion had effects on the second LIM domain, the homeodomain and most of the carboxy-terminal region and therefore resulted in a non-functional *Lmx1b* protein.

### **2.11.3. Dissection of limb buds for RNA preparation**

*Lmx1b* wildtype and mutant embryos were harvested on E11.5 as well as C57Bl/6 embryos on E11.5, 12.5 and 13.5 and transferred to dishes (Ø: 35mm) containing SYLGARD184 silicone (Dow Corning, Midland, MI, USA) and RNA/*later* solution (Ambion, Austin, TX, USA) to save RNA from degradation. Embryos were fixed on the silicone subsurface using insect needles (Fine Science Tools, Foster City, CA, USA) and limb buds were removed with fine forceps (Fine Science Tools, Foster City, CA, USA) and transferred to a 1.5 ml tube containing RNA/*later*. Before RNA was prepared as described in 2.2.3., the tubes were centrifuged, RNA/*later* was removed and the limb buds were directly covered with the lysis buffer of the RNA preparation kit.

## **2.12. Immunohistochemistry**

To localize proteins in cells, the cDNA of a gene of interest was cloned into a pcDNA-3.1<sup>+</sup>-V5/HisA expression vector (figure 13; Invitrogen, Carlsbad, CA,

USA) and transfected as described previously (2.9.2.). 36 hours after transfection, the cells were fixed with 4 % PFA/ PBS for 15 min, permeabilized with 0.1 % Triton-X100 for 10 min and blocked with 1 % BSA for 30 min.

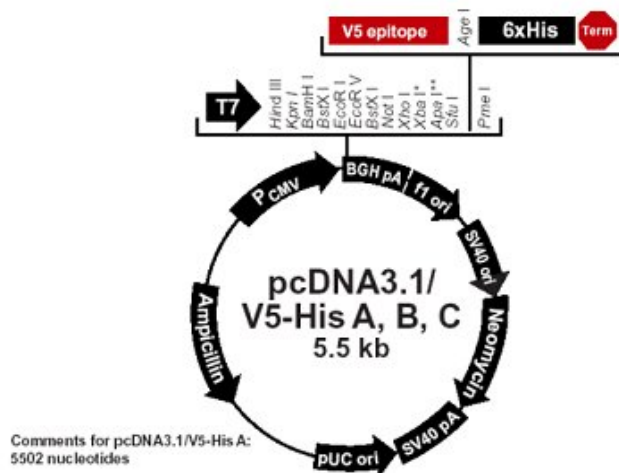


**Figure 13: Vector map of pcDNA3.1/V5-His A, B, C.**

Source: [http://www.invitrogen.com/content/sfs/manuals/pcdna3.1v5his\\_man.pdf](http://www.invitrogen.com/content/sfs/manuals/pcdna3.1v5his_man.pdf).

Exploiting the principle of antigen localization by the use of fluorescent antibodies [Coons and Kaplan, 1950], the cells were incubated with a 1:200 dilution of anti-V5 primary antibody (Invitrogen, Carlsbad, CA, USA) for 1 hour, washed with 1 x PBS, incubated with a 1:300 dilution of goat anti-mouse IgG, Cy3-conjugated secondary antibody (Chemicon, Temecula, CA, USA) for 1 hour, washed with 1 x PBS and mounted in 2 drops of VECTASHIELD antifading mounting medium (Vector Laboratories, Burlingame, CA, USA) per slide. Since the secondary antibody was conjugated with Cy3, the protein was detected with a Texas Red fluorescence filter (595-605 nm) in a Axioplan 2 microscope (Zeiss, Jena, Germany), while the DAPI stained nuclei appeared blue with a DAPI filter (456nm). Co-localization with vinculin was shown by using a monoclonal antibody for vinculin (1:200; Chemicon, Temecula, CA, USA), a biotin conjugated donkey anti-mouse IgG (1:300; Chemicon, Temecula, CA, USA) as a secondary antibody and DTAF-conjugated Streptavidin (1:300; Jackson ImmunoResearch Laboratories, West Grove, PA, USA) for the detection at 520nm (FITC).

## 2.13. Bioinformatic

### 2.13.1. Batched Sequence Analysis of EST sequences

For high throughput sequence analysis of 5000 EST sequences, the W2H web interface of the HUSAR (Heidelberg Unix Sequence Analysis Resources) Bioinformatics Lab at the German Cancer Research Center (DKFZ, Heidelberg, Germany; <http://genome.dkfz-heidelberg.de/>) was used.

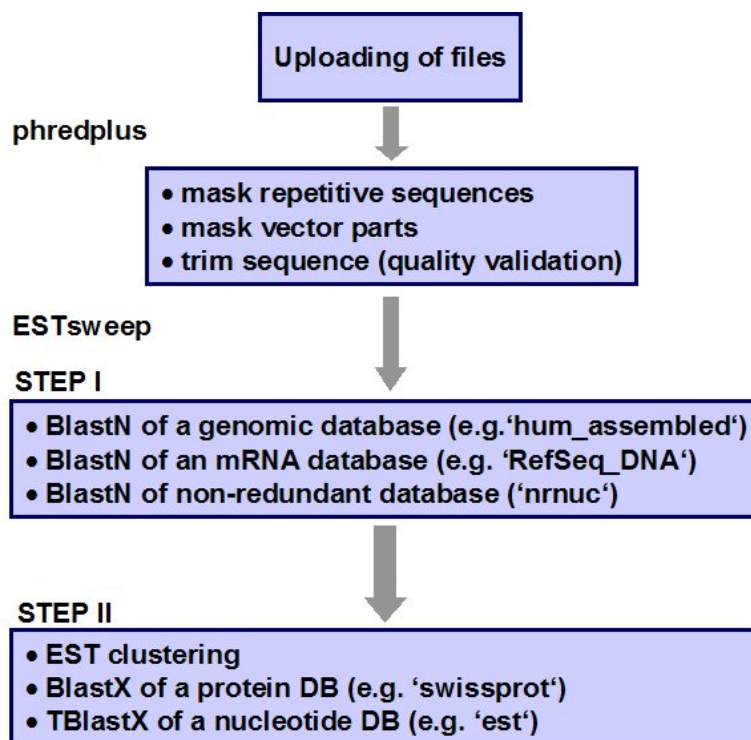


**Figure 14: Chartflow of EST-annotation** [source: German Human Genome Project (DHGP) description of project „Molecular identification of genes and pathways involved in skeletogenesis by EST generation, full length cDNA isolation and expression profiling“; <http://www.dhgp.de/research/projects/abstracts/pdf/9956>.

Sequences were automatically uploaded, the program phredplus masked repetitive sequences and vector parts and trimmed the sequence. Blast was performed automatically with the program ESTsweep that ran in 2 steps.

Their service allowed automated batch queries with a program package called ESTsweep, an EST identification task, based on the program ‘GCG’ [Devereux et al., 1984] that was established for this EST project in close collaboration with the HUSAR bioinformatic team. The package was later further developed and published as ESTAnnotator [Hotz-Wagenblatt et al., 2003].

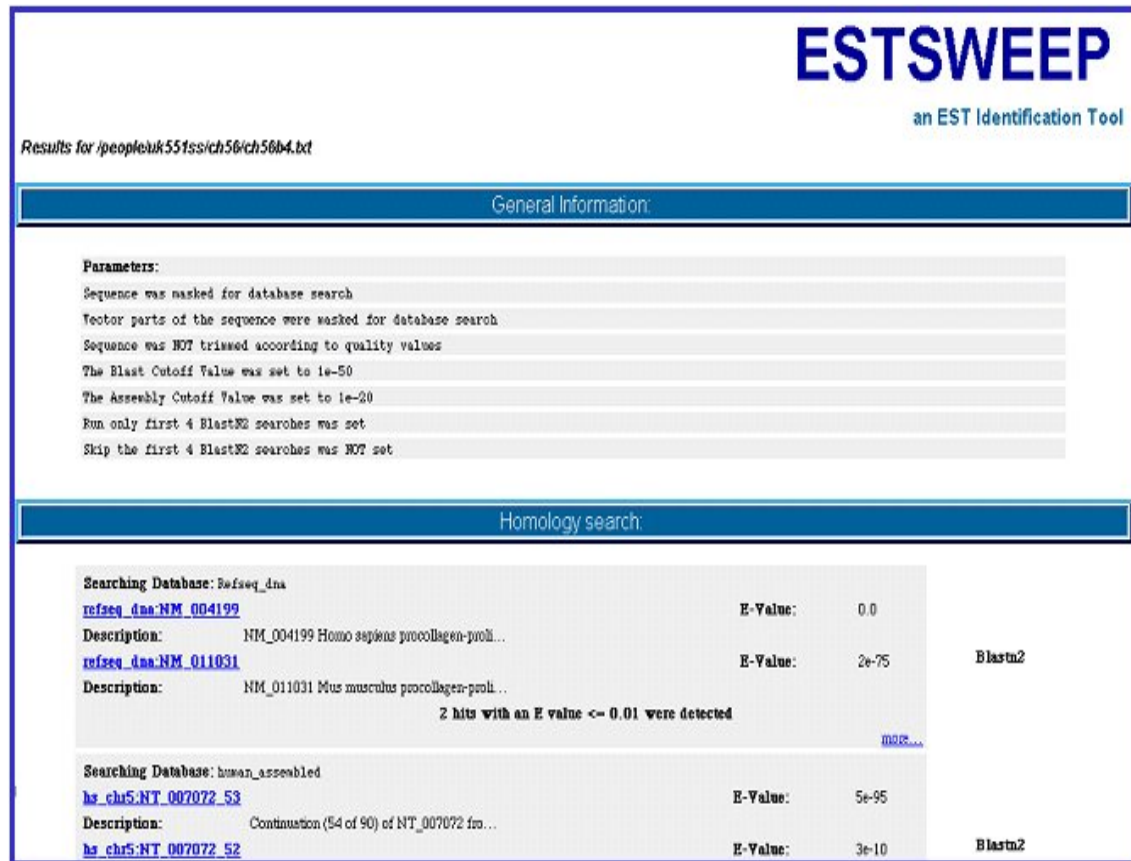


Figure 15: Example of an ESTsweep result file

As shown in the flowchart (figure 14), ESTsweep allowed direct upload of MeagBACE sequencing files, generated by GENterprise (Mainz, Germany) on the HUSAR server. In a first step, the HUSAR application 'phredplus' masked all repetitive sequences and vector parts and converted the trace files to high-quality sequences. The actual ESTsweep application worked in two steps. First, the masked EST sequences underwent BlastN analysis using 'hum\_assembled' (genomic human database), 'RefSeq\_DNA' (mRNA database) and the non-redundant database 'nrnuc' [Wheeler et al., 2001]. Second, the sequences were analyzed using clustering applications and protein databases, like 'Swissprot' [Watanabe and Harayama, 2001] and 'est'. A summary of the analysis was generated for each sequence. A portion of such a result file is shown in figure 15.

### 2.13.2. Analysis of single sequences

Standard analysis of DNA, RNA or protein sequences were usually performed with BLAST applications [Basic Local Alignment Search Tool [Altschul et al.,

1990; McGinnis and Madden, 2004; Wheeler et al., 2001] on the web interfaces of NCBI (National Center for Biotechnology Information, Bethesda, MD, USA; <http://www.ncbi.nlm.nih.gov/BLAST/>), Ensembl [EMBL (Heidelberg, Germany) and Sanger Institute (Cambridge, UK); <http://www.ensembl.org/Multi/blastview>] and UCSC Genome Browser (Santa Cruz, CA, USA; <http://genome.ucsc.edu>).

Further analysis of protein sequences were performed with databases from the ExPASy Proteomics Server (<http://us.expasy.org/>; Geneva, Switzerland).

### **2.13.3. Affimetrix normalization and analysis**

Data obtained by micro array experiments were normalized using RMA (robust multi-array average), an algorithm that creates an expression matrix from Affymetrix data [Harr and Schlotterer, 2006; Irizarry et al., 2003].

The variability among the hybridizations was pictured with scatter plot matrixes, a technique for viewing all the pair wise relationships between the variables [Craig and Kennedy, 2003]. A comparison of biological replicates shows the highest degree of conservation and therefore a mostly 45 degree line, a comparison between samples with less conservation instead a diffuse diagonal.

Differences in the quality of the genetic samples used for the array experiments were illustrated by creating a RNA digestion plot. RNA degradation plots show expression as a function of 5'-3' position of probes. For each array and within each probe-set, probes are arranged by their proximity to the 5' end of the gene [Archer et al., 2006]. The plot shows the average intensity of the probes classified by this order. Each line corresponds to an array and the slope of its trend indicates potential RNA degradation of the genetic material hybridized to the array. Since degradation of RNA usually starts at the 5' end and finishes in the 3', less truncated RNA molecules were expected to come from near the 5' end than from the 3' end. Therefore, probes matching close to the 5' end of the gene were found with lower intensity measures than probes matching closer to the 3' within each probe-set after the labeling and hybridization processes.

Genes that showed differential expression by microarray experiment were further investigated with qRT-PCR (2.3.7.), WISH (2.5.2.4.), and ISH (2.5.1.3.).

## 2.14. Material

### 2.14.1. Solutions

Alkaline phosphatase buffer (WISH)	0.1 M NaCl 50 mM MgCl <sub>2</sub> 0.1 M Tris pH 9.5 1 mM Levamisole
Blocking solution (FISH)	50 % nonfat powdered milk powder 0.5% Tween 20
Blocking solution (WISH)	1 x TBST 5% heat inactivated goat serum 1 mg/ ml BSA, IgG-free
Canada balsam	5 g Canada balsam in 10 ml methyl salicylate
Church medium	7% SDS 0.5 M sodium phosphate pH 7.2 1 mM EDTA mg/ ml tRNA from brewers yeast 1 % BSA
DEPC-H <sub>2</sub> O	0.1 % DEPC in H <sub>2</sub> O
5 x 1 <sup>st</sup> strand buffer	250 mM Tris-HCl pH 8.3 375 mM KCl 15 mM MgCl <sub>2</sub>
2 x FM (freezing medium)	65 % Glycerin 100 mM MgSO <sub>4</sub> 25 mM Tris/ HCl pH 8.0
Heparin solution	50 mg / ml in 4x SSC
Hoersch dye	10mg /ml in DMSO, freeze aliquots at -80°C.

Hybridisation buffer (aCGH)	50% deionized formamide 10% dextran sulphate 2 x SSC 2% SDS
Hybridization buffer (ISH)	50% deionized formamide 0.3 M NaCl in 20 mM Tris/ HCl pH 8.0 5 mM EDTA 10% dextran sulfate 0.02% Ficoll 0.02% BSA 0.02% polyvinylprolidone 0.5 mg/ ml bakers yeast RNA (RNase free) 10 mM DTT (to be added before use) 250 $\mu$ M $\alpha$ -S-thio-ATP (to be added before use)
Hybridisation buffer (WISH)	50% deionized formamide 0.75 M NaCl 1 x PE 100 $\mu$ g/ ml tRNA 0.5 mg/ ml Heparin 0.1 % BSA 0.5 % SDS
LB medium	10 g tryptone 5 g bacto yeast extract 10 g NaCl adjust with solid NaOH to pH 7.5 add water to 1 L; autoclave
LB agar	1 L LB media 15 g bacto agar ; autoclave
5 x Ligation buffer	250 mM Tris-HCl pH 7.6 50 mM $MgCl_2$ 5 mM ATP 5 mM DTT 25% glycerol

5x NTE	0.5 M NaCl 10mM Tris 25 mM EDTA
NTES solution	50mM Tris pH 8.0 50 mM EDTA pH 8.0 100mM NaCl 1% SDS
NZY media	21,1 g NZY broth in 1 L H <sub>2</sub> O
NZY agar	1 L NZY media 15 g bacto agar
NZY top agarose	0,7 % agarose in NZY media
Orange G dye	15 g Sucrose 0,175 g Orange G add water to 50 ml
PBT	PBS + 0,1 % Tween 20
10 x PCR buffer	0.5 M KCl 100 mM Tris pH 8.3 15 mM Mgcl <sub>2</sub> % gelatine
10 x PE	100mM PIPES pH 6,8 10 mM EDTA pH 8,0
Proteinase K buffer	20 mM Tris pH 7 1 mM EDTA pH 8
RIPA buffer	0.05 % SDS 150 mM NaCl 1% NP-40 0.5 % sodium deoxycholate 2 mM EDTA pH 8 50 mM Tris pH 8
RNA loading dye	0.15% bromphenol blue 0.15% xylene cyanol 15% glycerol
RNase buffer	0.5 M NaCl 10 mM Tris/ HCl pH 7.5



	% Tween 20
SOB medium	20 g tryptone
	5 g bacto yeast extract
	0.5 g NaCl
	2.5 ml KCl
	adjust to pH 7.0 with 10 M NaOH
	add water to 1 L; autoclave
	add 10 ml sterile 1 M MgCl <sub>2</sub> before use
Solution 1	50 mM glucose
	25 mM Tris-HCl pH 8.0
	10 mM EDTA pH 8.0
	100 µg/ ml RNase A
Solution 2	0.2 N NaOH
	1% SDS
Solution 3	3 M potassium acetate
	11,5 % glacial acetic acid
SSC/FA/Tween20	2 x SSC pH 7.0
	50% DI Formamide
	0.1% Tween 20
20x SSC	3 M NaCl
	0,3 M tri-Natriumcitrat-Dihydrat
	adjust to pH 7.0; autoclave
Staining solution	5 ml alkaline phosphatase buffer
	17.5 µl BCIP
	22.5 µl NBT
25 x TBE pH 8.3	270 g Tris (M: 121,14)
	137.5 g Borsäure
	23.25 g EDTA
	ad 1 L H <sub>2</sub> O
TBF I	30 mM KC <sub>2</sub> H <sub>3</sub> O <sub>2</sub> (potassium acetate)
	50 mM MnCl <sub>2</sub>
	100 mM KCl
	10 mM CaCl <sub>2</sub>

	15 % glycerol
	adjust pH 5,8 with acetic acid
	sterile filter the solution
TBF II	10 mM Na-MOPS pH 7,0
	75 mM CaCl <sub>2</sub>
	10 mM KCl
	15 % Glycerin
	sterile filter the solution
1 x TE	10 mM Tris HCl
	1 mM EDTA pH 8.0
10 x TBST	80 g NaCl
	2 g KCl
	250 ml 1M Tris pH 7,5
	100 ml Tween 20
	add water to 1 l

#### 2.14.2. Chemicals

Acetic acid	Fisher Scientific, Fair Lawn, NJ, USA
Agarose	GenMate, Bioexpress, Kaysville, UT, USA
Alkalische Phosphatase	Roche, Indianapolis, IN, USA
Artisan™ Mayer's Hematoxylin	DAKO, Glostrup, Denmark
α-S-thio-ATP	Roche, Indianapolis, IN, USA
Bacto agar	Difco, Becton Dickinson, Sparks, MD, USA
BCIP	Roche, Indianapolis, IN, USA
Bluing reagent/	
1x Scott's tap water	Sigma-Aldrich Corp., St. Louis, MO, USA
BSA	Sigma-Aldrich Corp., St. Louis, MO, USA
Canada Balsam	Fisher Scientific, Fair Lawn, NJ, USA
Chloroform	Fisher Scientific, Fair Lawn, NJ, USA
Collagenase Typ II	Gibco (New York, USA)
DEPC	Sigma-Aldrich Corp., St. Louis, MO, USA
Developer	VWR, West Chester, PA, USA

DIG-ab coupled to	Roche, Indianapolis, IN, USA
Alkaline phosphatase	Roche, Indianapolis, IN, USA
DMEM	Invitrogen, Carlsbad, CA, USA
DMF	Sigma-Aldrich Corp., St. Louis, MO, USA
DMSO	Sigma-Aldrich Corp., St. Louis, MO, USA
DNase I, RNase-free	Roche, Indianapolis, IN, USA
dNTP's	Amersham Bioscience/ GE Healthcare Life Science, Pittsburgh, PA, USA
Eosin	Sigma-Aldrich Corp., St. Louis, MO, USA
Eosin Y Solution Alcoholic	Sigma-Aldrich Corp., St. Louis, MO, USA
Ethanol	AAPER Alcohol & Chemical Co., Shelbyville, KY, USA
ExpressHyb Solution	Clontech, Mountain View, CA, USA
Fixer	VWR, West Chester, PA, USA
Formaldehyd 37 %	Sigma-Aldrich Corp., St. Louis, MO, USA
Formamid (deionized)	Fisher Scientific, Fair Lawn, NJ, USA
25% Glutaraldehyde	Sigma-Aldrich Corp., St. Louis, MO, USA
Glycerol	Sigma-Aldrich Corp., St. Louis, MO, USA
Harris Hematoxylin Solution	Sigma-Aldrich Corp., St. Louis, MO, USA
Heparin	Sigma-Aldrich Corp., St. Louis, MO, USA
Histoclear	Engelbrecht Medizin- und Labortechnik GmbH, Edermünde, Germany
H <sub>2</sub> O <sub>2</sub>	Sigma-Aldrich Corp., St. Louis, MO, USA
Hoersch dye 33258	Sigma-Aldrich Corp., St. Louis, MO, USA
Iso amylalcohol	Fisher Scientific, Fair Lawn, NJ, USA
Isopropanol	Fisher Scientific, Fair Lawn, NJ, USA
Klenow, labeling grade	Roche, Indianapolis, IN, USA
LB broth	Molecular Biol. Lab., Solana Beach, CA, USA
Levamisole	Sigma-Aldrich Corp., St. Louis, MO, USA
L-glutamine	Invitrogen, Carlsbad, CA, USA
Lipofectamine 2000	Invitrogen, Carlsbad, CA, USA
Methyl Salicylate	Sigma-Aldrich Corp., St. Louis, MO, USA

M-MLV RT	Invitrogen, Carlsbad, CA, USA
NBT	Roche, Indianapolis, IN, USA
NZY broth	Teknova, Hollister, CA, USA
Orange D	Sigma-Aldrich Corp., St. Louis, MO, USA
Polyvinylprolidone (PVP)	Sigma-Aldrich Corp., St. Louis, MO, USA
NP40/ Tergitol	Sigma-Aldrich Corp., St. Louis, MO, USA
PIPES	Sigma-Aldrich Corp., St. Louis, MO, USA
Proteinase K	Roche, Indianapolis, IN, USA
Random Hexamers	Promega, Madison, WI, USA
RNA Polymerase Sp6	Roche, Indianapolis, IN, USA
RNA Polymerase T7	Roche, Indianapolis, IN, USA
RNA Polymerase T3	Roche, Indianapolis, IN, USA
RNase A	Sigma-Aldrich Corp., St. Louis, MO, USA
RNase-Inhibitor	Promega, Madison, WI, USA
Sodium Deoxycholate	Sigma-Aldrich Corp., St. Louis, MO, USA
Tissue-Tek <sup>®</sup> O.C.T. compound	Sakura, Torrance, CA, USA
Transferrin	Roche, Indianapolis, IN, USA
tRNA from brewers yeast	Roche, Indianapolis, IN, USA
Trizol	Invitrogen, Carlsbad, CA, USA
Tryptone	Difco, Becton Dickinson, Sparks, MD, USA
Tween 20	Sigma-Aldrich Corp., St. Louis, MO, USA

### 2.14.3. Miscellaneous materials

CapSure <sup>®</sup> Macro LCM Caps View,	Arcturus/ Molecular Devices, Mountain CA, USA
Cytoseal XYL (Xylene based)	Richard Allan Scientific, Kalamazoo, MI, USA
Hybond-XL	Amersham Bioscience/ GE Healthcare Life Science, Pittsburgh, PA, USA
Kodak BioMax X-ray film	Eastman Kodak Company, New Haven, CT, USA
micro cover slides	VWR, West Chester, PA, USA

MicroSpin G-50 Columns	Amersham Bioscience/ GE Healthcare Life Science, Pittsburgh, PA, USA
Ready-to-go DNA-Lab. Beads	Amersham Bioscience/ GE Healthcare Life Science, Pittsburgh, PA, USA
SYLGARD184 silicone	Dow Corning, Midland, MI, USA
2-well Lab-Tek™ II Chamber Slide™ System	Nunc, Rochester, NY, USA

#### 2.14.4. Kits

BCA™ Protein Assay kit and Micro BCA™ Protein Assay kit	Pierce, Rockford, IL, USA
Digoxigenin RNA Labeling Kit	Roche, Indianapolis, IN, USA
Dynabeads® mRNA Purification Kit	Dynal/ Invitrogen, Carlsbad, CA, USA
GenElute Mammalian RNA Purification Kit	Sigma-Aldrich Corp., St. Louis, MO, USA
Genomic DNA Purification Kit (D-5500)	Gentra, Minneapolis, MN, USA
PicoGreen® dsDNA Quantification Kit	Molecular Probes/ Invitrogen, Carlsbad, CA, USA
PicoPure® RNA Isolation Kit	Arcturus/ Molecular Devices, Mountain View, CA, USA
RiboGreen RNA/ cDNA Quant. Kit	Molecular Probes/ Invitrogen, Carlsbad, CA, USA
QIAEX II Gel Extraction Kit	Qiagen, Hilden, Germany
Versagene™ RNA isolation kit	Gentra, Minneapolis, MN, USA
Wizard® SV Gel and PCR Clean-Up System	Promega, Madison, WI, USA

### 2.14.5. Equipment

Bacteria Incubator	ORBITAL Incubator Shaker, Gyromax™737; Amerex Instruments Inc., Lafayette, CA, USA
Balances	sartorius BP121S and sartorius LP6200; Sartorius AG, Goettingen, Germany
Cell culture incubators	Series II 3110 Water Jacketed Incubator; Thermo Electron Corporation, Waltham, MA, USA
Centrifuges	Avanti™ J-25 I; Beckman, Fullerton, CA, USA Eppendorf 5417 R and 5810 R; Brinkmann Instruments, Hamburg, Germany Z233M2 and Z233MK2; Hermle Labortechnik, Wehingen, Germany
Electrophoresis system	EasyCast™ Mini Gel Electrophoresis System; Owl Separation Systems, NH, USA
Gel imaging system	Eagle sight; Stratagene, La Jolla, CA, USA
Homogenisator	IKA Ultra Turrax T 25; Janke & Kunkel GmbH, Staufen, Germany
Hybridization oven	Hybridiser HB-1D; Techne, Duxford Cambridge, U.K.
Laser Capture Microscope	PixCell® Ile LCM Instrument with PixCell II Image Archiving Workstation (110 volts); Arcturus/ Molecular Devices, Mountain View, CA, USA
Lightcycler	LightCycler® 2.0; Roche, Indianapolis, IN, USA
Liquid Scintillation Analyzer	Tri-Carb 2100 TR; Perkin Elmer, Wellesley, MA, USA

Microscopes	Axioplan 2; Zeiss, Jena, Germany SMZ150; Nikon, Kanagawa, Japan
pH meter	Corning pH meter 430; Corning Incorporated Life Sciences, Aceton, MA, USA
Plate reader	FLUOstar OPTIMA; BMG LABTECH GmbH, Offenburg, Germany
Spectrophotometer	ND-1000; NanoDrop Technologies, Wilmington, DE, USA
Thermal cycler	PTC-200; Applied Biosystems, Foster City, CA, USA
UV-crosslinker	Stratalinker® 1800 UV Crosslinker; Stratagene, La Jolla, CA, USA
Water bath	Isotemp 215; Fisher Scientific, Fair Lawn, NJ, USA C10-B3 Heating Circulator Bath; Haake, Karlsruhe, Germany

#### 2.14.6. Plasmids

pGEM-T <sup>®</sup> Vector	Promega, Madison, WI, USA
pcDNA3.1/V5-His A, B, C	Invitrogen, Carlsbad, CA, USA
pCR <sup>®</sup> II-TOPO <sup>®</sup>	Invitrogen, Carlsbad, CA, USA

#### 2.14.7. Oligos (in 5' → 3' direction):

##### 2.14.7.1. Common oligos

T <sub>3</sub> A	ATTAACCCTCACTAAAGGG
T <sub>7</sub> A	AATACGACTCACTATAGGG

M13F	GTAAAACGACGGCCAGT
M13R	CAGGAAACAGCTATGAC
MAKT1	GTGGGCCGCTCTAGGCACCA
MAKT2	TAGCCCTCGTAGATGGGCACAG
HPRT-F	ATTGACACTGGGAAAACAATGC
HPRT-R	TCCAACACTTCGTGGGGTCC
Hprt-F	AGCGATGATGAACCAGGTTA
Hprt-R	GTTGAGAGATCATCTCCACC

#### 2.14.7.2. *Lmx1b* genotyping oligos

47B2(A)	GATAGGGCATTCAACCAGGACGAGCA
47B2(B)	AAACAGAAGCCACAGAGAGCCAAGGA
NEOI	GGTGCCACTCCCCTGTCCTTTCCTAA

#### 2.14.7.3. Oligos to amplify inserts in pcDNA 3.1 and pcDNA 3.1/V5-HisA:

pcDNA3.1/V5-HisA-F	TAATACGACTCACTATAGGG
pcDNA3.1/V5-HisA-R	TAGAAGGCACAGTCGAGG

#### 2.14.7.4. Oligos used for qRT-PCR

##### Human:

LMX1B-F (0976)	TTCCATGACATCGACAGCGATACC
LMX1B-R (1096-L22)	AGGAGGCGAAGTAGGAACTCTG

Universal Probe Library reaction (LMX1B):

Left primer	CAGCAGGAGCAGCAGAACT
Right primer:	GGCGTGTAGGAAGCCATC

NR5A1-F	CTCTAATGGCCAGCCTCCTTCT
NR5A1-R	TCGTCTGACGAATAGTCCATGC
NR6A1-F	GCAAGGAATGACCTGTTCCAG
NR6A1-R	TTGGCTGCATTCACACAAAAG
HPRT-F	ATTGACACTGGGAAAACAATGC
HPRT-R	TCCAACACTTCGTGGGGTCC



**Murine:**

Agc1-F	CAACACCTACAAGCACAGGCTACAG
Agc1-R	AAAAAGCGACAAGAAGACACCA
Asb4-F	ATGTAGCAGGTTTTGTGAGTGA
Asb4-R	ACATGAGAGCTGGAGTGTAGAATA
Cbln1-F	CTCTGAACCCTGCCACTTACTGA
Cbln1-R	GAACAGGACAGAAATACGGAATAC
Col11a1-F	CTATTTGGATTTTCGTTGGTGCTGTA
Col11a1-R	CTATCTTTGATGGATGGGAATGAG
Dbn-F	GGAAGAGTTCGCCCCAATCAG
Dbn-R	ACCAACGGGAGGAAAACCAAGTCAA
Dcn-F	TGTAATCATAAATGTCAACC
Dcn-R	AAGGCTTCACCAATAATA
En1-F	TTTTTGAAACGGGAGTAAG
En1-R	ATTAAATATATACACGGTCGAAAG
Egfr-F	AAGACACTTCCGTGGCAAGACAATA
Egfr-R	TCACAATACTGATGGTTTGAATGGGT
Fgf8-F	CTCAACTACCCGCCCTTCAC
Fgf-R	AGCTCCCGCTGGATTCCT
Fgf10-F	CACTTTGCCATTTAGATTAC
Fgf10-R	ACGGAGGCAGAACTCAC
Fgf12-F	CCAAGGACGAAAACAGCGACTA
Fgf12-R	ATTCTGGGGTAAAAACATCTGA
Fmod-F	GGTGCTTAGACTGTGCTACGG
Fmod-R	TCTTCAGAGGCAGGATGGTGATAC
Gas1-F	ATGAGGACGCCCATGCCA
Gas1-R	GCGCCATCAGGCACAGCAAG
Gdf10-F	AAAGGTGACCCCAATGACTCTACTAT
Gdf10-R	CCCGTTTATGTCTCTCCCACTTAC
Hoxc5-F	TATAAGCAGAGCCCCAATATCC
Hoxc5-R	AATCCGCCGTAGCAGTACC
Klf1-F	ACTGGGGATGAAATAAGAGTG
Klf1-R	CCTGAAGGCTCCTTTGTATGGT
Krt1-15-F	AGATCGGGACTACAGCCATTACTT

Krt1-15-R	GTTATACGCCACCTCCTTGTT
Krt2-8-F	TATGGCAGAGTGCAGGGAAGTAGAGA
Krt2-8-R	AAATACAAGTGAATTGGGTTTGG
Matn1-F	GGGTGGGCTTGGTCAACT
Matn1-R	ATGGCAGGCACAGGTGTAGGAG
Matn4-F	CGCTCTCAGGATGACATTTTCAG
Matn4-R	AACTCCGATGGTTCCGAT
mTrps1-F2	AGCGAGAAGTCTGCATCTCTTACC
mTrps1-R3	CACTTAAGTGATCTTCTGACCTCC
Ogn-F	ACCGTTTTATCTCACTATGATGGA
Ogn-R	AAATGTTTGCTTGCGTGTG
Pitx1-F	CTGGAGGTGGGGGTAAAGTTG
Pitx1-R	CTTGACCGGGTGAACGAT
Pmaip1-F	ACTGAAGCTCGGTGCGTCTG
Pmaip1-R	TCCAATACCAGGCATTTCCATC
Rfng-F	GTGTCCTATGAAGAACAGGGTTGA
Rfng-R	CTTTCTCTCTTCCTGGACGGT
Slc4a1-F	TAGAGGGAGGGTGAGAGGGTTGTA
Slc4a1-R	CAAACGCTTTTCTTAGACCTT
Sostdc1-F	TCCCTAAACCCCTTCCCAAAC
Sostdc1-R	AAACTAACCCCTGGCTGTCAAACAT
Tbx5-F	TGTATGCCAGCTCCGCTCCC
Tbx5-R	TGCCGACGCCGTGTACC
Tgfr2-F	TACCAAAAATCAAAGAAGACCGTT
Tgfr2-R	GACTGGGGTGGGTGTGAGTAAT
Tmeff2-F	GCGGGGTCTGAGAAAGGTATC
Tmeff2-R	GTGGGGGCATTTGTTTGGTAG
Vnn1-F	GCATCCAATGCTTCCTCAGACT
Vnn1-R	GGTCCATGAGAGAACGGAAATG
Wisp1-F	TCATCATCCTTTTCTTGTTCTAC
Wisp1-R	CCTTTTCTGTCCAGTTTAGGT
Wnt7a-F	CCTATCCTTTTGCCCTTTACAGTT
Wnt7a-R	TCTGCCCTGAGTGAGTACC
Zfx1b-F	GCAGTTCAGCCAAGACAGAGTTAG

Zhx1b-R TTCCTTCACATCCAGGTCACTTTA

#### 2.14.7.5. Oligos used for EST clone ch11g10/ *LRRC59*

##### murine

NM\_133807-3'UTR-F CCAGGCTCTCATTCCAGTTTTCT

NM\_133807-3'UTR-R TCTGCCCTGGTTGTGCTAATGTTT

5HPPSK TTGGCCGATTCATTAATGCAGGG

MHPP341c05-R GGCAGGAGAGAGGAATGAGG

5Hprev TGAAGAAAGTTGAGGAGAGTTTTTC

check-Xma-F GCCAGTAATGAATTTGTCCTGGTT

check-Kpn-F GACAGCCAGGGCTATACAGAGAAA

##### human

PrEfc361-1F AGCAGTGTGCAAACAAGGTG

PrEfc361-1R GCAGAACCCAATTCCATAGG

#### 2.14.7.6. Screening oligos for *LMX1B*, *TBX4*, *WNT4*, *WNT7A*

LMX1B-1F GCCAGACGGACTGCGCCAAG

LMX1B-1R GCGACTGGAGCTGCTCTGTC

LMX1B-2F CCCGGTGCGACCGGGACGCCGGG

LMX1B-2R TGACCGGGCTCGAGTGCCGGGCG

LMX1B-3F GACTTCTGAGCACCGCCAAC

LMX1B-3R GCATGTACCATCTGTGTGCA

LMX1B-4F GAGCCACGGCAGGTGTCAACA

LMX1B-4R GAGATGGAGGATGGAGGGATGTCC

LMX1B-5F ATCTCTCCGCACATCCCATCATAC

LMX1B-6R CGCAGTGAGTGTGAGTAGACTGTT

LMX1B-7F GATGCAGCGCAGAATCACTATTGC

LMX1B-7R CGATGTCATGGAAGATGGAGTCGT

LMX1B-8F CTAGTCAGCAGGCCATCCTGTCTC

LMX1B-8R GGGCACCGTATGGCTGTCT

TBX4-1F GTTCCTCCTCCAGCTCAG

TBX4-1R	AGCCATGTCCAGTGGAGAAC
TBX4-2F	AGCTGTTCTGGGTCTGGTTCT
TBX4-2R	GAAGGGAGGTGGCACTGAC
TBX4-3F	TGAGTTGTGCAGGTCACACA
TBX4-3R	CAGTTCCAGGCAGTGGACTC
TBX4-4F	TGCTCTCTCCTCCTCAGCAT
TBX4-4R	TCAGAGGCTTGAGCTCCTTC
TBX4-5F	GGCCAGAAGAATGAGGTCAA
TBX4-5R	CCGAGGGACTCTAGGC
TBX4-6F	TTTGTGTGC CTCACACTGGT
TBX4-7R	CCAAAGGCAGCATGAGAGAT
TBX4-8F1	CTGTCCCAGCATCCAACAG
TBX4-8R1	CAGAAGATGGATGCTCTCCAA
TBX4-8F2	GGACCGTGTTGCTCCAGTAT
TBX4-8R2	CAGCTGAGGCGTGTTTCATA
WNT4-1F1	CTCTGGGGCGGCGCTGACAG
WNT4-1R1	GCGGCTGAGAAGACGGCGAAGA
WNT4-1F2	CTCAGCCGCCGCGAGCAA
WNT4-1R2	GAGCGAGCGAGCCTCCGGTCCC
WNT4-2F	AAGCATTTCCACTCCCTTG
WNT4-2R	ATGACCTGCAATAGTCCCG
WNT4-3F	TTACAAAGGAGGGTGCAGG
WNT4-4R	AATGTTTTCTGAGTGGCCG
WNT4-5F	TCCTTGCCATCTCCTGAT
WNT4-5R	GACCCAAAAACCAAACCAGA
WNT7A-1F	CGGCGGCCAATCGGGACTATGA
WNT7A-1R	CCGCGCCTCCTGAGAGAGTTCG
WNT7A-2F	ACATGAGTTAGGGGTGCAGG
WNT7A-2R	AGAGGGCACCTGAGGGTATT
WNT7A-3F	CTCACTCTTCAGTCAGGCCC
WNT7A-3R	CTGTGGCTCCTCAACAGACA
WNT7A-4F	TGACCTGTGCTGTGCTCTTC
WNT7A-4R	TCTACACGGCTCCTTGTCCT

**2.14.7.7. Oligos used to generate ISH/WISH probes**

Dbn1-F	ACCAACGGGAGGAAAACCAGTCAA
Dbn1-R	GGAAGAGTTCGCCCCAATCAG
Lmx1b-F	CGAGAGACATTGGCAGCAG
Lmx1b-R	GGGCACCGTATGGCTGTC
Nrp2-F	GCCTGGGTGTTACTGCTGATCTTG
Nrp2-R	GGGAGAGCGTGGAGGTAATGTG
Ppargc1-F	TTGTTCTTGTTCTGGTATGGTTGTT
Ppargc1-R	TGACTCTCTGGATTTTGATAGTTTACTG
Shox2-F	GGGAGCTTGTTTCATATTGCTATT
Shox2-R	TCTGTTTTGTTTTCTTGGACCATT
Ssbp2-F	AATGGCATTTTAACAGTGGTTGATAG
Ssbp2-R	TTCACAGTAAGAAAGTCAGGTGGTTAAG
Vnn1-F	GCATCCAATGCTTCCTCAGACT
Vnn1-R	GGTCCATGAGAGAACGGAAATG

**2.14.8. Molecular weight marker**

λ Hind III fragments	Invitrogen, Carlsbad, CA, USA
1 kb plus ladder	Invitrogen, Carlsbad, CA, USA
100 bp ladder	Invitrogen, Carlsbad, CA, USA
RNA Ladder 0.24-9.5 kb	Invitrogen, Carlsbad, CA, USA

### 3. Results

#### 3.1. EST project

A human fetal growth plate cartilage library (20 weeks prenatal - 2 years postnatal) was the starting material for an EST sequencing project that was undertaken to identify and characterize potential new genes involved in processes of skeletogenesis. Cartilage collection and library construction were done by Mirta Machado and Dr. Brendan Lee at Mount Sinai School of Medicine, New York/ NY, USA (now both at Texas Medical Centre in Houston/ TX, USA). Pre-screenings for redundant genes like ribosomal RNAs, actin, etc. were performed by Dr. Christiane Stelzer (Children's Hospital, Mainz) [Stelzer, 2000]. For this thesis, 5000 ESTs with an insert size bigger than 400 bp were sequenced by Prof. Tom Hankeln and Prof. Erwin Schmitt at GENTERprise (University of Mainz, Germany) and evaluated through database searches (2.13.) by the groups of Prof. Andreas Winterpacht (Human Genetics, Erlangen, Germany), Prof. Thomas Hankeln and Prof. Erwin Schmidt GENTERprise (Mainz, Germany), and Prof. Bernhard Zabel at Children's Hospital, Mainz (now Freiburg University Hospital, Freiburg, Germany).

##### 3.1.1. Results from database searches

Results from database searches (2.13.1. - 2.13.2.) of the 5000 EST sequences were summarized in an excel spread sheet (figure 16) containing symbol, gene title, mRNA accession number, genomic locus, link to NCBI 'OMIM' (Online Mendelian Inheritance in Man™) database [McKusick, 2007], information about protein domains, Unigene cluster, frequency within the total number of sequenced ESTs, the homologous mouse gene, as well as the Human Genome U133 Plus 2.0 Array Probe Set ID and the Biological Process Description, Molecular Function Description, Cellular Component Description and corresponding pathway description as identified with the help of the 'Affimetrix NetAffx™ Analysis Center' (<http://www.affymetrix.com>) and the 'Gene Ontology' (GO) web interface (<http://www.geneontology.org>).

The following categories were interactively linked with their corresponding hyperlink: gene symbol with the 'NCBI Entrez Gene' database, Unigene number with human cluster from 'NCBI UniGene' database, OMIM number with known genetic diseases from 'NCBI OMIM' database, and the domains with corresponding entries to the 'SMART' or 'NCBI Structure Group' containing 'Conserved Domains' databases (<http://smart.embl-heidelberg.de>; <http://www.ncbi.nlm.nih.gov>).

Genes were categorized according to their biological functions. Therefore, the gene title was color-coded which allowed a quick differentiation between genes involved in cell division/ cycle and DNA replication (yellow), cell signaling/ communication and transport (green), cell structure and motility (blue), cell/ organism defense and apoptosis (red), gene/ protein expression, transcription factors, and posttranslational modification (brown), proteolysis (grey), and metabolism (orange). When genes qualified for more than one category, it was deliberated about the different sources, and the more likely category was picked.

A	B	C	D	E	F	G	H	I	J	K	L	M	N	O
Human Ge	symbol	mRNA acc.	Gene Title	Locus	OMIM	domain	GO Biological F	GO Molecular F	GO Cellular C	Pathway	frequ	Unigene	M. musculus gene	
244580_at	SCUBE3													
212154_at	SDC2	NM_002998	syndecan 2 (heparan sulfate proteoglyc	8q22-q23	142460	Syndecan	---	cytoskeletal protein	integral to plasm	---	2	Hs.1501	Sdc2	
212158_at	SDC2													
212157_at	SDC2													
1954864_at	SDC3	NM_014654	syndecan 3 (N-syndecan)	1pter-p22	186357	Syndecan	---	cytoskeletal protein	membrane // int	---	1	Hs.158287	Sdc3	
202898_at	SDC3													
202071_at	SDC4	NM_002999.1	syndecan 4 (amphiglycan, ryudocan)	20q12	600017	Syndecan	---	cytoskeletal protein	integral to plasm	---	2	Hs.532267	Sdc4	
236797_at	SDC4													
200958_at	SDCBP	NM_006251	syndecan binding protein (syntenin)	8q12	602217	PDZ_signalin	protein targeting to	interleukin-5 recepti	nucleus // endo	---	3	Hs.200804	Sdcbp	
218427_at	SDCCAG3	NM_006843	serologically defined colon cancer antig	9q34.3		Myosin_tail_1	---	---	---	---	2	Hs.34300	Sdccag3	
238111_at	SDCCAG3													
205695_at	SDS	NM_006843	serine dehydratase	12q24.13	182128	CysK, PALP	gluconeogenesis //	L-serine ammonia-1	---	Fatty acid elc	1	Hs.439023	Sds	
1555539_at	SDS													
207707_at	SEC13L1	NM_030673.1	SEC13-like 1 (S. cerevisiae)	3p25-p24	600152	WD40	intracellular protein	---	---	---	1	Hs.166924	Sec13l	
239617_at	SEC13L1													
244695_at	SEC13L1													
204344_at	SEC23A	NM_006364	Sec23 homolog A (S. cerevisiae)	14q21.1	610511	Sec23-like, G1	intracellular protein	protein binding // pr	endoplasmic reti	---	1	Hs.272927	Sec23a	
212687_at	SEC23A													
215209_at	SEC24D	NM_014822	SEC24 related gene family, member D (S	4q26	607186	Sec24-like, G1	intracellular protein	protein binding // zi	endoplasmic reti	---	1	Hs.189641	Sec24d	
202375_at	SEC24D													
215641_at	SEC24D													
232405_at	SEC24D													
216816_at	SEC31A	NM_016211	SEC31 homolog A (S. cerevisiae)	4q21.22	610257	WD40	ER to Golgi vesicle	---	COPII vesicle oc	---	2	Hs.370024	Sec31a	
200945_at	SEC31A													
1556416_at	SEC31A													
215009_at	SEC31A													
243765_at	SEC31A													
236727_at	SEC31A													
222395_at	SEC61A1	NM_013336	Sec61 alpha 1 subunit (S. cerevisiae)	3q21.3	609213	SecY	protein targeting //	protein translocase	endoplasmic reti	---	7	Hs.518236	Sec61a1	
217716_at	SEC61A1													
203133_at	SEC61B	NM_006808	Sec61 beta subunit	9q22.32+	609214	Sec61_beta	protein targeting //	---	endoplasmic reti	---	2	Hs.191887	Sec61b	
244700_at	SEC61B													
223070_at	SELK	NM_145281.1	selenoprotein K	3p21.31	607316		---	selenium binding	---	---	3	Hs.58471	Selk	
226051_at	SELM	NM_080430	selenoprotein M	22q12.2			---	selenium binding	endoplasmic reti	---	3	Hs.55240	Selm	
223209_at	SELS	NM_018445.1	selenoprotein S	15q26.3	607318		redox signal respon	receptor activity //	endoplasmic reti	---	1	Hs.32149	Hsl2	
215259_at	SEMA4A5	NM_022367	sema domain, immunoglobulin domain	1q22	607232	PSI_Sema	DNA metabolism //	DNA binding // reo	membrane // int	---	1	Hs.408546	Sema4a	
234072_at	SEMA4A5													
224625_at	SERF2	NM_005770	small EDRK-rich factor 2	15q15.3	605054		---	---	---	---	3	Hs.424126	Serf2	
217756_at	SERF2													
200970_at	SERP1	NM_014445	stress-associated endoplasmic reticul	3q25.1		BAMP4	protein modification	---	endoplasmic reti	---	2	Hs.518326	D3Ucl1	
200963_at	SERP1													
200971_at	SERP1													
202376_at	SERPINA1	NM_001095	serpin peptidase inhibitor, clade A (alpha	14q32.1	107280	alpha-1antitry	acute-phase respon	DNA binding // pro	extracellular regi	---	4	Hs.534233	Serpina3n	
212190_at	SERPINE1	NM_006216	serpin peptidase inhibitor, clade E (neut	2q33-q35	172701	PAI-1_neutrin	nervous system de	serine-type endope	extracellular regi	---	11	Hs.38449	Serpine2	
236599_at	SERPINE2													
210231_at	SET	NM_003011	SET translocation (myeloid leukemia-as	9q34	600960	NAP	DNA replication //	protein phosphatas	nucleus // nucle	---	4	Hs.436687	Set	
213048_at	SET													

**Figure 16: Partial EST annotation sheet** with columns containing the following information: A: Human Genome U133 Plus 2.0 Array Probe Set ID; B: symbol; C: mRNA accession number; D: gene title; E: locus; F: OMIM number; G: conserved domains; H: GO biological process description; I: GO molecular function description; J: GO cellular component description; K: pathway; L: pathway hyperlink; M: frequency; N: Unigene number; O: homologous mouse gene. Color code as described in the text.

According to these categories, the 5000 ESTs were statistically evaluated.

### 3.1.2. Statistical annotation of EST sequences

The statistical evaluation of the 5000 sequenced ESTs revealed that 80% of the sequences could be categorized by their functions (figure 17, left panel), while the remaining 20% included unreadable sequences (10%), contaminations with genomic or bacterial material (5%), sequences that did not show a match (1%) to any of the utilized databases, as well as sequences that are transcribed but cannot be classified yet as a result of insufficient information about these transcripts (4%). The biggest fraction, almost 40% of the 5000 sequences, match to genes that are involved in gene/protein expression and posttranslational modification, as well as transcription factors. 12% of the genes are involved in cell signaling, cell-to-cell communication and transport, 10% contribute to cell structure and motility, 7% transcribe genes that are active in cell defense and apoptosis, another 7% contain metabolic genes. Smaller fractions summarize genes that are responsible for cell division, cell cycle and DNA replication (3%), as well as proteolysis (2%).

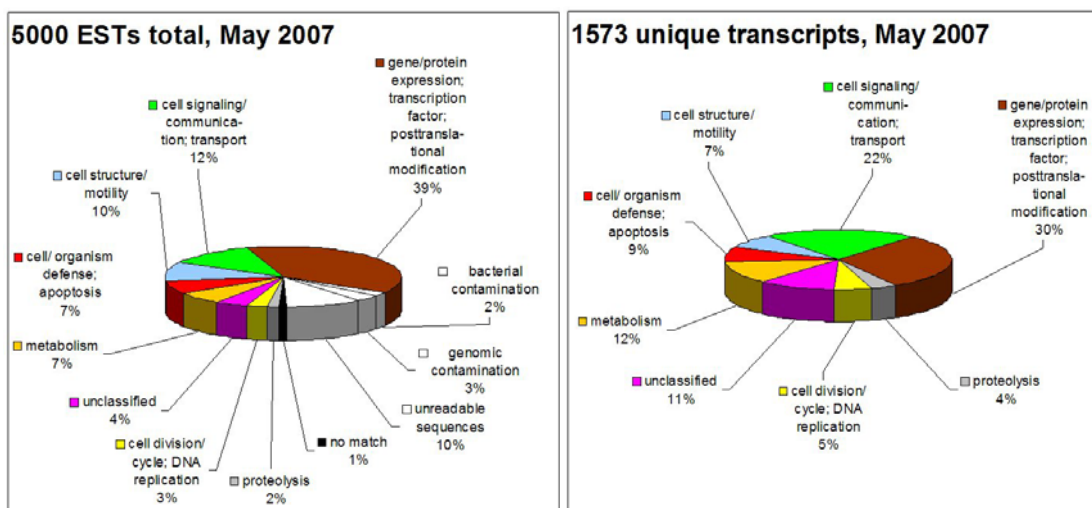


**Figure 17: Percentage functional distribution of analyzed EST sequences** after a final examination in May 2007: left panel shows percentages within the 5000 ESTs, right panel within the 1573 unique transcripts.



*In silico* analysis of the 5000 ESTs and independent reexamination of previously published data [Tagariello et al., 2005] in May 2007, revealed 1573 individual transcripts (figure 17, right panel), corresponding to 1400 known and 173 unclassified transcripts that represent potential novel genes and those that could not be classified due to insufficient information. Most of the unique transcripts were transcription factors or involved in gene/protein expression and posttranslational modification (30%). Genes in cell signaling/ communication and transport (22%) represented the second largest portion, followed by metabolic genes (12%). Unclassified transcripts constituted 11%, genes in cell/ organism defense and apoptosis 9%, transcripts for cell structure and motility 7%, cell division/ cycle and DNA replication factors 5%, and genes in proteolysis 4%.

Within the 5000 ESTs, most of the transcribed sequences were represented only once. Only 28 genes were represented at least 20 times (figure 18).

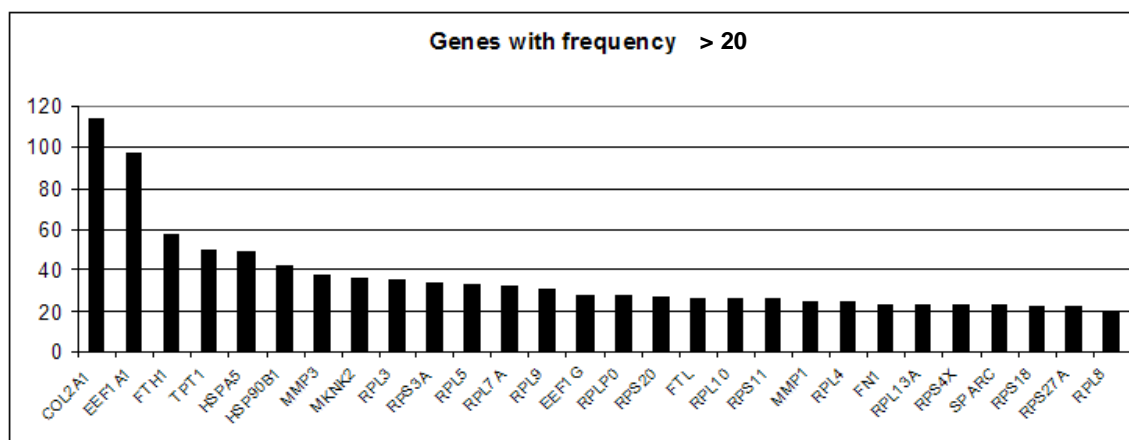


**Figure 18: Genes with the highest frequencies within the 5000 ESTs**, further description in the text.

Within these 28 genes, there were 15 ribosomal proteins, 2 matrix metalloproteinases (*MMP1*, *MMP3*), 2 ferritins (*FTH1*, *FTL*), 2 heat shock proteins (*HSPA5*, *HSP90B1*), 2 eukaryotic translation elongation factors (*EEF1A1*, *EEF1G*), the tumor protein *TPT1*, as well as MAP kinase interacting serine/threonine kinase 2 (*MKNK2*), and the two ECM proteins fibronectin (*FN1*) and osteonectin (*SPARC*). Type II collagen (*COL2A1*) was the most presented gene within the library (114 times).

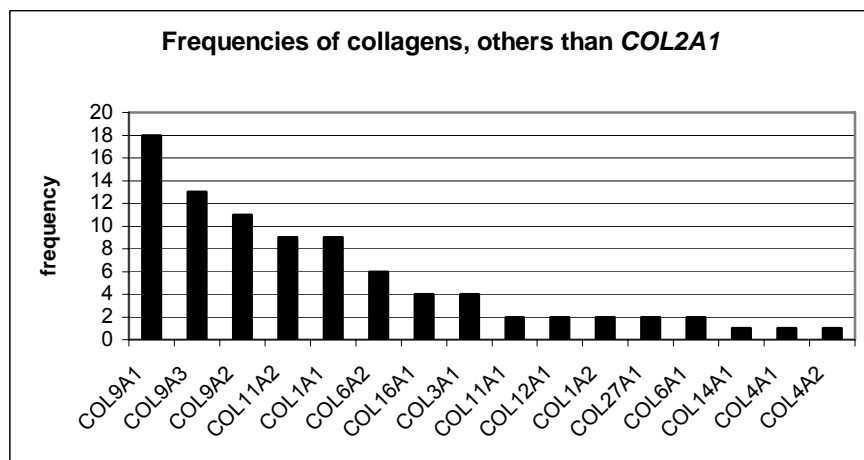


**Figure 19: Frequencies of collagen genes** within the 5000 ESTs as in May 2007.

Beside *COL2A1*, a couple of other collagens were presented in the cartilage library (figure 19). Three type IX collagens show the highest frequency, followed by *COL11A2* and *COL1A1*. Overall, 17 collagens, including *COL2A1*, were found within the 5000 ESTs, representing 4.02% (201) of all the sequences. In comparison to previously published data [Tagariello et al., 2005], the number therefore increased from 3.8% by 0.22% with final examination in May 2007.

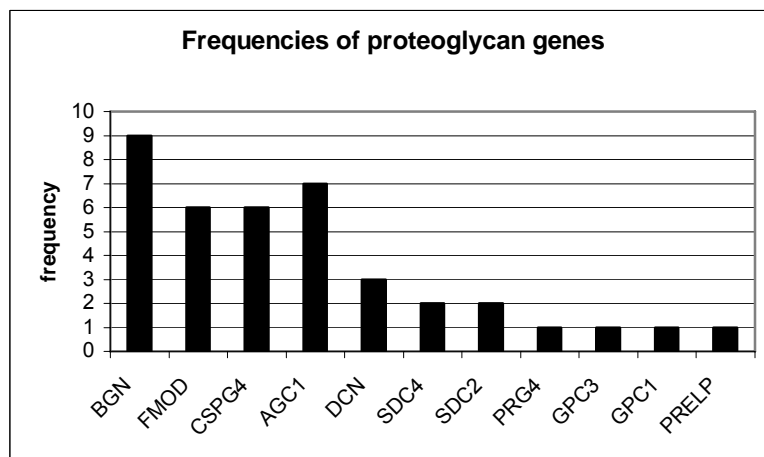


**Figure 20: Frequencies of proteoglycan constituents of the extracellular matrix** within the 5000 ESTs as in May 2007. *BGN*: biglycan; *FMOD*: fibromodulin; *CSPG4*: chondroitin sulfate proteoglycan 4; *AGC1*: aggrecan; *DCN*: decorin; *SDC4*: syndecan 4; *SDC2*: syndecan 2; *PRG4*: proteoglycan 4; *GPC3*: glypican 3; *GPC1*: glypican 1; *PRELP*: proline arginine-rich and leucine-rich protein.

Within the proteoglycans, highest frequency was seen for biglycan, followed by aggrecan, fibromodulin, and chondroitin sulfate proteoglycan 4. Lower

frequencies were found for decorin, syndecan 2 and 4, proteoglycan 4, glypican 1 and 3, as well as *PRELP* (figure 20).

Within the non-collagen/ non-proteoglycan ECM components, Osteonectin (*SPARC*) and fibronectin 1 were found at highest frequency, while others were much less represented (figure 21).

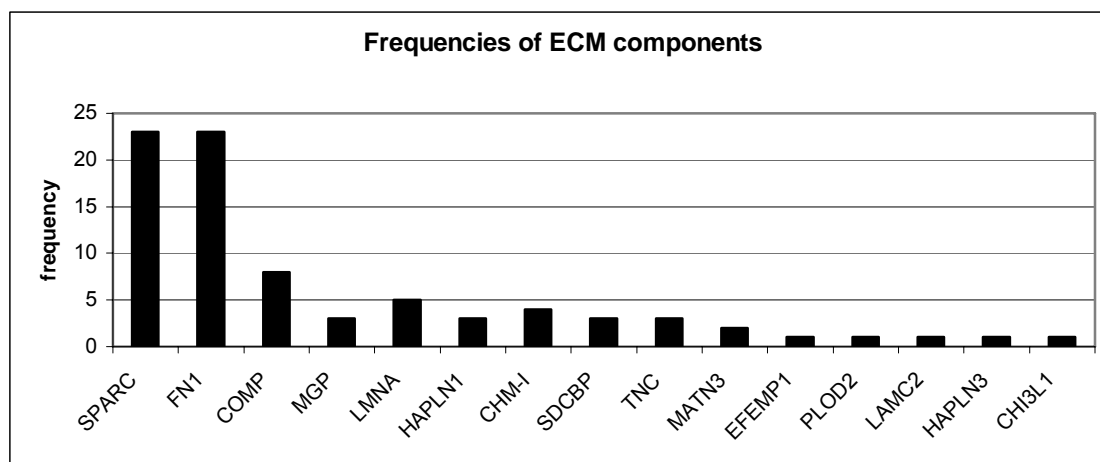


**Figure 21: Frequencies of non-collagen/ non-proteoglycan ECM constituents** within the 5000 ESTs as in May 2007. *SPARC*: osteonectin; *FN1*: fibronectin; *COMP*: cartilage oligomeric matrix protein; *MGP*: Matrix Gla protein; *LMNA*: Lamin A/C; *HAPLN1*: hyaluronan and proteoglycan link protein 1; *CHM-1*: chondromodulin; *SDCBP*: syndecan binding protein; *TNC*: tenascin; *MATN3*: matrilin 3; *EFEMP1*: EGF-containing fibulin-like ECM protein; *PLOD2*: procollagen lysine 2-oxoglutarate 5-dioxygenase 2; *LAMC2*: laminin gamma 2; *HAPLN3*: hyaluronan and proteoglycan link protein 3; *CHI3L1*: chitinase 3-like 1.

The analysis of the 5000 EST sequences showed a typical distribution compared to previously described cartilage EST projects [Kumar et al., 2001; Okihana and Yamada, 1999; Pogue et al., 2004; Zhang et al., 2003]. For instance, the frequencies of the collagens showed highest values for type II collagen, alpha 1 throughout all the libraries (table 3), as well as a low copy number for type 10 collagen, alpha 1. Hypertrophic chondrocytes that express *COL10A1*, were underrepresented within the library as tissue from the chondro-osseous junction was avoided during tissue collection to minimize contaminations from bone marrow [Tagariello et al., 2005].

	Murine postnatal growth cartilage (4 <sup>th</sup> week) [Okihana and Yamada, 1999]		Human fetal cartilage (8 <sup>th</sup> -12 <sup>th</sup> week) [Zhang et al., 2003]		Human fetal cartilage (18 <sup>th</sup> -20 <sup>th</sup> week) [Krakow et al., 2003; Pogue et al., 2004]		Final distribution of human cartilage (20 <sup>th</sup> week – 2 <sup>nd</sup> year) [Tagariello et al., 2005]		Human adult normal cartilage [Kumar et al., 2001]	
Σ	1401		13333-13500		6266		5000		5226	
sequenced	769		13155				5000			
readable	608						4486		4415	
contaminated / repetitive			2549				289			
no match							57			
known	410		8696				3917		1590	
unknown			1857				223		1110	
novel	196		53						119	
polyA	2									
individual			2448		2404		1573		2819	
individual known			1896		1775		1400			
Individual unknown			552		629		173			
	cn	% (n=769)	cn	% (n=13333-13500)	cn	% (n=6266)	cn	% (n=5000)	cn	% (n=5226)
<b>Collagens</b>										
COL10A1	p				1	0.02	0		p	
COL11A1	p		46	0.34	79	1.26	2	0.04	p	
COL11A2	p		34	0.25	43	0.69	9	0.18		
COL12A1			10	0.07			2	0.04		
COL14A1							1	0.02		
COL16A1	p				5	0.08	4	0.08		
COL1A1	p		90	0.67	3	0.05	9	0.18	p	
COL1A2	p		154	1.15	3	0.05	2	0.04	p	
COL27A1							2	0.04		
COL2A1	55	7.15	172	1.28	260	4.15	114	2.28	p	
COL3A1			54	0.4			4	0.08		
COL4A1							1	0.02		
COL4A2							1	0.02		
COL6A1	p				8	0.13	2	0.04		
COL6A2					6	0.1	6	0.12		
COL6A3	p						0			
COL9A1	p		74	0.55	230	3.67	18	0.36		
COL9A2	p		21	0.16	44	0.70	11	0.22		
COL9A3	p		26	0.19	70	1.12	13	0.26	p	

**Table 3: Composition of clones in present (in blue) and previous cartilage EST sequencing projects** [Krakow et al., 2003; Kumar et al., 2001; Okihana and Yamada, 1999; Pogue et al., 2004; Zhang et al., 2003] Distribution of collagens as given in copy numbers (cn) as well as in percentages; fr.: frequency, p: present.

This is also supported by the fact that matrix metalloproteinase 9, an additional marker for hypertrophy [Engsig et al., 2000], was not detected. But then, *MMP1*, *MMP3* and *MMP13* – all expressed in hypertrophic chondrocytes [Haeusler et al., 2005] - were found at relative high copy numbers. *MMP3* was also seen with high frequency in adult cartilage, as well as in tissues from the 18<sup>th</sup> – 20<sup>th</sup> week of gestation that also contained a high copy number of *MMP13* transcripts (table 4).

	Murine 4 <sup>th</sup> week		Human 8 <sup>th</sup> – 12 <sup>th</sup> week		Human 18 <sup>th</sup> -20 <sup>th</sup> week		Human 20 <sup>th</sup> week - 2 <sup>nd</sup> year		Human adult	
	cn	% (n=769)	cn	% (n=13333-13500)	cn	% (n=6266)	cn	% (n=5000)	cn	% (n=5226)
<b>Proteoglycans</b>										
AGC1	p		14		5	0.08	7	0.14	18	0.34
BGN	p				5	0.08	9	0.19		
CSPG4							6	0.12		
DCN			14		15	0.24	3	0.06	174	3.33
FMOD	p		8		43	0.69	6	0.12	p	
GPC3			15				1	0.02		
HSPG2	p						0			
PRELP							1	0.02	13	0.25
PRG4			9				1	0.02		
SDC2			8				2	0.04		
SDC4					6	0.1	2	0.04		
LUM			8				0		12	0.23
<b>ECM components</b>										
CHI3L1							1	0.02	22	0.42
CHM-I	p		15		15	0.24	4	0.08		
CILP			1				0		p	
COMP	p		2		7	0.11	8	0.16	24	0.46
EFEMP1							1	0.02		
FN1	p		16		16	0.26	23	0.46	25	0.48
HAPLN1			20		47	0.75	3	0.06		
HAPLN3							1	0.02		
LAMC2							1	0.02		
LMNA					8	0.13	5	0.1		
MATN1			42		16	0.26	0			
MATN3			7		21	0.34	2	0.04		
MGP	p		6				3	0.06	22	0.42
OPN	p						0			
PLOD2			2				1	0.02		
SDCBP							3	0.06		
SPARC	54	7.02	42		96	1.53	23	0.46	p	
TNC							3	0.06		
<b>Matrix metalloproteinases</b>										
MMP1							24	0.48		
MMP13			1		58	0.93	4	0.08		
MMP15			2				0			
MMP19			1				0			
MMP2			10				1	0.02		
MMP3					129	2.06	37	0.74	40	0.77
<b>Bone morphogenetic proteins</b>										
BMP1			1				1	0.02		
BMP6					6	0.1	1	0.02		
BMP7			1				0			

**Table 4: Distribution of matrix components in present (in blue) and previous cartilage EST sequencing projects** [Krakow et al., 2003; Kumar et al., 2001; Okihana and Yamada, 1999; Pogue et al., 2004; Zhang et al., 2003] as given in copy numbers (cn) as well as in percentages; p: present.

All typical proteoglycans, like aggrecan 1 (*AGC1*), biglycan (*BGN*), fibromodulin (*FMOD*), decorin (*DCN*), and chondroitin sulfate proteoglycan 4 (*CSPG4*) were present within the libraries (table 4), as well as further ECM components like fibronectin (*FN1*), osteonectin (*SPARC*), cartilage oligomeric matrix protein (*COMP*), and lamin A/C (*LMNA*).

	Murine 4 <sup>th</sup> week		Human 8 <sup>th</sup> – 12 <sup>th</sup> week		Human 18 <sup>th</sup> -20 <sup>th</sup> week		Human 20 <sup>th</sup> week - 2 <sup>nd</sup> year		Human adult	
	cn	% (n=769)	cn	% (n=13333-13500)	cn	% (n=6266)	cn	% (n=5000)	cn	% (n=5226)
<b>Ribosomal proteins</b>										
RPA0							0		p	
RPL10			53				26	0.52		
RPL13A			64				23	0.46		
RPL21							18	0.36	p	
RPL3					22	0.35	35	0.7		
RPL37a			56				8	0.16		
RPL4	p									
RPL5							33	0.66		
RPL7A			45				32	0.64		
RPL8							20	0.4		
RPL9			47				31	0.62		
RPLP0			56		30	0.49	28	0.56		
RPS11							26	0.52		
RPS18							22	0.44		
RPS20			42				27	0.54		
RPS27A							22	0.44		
RPS3	p									
RPS4X					9	0.14	23	0.26		
RPS8			42				14	0.28		
RPS9							7	0.14	p	
<b>others</b>										
ANXA2			14		37	0.59	3	0.06	p	
ANXA5			9		12	0.19	8	0.16		
ANXA7	p									
APOD							0		40	0.77
CFH							0		24	0.46
CLU							12	0.24	71	1.36
CTGF			6		12	0.19	0		14	0.27
EEF1A1			150		119	1.9	97	1.94		
EEF1G					14	0.22	28	0.56		
EEF2			16				13	0.26		
ENO1			16		15	0.24	16	0.32		
FTH1					7	0.11	57	1.04	p	
FTL							26	0.52		
GPX3							3	0.06	140	2.68
H19			25				10	0.2		
HSP70	p									
HSP90			11		32	0.51	21	0.42		
IGF2			24				1	0.02		
ITM2B			10				2	0.04		
RUNX2							0			
S100A6			15				7	0.14		
SERPINA3					7	0.11	4	0.08	15	0.29
SOD3							0		12	0.23
SOX9					2		1	0.02	p	
OPG					15	0.24	0			
TPT1					24	0.38	50	1	24	0.46
TRERF1			16				0			
TSC22D3							0		22	0.42
TXNIP							0		30	0.57
VIM					21	0.34	8	0.16	27	0.52

**Table 5: Distribution of ribosomal and other proteins in present (in blue) and previous cartilage EST sequencing projects** [Krakow et al., 2003; Kumar et al., 2001; Okihana and Yamada, 1999; Pogue et al., 2004; Zhang et al., 2003] as given in copy numbers (cn) as well as in percentages. Gene symbols in red identify disease genes [Superti-Furga and Unger, 2007]; p: present.

Unfortunately, detailed information about the copy numbers from all the marker genes was not available and the variable percentages, probably due to different ages of the collected tissues, as well as modifications in the preparation of the libraries, were difficult to compare.

Overall, the human fetal cartilage library showed comparable copy numbers for all major marker genes that are known to be important for cartilage development and maturation, thus indicating that the generated EST library is a representative data set and therefore a very valuable tool to identify important genes in normal chondrogenesis. Ribosomal proteins and ubiquitously expressed genes (table 5) were also identified confirming that this library is representative for detailed investigations. This included the characterization of novel EST clones that were considered candidate genes in skeletogenesis and mutations in these newly identified genes might be responsible for chondrodysplasias with as yet unknown molecular pathogenesis.

### **3.1.3. Characterization of selected EST clones**

Single EST clones were selected for further characterization based on their protein domains or genomic localization which suggested a link to known genetic players in skeletogenesis or disease loci of chondrodysplasias.

#### **3.1.3.1. Characterization of clone B-C12**

Clone B-C12 mapped in a zinc finger cluster on human chromosome 19q13.41 (NCBI, Blast the Human Genome) and showed 100% identity with the hypothetical protein *MGC4400* (accession number NM\_032679, 1437 bp) in a homology search with the EST sequence against the database 'Nrnc' in autumn 2003. The gene title was changed to zinc finger protein 577 (*ZNF577*) in March 2006 because of the eight C<sub>2</sub>H<sub>2</sub> zinc finger domains. Additionally, *ZNF577* contains a Krüppel-associated box ('KRAB') that is located at the NH<sub>2</sub>-terminus of the zinc finger domain (figure 22). The KRAB domain is a 75-amino acid transcriptional repressor module associated with eukaryotic zinc finger proteins that requires binding to the co-repressor *KAP1/ CDKN3* to mediate gene silencing [Peng et al., 2000].

Screening human protein databases showed a high homology between *ZNF577* and *ZBRK1/ ZNF350* (48% over 517 amino acids) that was identified as an interaction partner of the tumor suppressor gene *BRCA1* [Zheng et al., 2000].

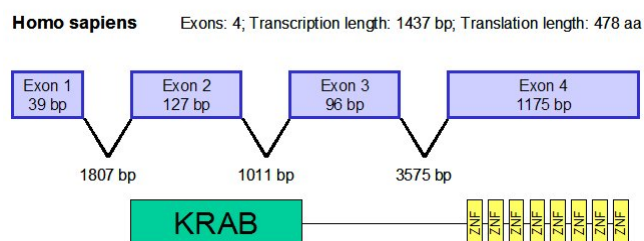


**Figure 22: Exon-intron structure of the human *ZNF577*.** Exons are shown as blue boxes, the length of the introns is given below. Indicated are the number of exons, as well as the length of the transcript and of the protein. The lower panel indicates the orientation of the KRAB domain and the eight zinc fingers.

Because of this similarity, it was likely that *ZNF577* would interact with another tumor suppressor gene.

Unfortunately, no mouse gene was published and screening the commonly used 'Ensembl', 'NCBI', and 'Celera' mouse databases did not reveal an orthologue gene. Additionally, screening a mouse E8.5 phage library with a human probe did not result in a positive clone. Therefore, only the size of the open reading frame was confirmed in HTB94 human chondrosarcoma cells by Northern blot hybridization (data not shown) confirming a single transcript with the predicted size. Further investigations were not initiated because of the lack of human tissues.

### 3.1.3.2. Characterization of clone ch11g10

Database analysis mapped clone ch11g10 on human chromosome 17q21.33 (NCBI, Blast the Human Genome). 17q contains genes like *WNT3*, *TBX4*, *COL1A1* and a cluster of *HOXB* genes, all important during development. The first three genes are mutated in diseases involving the skeleton and the *HOXB* genes (17q21.32) are important in the establishment of the anterior-posterior and the dorsal-ventral axis during vertebrate embryogenesis [Godsave et al., 1994]. *WNT3* (17q21.32) was previously associated with Tetra-amelia [Niemann et al., 2004], *TBX4* (17q23.2) with Small patella syndrome [Bongers et al., 2004], *COL1A1* (17q21.33) with Osteogenesis Imperfecta [Byers et al., 1982].

Homology search with the EST sequence against 'Nrnc' database showed a 100% identity with the hypothetical protein *PRO1855/ FLJ21675* (accession number AF119857, 2341 bp) that belonged to the UniGene cluster Hs.370927.



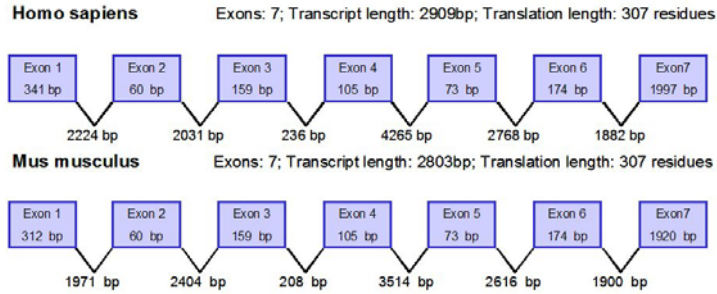


**Figure 23: Exon-intron organization of the human *PRO1855* and its murine orthologue.** Exons are shown as blue boxes, the length of the introns is given below. Indicated as well are the number of exons, the transcript and the translation length.

Analysis of the consensus sequence revealed an open reading frame of 2909bp (figure 23). The orthologous mouse sequence at that time (89% identities) had an open reading frame of 2803 bp and was described as ‘Mus musculus 16 days embryo heart cDNA, RIKEN full-length enriched library, clone: I920194F17 product; similar to hypothetical protein PRO1855 (P34 protein homolog)’ (accession number AK169390) belonging to mouse UniGene cluster Mm.172720. The orthologous genes showed a similar exon-intron structure and both proteins were 307 amino acids long (figure 23).

Homo sapiens	1	MTKAGSKGNNLRDKLDGNELDLSLSDLNEVPVKEAALPKATITLDSCKNLSTLPSPFCG	60
Mus musculus	1	MTKAGSKGNNLRDKLDGNELDLSLSDLNEVPVKEAALPKATITLDSCKNLSTLPSPFCG	60
Rattus norvegicus	1	MTKAGSKGNNLRDKLDGNELDLSLSDLNEVPVKEAALPKATITLDSCKNLSTLPSPFCG	60
Xenopus laevis	1	MARANGSQNNLRDKLDGNELDLSLSDLSEVPVRLVAIPKATITLDSCKNLSTLPSPFCG	60
Drosophila melanogaster	1	MPKPGDK--NVRERVVDCTCDLSLSESEIPVREIASFKRVTVDLSNRLVNLGNFSI	63
Anopheles gambiae	21	NVRDLTDNVLDLSLNNISRVVQEIKTLLRATITLDSNIRISITENFTD	69
Caenorhabditis elegans	11	LKNLQEDDELDSASGIEPFP-NAIVQLPRLTKLDSNAITFLPSPFCG	59
Homo sapiens	61	LTHLVKLDLSKNNLQQLPADPGRVLNQLHLDLLNNRLVTLFVSFAQLKRLKWLDKDNPL	120
Mus musculus	61	LTHLVKLDLSKNNLQQLPADPGRVLNQLHLDLLNNRLVTLFVSFAQLKRLKWLDKDNPL	120
Rattus norvegicus	61	LTHLVKLDLSKNNLQQLPADPGRVLNQLHLDLLNNRLVTLFVSFAQLKRLKWLDKDNPL	120
Xenopus laevis	61	LSHIVRLDLSKNQIVQLPSEFGRLLMQLHLDLLQNHIMS LVSFAQLKSLKWLDKDNPL	120
Drosophila melanogaster	64	LTRLVRLDLSKNQIKFLPEDFGQLEQLRHLDLYNNCEHLPLSPGQLRLRLYLDLKNPL	123
Anopheles gambiae	70	LTQLTQIDLSKNRITTTICDDPGLLTNLRRLDLYKNQLTRLPLTFGRLLKRLYLDLKENPL	130
Caenorhabditis elegans	60	MTKLIRLDFGSCQLHHLDPGIGLLTSLQHLNLYNNQIEDLPLSFANLKS LKWLDKKNPL	119
Homo sapiens	121	DPVLAKVAGDCIDEKQCKQCANVLOHMKAVQADQERERQRRLEVERAEKKREAKQAK	180
Mus musculus	121	DPVLAKVAGDCIDEKQCKQCANVLOHMKAVQADQERERQRRLEVERAEKKREAKQAK	180
Rattus norvegicus	121	DPVLAKVAGDCIDEKQCKQCANVLOHMKAVQADQERERQRRLEVERAEKKREAKQAK	180
Xenopus laevis	121	KPD LAKVAGDCIDEKQCKQCAQVLOHMKSVQSDHEITLQRLQLDKERKKKLEAKQRVK	180
Drosophila melanogaster	124	TPAWEKIVGCCSTQKDCQQAARNTV	148
Anopheles gambiae	131	NPAFKKIIGTCSDTNDCLVAATRAVDFMK	160
Caenorhabditis elegans	120	NSKLAAIAGNCGTDAECKQAARQV	144
Homo sapiens	181	EAQERE LRKREKAEERERRRKEYDALKAAREQEKKKKEANQAPKSKSGSRPRKPPPRK	240
Mus musculus	181	EAKERE LRKREKAEERERRRKEYDAKASKREQEKKKKEANQAPKSKSGSRPRKPPPRK	240
Rattus norvegicus	181	EAKERE LRKREKAEERERRRKEYDAKASKREQEKKKKEANQAPKSKSGSRPRKPPPRK	240
Xenopus laevis	181	EEQEREMRKKKQKQKERRRRDYNAMQEAERALNSNKAEEEPTEHMKMATPREKKLAQ	240
Homo sapiens	241	HTRSWAVLRLLLLLLFGVAGGLVACRVTELQQQLPCTSVNTIYDNAVQGLRHHEILQW	300
Mus musculus	241	HTRSWAVLRLLLLLLFGVAGGLVVCRTVGLHQQLPCTSVNTIYDNAVQGLRHHEILQW	300
Rattus norvegicus	241	HNRSWAVLRLLLLLLFGVAGGLVVCRTVGLQQQLPCTSVNATYDNAVQGLRHHEILQW	300
Xenopus laevis	241	RQSRLRIACILLFGLLVVLVVACRFTDLKAINMCTSVNATYKETISALHSNVLRF	300
Homo sapiens	301	LQTDSSQ	307
Mus musculus	301	LQTDSSQ	307
Rattus norvegicus	301	LQTDSSQ	307
Xenopus laevis	301	LQDPSSQ	307
		LRR1	
		LRR2	
		LRR3	
		LRR4	
		Coiled-coil	
		TMD	

**Figure 24: Alignment of the protein sequence of *LRRC59* of 7 different species.** 4 leucine rich repeats (LRR1-4) are indicated by green shaded boxes, the coiled coil motif by the brown box, the transmembrane domain (TMD) by the gray box

Since the first database search, done in late 2003, additional sequences were submitted for this potential gene and the name 'PRO1855' was changed to 'leucine rich repeat containing 59' (*LRRC59*, accession number NM\_018509) because of the four leucine rich repeats (LRR) that were highly conserved between different species, as well as the coiled coil motif and the transmembrane domain (figure 24).

The expression was detected by qRT-PCR on a variety of tissues of adult and newborn mice (figure 25). The highest expression was seen in testis and ovary of adult mice, as well as in calvarias of newborn mice.

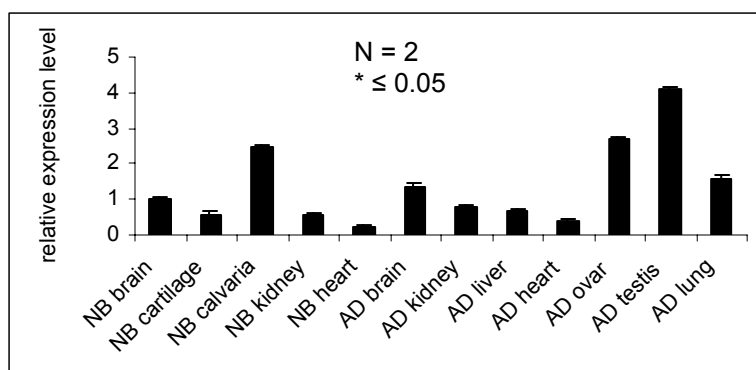


**Figure 25: Quantitative RT-PCR for *Lrrc59* on a variety of tissues** of adult (AD) and newborn (NB) mice using *Lrrc59* specific primers NM\_133807-3'UTR-F/R

Northern blot hybridization using rat, murine and human cell lines confirmed the size of the open reading frame in the orthologous genes. The transcript was detected in human chondrosarcoma cells (HTB94), rat chondrosarcoma cells (RCS) and murine chondrocytes (MCT), but not in rat osteosarcoma cells (ROS17) or murine fibroblastic 10T $\frac{1}{2}$  (figure 26). Although more cell lines should have been included, it appeared that the transcript is expressed in cell lines of chondrogenic, but not osteoblastic origin. That suggested a specific function in chondrocytes that needed further investigation.

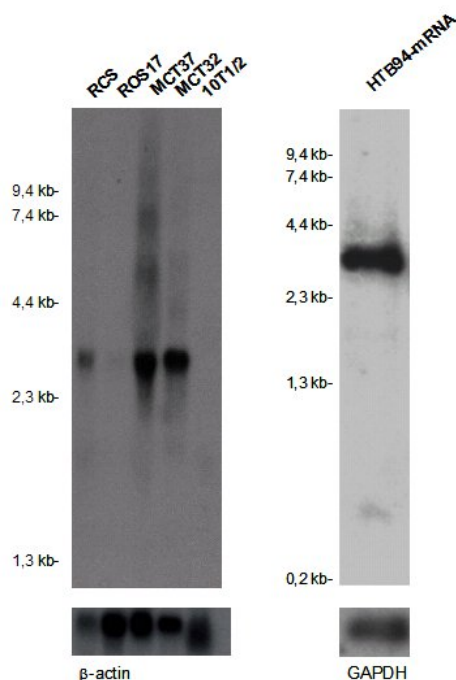


**Figure 26: Northern blot hybridization of rat/murine and human RNA samples using a *Lrrc59/ LRRC59* specific probe:** The transcript was detected in RNA of rat chondrosarcoma cells (RCS) and murine hypertrophic chondrocytes (MCT 32/ MCT37), but not in 10T1/2 fibroblasts or rat osteosarcoma cells (ROS17) (left panel). In human chondrosarcoma cells (HTB94) the transcript size was confirmed (right panel). The murine/ rat probe was generated with gene specific primers NM\_133807-3'UTR-F/R, the human probe with PrEfc361-1F/1R.

*In situ* hybridization on sagittal sections revealed a specific expression in proliferating chondrocytes at E13.5 and in the inner cortex of long bones at E17.5 (figures 27 B, E). Hybridization on extremities at E15.5 with probes for murine PRO1855/ *Lrrc59* and type X collagen showed that the two genes are not co-localized, but *Lrrc59* “surrounded” the areas of *Col10a1* expression (figures 27 H, I).

Whole mount *in situ* hybridization for E11.5, 12.5, 13.5 did show only weak, unspecific signals while the sense controls remained unstained (figure 28).

Screening human protein databases showed a high homology with other LRR containing proteins (figure 29) like fibromodulin (accession number NP\_002014), biglycan, decorin (accession number NP\_001702), lumican (accession number NP\_002336), and chondroadherin (accession number NP\_001258) over the first 104 amino acids of *LRRC59* (accession number NP\_060979). All these proteins were previously described as collagen binding small leucine-rich proteoglycans (SLRP) [McEwan et al., 2006].

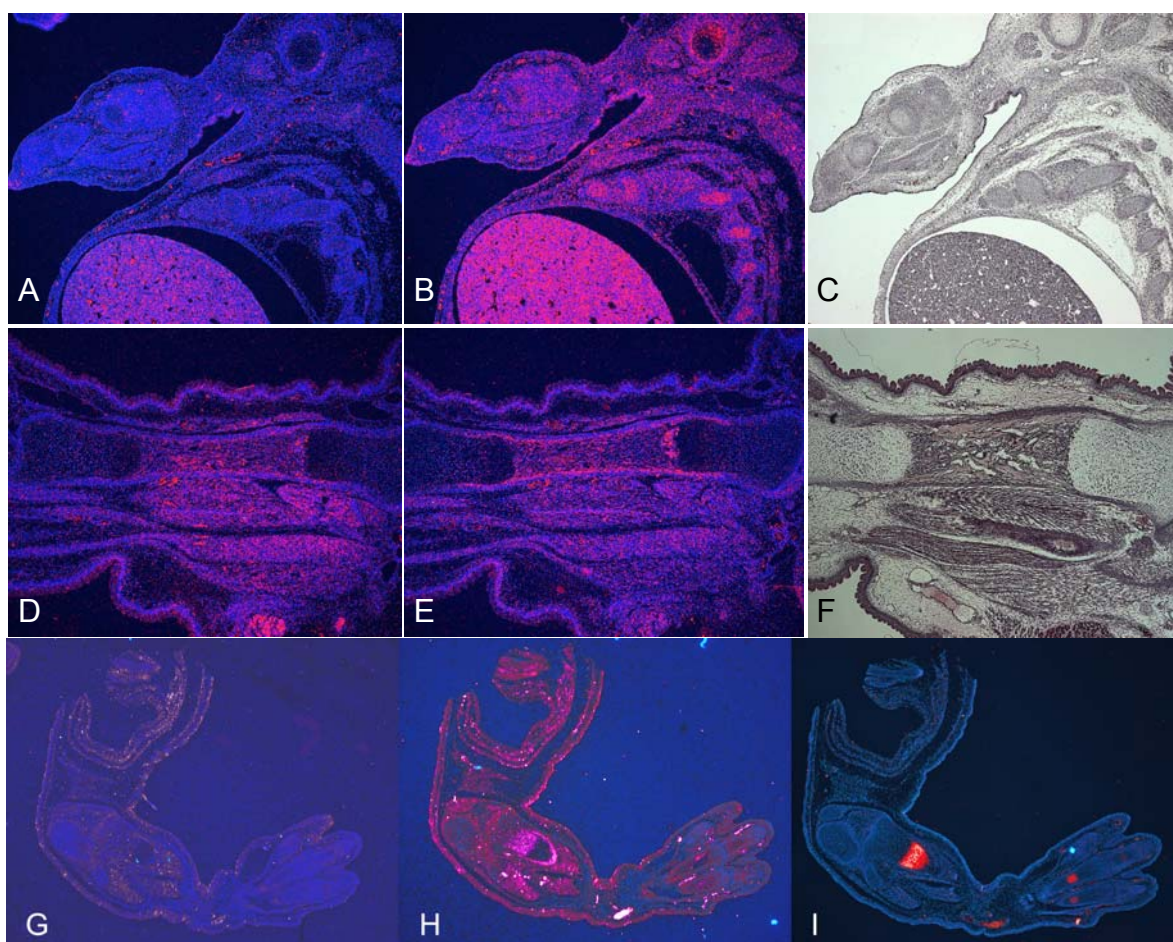


**Figure 27:** *In situ* hybridization of *Lrrc59* on sagittal sections of E13.5 (A-C), long bones at E17.5 (D-F), and long bones at E15.5 (G-I). Sense control probe was used in A, D, and G, where sections remained unstained, while hybridization with an antisense probe revealed specific signals (B, E, and H). Vital staining was used for better orientation (C and E), as well as hybridization with a type X collagen antisense probe (I); Probes for *Lrrc59* were generated with gene specific primers NM\_133807-3'UTR-F/R.

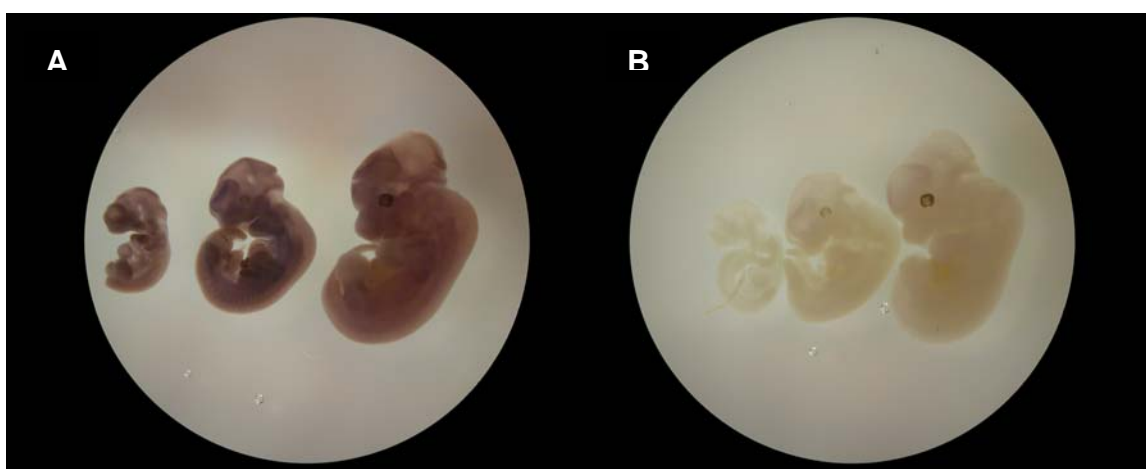


**Figure 28:** WISH with *Lrrc59* specific probe on E11.5, E12.5, and E13.5, tail partly disrupted. A: embryos hybridized with antisense probe; B: embryos hybridized with sense probe.



fibromodulin precursor	9	L A G L F S L S Q A Y E D D P H W F H Y L R S Q Q S T Y Y D P Y D P Y P Y E T Y E P Y P Y
biglycan preproprotein	7	L V S L L A L S Q A L P F E Q R G F W D F T L ----- D D G P F M M N D E A S
decorin isoform a preproprotein	7	L L L L A Q V S W A G P F Q Q R G L F D F M L ----- E D ----- E A S
lumican		P L S I Y G Q S S P ----- N ----- C A P E C N C P E S Y -- P S A M Y C
fibromodulin precursor		G V D E G P A Y T Y G S P S P P D P R D ----- C P Q E C D C P P N F -- L T A M Y C
biglycan preproprotein		G A D T S G V L D P D S V T P T Y S A M ----- C P F G C H C --- H -- L R V V Q C
decorin isoform a preproprotein		G I G P E - V P D R D P E V P D R D F E P S L G P V C P F R C Q C --- H -- L R V V Q C
chondroadherin precursor		A A ----- C P Q N C H C --- H S D L Q H V I C
LRRC59		1 M T K A G S K G G N L R D K L D G N E L D L
lumican		D E L K I K S V F - M - V P -- F G I K Y I Y L R N N Q -----
fibromodulin precursor		D N R N L K Y L F - F - V P -- S R M K Y Y F Q N N Q -----
biglycan preproprotein		S D L G L K S V F - K E I S -- P D T T L D L Q N N D -----
decorin isoform a preproprotein		S D L G L D K V F - K D L P -- P D T T L D L Q N N K -----
chondroadherin precursor		D K V G L Q K I F - K - V S -- E K T K L N L Q R N F P V L A A N S F R A M P N L V L S H
LRRC59		S L S D L N E V E V K E I A A L P K A T I L D L S C N K -----
lumican		----- I D H I D E K A F E N V T D L Q W L I L D H N L L E N S K I K G R V F S K I K Q L K
fibromodulin precursor		----- I T S I Q E G V F D N A T G L L W I A L H G N Q I T S D K V G R K V F S K L R H L E
biglycan preproprotein		----- I S E I R K D D F K G I Q H L Y A L V L V N N K I S -- K I H E K A F S P L R K L Q
decorin isoform a preproprotein		----- I T E I K D G D F K N L K N L H A L I L V N N K I S -- K V S G A F T P L V K L E
chondroadherin precursor		L Q H C Q I R E V A A G A F R G L K Q L I Y I Y L S H N D I R -- V V R A G A F D D L T E L T
LRRC59		----- L T T L P S - D F C G L T H L V K L D L S K N K L Q -- Q L - E A D F G R L V N L Q
lumican		K L H I N H N N L T E S V G P L
fibromodulin precursor		R L Y L D H N N L T R M P G P L
biglycan preproprotein		K L Y I S K N H L V E I F P N L
decorin isoform a preproprotein		R L Y L S K N Q L K E L P E K M
chondroadherin precursor		Y L Y L D H N K V T E L P R G L
LRRC59		H I D L L N N K L V T L P V S F 104

**Figure 29: Alignment of 5 small leucine-rich proteoglycans (SLRP) with *LRRC59*.** Conform amino acids with *LRRC59* are marked in green. conform amino acids within the SLRPs are marked in yellow.

To find out whether *Lrrc59* could be a component of the cytoskeleton, colocalization with vinculin was investigated by immunohistochemistry in COS7 cells. Vinculin is a membrane-cytoskeletal protein involved in linkage of integrin adhesion molecules to the actin cytoskeleton, and integrin can act as a receptor for collagen-binding SLRPs [Camper et al., 1997] or for collagen directly [White et al., 2004]. Focal contacts were detected with a vinculin specific antibody (figure 30).

*Lrrc59* indeed co-localized with the membrane-cytoskeletal protein vinculin and may therefore be connected to the actin/ integrin network, and function in collagen fibrillogenesis as described for SLRP [McEwan et al., 2006].

*In situ* hybridization showed that *Lrrc59* might have an important role in proliferating chondrocytes. Its protein structure and the co-localization with

vinculin connect *Lrrc59* indirectly to the ECM, via intramembranous proteins like integrin. Whether *Lrrc59* has an influence on the fibrillogenesis in the ECM, needs to be further investigated. Therefore, a mouse model could be helpful.

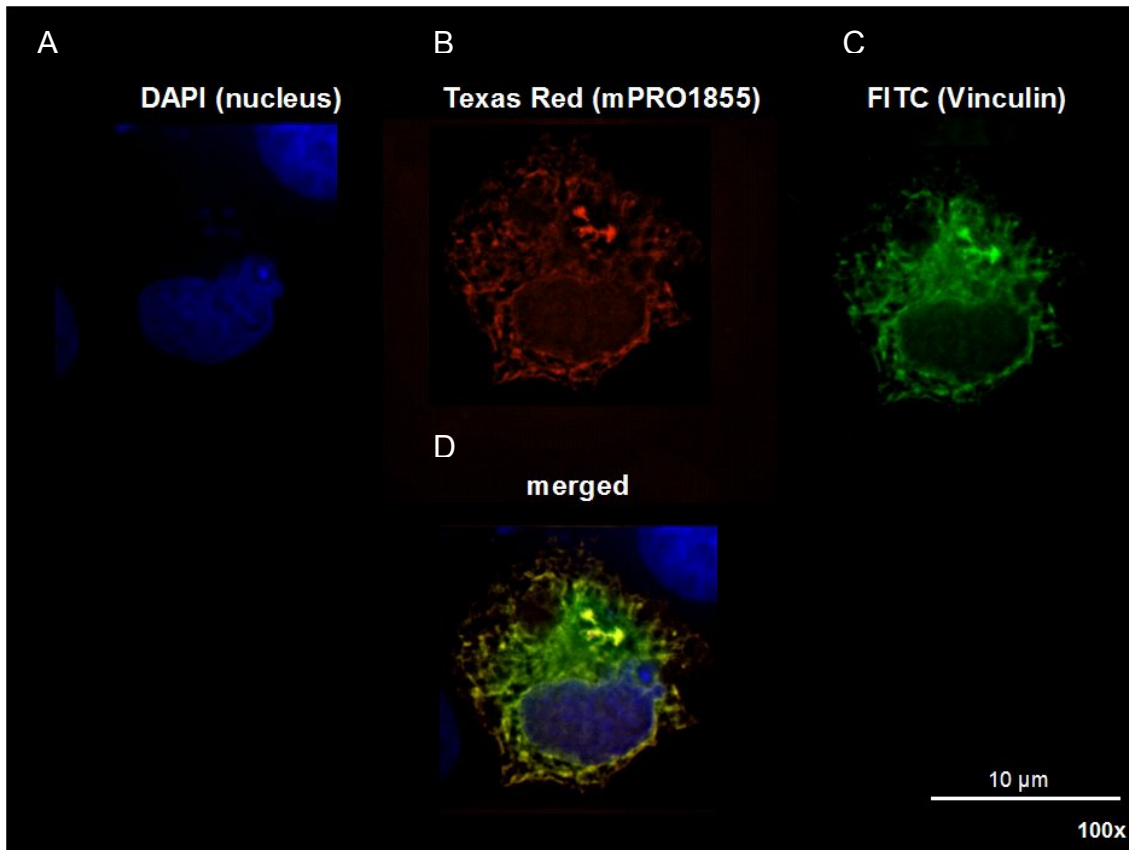


**Figure 30: Co-localization of murine *Lrrc59* with Vinculin in COS7 cells.** Immunofluorescence staining after co-transfection of COS7 cells with full length *Lrrc59*, cloned in pcDNA3.1/V5-His A, and Vinculin (Vcl). A: Nucleus was stained with DAPI; B: *Lrrc59* detected with V5-ab and goat-anti-mouse IgG-Cy3; C: Vcl detected with a monoclonal Vcl-ab, biotin-donkey-anti-mouse IgG and Streptavidin DTAF; D: merged image to visualize co-localization of the two genes.

### 3.1.3.2.1. Knock-out model for *Lrrc59*

A mouse model for *Lrrc59* inactivation was initiated by finding the MICER (Mutagenic Insertion and chromosome Engineering Resource) clones MHPN88m09 and MHPP341c05 from Sanger Center (Cambridge, UK) [Adams et al., 2004; Zheng et al., 1999]. Both clones contain exons 1-4 in the same orientation, but in two different vectors. No clone containing exons 5-7 exists to date. Using both vectors from these libraries would have been useful to increase the chance to inactivate the *Lrrc59* gene, but DNA preparation for MHPP341c05

failed several times. Therefore, only MHPN88m09 was further used. MHPN88m09 belongs to the 5'HPRT library clones and therefore contains the 5' half of the drug resistance gene *Hprt* minigene, as well as the neomycin resistance gene, a *loxP* recombination sequence, and a tyrosinase (Tyr) minigene that gives coat color to an otherwise albino mouse (figure 31) [Zheng et al., 1999].

Three restriction strategies were considered for *Lrrc59* inactivation: using *SacII* to cut out exon 1, *XmaI* cuts out exons 2 and 3, and *KpnI* would eliminate exons 2-4. In any case, a single cutter *SwaI* could be used for linearization of the constructs (figure 31). Forward primer 5HPPSK was used to check unrestricted clones for their genomic insert, as well as clones lacking the *SacII* fragment. Two more forward primers, check-Xma/ Kpn-F, were used to confirm clones digested with *XmaI* or *KpnI*. The reverse primer 5Hprev was used to sequence the clones for their genomic insert from the tyrosinase site (figure 31).

Initial restriction digests were performed and worked as described, but further procedures could not be performed in the time frame of this thesis.

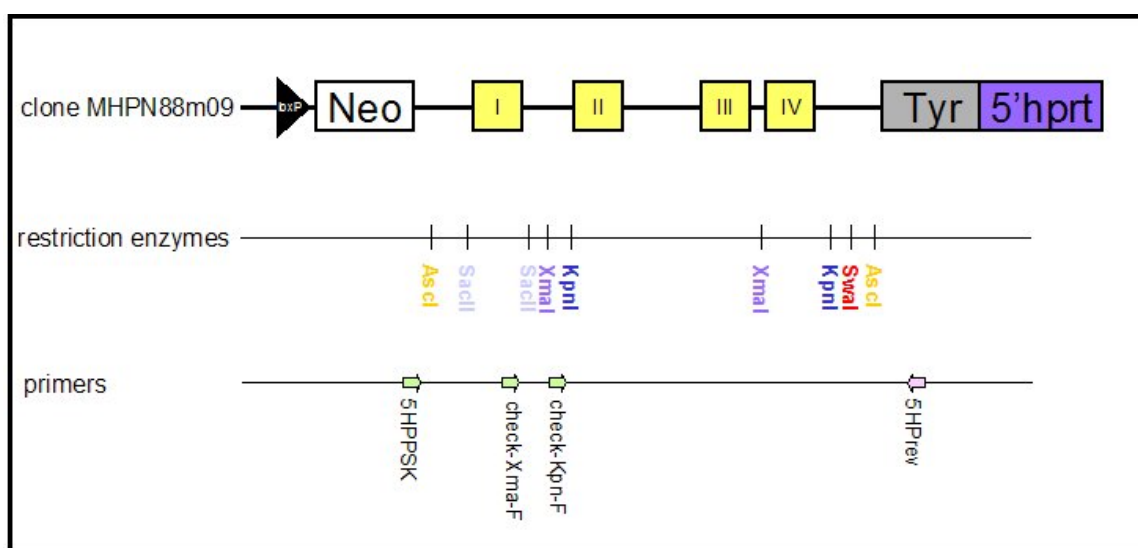


**Figure 31: Composition of clone MHPN88m09** with *loxP* site (black triangle), neomycin resistance gene (white box), exons 1-4 of *Lrrc59* (yellow boxes), the tyrosinase minigene (grey box), and the 5' half of the *hprt* minigene (blue box). Localization of restriction enzyme cut sites given in the middle pattern, localization of primers shown below.

### 3.1.3.3. Characterization of clone ch32F03

Clone ch32F03 showed 100% similarities to *CRELD2* (cysteine-rich with EGF-like domains 2, accession number NM\_024324) that appeared four times among the 5000 sequenced ESTs in the human fetal cartilage library and is part of the Unigene cluster Hs.211282. According to its GenBank entry, *CRELD2* mapped on human chromosome 22p13, but mapping by FISH showed a location on the opposite arm, 22q13 [Maslen et al., 2006a].

Blast searches with a deduced amino acid sequence for CRELD1 were used to identify CRELD2 [Robinson et al., 2003; Rupp et al., 2002]. The coding regions of the two genes show 51% homology. CRELD1 (accession number NP\_056328) has two type III transmembrane domains in its C-terminus, while CRELD2 has none. But the sequence identity and the similar arrangement of their other protein domains, indicate that the two genes are closely related and belong to one protein family. Interestingly, Rupp and co-workers published whole mount *in situ* hybridizations of chick embryos for *CRELD1* and saw specific staining in the limb buds and the mandible [Rupp et al., 2002].

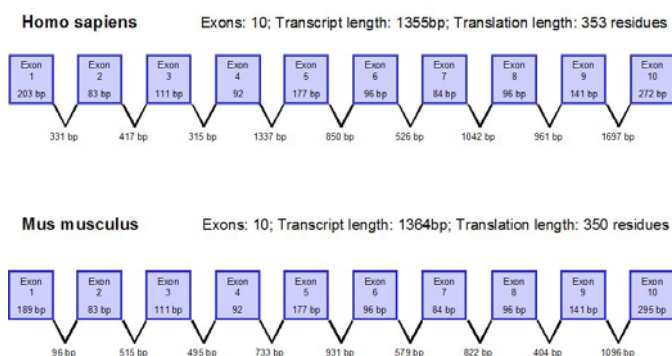


**Figure 32: Exon-intron organization of the human *CRELD2* and its murine orthologue.**

Exons are shown in blue boxes, the length of the introns is given below. Indicated as well are the number of exons, the length of the transcript and the number of amino acid residues.

The Human and the mouse gene (*Creld2*, accession number NM\_029720) consists of ten exons that result in a transcript length of 1355 bp for the human gene and 1364 bp for the mouse orthologue, respectively (figure 32).



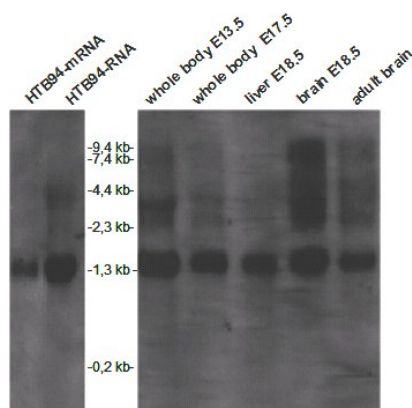


**Figure 33: Northern Blot hybridization for *Creld2*/ *CRELD2*** using total RNA and mRNA of human chondrosarcoma cells in the left panel and total RNA of E13.5, E17.5, liver and brain of E18.5 and adult brain in the right panel to confirm the transcriptional length of ~1350 bp of *CRELD2* and *Creld2*.

Recently, *CRELD2* was described as ubiquitously expressed during development and by mature tissues with the highest levels seen in adult endocrine tissues [Maslen et al., 2006a]. The transcriptional length of the gene was confirmed by Northern blot hybridization using total RNA and mRNA of human chondrosarcoma cells, as well as total RNA of E13.5 and E17.5, liver of E18.5, and brain of E18.5 and adult mice (figure 33). The transcript length was confirmed in all the RNA samples. Additional bands could be due to alternative transcripts, since five *Creld2* isoforms have already been published to date [Maslen et al., 2006a]. A cross-hybridization with family member *CRELD1* is unlikely, but other family members might be found in the future.

The protein length slightly differed with 353 amino acids for *CRELD2* (accession number NP\_077300) vs. 350 for *Creld2*. 'Blast 2 Sequences' (NCBI tool) predicted 76% identity between the two proteins. According to the domain identification program 'SMART', each protein contains a calcium-binding epidermal growth factor (EGF)-like domain at the NH<sub>2</sub>-terminus and therefore likely binds calcium for its full biological function (figure 34). The two additional furin-like repeats suggest that these proteins may be further processed and involved in a signaling pathway.

Homo sapiens	1	MRLPRRAALGLLPLLLLPAPAEAA	25
		L AA GLL LL PP A	
Mus musculus	1	MHLLIAAFGLLLLL—PPPGASRA	23
26		KKPTPCHRCRGLVDKFNQGMVDIAKKNFGGGNTAWEKTL SKYESSEIRLLEILEGLCES	85
		+KPT C RCR LVDKFNQGM +TA+KNFGGGNTAWEKTL SKYE SEIRLLEI+EGLC+S	
24		RKPTMCQRCTLVDKFNQGMANTARKNFGGGNTAWEKTL SKYEFSEIRLLEIMEGLCDS	83
86		SDFECNQMLEAQEEHLEAWWLQKSEYPDLFEWFVCVTKLVCCSPGTYPDC	145
		SDFECNQ+LE QEE LEAWW LK E+P+LFEWFVCV TLK CC PGTYGPD	
84		SDFECNQLEQQEEQLEAWWQTLKKEHPNLFWFVCVHTLKACCLPGTYGPD	143
146		RPCSGNGHCSGDGSRQGDGSCRCHMGYQGFLCTDCMDGYFSSLRNETHS	205
		RPCSGNG+CSGDGSRQGDGSC+CH GY+GPLC DC DG+FS RNETHS	
144		RPCSGNGYCSGDGSRQGDGSCQCHTGYKGPLCIDCTDGFFSLQRNETHS	203
206		CSGLTNRDCGECEVGWVLDDEGACVDVDECAAEPPPCSAQFCKNANGSYTCE	265
		CSG +N+DC +CEVGW E ACVDVDECAAE PCS Q+C+N NGSYTCE+CDS+CVG	
204		CSGFSNKDCIQCEVGWVARVEDACVDVDECAAEISPCSDGQYCENVNGSYTCE	263
266		CTGEGPFGNCKECISGYAREHGQCADVDECALAEKTCVRKNENCYNTPGSYVCVCPDGFEG	325
		CTG+GP NCKECI+GY +E GQC D+DEC+L EK C RKNENCYN PGS+VCVCP+GFE	
264		CTGKGFPANCKECIAGYTKESGQCTDIDECSLEEKAKRKNENCYNVPGSFVCVCPGFE	323
326		TEDACVPPAEAEATEGESPTQLPSREDL	353
		TEDACV AE + TE E+PTQ PSREDL	
324		TEDACVQTAEQKVTE-ENPTQPPSREDL	350



**Figure 34: Alignment of the protein sequence of the human CRELD2 and the murine Creld2.** A green shaded box indicates the calcium binding EGF-like domain, the furin-like repeats by the blue boxes.

The NCBI Conserved Domains' database is linking NP\_077300 to the matrilin protein family that contains EGF-like domains and could be specifically expressed in developing cartilage rudiments to provide extracellular matrix molecules and might mediate cell-matrix and matrix-matrix interactions.

No specific *Creld2* expression was seen in developing cartilage by whole mount *in situ* hybridizations and *in situ* hybridization at E10.5 - E13.5 (not shown). This contradicts the above described findings. To elucidate whether CRELD2 is really not expressed in cartilage or whether our assay did not work properly, RT-PCR using different sources of templates was performed.

RT-PCR was performed using the same amounts of human and mouse template cDNAs (figure 35). The human transcript was detectable in undifferentiated MSC, adipogenic differentiated MSC, the chondrosarcoma cell line HTB-94 and in fibroblasts, so was *COL1A2* and the ubiquitously expressed housekeeping gene glyceraldehyde-3-phosphate dehydrogenase (*GAPDH*). *COL2A1* and aggrecan (*AGC1*) expression was not seen in any of the above sources.

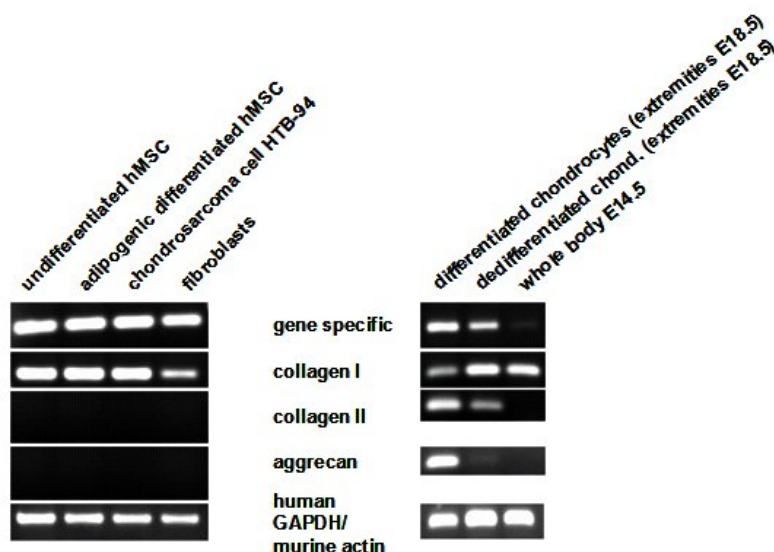


**Figure 35: RT-PCR for CRELD2/ *Creld2*** (gene specific), type I collagen, type II collagen, aggrecan, and housekeeping genes using human and murine cDNA templates. CRELD2, type I collagen was detectable in undifferentiated human MSC, adipogenic differentiated MSC, HCS cells, and fibroblasts, while no type II collagen and aggrecan expression was seen. *Creld2* and type I collagen expression was found in differentiated and undifferentiated chondrocytes, as well as in cDNA from whole embryo E14.5, while no type II and aggrecan expression was seen in E14.5. Human GAPDH and murine  $\beta$ -actin were used as housekeeping control genes.

*Creld2* was strongly expressed in differentiated and weaker in retinoic acid treated dedifferentiated epiphyseal chondrocytes dissected at E18.5 (2.2.4.), while the expression was almost undetectable in cDNA from whole embryos at E14.5. Control RT-PCRs were performed with *Col1a2*, *Col2a1*, aggrecan (*Agc1*), and the housekeeping gene  $\beta$ -actin. While *Col1a2* and  $\beta$ -actin expression was seen in all templates, *Col2a1* and *Agc1* were, as expected, strongly expressed in differentiated chondrocytes, much weaker in dedifferentiated chondrocytes [Dietz and Sandell, 1996] and undetectable in cDNA from a whole E14.5 embryo, when a lot of chondrocytes are already present.

During investigations, no results gained by WISH, ISH, and qRT-PCR linked *Creld2/ CRELD2* to a major function in cartilage development. Therefore, no further experiments were performed. Meanwhile, five CRELD2 isoforms that differ significantly in their composition were identified. One isoform of CRELD2 - called hCRELD2beta - acted as a specific regulator of human nicotinic acetylcholine receptor  $\alpha 4$  and  $\beta 2$  subunits in the thalamus and the cortex [Maslen et al., 2006a; Ortiz et al., 2005], while mutations in *CRELD1* were associated with

common cardiovascular atrioventricular septal defects [Robinson et al., 2003], also seen in Down syndrome [Maslen et al., 2006b]. Furthermore, the *CRELD1* gene was deleted in the human cytogenetic disorder 3p- syndrome and was located in the region of loss of heterozygosity for several types of cancers [Rupp et al., 2002]. An osteo- or chondrodysplasia defect involving one of the two family members is not known so far and their functions, especially for *CRELD2*, remains poorly understood to date.

### **3.1.4. Microarray experiment**

#### **3.1.4.1. Normalization and evaluation of microarray data**

No human fetal cartilage was available for further characterization of selected EST sequences. Therefore, part of the analysis was then carried out using mouse tissues. The importance of the sequenced ESTs in skeletal development was validated by a comparative microarray experiment that was performed with RNA isolated from E11.5, E 12.5 and E13.5 fore limb buds. Two sets of RNA probes were hybridized on Mouse 430 2.0 GeneChip® arrays (Affymetrix, Santa Clara/ CA, USA). Genes showing significant changes in expression over time were expected to have important roles in limb bud development.

Data obtained from microarray experiment were normalized using RMA (Robust Multi-Array). Genes that showed at least a 2-fold difference in expression were listed and further investigated. The quality of the included probes was validated using scatter plot matrixes to picture the degree of conservation between the probes, as well as RNA digestion plots to determine the degree of degradation from each set of probes (2.13.3.).

116 genes showed statistically significant differences in expression over time and genes with the same expression pattern were grouped together. 98 individual genes were found differentially expressed and categorized according to their biological function (figure 36, table 11 in 8.2.). The largest part (35%) of the genes were involved in cell structure and motility. 24% assured transport, cell signaling and cell-to-cell communication, 18% represented transcription factors

or genes for gene/ protein expression and posttranslational modification, 5% were metabolic genes or genes involved in cell division/ cycle and DNA replication, while 2% functioned in proteolysis or cell/ organism defense and apoptosis. 9% were not categorized because of insufficient information about their function.

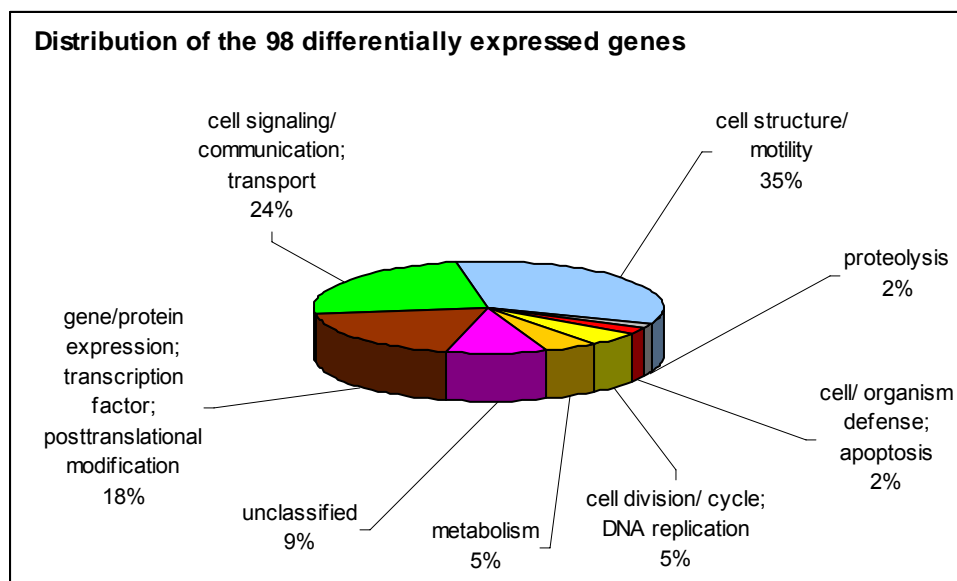


**Figure 36: Distribution of the biological function of the 98 individual genes** that were found differentially expressed over time by micro array experiment.

### 3.1.4.2. Evaluation of microarray data using qRT-PCR

The validation of micro array data by quantitative RT-PCR was performed for a random selection of 21 out of the 98 differentially expressed genes (figure 37). The so obtained data were compared with the results from the micro array analysis. In some cases – like fibromodulin (*Fmod*), multiple probes were spotted on the array and were compared with the real time data.

Decreasing expression over time (E11.5-E13.5) that was seen in the microarray experiments for matrilin 1 (*Matn1*), growth differentiation factor 10 (*Gdf10*), osteoglycin (*Ogn*), matrilin 4 (*Matn4*), decorin (*Dcn*), fibromodulin (*Fmod*, figure 37 top left), type XI collagen (*Col11a1*), aggrecan 1 (*Agc1*), and WNT1 inducible signaling pathway protein 1 (*Wisp*) was validated by qRT-PCR.

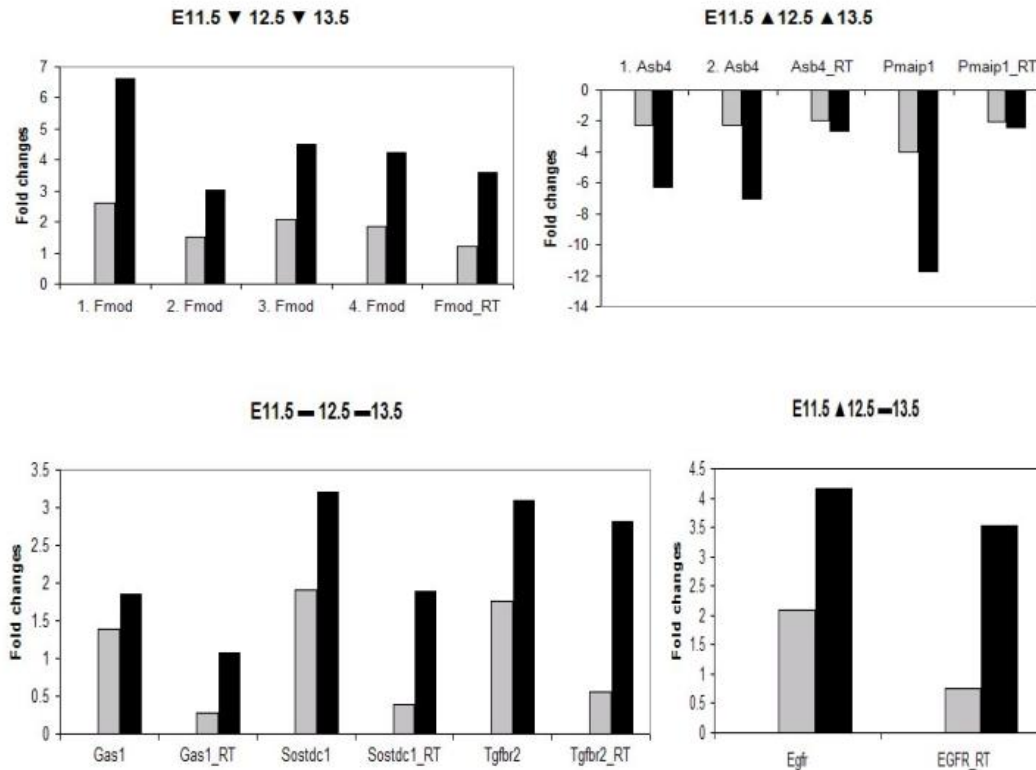


**Figure 37: Micro array data vs. qRT-PCR:** Micro array data showing normalized expression value differences. Data were converted into fold changes to allow direct comparison with fold changes obtained from quantitative RT-PCR (marked with '\_RT'). Expression at E11.5 was set to 0 and is therefore invisible. Expression at E12.5 was illustrated by the grey bar, expression at E13.5 by the black bar. Due to normalization, tendencies of fold changes do not represent tendencies in expression. Decreasing expression over time was shown for fibromodulin (*Fmod*); Increasing expression over time was confirmed for ankyrin repeat and SOCS box-containing protein 4 (*Asb4*) and phorbol-12-myristate-13-acetate-induced protein 1 (*Pmaip1*); Constant expression over time was validated for growth arrest specific 1 (*Gas1*), sclerostin domain containing 1 (*Sostdc1*), and transforming growth factor, beta receptor II (*Tgfb2*); First increasing, then constant expression was found in epidermal growth factor receptor (*Egfr*).

Increasing expression over time was validated for ankyrin repeat and SOCS box-containing protein 4 (*Asb4*), and phorbol-12-myristate-13-acetate-induced protein 1 (*Pmaip1*, figure 37 top right). Same expression levels at E11.5 and E12.5 and increasing expression at E13.5 were confirmed for solute carrier family 4, member 1 (*Slc4a1*) and cerebellin 1 precursor protein (*Cbln1*). Same expression levels at E11.5 and E12.5 and decreasing expression at E13.5 were validated for zinc finger homeobox 1b (*Zfhx1b*), Krüppel-like factor 1 (*Klf1*), and keratin complex 2, basic, gene 8 (*Krt2-8*). Increasing expression from E11.5 to E12.5 that stayed constant afterwards was validated for epidermal growth factor receptor (*Egfr*, figure 36 bottom right). As a control (figure 37, bottom left),

constant expression at all three time points was verified for sclerostin domain containing 1 (*Sostdc1*), transforming growth factor, beta receptor II (*Tgfb2*), fibroblast growth factor 12 (*Fgf12*), and growth arrest specific 1 (*Gas1*).

The qRT-PCR results from only two genes, *Matn1* and *Fgf12*, did not correlate with the micro array data, indicating that quantitative RT-PCR is a reliable method to validate the produced microarray data.

Investigations involving ISH and WISH will be needed to further evaluate the value of the obtained data. The creation of the micro array data was seen as an additional source of information to study the function of the identified genes in the human fetal cartilage cDNA library. Unfortunately, only 19 orthologues genes of the 98 differentially expressed mouse genes could be found in the human EST library.

### **3.2. *Lmx1b***

Appropriate limb development is partly due to *Lmx1b*, a LIM-homeodomain transcription factor, strongly expressed in dorsal mesenchymal tissues, as well as in anterior structures of the murine limb; this pattern of expression mimicks the anterior to posterior gradient of joint and nail dysplasia as seen in Nail-patella syndrome patients who harbors autosomal dominant LMX1B mutations [Dreyer et al., 2000]. Furthermore, *Lmx1b* is expressed in podocytes where it directly regulates the coordinated expression of the alpha-3(IV) and alpha-4(IV) collagen required for normal GBM morphogenesis [Morello et al., 2001]. Beside these two collagen chains and a couple of podocyte differentiation markers, no *Lmx1b* downstream targets have been identified in the limb to date. Therefore, tissues from kidneys and limbs isolated from wild type and mutant *Lmx1b* mice were utilized for further investigation.

### 3.2.1. Finding a downstream target of *Lmx1b*

Two approaches were performed to identify putative *Lmx1b* downstream targets, one proteomic based, the other one on RNA transcription level.

2D-gel electrophoresis with proteins isolated from E13.5 fore limbs (done by Dr. Dobrawa Napierala, Baylor College of Medicine, Houston, TX, USA) and newborn kidneys from *Lmx1b* knock-out vs. wild type mice were performed to find proteins that are differentially translated.

After computerized comparison of the 2D patterns (2.6.), twelve potentially interesting spots were sent to Dr. Arnie Falick (Howard Hughes Medical Institute Mass Spectrometry Laboratory, UC Berkeley, Berkeley, CA, USA) for protein identification (table 6).

Molecular weight	+/+ (Spot %)	-/- (Spot %)	Difference	Identified by mass spec	Accession #
E13.5 FORE LIMBS					
87,288	0.01	0.05	4.83	too weak	/
25,474	0.01	0.05	3.32	HMG-1	P07155
29,029	0.07	0.02	-4.22	<b>Carbonic anhydrase II</b>	NP_033931
27,080	0.03	0.00	-9.60	Ube2n (ubiquitin-conjugating enzyme E2N)	NP_542127
14,262	0.04	0.01	-5.08	Myosin light chain	
Not detectable	0.11	0.03	-4.02	Ubiquitin-conjugating enzyme	
NEWBORN KIDNEYS					
45,339	0.00	0.01	118.90	Proteasome subunit p45	P47210
24,648	0.02	0.08	5.09	Transforming protein RhoA	Q9QU10
18,049	-	0.06	+++	Fatty acid binding protein and Histone H4	P11404
146,373	0.07	0.01	-6.19	TER ATPase	Q01853
22,291	0.06	-	+++	<b>Agrn protein</b>	28175533
20,036	0.10	0.01	-12.34	Stathmin	P54227
14,245	0.52	0.07	-7.11	PPlase	P17742

**Table 6: Results from mass spectrometry analysis.** Increased polypeptide spots with a fold difference of  $\geq 3$  are highlighted in blue while decreased spots with a fold difference of  $\leq -3$  are highlighted in red.

From the initial twelve spots 2 proteins were of particular interest: Agrin (*Agrn*) that was less secreted in the kidneys of *Lmx1b* mutant mice, and carbonic anhydrase 2 (*Car2*) that was decreased in the *Lmx1b* mutant fore limbs. The other detected proteins have either functions in cell signaling and metabolism and are therefore ubiquitously expressed like the two ubiquitin-conjugating enzymes, prolyl isomerase (PPlase), proteasome subunit p45, fatty acid binding protein and histone H4, TER ATPase, and high mobility group 1 (HMG-1), or they are more generally involved in cytoskeleton assembly and function. RhoA for



instance is a small GTPase protein involved in the formation of stress fibers of the actin cytoskeleton. Myosins are responsible for actin-based motility in eukaryotic tissues, and stathmin regulates the dynamics of microtubules, one of three major components of the cell's cytoskeleton. A direct correlation between *Lmx1b* and these genes would have been more difficult to investigate with our current knowledge of limb and kidney formation..

Further analyses on the neuronal aggregating factor *Agrin*, a crucial molecule for the formation of neuromuscular junctions, did not confirm a down regulation at the RNA level: qRT-PCR did not show a significant difference of *agrin* expression in brain or kidney of newborn *Lmx1b* wild type mice vs. their knock-out littermates, nor did Northern blot hybridization on RNA derived from undifferentiated and differentiated podocyte cells [Mundel et al., 1997]. As *Lmx1b* deficient mice, *Agrin*-knock-out mice die right after birth. They do not form functional neuromuscular synapses [Bezakova and Ruegg, 2003]. *Lmx1b*-null mice show very poor breathing that could be due to non-functional synapses in the diaphragm, but immunohistochemical experiments with diaphragms of *Lmx1b* wild type and knock-out mice did not show differences for the neuronal markers neurofilament and  $\alpha$ -bungatoxin.

*Car2* deficiency was identified as the primary defect in osteopetrosis with renal tubular acidosis and cerebral calcification [Sly et al., 1983]. It is highly expressed in osteoclasts during bone resorption and mice exposed prenatally to acetazolamide - a *Car*-specific inhibitor and teratogen - develop an increased frequency of limb malformations [Scott et al., 1990].

To see whether a more sensitive method on RNA level can confirm the down regulation of *Agrin* and *Car2* in *Lmx1b* mutant mice, a micro array with RNA from whole kidneys of *Lmx1b* newborn wild type versus mutant mice was performed.

Unfortunately, not even the known *Lmx1b* downstream targets like *Col4a4*, or *Col4a3* appeared to be down regulated in this experiment. Only podocin expression was strongly reduced (data not shown), while *Agrin* expression remained unchanged. In the same experiment, expression of *Car2* remained unchanged, as well as in E11.5 *Lmx1b* mutant fore limbs.

These data suggested that RNA from whole kidneys was not useful to find downstream targets of a gene that is expressed specifically in podocytes only.

Therefore, glomeruli containing podocyte cells were laser captured and used for RNA preparation, amplification and micro array hybridization.

This time reduced expression of *Lmx1b* downstream targets like *Col4a3* and podocin was seen. Within the 60 most down regulated genes, only podocalyxin-like (*Podxl*) and Vanin 1 (*Vnn1*) appeared to be reasonable candidates. *Podxl* is thought to be a major component of the glycocalyx that covers foot processes of podocytes on their apical surface [Takeda et al., 2001], while *Vnn1* encodes a glycosylphosphatidylinositol-linked membrane-associated pantetheinase that is expressed in a sex-specific manner in mice. It was found to be co-expressed with the transcription factors *SF1* and *SOX9* and seemed to be necessary for normal Sertoli cell development [Wilson et al., 2005].

Further studies were not very successful, and this was also due to the fact that *Lmx1b*-deficient mice die a few hours after birth, when a good percentage of podocytes haven't yet reached full maturity.

To identify *Lmx1b* downstream targets in the limb instead, a third approach based on RNA transcriptional level was taken: RNA was extracted from wild type and knock-out *Lmx1b* E11.5 fore limb buds and further processed for micro array analysis.

#### **3.2.1.1. Differentially expressed genes in fore limb buds**

After normalization, 1295 genes showed at least a significant 2-fold difference of expression in the mutant E11.5 compared to the wild type limb buds.

Within the first 20 most down regulated genes (table 7), there were some with known functions in endochondral bone and joint development, like *Smad6*, *Gdf5*, and *Fzd2*. Others were less clearly linked to these processes and could be potential new candidate genes. After searching the literature, Neuropilin 2 (*Nrp2*), single-stranded DNA binding protein 2 (*Ssbp2*), peroxisome proliferative activated receptor gamma, co-activator 1 alpha (*Ppargc1a*) and short stature homeobox 2 (*Shox2*) were selected for further analysis.

ProbeSet	Gene Symbol	RMA_KO-WT	Gene Title
1456778_at	<b>Nrp2</b>	-2.164	Neuropilin 2, mRNA (cDNA clone IMAGE:3968483)
1435349_at	<b>Nrp2</b>	-2.08	neuropilin 2
1422616_s_at	Wdr54	-1.988	WD repeat domain 54
1449054_a_at	Pcbp4	-1.946	poly(rC) binding protein 4
1418532_at	Fzd2	-1.915	frizzled homolog 2 (Drosophila)
1460336_at	<b>Ppargc1a</b>	-1.893	peroxisome proliferative activated receptor, gamma, coactivator 1 alpha
1416746_at	H2afx	-1.834	H2A histone family, member X
1418139_at	Dcx	-1.832	doublecortin
1422771_at	Smad6	-1.825	MAD homolog 6 (Drosophila)
1422440_at	Cdk4	-1.793	cyclin-dependent kinase 4
1427739_a_at	Trp53	-1.765	transformation related protein 53
1418476_at	Cr1f1	-1.735	cytokine receptor-like factor 1
1437192_x_at	Vdac1	-1.726	voltage-dependent anion channel 1
1433496_at	Glt25d1	-1.697	glycosyltransferase 25 domain containing 1
1449815_a_at	<b>Ssbp2</b>	-1.685	single-stranded DNA binding protein 2
1439148_a_at	Pfkl	-1.671	phosphofructokinase, liver, B-type
1417359_at	Mfap2	-1.654	microfibrillar-associated protein 2
1416183_a_at	Ldh2	-1.641	lactate dehydrogenase 2, B chain
1419139_at	Gdf5	-1.639	growth differentiation factor 5
1438042_at	<b>Shox2</b>	-1.565	short stature homeobox 2

**Table 7: 20 most down regulated genes in microarray experiment performed with E11.5 wild type vs. knock-out fore limb buds.** Potential *Lmx1b* downstream targets are indicated in red.

Although *Nrp2* was mainly described in neuronal development, it is also expressed in podocytes and during limb development [Giger et al., 2000; Villegas and Tufro, 2002]. *Ppargc1* was identified as a co-activator of *Sox9* during chondrogenesis [Kawakami et al., 2005], and may therefore be important during mesenchymal condensation. *Shox2* was shown to act upstream of the *Runx2* gene, another key regulator of chondro-osteogenesis [Cobb et al., 2006], and *Ssbp2* interacts with the homeodomain transcription factors *Ldb1* (in mouse) and *Chip* (in *Drosophila*), and was found to be important for *Drosophila* wing development [van Meyel et al., 2003]. Because this evidence appeared to link the potential candidate genes to chondrogenesis or limb development, further investigations were undertaken to gain additional insights.

### 3.2.1.2. Evaluation of micro array experiment using qRT-PCR

Gene expression was investigated by qRT-PCR with newly generated cDNA from *Lmx1b* wild type and mutant E11.5 fore limb buds for several genes that have defined functions in limb bud and/or cartilage development. Due to the numerous qRT-PCRs performed and the limited amount of material, every experiment was done only once and has therefore no statistical relevance. Nevertheless, the results illustrated a consistent pattern between wild type and mutant tissues, suggesting a generalized downregulation of several genes involved in endochondral bone formation.

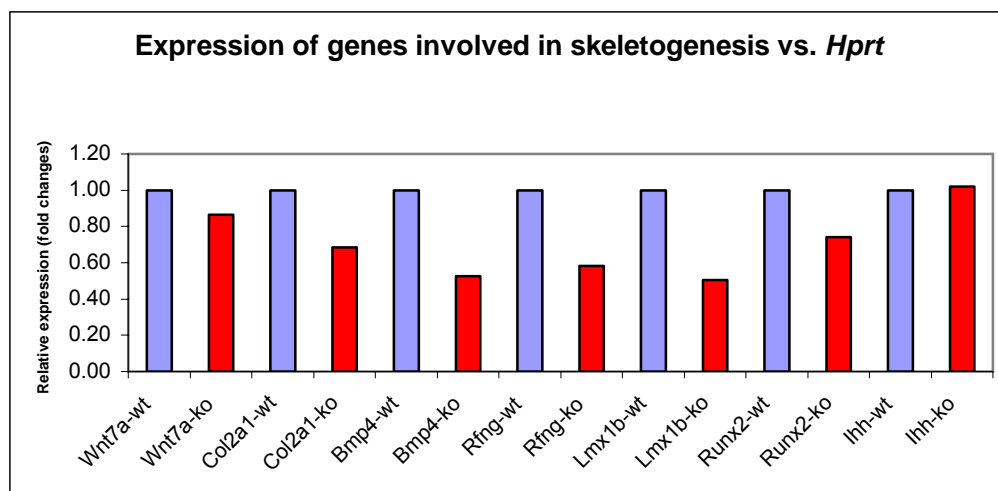


**Figure 38: Expression** (illustrated in fold changes) **of genes involved in skeletogenesis vs. housekeeping gene *Hprt***. Blue bars correspond to relative expression in wild type (wt) tissues, while red bars correspond to the expression in mutant (ko) tissues. *Wnt7a*: wingless-type MMTV integration site family, member 7A; *Col2a1*: procollagen, type II, alpha 1; *Bmp4*: bone morphogenetic protein 4; *Rfng*: radical fringe gene homolog; *Lmx1b*: LIM homeobox transcription factor 1 beta; *Runx2*: runt related transcription factor 2; *Ihh*: Indian hedgehog.

*Lmx1b* expression was reduced by 50% in the mutant tissue (figure 37). *Wnt7a*, an upstream inducer of *Lmx1b*, remained almost unchanged, as well as *Ihh* and the ventrally expressed *En1* (figures 38, 39), that have important functions during chondrogenesis and limb bud development.

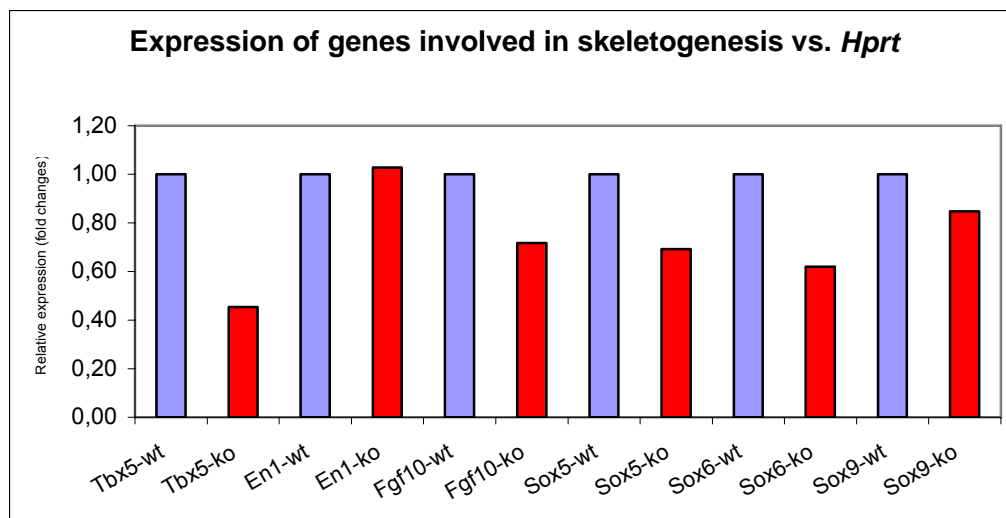


**Figure 39: Expression** (illustrated in fold changes) **of genes involved in skeletogenesis vs. housekeeping gene *Hprt***. Blue bars correspond to relative expression in wild type (wt) tissues, while red bars correspond to the expression in mutant (ko) tissues. *Tbx5*: T-box 5; *En-1*: engrailed 1; *Fgf10*: fibroblast growth factor 10; *Sox5*: SRY-box containing gene 5; *Sox6*: SRY-box containing gene 6; *Sox9*: SRY-box containing gene 9.

About 40-60% reduction was seen for *Rfng*, *Tbx5*, *Bmp4*, and *Sox6*, while *Sox9*, *Sox5*, *Col2a1*, *Fgf10*, and *Runx2* showed about 15-40% less expression in the mutant tissue (figures 38, 39).

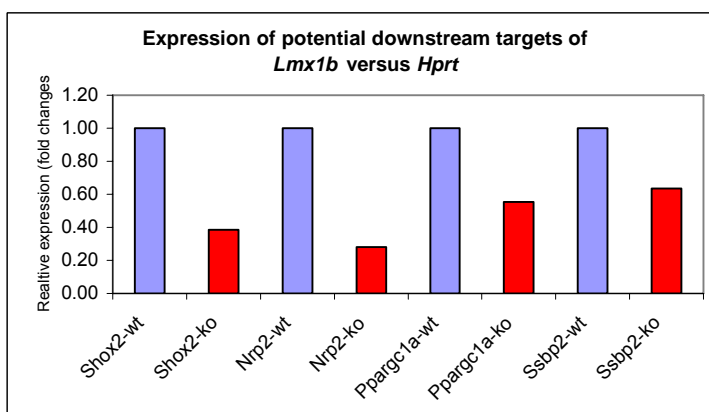


**Figure 40: Relative expression** (illustrated in fold changes) **of potential *Lmx1b* downstream targets versus housekeeping gene *Hprt***. Blue bars correspond to relative expression in wild type tissues, while red bars correspond to the expression in mutant tissues. *Shox2*: Short stature homeobox 2; *Nrp2*: Neuropilin 2; *Ppargc1*: peroxisome proliferative activated receptor, gamma, co-activator 1 alpha; *Ssbp2*: single-stranded DNA binding protein 2.

For the four potential *Lmx1b* downstream targets -*Shox2*, *Nrp2*, *Ppargc1a*, and *Ssbp2*- that were selected after the micro array experiment, a down regulation in the mutant tissue was confirmed by qRT-PCR (figure 40), and further investigations by WISH were also performed.

### 3.2.2. Evaluation of microarray experiment using WISH

#### 3.2.2.1. Whole mount *in situ* hybridization for *Lmx1b*

To have a reference for further hybridizations of wild type and knock-out *Lmx1b* mouse embryos, whole mount *in situ* hybridization was first performed for *Lmx1b* itself (figure 41). The probe, a 565 bp product from the 3'UTR of *Lmx1b*, was previously generated from mouse adult total kidney RNA [Dreyer et al., 2004]. As expected hybridizing an E11.5 wild type embryo with the *Lmx1b* antisense probe resulted in specific staining of the dorsal part of the limb bud (figure 40A middle and 40B), while the same hybridization of a mutant embryo showed reduced staining in the same tissues (figure 41, right), and the control hybridization with the sense probe remained unstained (figure 41A, left).

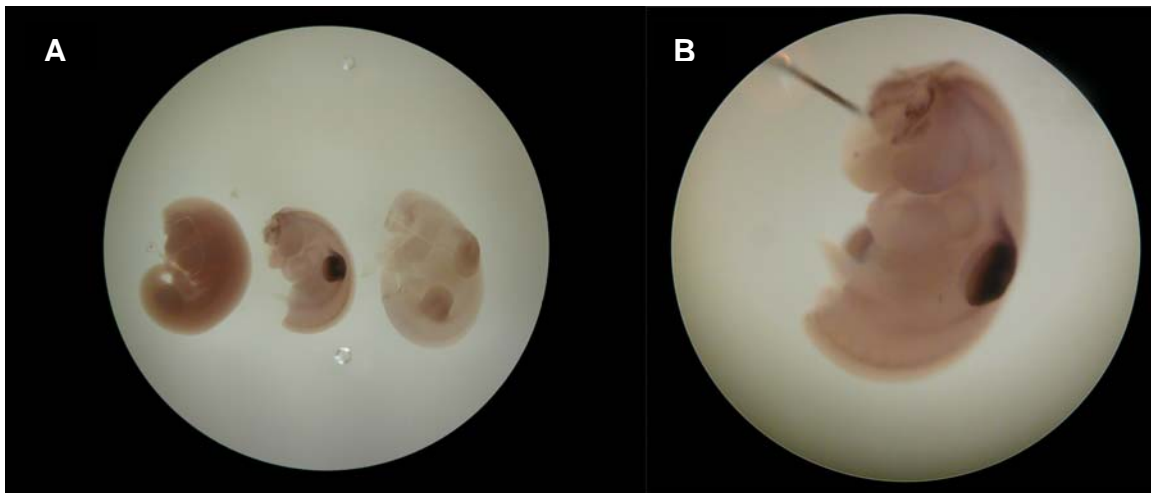


**Figure 41: WISH with *Lmx1b* specific probe on E11.5 embryos**, head and hind limbs partly disrupted. A: wild type hybridized with sense probe, wild type hybridized with antisense probe, mutant hybridized with antisense probe; B: wild type hybridized with antisense probe.

#### 3.2.2.2. Whole mount *in situ* hybridization for putative *Lmx1b* downstream targets

Whole mount *in situ* hybridization was performed for all four potential *Lmx1b* downstream targets *Shox2*, *Nrp2*, *Ppargc1*, and *Ssbp2*. Specific staining was obtained for all four genes (data not shown), but only *Shox2* and *Nrp2* showed specific expression in the limb buds (figures 42, 43). While the expression for *Shox2* was almost unchanged in the mutant embryos compared to wild type littermates, the expression of *Nrp2* was clearly reduced in the knock-out (figure

42A). Interestingly, the expression pattern of *Nrp2* in the limb buds was similar to what was found in WISH for *Lmx1b* (figures 40B, 41B) - both genes being expressed in the dorsal mesenchyme of the limb bud.



**Figure 42:** From left to right, **WISH with *Shox2* specific sense probe** on E12.5 embryo (head partly disrupted), and with *Shox2* specific antisense probe on E13.5, E12.5, and E11.5 embryos.

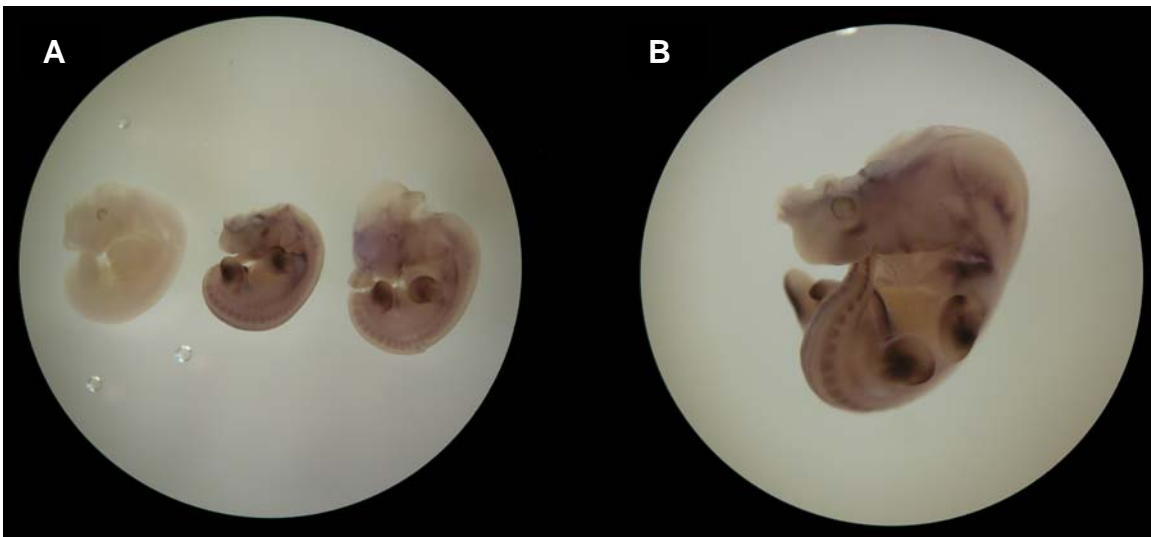


**Figure 43:** **WISH with *Nrp2* specific probe** on E11.5 embryos, heads partly disrupted. A: From left to right, wild type hybridized with sense probe, wild type hybridized with antisense probe, mutant hybridized with antisense probe; B: wild type hybridized with antisense probe.

### 3.2.3. Neuropilin 2 (*Nrp2*)

From these data, *Nrp2* appears to be an interesting potential *Lmx1b* downstream target. Importantly, *LMX1B* binding sites that were described in previous studies [Dreyer et al., 1998; German et al., 1992; Miner et al., 2002], were found at a

high score in the putative *Nrp2* promoter with the 'Patser' tool [Hertz and Stormo, 1999], suggesting a likely upstream role of *Lmx1b* in the transcriptional regulation of *Nrp2* (personal communication with Dustin Baldrige and Dr. Rui Chen at Baylor College of Medicine, Houston, TX, USA).

Mice deficient for *Nrp2* had been generated by others [Giger et al., 2000] and were requested. Further analyses and interaction studies are on their way and will hopefully confirm the hypothesis that *Nrp2* is a novel *Lmx1b* downstream target during limb bud development.

### 3.3. Genitopatellar Syndrome (GPS)

To investigate the pathogenic mechanism of the rare GPS that has a similar clinical phenotype to NPS, six patients with clinical Genitopatellar syndrome (table 8) were involved in this study. Mutation screening, array based comparative genome hybridization (aCGH), fluorescence *in situ* hybridization, as well as quantitative RT-PCR were performed to identify the chromosomal region and the candidate genes that might be responsible for GPS. With one newly added patient (#152-01-01), only 16 patients were described in the literature to date [Schlaubitx et al., 2007].

#### 3.3.1. Patient # 152-01-01

Patient # 152-01-01 is a Caucasian female (figures 44 A-E) that was born in August 1994 by Cesarean-section delivery at 36 weeks gestation when her length was 48.3 cm, the weight 2.5 kg, and the head circumference 30.2 cm. Initial exam revealed an innocent heart murmur that resolved spontaneously, and bilateral club feet which were treated with serial casting and surgery. At six months of age, hypoplastic ridged fingernails (figure 44B), and unusual knee contours were noted (figure 44C), and she was diagnosed with Nail-Patella syndrome [Schlaubitx et al., 2007].



Patient number		152-01-01	152-02-01	152-03-01	152-04-01	152-05-01	152-06-01
Physician/ Publisher		Smith/ Keller	Reardon (2002)	Abdul-Rahman et al. (2006)	Abdul-Rahman et al. (2006)	Lammer & Abrams (2002)	Lifchez et al. (2003)
Sex		♀	♂	♂	♀	♀	♂
Karyotype		46, XY	46, XY	46, XY	46, XX	46, XX	46, XY
Current Age & Life Status		12 years, alive	5 years, alive	3 years, alive	1 years, alive	7 years, alive	4 years, alive
Neurologic	Microcephaly	-	+	+	+	+	+
	ACC	-	+	+	+	-, thin	+
	Hypoplasia	as infant		+	+	+	as infant
	Hearing loss	-	-	+	+, mild	-	
Minor facial anomalies	Hair	thick	thin scalp	thin scalp	thin scalp	thin scalp	thin scalp
	Broad large nose	+	+	+			+
	Micrognathia	-	+			-	-
	Low ears	+		+	+	-	+
	Chin	small, pointed				normal	disproportiona l long
Flexion deformities	Hypertelorism					+	
	Hips	+	+	+	+	+	-
	Knees	+	+	+	+	+	+
	Club feet	+	+	+	+	+	+
	Elbow	+	-		+, radioulnar synostosis	hyper- extensible	+
	Toes/ talipes	equinovarus	+		overlapping toes	+	+, mild
Skeletal	Brachydactyly	-	-			-	
	Hip dislocation	-	-			-	
	Pelvic hypoplasia	-	-		+	-	
	Radial head deformity	+	-		+, radioulnar synostosis	-	
	Ribs	right 11, left 10			cervical	11 pairs	hypoplastic first pair
	Scoliosis	+, mild	-			-	
	Delayed tooth eruption					+	+
Patellae	Rudimentary	+					
	Displaced	+					
	Normal size (Clinically) absent		+	+	+	+	+
Cardiac		HM at birth, - at 8 years	- HM at 4 years	PDA	ASD, PA sling	ASD Secundum	
Lung		-	-	T	Pulmonary, Hypopl.	+, mild T	T, L, PRE
Renal		O	H	P, H	H, MCK Hypoplasia	AU	U, H
Anogenital anomalies	Clitoral abnormality					Hypoplasia	
	Scrotal hypoplasia	+	+	+		N/A	+
	Cryptorchidism	+	+, No left- sided gonad	+, bilateral		N/A	
	Hermaphrodite	+	-			N/A	
	Ovotestes	+	-			N/A	
	Displaced anus	-	-		+	+	
Others	Hypoplastic & ridged nails	+				-	
Early Development	Nipples	hypoplastic				inverted	
		Rolling at 7 months	No speech at 4 years, sits securely	No language, at 2.5 years, sits only with support	~ Develop- mental age of 1 month at 7 months	No language at 40 months	~ Develop- mental age of 5 months, motor age of 3 months at 2 years
		Sitting at 12 months	Bottom shuffles				
		Walking at 24 months					

**Table 8: Phenotypic comparison among Genitopatellar Syndrome patients;** Hypopl.: hypoplasia; ACC: Agenesis of corpus callosum; HM: Heart murmur; T: Tracheomalacia; L: Laryngomalacia; PRE: poor respiratory effort; O: Oligohydramnios; P: Polyhydramnios; U: Ureterohydronephrosis; H: Hydronephrosis; MCK: Multicystic kidneys; AU: Abnormal ultrasound; PDA: Patent Ductus Arteriosus; ASD: Atrial Septal Defect; PA: Pulmonary Atresia.

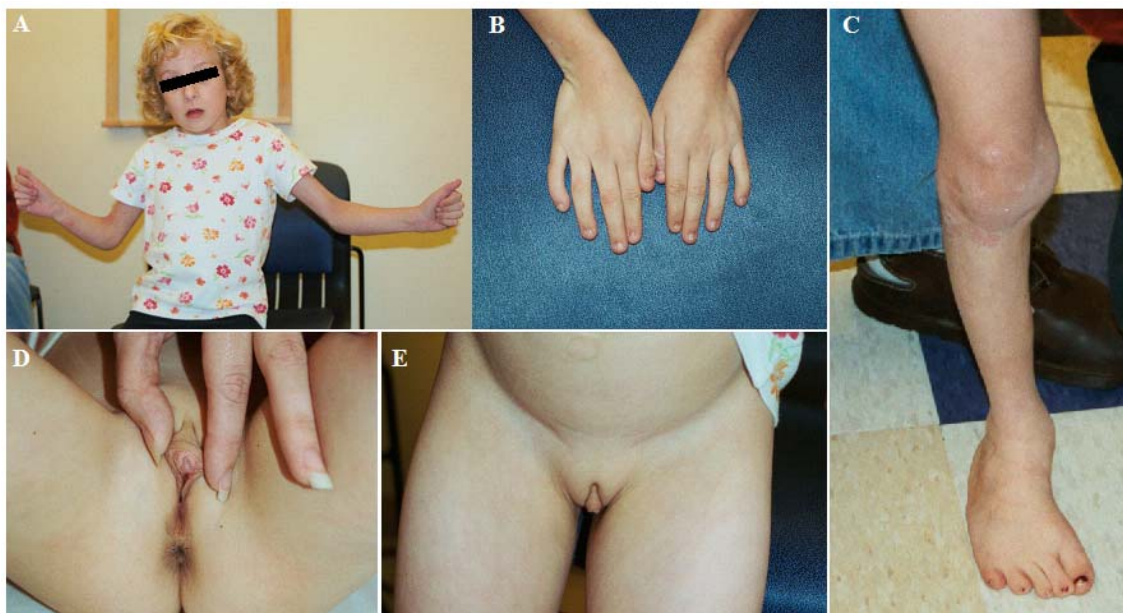


**Figure 44: Patient # 152-01-01;** A: patient at 8 4/12 years of age with flexion deformities of the elbow and a long nose with broad nasal tip; B: Hands with hypoplastic fingernails; C: Right leg with rudimentary and displaced patellae and surgical corrected clubfoot; D-E: Ambiguous external genitals: phallic structure with retractable foreskin as well as vaginal introitus. Anus was not displaced (pictures provided by Laurie D. Smith).

Genital exam performed at that time revealed a normal appearing vaginal introitus and clitoromegaly. At one year of age, bilateral inguinal hernias were noted. During herniorrhaphy, inguinal testes were discovered and laparoscopic evaluation failed to demonstrate the presence of an uterus. Histopathologic evaluation of the excised gonadal tissue revealed bilateral ovotestes with attached Müllerian and Wolffian duct remnants (figure 45).

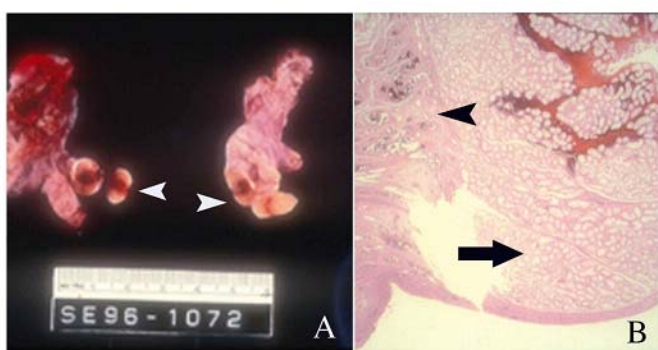


**Figure 45:** A: Gross pathology of ovotestes and associated structures, arrows point to ovotestes; B: Histopathology of ovotestes, arrow points to testicular tissue, arrowhead point to ovarian tissue. Note juxtaposition of ovarian and testicular tissue (pictures provided by Laurie D. Smith).

Chromosome analysis in blood revealed a 46,XY karyotype (figure 46), and fluorescent *in situ* hybridization for *SRY* and the chromosome X centromere

(figure 47), as well as subtelomeric FISH evaluation confirmed the typical male pattern.

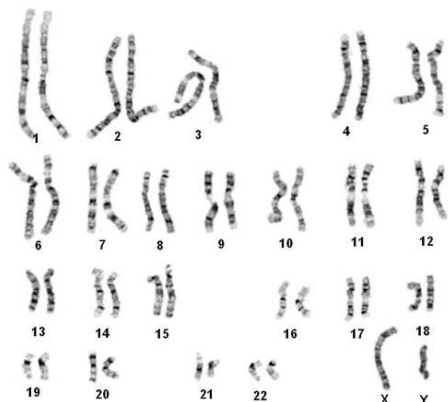


**Figure 46: Karyotype of patient # 152-01-01 demonstrating a 46,XY karyotype** (picture provided by Laurie D. Smith).

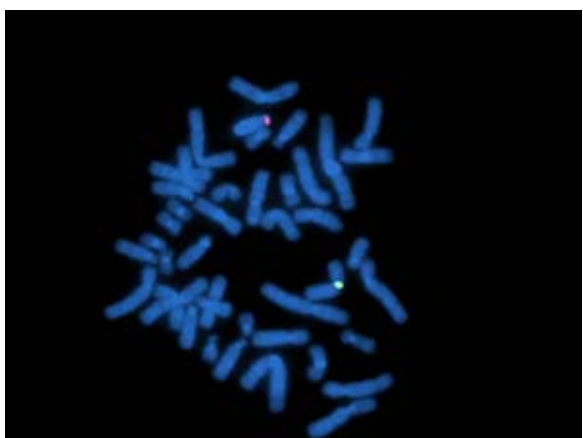


**Figure 47: FISH analysis for a SRY specific probe (red signal) and a centromer probe (green signal)**, picture provided by Laurie D. Smith.

Her 7-dehydrocholesterol levels were normal, excluding Smith-Lemli-Opitz syndrome (SLOS). A review of the patient's development revealed global developmental delay. She rolled over at 7 months, sat at 12 months, and walked at 24 months of age. She experienced secondary encopresis after 2 years of age, but this spontaneously resolved by 6 years of age. She is currently enrolled full time in a junior high school special education program. She knows her letters, some colors, and some body parts. She can count to 100 and is unusually skilled at putting together jigsaw puzzles. On examination, she readily and independently completed a 70 pieces puzzle. She has partially unintelligible

speech with echolalia and preservation. Her adaptive age at her most recent examination, performed at 11 years and 2 months, was 2 years and 9 months. At that time, her height was 109.6 cm (<5%, mean for 5-6 years), her weight was 24.4 kg (<5%, mean for 7-8 years) and her OFC was 52.7 cm (75-80% for age). She had coarse facies, a prominent metopic suture with ridging, large forehead, a broad nasal tip, slightly down slanting palpebral fissures and small, slightly low-set ears, a high arched palate, and a pointed chin (figure 43A). There was significant nuchal webbing and thick hair. Her nipples were widely spaced and hypoplastic. Her abdomen was normal with the exception of a small umbilical hernia. Genital exam revealed what appeared to be an elongated clitoris with a redundant clitoral hood (figure 44E). The urethral meatus was situated at the tip of this clitoric structure. A small opening suggestive of a vaginal introitus or a residual urogenital fold and sinus was present. The anus was patent and not displaced (figure 44D). Musculoskeletal exam revealed severe elbow contractures with inability to extend beyond 55 degrees and mild pterygia of the right elbow (figure 44A). Patellae were rudimentary bilaterally and displaced superiolaterally (figure 44C). Fingers and wrists were mildly hyperextensible. Fingernails and toenails were ridged and hypoplastic with radial digits more severely affected (figure 44B). There was impressive scapular winging bilaterally. A skeletal survey revealed mild valgus deformity of the lower extremities with shortening of the proximal and distal fibulae, bilaterally dislocated radial heads and mild scoliosis of the spine. There were 11 ribs on the right and 10 on the left. Mildly delayed bone age -estimated at eight years and ten months of age- was also present. Based on the laboratory and clinical findings, this patient was diagnosed with evidence of sex-reversal and features of nail patella syndrome that together fit within the spectrum of genitopatellar syndrome.

### 3.3.2. Mutation screening

Mutation screening for *LMX1B* was performed, because of the knee abnormalities that are common to both GPS and NPS. Since no pathogenic mutation in *LMX1B* was detected, *WNT7A* was screened next, as it was shown

to be an upstream regulator of *Lmx1b* in mouse models and involved in the development of the Müllerian ducts, and hence, in the establishment of the mammalian female reproductive tract [Chen and Johnson, 2002; Parr and McMahon, 1998]. More recently, mutations in *WNT7A* were shown to cause a range of limb malformations, including Fuhrmann Syndrome and Al-Awadi/ Raas-Rothschild syndrome (AARRS) and Schinzel-phocomelia syndrome [Woods et al., 2006]. Although the patient has a XY,46 karyotype, *WNT4* was screened as well, because of its involvement in the initial development of the Müllerian duct in both sexes and the suppression of Leydig cells by upregulation of *DAX1* (dosage-sensitive sex reversal, adrenal hypoplasia congenital, critical region on the X chromosome, gene-1/ *NR0B1*) that is necessary for gonad development [Jordan et al., 2001; Meeks et al., 2003]. It was also reported that targeted deletion of *Wnt4* in mice causes the masculinization of XX pups [Vainio et al., 1999]. Therefore, *WNT4* seemed a strong candidate gene for sex-reversal phenotypes in human [Jordan et al., 2001]. *TBX4* that is associated with Small Patella Syndrome (SPS) characterized by aplastic or hypoplastic patella, foot and femur anomalies, but no renal pathology [Bongers et al., 2004], was screened as well, although it seemed a less likely candidate for such a complex phenotype. Overall, no pathogenic mutations were found in *LMX1B*, *WNT7A*, *WNT4*, or *TBX4*.

### 3.3.3. Array-based comparative genomic hybridization

To identify possible genome wide imbalances and aberrations, array-based comparative genomic hybridization was performed with two different BAC DNA micro arrays. The first BAC array was consisting of over 20,000 individual clones prepared as described previously [Cai et al., 2002; Yu et al., 2003]. This was followed by a second, independent, array analysis using a higher density BAC array consisting of 32,447 BAC clones [Ishkanian et al., 2004; Krzywinski et al., 2004], using similar procedures described previously [de Vries et al., 2005]. Because of the finding of sex reversal, patient # 152-01-01 was hybridized against a female control pool, while the other five patients were hybridized

against pooled DNA from the opposite gender. A 3.07 Mb deletion including the loci for *NR5A1*, *NR6A1*, *PBX3*, *LMX1B*, *ANGPTL2*, and *GARNL3* was detected in the patient 152-01-01 using both aCGH platforms (figures 48, 49, table 9), whereas the other 5 patients showed normal aCGH profiles.

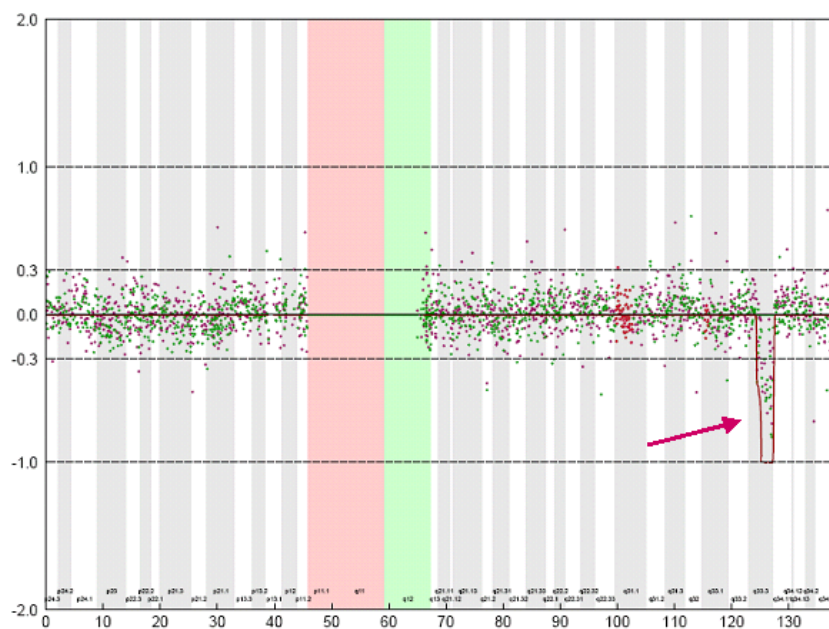


**Figure 48: Array CGH profiles of chromosome 9 of patient # 152-01-01;** profile obtained by tiling resolution aCGH containing 32,447 BAC clones (2. performed array). On the x-axis, all 1,219 chromosome 9 clones are ordered by Mb position and on the y-axis log<sub>2</sub> T/R ratios are shown. Hidden Markov Model (gray line) was used to identify duplications and deletions. Patient 152-01-01 shows a 3.07 Mb deletion on 9q33.3 (arrow); picture provided by Lisenka E. Vissers.

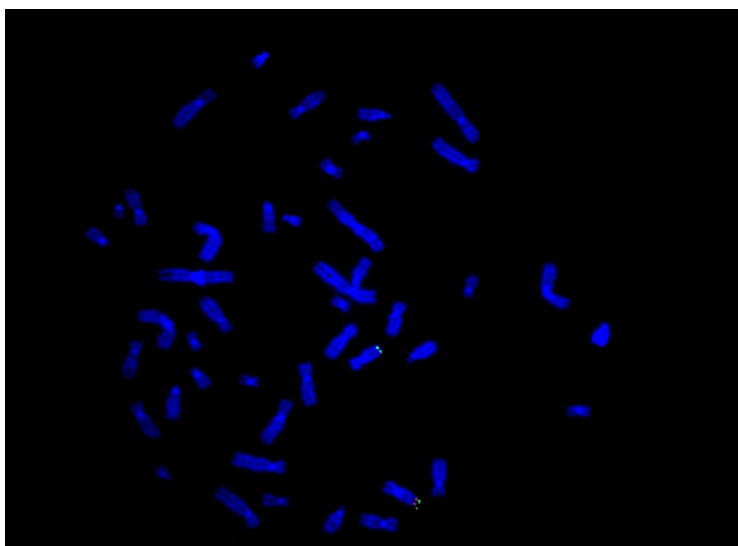


**Figure 49: FISH for *LMX1B* (red signal) and telomere control probe (green signal);** picture provided by Svetlana A. Yatsenko.

Additional attention was given to the chromosomal loci of genes that were previously screened for mutations as well as genes that are associated with abnormalities in genitourinary development, like *WT1*, *DAX1*, *SOX9*, *DMRT1*, *DMRT2*, *GATA4* or *PAX2*. However, aCGH did not reveal alterations on 3p25.1 (*WNT7A*), 17q23.2 (*TBX4*), 1p36.12 (*WNT4*), Xp21.2 (*DAX1*), 17q24.3 (*SOX9*), 9p24.3 (*DMRT1* and *DMRT2*), 8p23.1 (*GATA4*), 10q24.31 (*PAX2*) and 11p13 (*WT1*) in any of the patients' DNAs that were analyzed.

### 3.3.4. Determination of the breakpoints

Probes	Approximate physical map position (Mp) <sup>*</sup>	Genetic marker	Signal on del (9)	Performed analysis
RP11-259C15	124.105-124.268	<i>PSMB7</i>	+	FISH
RP11-13C11	124.272-124.316	<i>GPR144</i>	+	aCGH
G248P87289H2	124.278-124.318	<i>GPR144</i>	+	FISH
RP11-412C6	124.282-124.433	<i>NR5A1</i>	+ dim	FISH
G248P85560F9	124.296-124.338	<i>NR5A1</i>	+ dim	FISH
RP11-121K12	124.330-124.517	<i>NR6A1</i>	-	aCGH
RP11-164H5	124.339-124.513	<i>NR6A1</i>	-	FISH
RP11-85C21	124.352-124.519	<i>NR6A1</i> / <i>D9S1840</i>	-	aCGH
RP11-599P14	124.582-124.758	<i>D9S117</i>	-	aCGH
RP11-474P12	124.758-124.887	<i>D9S1723</i>	-	FISH
RP11-314M22	124.865-125.007	<i>D9S1825</i>	-	aCGH
RP11-924K18	125.130-125.327	<i>D9S1925</i>	-	aCGH
RP11-161P7	125.143-125.317	<i>GAPVD1</i>	-	aCGH
RP11-184B22	125.144-125.331	<i>D9S1925</i>	-	FISH
RP11-12A16	125.437-125.438		-	FISH
RP11-65F7	125.689-125.878	<i>PBX3</i>	-	aCGH
RP11-106B17	125.950-126.129	<i>D9S1139</i>	-	aCGH
RP11-343J18	125.955-126.116	<i>D9S1139</i>	-	FISH
RP11-516D6	126.236-126.389	<i>C9orf28</i>	-	aCGH
RP11-205K6	126.296-126.460	<i>D9S1821</i>	-	aCGH
G248P85477D7	126.360-126.396		-	FISH
RP11-123K19	126.391-126.570	<i>LMX1B</i>	-	FISH/ aCGH
G248P81148A7	126.402-126.441	<i>D9S1821</i>	-	FISH
G248P800687F3	126.438-126.480	<i>LMX1B</i>	-	FISH
G248P88856C3	126.468-126.508	<i>LMX1B</i>	-	FISH
RP11-489N22	126.497-126.680	<i>LMX1B</i>	-	FISH
G248P84893D6	126.505-126.548	<i>LMX1B</i>	-	FISH
RP11-809P3	126.680-126.909	<i>RALGPS1</i>	-	aCGH
RP11-106H5	126.702-126.727	<i>RALGPS1</i>	-	aCGH
RP11-926G7	126.877-127.055	<i>ANGPTL2</i>	-	aCGH
RP11-1M19	126.930-126.964	<i>ANGPTL2</i>	-	FISH
RP11-689B7	126.971-127.149	<i>GARNL3</i>	-	aCGH
RP11-430F11	126.980-127.178	<i>GARNL3</i>	-	FISH/ aCGH
RP11-356B19	127.186-127.411	<i>SLC2A8</i>	+	FISH
RP11-81N19	127.190-127.379	<i>D9S1819</i>	+	aCGH
RP11-373J8	127.409-127.430	<i>C9orf88</i>	+	FISH
RP11-42D4	127.421-127.584	<i>STXBP1</i>	+	aCGH

**Table 9: Summary of analysis defining breakpoints on chromosome 9q33.3-q34.11 for patient # 152-01-01;** <sup>\*</sup>The map position and location of genetic markers is based on information from the UCSC genome browser, freeze 2004 (<http://genome.ucsc.edu>); +: not deleted; -: deleted; + dim: partially deleted

The distal and proximal breakpoints of the micro deletion in patient # 152-01-01 were confirmed by fluorescent *in situ* hybridization (FISH) that was performed following routine procedures using GTG-banded metaphase chromosomes from peripheral blood leukocytes of all six patients at 550-600-band resolution. The BAC and fosmid clones spanning the region of interest were selected from UCSC genome browser and are listed in table 9. Two fosmids, G248P87289H2 and G248P85560F9, were selected for fine mapping of the proximal breakpoint just upstream of *NR5A1* in patient # 152-01-01 (figure 50). FISH using BAC clones RP11-430F11 and RP11-356B19, with the first one being deleted but not the second, identified the distal breakpoint of the deletion in patient # 152-01-01.

Additionally, five fosmids (G248P85477D7, G248P81148A7, G248P800687F3, G248P88856C3, G248P84893D6) spanning the 5' end of *LMX1B* as well as 100 kb upstream of the *LMX1B* start codon, were used for FISH to exclude possible inversions of putative regulatory elements located between *LMX1B* and *NR5A1* in any of the patients (personal communication with Dr. Ian McIntosh), but none were found (data not shown).

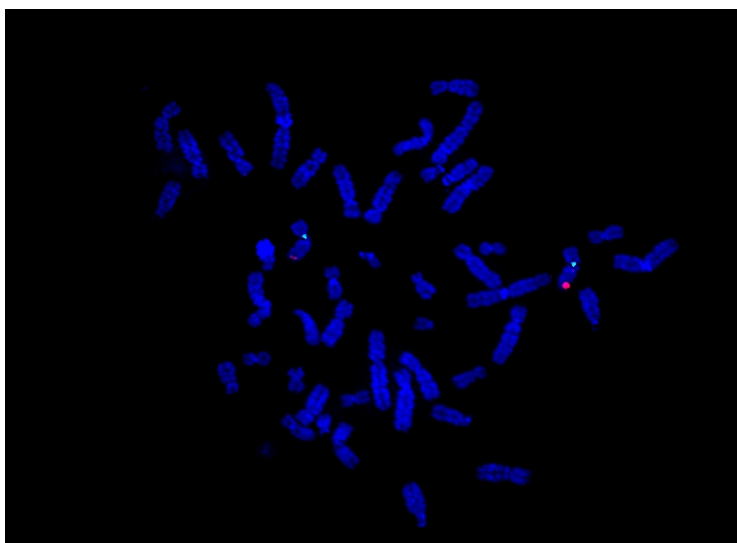


**Figure 50: FISH for G248P85560F9 (red signal) and control centromere probe (green probe) to verify proximal breakpoint; picture provided by Svetlana A. Yatsenko.**

### 3.3.5. Quantitative RT-PCR for genes within the micro deletion

A dosage dependent effect of genes located within the micro deletion of patient # 152-01-01 was investigated using material from EBV-transformed lymphoblasts



for qRT-PCR. First, cDNA from EBV-transformed lymphoblasts was used in a standard reaction with *LMX1B*-specific primers and LightCycler® FastStart DNA Master SYBR Green I (Roche, Indianapolis/IN, USA). Different primers and MgCl<sub>2</sub> concentrations and template amounts did not allow a specific amplification of the *LMX1B* gene. Therefore, the *LMX1B* gene specific Universal Probe Library #28 (Roche, Indianapolis/IN, USA) was used for further investigations. The Universal Probe Library is a set of 165 real-time PCR probes that allows amplification of any transcript. The probes are only 8-9 nucleotides long and dye labeled at their 5' and 3' end. Amplification was performed with a set of PCR primers, designed with the ProbeFinder software (Roche, Indianapolis, IN, USA), in a qRT-PCR reaction with LightCycler® TaqMan® Master (Roche, Indianapolis/IN, USA) and the Universal Probe. The gene specific primers supposedly allowed the amplification of the transcript that the specific Universal Probe binds to. The binding of the probe is detected by its degradation during PCR amplification thus setting free the bound fluorescence dye that gets detected. Although the conditions were optimized, amplification of the extreme GC-rich *LMX1B* gene failed. To by-pass influences of transcribing the lymphoblast RNA into cDNA, one-step RT-PCR reactions using the LightCycler® RNA Amplification Kit SYBR Green I (Roche, Indianapolis, IN, USA) was performed next, but no reproducible results were obtained for *LMX1B*, as well as for *NR5A1* and *NR6A1* and housekeeping gene *HPRT*. After all, it was not clear whether EBV-transformed lymphoblasts could be used to research dosage dependent effects, since the transformation procedure may have a certain impact on the copy number of each gene.

## 4. Discussion

The Nosology Group of the International Skeletal Dysplasia Society reported 372 osteochondrodysplasias and genetically determined dysostoses in 2007 [Superti-Furga and Unger, 2007]. For 215 of these conditions, an association with one or more genes can be recognized, while the molecular changes, responsible for the remaining 157 syndromes, remain elusive to date. Although several new genetic disorders were characterized since the previous report [Hall, 2002], more investigations will be needed in the future.

But bone and cartilage are inconvenient tissues to work with. Especially cartilage is hard to obtain, and the amount is stunted. Extraction of nucleic acids or proteins is difficult because of the collagen fibers and ECM proteins that make it a partly elastic, partly hard tissue. Therefore, resources for research are very limited and efficient screening approaches needed to obtain a maximum of information.

In this thesis two different approaches were followed. Firstly, a high throughput EST sequencing project from a human fetal cartilage library was performed to identify novel or known genes involved in early skeletal development (20<sup>th</sup> week of gestation until 2<sup>nd</sup> year of life); these could then be investigated as potential candidate genes for one or more of the 157 bone disorders with underlying gene mutation or pathogenic mechanism that are still unknown to date.

Secondly, a disease-orientated approach was undertaken to identify downstream targets of *LMX1B*, the gene causing Nail-Patella syndrome (NPS), to better understand the dorsal-ventral patterning of the limb. This process may help to find out the molecular mechanisms behind other conditions with aplasia or hypoplasia of the patella, including isolated patella aplasia hypoplasia (PTLAH), Meier-Gorlin syndrome, and genitopatellar syndrome which remain elusive to date [Bongers et al., 2005b]. Beside two proteomic approaches, three microarray experiments with murine tissues were performed to investigate potential downstream targets.

Furthermore, six patients with genitopatellar syndrome could be enrolled in a study to investigate the molecular changes responsible for this relatively rare

disease. This syndrome usually presents as a distinct entity from NPS but with a similar clinical phenotype.

#### **4.1. EST project**

Three high throughput strategies are used in molecular biology to identify and characterize expressed genes within a tissue of interest: serial analysis of gene expression (SAGE), microarray technology, and expressed sequence tag (EST) sequencing. SAGE is a method for comprehensive analysis of gene expression patterns and generates libraries from RNA material of interest [Velculescu, 1999; Wang, 2007]. During the SAGE procedure, a short sequence tag (10 -14 bp) from a defined location within a transcript is generated that contains sufficient information to identify uniquely that transcript. Several tags are arranged in concatemers that are cloned and sequenced afterwards. Determining the abundance of individual tags and identifying the gene corresponding to such tag can quantitatively evaluate the expression pattern of any population of transcripts. ([www.sagenet.org](http://www.sagenet.org)). Doing so, the expression of mRNA from two different tissues can be compared. Microarray technology allows fast analysis of gene expression in a parallel format [Schena et al., 1995; Stears et al., 2003] by using RNA from different tissues of interest. Microarrays contain a large number of genes and are therefore useful to quickly survey a certain number of them or when the sample to be studied is small. Microarrays may be used to assay gene expression within a single sample or to compare gene expression in two different cell types or tissue samples, such as in healthy and diseased tissue. Because the expression of hundreds or thousands of genes can be examined at once, microarray studies represent an important and necessary tool in understanding and cataloging the transcriptome ([www.ncbi.nlm.nih.gov](http://www.ncbi.nlm.nih.gov)). EST sequencing projects allow the systematic sequencing of random cDNA clones, resulting in short Expressed Sequence Tags (EST) that are usually long enough to identify the transcript of origin [Adams et al., 1991; Nagaraj et al., 2007]. Sequencing of cDNA libraries to generate large numbers of ESTs, combined with bioinformatics, was proven to be a useful procedure to

evaluate the gene expression profiles in tissues of interest and to identify novel genes that might be tissue specific and key players during growth, differentiation and/or tissue/organ homeostasis.

Cartilage EST sequences are underrepresented in the published gene clusters [Tagariello, 2005], that provide transcriptional information about each gene and are stored in public databases like NCBI UniGene. 31 UniGene libraries from connective tissues are available, but most of them were generated from chondrosarcoma cell lines or rheumatoid arthritic tissue that are of little use for investigations of early skeletogenesis processes in healthy humans or other species. Beside the previously described four cartilage libraries [Tagariello, 2005], including one library from normal cartilage and three from osteoarthritic cartilage, representing a total of 17,598 sequences, only two libraries from chondrocyte cell culture provide additional information (HCHON2, Lib. # 18386 with 9,357 ESTs; CONS2, Lib. # 12662 with 2,501 ESTs). Within the last two years, the total numbers of ESTs increased from about 5 millions to 6.73 millions, and the number of clusters from 53,256 to 123,993 (as of June 2007) [Tagariello, 2005]. The number of cartilage libraries stayed the same, indicating the fact that cartilage sequences are overall still underrepresented. Published data were obtained from a murine growth plate cartilage library of 4 weeks old BALB/c mice [Okihana and Yamada, 1999], the comparison of 5,000 ESTs from human adult normal and osteoarthritic cartilage [Kumar et al., 2001], more than 13,000 ESTs from fetal femoral cartilage (8<sup>th</sup> –12<sup>th</sup> week) [Zhang et al., 2003], as well as 6,266 ESTs from articular surfaces of two fetuses (18<sup>th</sup> –20<sup>th</sup> week) [Krakow et al., 2003; Pogue et al., 2004]. No data were available from genes specifically expressed within the second half of gestation until early childhood. While primary ossification centers are already established before birth, secondary ossification centers develop after birth. Therefore, the present EST study, examining material from the 20<sup>th</sup> week of gestation until the 2<sup>nd</sup> year of age, analyzes genes that are involved in these important processes and were not considered in previous studies. This may indeed provide critical novel information about these early stages of skeletogenesis.

#### 4.1.1. Comparison of the present library with previously published studies

Aside from pilot studies involving the sequencing of 250 ESTs [Stelzer, 2000], the project was started in 2000. Since the library was already generated, RNA was not available anymore and EST sequencing was the only possible method to identify the genes expressed in this tissue. In May 2001, 850 sequences were analyzed and 74% of them matched with known genes and ESTs/ cDNAs. This number increased to 76% in September 2002 (4748 ESTs total), and reached 80% in May 2007 (figure 17). This indicates the constantly increasing amount of information within the databases that made it possible to identify more sequenced ESTs over time. Categorization regarding their function (figure 17) was possible with the help of databases like 'Geneontology' (<http://www.geneontology.org>) that started their service in 2002 and was therefore not available for previous analysis.

In comparison to other cartilage EST projects [Jung et al., 2004; Zhang et al., 2003], the 5000 EST sequences, consisting of 1573 individual transcripts, showed an analog distribution. As described earlier [Tagariello et al., 2005], the highest percentage was observed for genes involved in regulation of gene expression and posttranslational modifications (30%, figure 17), followed by cell signaling genes (22%) and metabolic genes (12%). A similar distribution was seen for the fetal cartilage library from 8<sup>th</sup> –12<sup>th</sup> week [Zhang et al., 2003], as well as in a library generated from the human chondrosarcoma cell line HCS 2/8 [Jung et al., 2004]. But in contrast to the cartilage tissue libraries, genes involved in cell structure and motility constituted the second largest group in the HCS 2/8 cells, and cell signaling genes ranked forth [Tagariello et al., 2005]. This might be due to an overall reduced cell signaling and dedifferentiation in the cancer cell culture.

Unfortunately, detailed information about the functional distribution were neither available from the murine cartilage ESTs, nor from the human adult and fetal cartilage projects (8<sup>th</sup> -12<sup>th</sup> week) [Kumar et al., 2001; Okihana and Yamada, 1999; Pogue et al., 2004].

However, more details were published about single genes. Highest frequency was seen for *COL2A1* in all the fetal libraries (table 3). This was expected, since *COL2A1* represents about 85% of the collagen in hyaline cartilage and

is considered the marker gene for proliferating chondrocytes. Type IX collagen is usually found in tissues containing *COL2A1*. And indeed, *COL9A1*, *COL9A2*, and *COL9A3* were found at high frequency in the present study (0.84%) as well as in cartilage from 8<sup>th</sup>–12<sup>th</sup> week (0.9%) [Zhang et al., 2003] and 18<sup>th</sup>–20<sup>th</sup> week (5.49%) [Pogue et al., 2004]. The expected molar ratio between the three type IX collagens (1:1:1) was not seen in any of the projects and *COL9A1* showed the highest frequency in all three libraries. Another collagen that is closely associated with both type II and type IX collagen in thin collagen fibrils of hyaline cartilage is type XI collagen. The chondrocyte marker gene *COL11A2* was found 9 times in the present study, representing 0.18% of all the ESTs. It was also found in cartilage from the 8<sup>th</sup>–12<sup>th</sup> week (0.25%) [Zhang et al., 2003], and 43 times in material from the 18<sup>th</sup>–20<sup>th</sup> week (0.69%) [Pogue et al., 2004].

Type I collagens are strongly expressed in mesenchyme and prechondrocytes, and their expression decreases during endochondral bone formation [Olsen et al., 2000]. That could explain the overall percentage decrease in tissues from the 8<sup>th</sup>–12<sup>th</sup> week, the 18<sup>th</sup>–20<sup>th</sup> week to the present study (1.82%, 0.1%, 0.24%, respectively). The expected ratio of *COL1A1*/*COL1A2* (1:2) was almost reached for cartilage from 8<sup>th</sup>–12<sup>th</sup> week (90:154 copy numbers), but not in the present study (9:2) and in cartilage from 18<sup>th</sup>–20<sup>th</sup> week (3:3), probably due to an insufficient amount of sequenced clones. During tissue collection for this study, zones of hypertrophic chondrocytes were avoided. Therefore, type X collagen was not identified and was also seen only once in cartilage from the 18<sup>th</sup>–20<sup>th</sup> week of gestation. As expected, it was present in the cDNA library from human adult cartilage material [Kumar et al., 2001].

Although type VI collagen has mainly been associated with muscle disorders [Lampe and Bushby, 2005], *COL6A1* and *COL6A2* were found within the collagens of the present study (0.16%), as well as in cartilage from the 18<sup>th</sup>–20<sup>th</sup> week (0.23%).

Beside *COL2A1*, there were 15 ribosomal proteins, 2 matrix metalloproteinases (*MMP1*, *MMP3*), 2 ferritins (*FTH1*, *FTL*), 2 heat shock proteins (*HSPA5*, *HSP90B1*), two eukaryotic translation elongation factors (*EEF1A1*, *EEF1G*), the tumor protein *TPT1*, as well as MAP kinase interacting

serine/threonine kinase 2 (*MKNK2*), and the two ECM proteins fibronectin (*FN1*) and osteonectin (*SPARC*) within the genes with frequencies  $\geq 20$  (figure 18). The strong presence of ribosomal proteins, heat shock proteins, eukaryotic translation elongation factors, and tumor protein is due to their ubiquitous expression and important function in almost all cellular processes. For instance, ferritin proteins assure the intracellular iron storage. Due to the high collagen content in bone and cartilage, matrix metalloproteinases, like *MMP1* that degrades collagen, need to be present. In contrast, *MMP3* is able to cleave other ECM proteins, like the highly presented *FN1* or *SPARC*, but not the fibrillar collagens. Although there are no comparable data available, the presence of the most frequent genes appears reasonable and the study therefore valuable.

In cartilage from the 8<sup>th</sup>-12<sup>th</sup> week [Zhang et al., 2003], the 10 most abundantly expressed genes included, beside *COL2A1*, four more collagens (*COL1A2*, *COL1A1*, *COL9A1*, and *COL3A1*), the eukaryotic translation elongation factors *EEF1A1*, and four ribosomal proteins. In cartilage from the 18<sup>th</sup>-20<sup>th</sup> week [Krakow et al., 2003; Pogue et al., 2004], six collagens were among the 14 highest expressed genes (*COL2A1*, *COL9A1*, *COL9A2*, *COL9A3*, *COL11A1*, and *COL11A2*), as well as three more ECM components (*FMOD*, *HAPLN1*, and *SPARC*), the two matrix metalloproteinases *MMP3*, and *MMP13*, two widely expressed heat shock proteins (*HSPA8*, *HSPA1A*), and the eukaryotic translation elongation factor *EEF1A1*. The list of the highest expressed genes in these two other fetal cartilage EST projects are overall well comparable to what was seen in the present study. A comparison with the most abundant genes in normal adult articular cartilage [Kumar et al., 2001] revealed a very different distribution. 14 genes were found more than 20 times. Within these genes, not a single collagen was present. Six of the most common ECM components (*DCN*, *FN1*, *VIM*, *COMP*, *MGP*, *CHI3L1*), the matrix metalloproteinase *MMP3*, the metabolic genes *GPX3* and *CLU*, the signaling proteins *APOD*, *TXNIP*, and *CFH*, the tumor protein *TPT1*, as well as the transcriptional regulator *TSC22D3* were found instead (figure 18). The authors explain the extremely low expression of collagens, especially *COL2A1*, with the long half-time of this protein in articular cartilage as described previously [Maroudas, 1980]. Additionally, adult cartilage does not

proliferate nearly as often as fetal cartilage, so genes mainly involved in proliferation, like collagens, are less expressed. The strong expression of the anti-oxidant enzyme *GPX3* was explained as being needed in articular chondrocytes to produce hydrogen peroxide for the depolymerization of hyaluronic acids [Tiku et al., 1990]. However, the strikingly different expression pattern in the adult cartilage library is probably due to its preparation from articular cartilage only, versus fetal cartilage libraries that were prepared from femoral cartilage [Zhang et al., 2003], growth plate and articular cartilage [Krakow et al., 2003], and growth plate cartilage (present study) [Tagariello et al., 2005]. Furthermore, adult cartilage is in a homeostatic phase, so genes involved in early skeletogenesis were not expected at high levels. The distribution of genes seen in adult cartilage is very different from what was previously seen in fetal cartilage. The present study investigated genes at the transition from fetal to adult cartilage and is therefore important to understand the changes observed.

When comparing proteoglycans, a certain amount of them were seen in each library (table 4), but the percentage distributions were found very variable. 11 proteoglycans were seen in the present study (0.79%), with the highest expression (9 times) for biglycan (*BGN*), followed by vimentin (*VIM*), aggrecan (*AGC1*), and fibromodulin (*FMOD*) (figure 20). Although biglycan is an important factor of the ECM and targeted disruption led to reduced bone growth [Corsi et al., 2002], biglycan expression was not reported for adult cartilage [Kumar et al., 2001] and cartilage of the 8<sup>th</sup>- 12<sup>th</sup> week [Zhang et al., 2003] and was less expressed in the 18<sup>th</sup> – 20<sup>th</sup> week [Pogue et al., 2004]. Vimentin instead was seen with higher expression in the 18<sup>th</sup> – 20<sup>th</sup> week [Pogue et al., 2004] and the adult study, but not at all in the 8<sup>th</sup>- 12<sup>th</sup> week [Zhang et al., 2003]. Aggrecan and fibromodulin were relatively strong detected in all the libraries. All other observed proteoglycans were found with very variable percentages (table 4).

Within other ECM components (table 4), osteonectin (*SPARC*), fibronectin (*FN1*), hyaluronan and proteoglycan link protein 1 (*HAPLN1/ CRTL1*), chondromodulin (*CHM-1*), cartilage oligomeric matrix protein (*COMP*), and matrix *Gla* protein (*MGP*) were seen at variable expression frequency.



The detected ECM components have functions in different cells and stages of skeletogenesis. While *FN1* is a marker of early cartilage development [Peters et al., 2002], *SPARC* as well as *HAPLN1* have important functions in hypertrophic chondrocytes [Alford and Hankenson, 2006; Watanabe and Yamada, 1999]. Biglycan and decorin were described to play important roles in the differentiation of osteoblast precursors, as well as in regulating osteoclast differentiation [Bi et al., 2006; Kamiya et al., 2001]. Together with fibromodulin, they belong to the family of small leucine-rich proteoglycans and are associated with the fibrillogenesis of collagens [Douglas et al., 2006; Font et al., 1998].

Unfortunately, no correlation could be made between the expression profiles of the ECM components and the frequency changes in the cartilage libraries from different time points.

After all, statements about frequencies and percentages must be reported with caution. Towards the end of the world wide human genome project in 2001, it was estimated that there are about 40,000 human genes [Venter et al., 2001]. Sequencing and analyzing only a couple of thousands ESTs from one tissue can therefore give just an idea of the real gene distribution. Not even the sequencing of 13,155 cartilage ESTs [Zhang et al., 2003] allowed realistic molar ratios between certain collagens. This suggests that a multiple amount of EST sequences of the 40,000 expected genes would be required to obtain data reflecting the *in vivo* situation, but that would increase the costs of the experiments dramatically.

Still, to obtain an overview of the genes expressed in cartilage at different time points, the comparison of cartilage cDNA libraries generated from cartilage RNA at different developmental stages can be a valuable tool for better understanding the different signaling pathways during cartilage development. More detailed studies are now performed by using microarray experiments which are considered a more accurate and cheaper method allowing the creation of expression profiles for several thousand of genes at the same time.

#### **4.1.2. Advances in skeletogenesis research**

Because most expression studies are now done by microarray technology, EST sequencing projects have become rare in these days. But while EST projects have the purpose to collect information about the genes that are represented in a tissue of interest, microarrays are mainly used as a comparative tool and hence needs two different types of tissues. During the analysis of the present study, possible array solutions were discussed. One possibility would be to spot a representative number of 50 bp-oligos, representing candidate and cartilage specific genes from the library, on arrays and to hybridize them with RNA from human mesenchymal stem cells, differentiated either toward the osteogenic or chondrogenic pathway. These cells were available through Prof. Dr. Franz Jakob (Orthopedic University Clinic, Würzburg, Germany). The cost for synthesizing the projected 500 50bp-oligos would have been too high, and although very interesting the project was therefore not further pursued.

Another approach would be to generate a full-length (and higher quality) cDNA library from 1g of mRNA isolated from human fetal growth plate cartilage (15<sup>th</sup> – 19.5<sup>th</sup> week) that was provided by Prof. Jerry Pelletier (McGill University, Montreal, Canada). The lengths of the clones in the present library were relatively short (1200 bp maximum) and a minority of the clones contained full-length genes. This was probably due to a high degree of RNA degradation during the library preparation in the early 1990s, when less than perfect techniques were available or published. To generate a high quality normalized and subtracted full-length cDNA library with a protocol provided by Dr. Piero Carninci (RIKEN Tsukuba Institute, Tsukuba, Japan), an extensive hands-on experience would have been required. Since the RIKEN Institute generated only mouse libraries at that time, Pierre Beurang from Five Prime Therapeutics (San Francisco, CA, USA) was contacted to generate a full-length library following the RIKEN protocol from human material. Unfortunately, the quality of the submitted RNA did not reach the standards of the company and a library could therefore not be generated. Subsequently, a previously considered generation of cDNA libraries from osteogenic and chondrogenic differentiated human mesenchymal stem cells was abandoned due to the associated expensive collecting efforts and lack of experience.

In the meantime, a great number of microarray experiments were published providing more knowledge about tissue specific expression in cartilaginous and bony tissues. The increased sensitivity of the microarray method was due to technical advances. Thanks to e.g. laser capture microscopy, even single cells can be extracted from a tissue, thus reducing the chances of contamination with unwanted material. New RNA extraction kits, and more reliable RNA amplification methods require less starting tissue material for downstream hybridization on improved microarrays. Especially for a tissue that is as difficult to obtain as human cartilage, these refinements will have a great impact in future cartilage research.

Most supportive for the present study are recently published microarray data that were performed using tissues obtained with laser captured proliferative and hypertrophic chondrocytes pooled from 6 and 7 weeks old rat growth plates [Wang et al., 2004], with murine E12.5 forelimb versus hindlimb autopod [Shou et al., 2005], or with laser captured articular and resting zone chondrocytes from E14 growth plate [Yamane et al., 2007]. The data obtained from different time points during cartilage development will help to further understand and interpret the expression pattern and function of several genes affecting skeletogenesis.

The most recent human study compared the profile of genes expressed in femur cartilage (18<sup>th</sup>-22<sup>nd</sup> week) to their expression in 34 non-cartilage tissues as stored in the CELSIUS database, generated by the UCLA microarray core (Los Angeles, CA, USA). As expected, cartilage-specific genes like *COL11A1*, *COL10A1*, *MMP13*, *AGC1*, and *HAPLN1* were found higher expressed in the femur dataset [Funari et al., 2007].

In the future, more disease oriented microarrays can be expected as well. Array hybridization utilizing RNA from affected vs. normal tissues may help to elucidate the genetic bases behind the 157 osteochondrodysplasias and dysostoses that are not yet understood.

To support and complement the present human EST sequencing study, the generation of a murine microarray was performed to obtain additional expression data for genes whose human orthologues were found in the EST project.

#### 4.1.3. Limb bud microarray

Human fetal cartilage is a rare and very difficult tissue to obtain. But the high homology between human and murine genes allows carrying out part of the analysis with murine tissues that are easier to obtain. To generate a set of supporting data that could help in the interpretation of detected human genes in the EST library, differential gene expression patterns over time was investigated in murine limb buds. Limb buds from E11.5, E12.5, and E13.5 were harvested to isolate RNA that was hybridized on Mouse 430 2.0 GeneChip® arrays (Affymetrix, Santa Clara, CA, USA), containing over 39,000 transcripts. The selected time points cover the timeframe just around the occurrence of precartilaginous mesenchymal condensation that starts at E12.0. In addition, the chosen time points fall in the beginning of the second half of mouse gestation. So they represent a similar time frame to that from which human material was used to generate the EST library (> 20<sup>th</sup> week). Genes that show significant changes in expression over time were expected to have important roles in limb bud development, and their orthologues should be considered as candidate genes for limb chondrodysplasias.

After normalization of the microarray data, 98 individual genes showed a statistically significant difference in the level of gene expression (at least 2-fold) (table 11, appendix 8.2.). Most of these genes (35%) were coding for structural and cell motility proteins. 9% of the genes were not further classified and could therefore represent genes with yet unknown roles in skeletogenesis. Within the structural protein, eight collagens (*Col5a1*, *Col5a2*, *Col6a1*, *Col6a2*, *Col6a3*, *Col8a2*, *Col11a1*, and *Col12a1*), and some of the known ECM components - fibromodulin (*Fmod*), gelsolin (*Gsn*), lumican (*Lum*), matrix Gla protein (*Mgp*), matrilin 1 and 4 (*Matn1*, *Matn4*), chondroitin sulfate proteoglycan 4 (*Cspg4*), and decorin (*Dcn*) - were detected (table 11, appendix 8.2.). Since the RNA was extracted from limb buds, the high percentage of ECM components was expected and therefore confirmed the quality of the data. Besides the ECM components other genes with known functions in limb development were also identified.

For instance, the signaling secreted protein frizzled B (FrzB) that controls the patterning of the developing body axis, is expressed in the anterior and posterior mesoderm and cartilaginous structures of the developing limb bud

[Leimeister et al., 1998] and showed an overall increase expression in the microarray study. This is supported by the fact that *Frzb* expression was weak in the fore- and hind limbs of E12.5, but uniformly distributed at E13.5 [Shou et al., 2005].

Dickkopf homolog 3 (*Dkk3*) was shown to affect *in vitro* and *in vivo* osteogenesis in C3H10T1/2 mesenchymal progenitor cells [Aslan et al., 2006].

Growth differentiation factor 10 (*Gdf10*) has dorsalizing activities and can induce endochondral bone formation in adult animals [Hino et al., 2004]. It is highly related to *Bmp3b* with which it defines a new subgroup within the larger TGF $\beta$ -superfamily [Cunningham et al., 1995].

Although this expression profile will help to understand the roles of single genes during mesenchymal condensation,, it is questionable whether the data obtained will help to complement the analysis of the human EST project since only 21 orthologue out of the 98 differentially expressed mouse genes were found in the human EST library (table 10).

Symbol	Name	Expression profile
<i>Anxa2</i>	annexin A2	•E11.5 — 12.5 ▼13.5
<i>Cspg4</i>	chondroitin sulfate proteoglycan 4	•E11.5 — 12.5 ▼13.5
<i>Col6a2</i>	procollagen, type VI, alpha 2	•E11.5 — 12.5 ▼13.5
<i>Fmod</i>	fibromodulin	•E11.5 — 12.5 ▼13.5
<i>Gsn</i>	gelsolin	•E11.5 — 12.5 ▼13.5
<i>Kcnk2</i>	potassium channel, subfamily K, member 2	•E11.5 — 12.5 ▼13.5
<i>MGI:2149786/Selm</i>	selenoprotein M	•E11.5 — 12.5 ▼13.5
<i>S100a10</i>	S100 calcium binding protein A10 (calpactin)	•E11.5 — 12.5 ▼13.5
<i>Smoc2</i>	SPARC related modular calcium binding 2	•E11.5 — 12.5 ▼13.5
<i>Col11a1</i>	procollagen, type XI, alpha 1	•E11.5 ▲12.5 —13.5
<i>Egfr</i>	epidermal growth factor receptor	•E11.5 ▲12.5 —13.5
<i>Samd4</i>	sterile alpha motif domain containing 4	•E11.5 ▲12.5 —13.5
<i>Agc1</i>	aggrecan 1	•E11.5 ▼ 12.5 ▼ 13.5
<i>Col6a1</i>	procollagen, type VI, alpha 1	•E11.5 ▼ 12.5 ▼ 13.5
<i>Cyt1</i>	cytokine like 1	•E11.5 ▼ 12.5 ▼ 13.5
<i>Dcn</i>	decorin	•E11.5 ▼ 12.5 ▼ 13.5
<i>Egfl6</i>	EGF-like-domain, multiple 6	•E11.5 ▼ 12.5 ▼ 13.5
<i>Lox</i>	lysyl oxidase	•E11.5 ▼ 12.5 ▼ 13.5
<i>Mgp</i>	matrix Gla protein	•E11.5 ▼ 12.5 ▼ 13.5
<i>Col12a1</i>	procollagen, type XII, alpha 1	•E11.5 ▼ 12.5 ▼ 13.5
<i>Tnc</i>	tenascin C	•E11.5 ▼ 12.5 ▼ 13.5

**Table 10: 21 out of 98 differentially expressed genes, whose orthologue genes were found in the cartilage EST project.**

Unfortunately, detailed expression data is only available for some of these 21 genes. An interpretation about the developmental expression pattern is therefore difficult, but was tried for some of the genes.

Although we currently don't know whether annexin2 or S100a10 expression decrease after day E12.5, it is reasonable to find the same expression profile for the two genes, since annexin2 is required for strong binding of S100A10 to the C-terminal domain of the protein Ahnak [De Seranno et al., 2006].

*Col11a1* transcripts were found to accumulate mostly in cartilaginous tissues, such as the chondrocranium and the developing limbs [Yoshioka et al., 1995]. An increase in its expression from E11.5 to E12.5 was observed which remained constant afterwards.

Detailed expression of *Col6a2* has not been described in early stages of development, E11.5-13.5. Its expression was found to be higher in articular versus growth plate cartilage [Yamane et al., 2007] which may explain the overall decrease over time.

Fibromodulin was expressed stronger in proliferating than in hypertrophic chondrocytes [Wang et al., 2004]: this might justify the tendency to decrease over time that was seen.

Examples of expression profiles inconsistent with the *in vivo* situation are those of decorin, matrix Gla protein (*Mgp*) and aggrecan1. *Mgp* is expressed by proliferating and late hypertrophic chondrocytes, but not by the intervening chondrocytes [Newman et al., 2001]. Decorin is related to chondrocyte hypertrophy and aggrecan is the main proteoglycan in articular cartilage and therefore a constant increase for both genes would have been expected. Unfortunately, qRT-PCR experiments for decorin and aggrecan1 confirmed microarray data which cannot be simply explained at this point.

Overall, mainly components of the ECM were present within these 21 genes as expected. An interpretation about all the genes is difficult, since detailed expression data are missing for most of them. Additional investigations using mesenchymal tissues at time of precartilaginous condensation will be needed to further confirm our data.

Some potential disease candidate genes were therefore analyzed, including their gene structure, conservation and expression in cartilaginous tissues.

Most of these investigations utilized murine tissues to overcome the lack of human material.

#### 4.1.4. EST clones B-C12 and ch32F03

EST clone B-C12 was selected for further investigations, because it is located on human chromosome 19q within a zinc finger gene cluster. Zinc finger genes mainly function as transcription factors and disfunctions in transcription factors often result in severe malformations. Most prominent examples in skeletogenesis are campomelic dysplasia caused by haploinsufficiency of the *SOX9* gene [Foster et al., 1994], or cleidocranial dysplasia caused by mutations in the transcription factor *RUNX2* [Mundlos et al., 1997]. Because of its 8 zinc finger domains, the previous gene nomenclature was change from *MGC4400* to *ZNF577*; it was found only once within the cartilage EST library. *ZNF577* also contains a KRAB domain, a transcriptional repressor module that can mediate gene silencing. Because the KRAB-containing, zinc finger transcription factor *Zfp60* was identified as a candidate regulator of cell differentiation in mouse calvaria primary cultures [Ganss and Kobayashi, 2002], and the KRAB-zinc finger protein *NT2* is a repressor of *Col11a2* cell-type-specific promoter activity [Tanaka et al., 2002], a similar important role in skeletogenesis was hypothesized for *ZNF577*. Unfortunately, no mouse gene could be identified to date and no data were obtained by the mouse limb bud microarray. Only the size of the human transcript was confirmed by northern blot hybridization. Further experiments were ruled out due to lack of human tissues to work with.

EST clone ch32F03 was selected for further studies because it showed 100% similarities to *CRELD2* which appeared four times in the cartilage EST library. *CRELD2* is a family member of *CRELD1* that showed specific staining in the mandibles and in the limb bud of chick embryos in whole mount *in situ* experiments [Rupp et al., 2002]. No statistically significant changes were seen for *Creld2* in the murine limb bud array. Therefore, the expression of *Creld2* was assayed in murine cell lines, tissues, and embryos by qRT-PCR, WISH, and ISH, but a specific expression in cartilage or bone was not found. Further experiments were therefore decided against. In the meantime, *CRELD1* was

associated with cardiovascular defects [Maslen et al., 2006; Robinson et al., 2003], while the function of *CRELD2* remains elusive to date.

#### 4.1.5. EST clone ch11g10 (Leucine rich repeat containing 59)

Homo sapiens leucine rich repeat containing 59 (*LRRC59*) was found twice within the 5,000 cartilage ESTs and was selected because of its interesting genomic location. *LRRC59* was mapped on human chromosome 17q21.33, near developmentally important genes like *WNT3*, *TBX4*, *COL1A1*, and *HOXB1-9*. While the *HOXB* genes are involved in the establishment of the anterior-posterior and the dorsal-ventral axis during vertebrate embryogenesis [Godsave et al., 1994], the other genes are mutated in skeletal diseases including tetra-amelia [Niemann et al., 2004], small patella syndrome [Bongers et al., 2004], and Osteogenesis imperfecta [Byers et al., 1982].

*LRRC59*, previously called *PRO1855* or *FLJ21675*, is highly conserved among a variety of species (figure 24) and its 307 amino acids contain four leucine rich repeats, a coiled coil motif and a transmembrane domain.

Quantitative RT-PCR showed highest expression in testis and ovary of adult mice, followed by newborn mouse calvarias and adult lung. Low expression was seen in newborn femoral cartilage, brain, heart, and kidney (figure 25), showing that *Lrrc59* is not a ubiquitously expressed gene.

The transcript of ~2900 bp was detected and confirmed by northern blot analysis in human chondrosarcoma cells, rat chondrosarcoma cells, and murine chondrocytes, but was not seen in rat osteosarcoma cells or murine fibroblasts (figure 26). From the study of these cell lines, it appears that the transcript is expressed in cell of chondrogenic, but not osteoblastic origin. The predominant expression in cartilaginous tissues was further confirmed by *in situ* hybridization, showing specific expression in proliferating chondrocytes at E13.5, but also in the inner cortex of long bones at E17.5 (figure 27 B, E). A parallel hybridization of *Lrrc59* and type X collagen on E15.5 limbs showed that the two genes are not co-localized. Instead, *Lrrc59* was expressed in areas surrounding the *Col10a1* positive hypertrophic chondrocytes (figure 27 H, I). Overall, the expression appeared weaker in the older specimens and less defined. Whole mount *in situ* hybridization did not show a specific expression, because *Lrrc59* is probably not expressed in embryos earlier than



E13.5. This is supported by the fact that significant expression changes were not seen in the limb bud array and that ISH had shown only a weak expression in proliferating chondrocytes of the ribs and even a weaker expression in the outgrowing limb buds. In summary, weak expression was seen in proliferating chondrocytes at E13.5 that became stronger in cells around hypertrophic chondrocytes at E15.5 and decreased in the inner cortex of long bones at E17.5. The fact that the transcript was detected in chondrogenic cell lines, but not in cells of osteoblastic origin, supports the hypothesis that *Lrrc59* could be primarily expressed in chondrocytes during skeletal development. As mentioned before though, it was also seen in other newborn and adult tissues.

To investigate its function, human databases were screened for proteins with similarity to LRRC59 (figure 29). The proteins fibromodulin, biglycan, decorin, lumican, and chondroadherin showed 33-41% homology to LRRC59, mainly within its first 104 amino acids. These proteins are all proteoglycans and their structural correlation to leucine-rich repeat containing proteins, like LRRC59, was described previously [McEwan et al., 2006]. Together they were classified into a family of small leucine-rich repeat proteins and proteoglycans (SLRP) that belongs to the leucine-rich repeat (LRR) superfamily. Their central LRR domain is flanked by conserved cysteine motifs. Additionally, most proteoglycans carry at least one glycoaminoglycan (GAG) chain of variable chemical composition which is an important feature for components of connective tissues.

All LRR proteins are thought to be involved in protein-protein interactions [McEwan et al., 2006; Weber et al., 1996]. SLRPs are involved in the organization of the ECM and have also effects on cell behaviour [Hocking et al., 1998]. The best described SLRP is decorin which interacts with fibronectin [Gendelman et al., 2003], type I collagen [Schonherr et al., 1995], thrombospondin [Winnemoller et al., 1992], epidermal growth factor receptor [Santra et al., 2002] and transforming growth factor-beta [Schonherr et al., 1998]. Decorin controls collagen fibrillogenesis and knock-out mice have fragile skin with markedly reduced tensile strength due to abnormal collagen morphology in skin and tendons [Danielson et al., 1997]. Mice deficient for other family members have similar phenotypes suggesting similar functions to

decorin, while double knock-out mice have more severe phenotypes [Ameye and Young, 2002].

LRR 1:ALPKATILDLSCNKLTTLPSTDFCG  
LRR 2:LTHLVKLDLSKNKLQQLPADFGR  
LRR 3:LVNLQHLDLLNNKLVTLPVSFQAQ  
LRR 4:LKNLKWLDLKDNPIDPVLAKVAGDC

**Figure 51: Leucine-rich repeats (LRR1-4) within LRRC59** contain the previously described LxxLxLxxNxL motif (marked in green) [Kajava, 1998]. A consensus leucine within the first LRR (LRR1) was substituted by a hydrophobic amino acid, here alanine.

LRR proteins consist of internal tandem repeats that are 20-29 amino acids long and rich in leucine and other small hydrophobic residues [McEwan et al., 2006]. These repeats contain a LxxLxLxxNxL motif [Kajava, 1998], with x being any amino acid and where the consensus leucines can be substituted by a hydrophobic amino acid. The LRRs within LRRC59 follow exactly this scheme (figure 51). Only within the first LRR, a consensus leucine was substituted by a hydrophobic amino acid, here alanine.

According to their phylogenetic relationship, the number of internal repeats and the spacing of cysteines, the proteoglycans were divided into subgroups (figure 52).

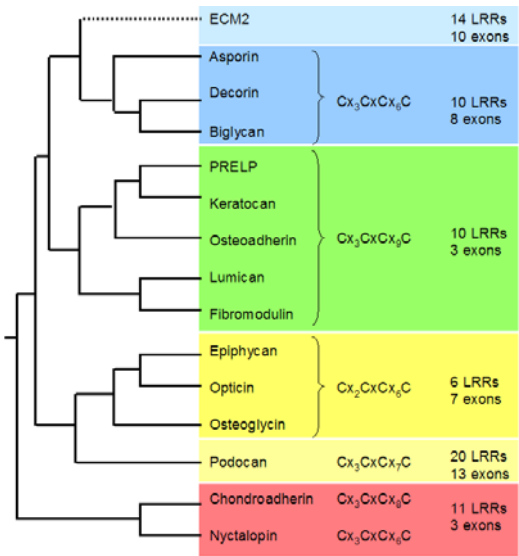


**Figure 52: Phylogenetic analysis of known SLRP** indicating the spacing of cysteines, the number of leucine-rich repeats (LRR) and the number of exons (adapted from McEwan et al., 2006; Ameye and Young, 2002; Henry et al., 2001).

Unfortunately, none of the previously described cysteine signatures can be seen in LRRC59 that in addition, has only 4 LRRs while the known SLRPs have 6-20 LRRs. Like LRRC59, asporin, decorin and biglycan consists of 8 exons, but these SLRPs all encode for 10 LRRs (figure 52).

Furthermore, other sequence characteristics like long stretches of negatively charged amino acids as seen in podocan and asporin [Henry et al., 2001; Lorenzo et al., 2001; Ross et al., 2003], or glycosylation sites were not found either.

Also the horse-shoe like 3D structure that has been reported for decorin [Scott et al., 2004], was not seen in LRRC59 (figure 53). Therefore, a putative interaction with the surface of collagen fibrils to protect them from cleavage by collagenases [Geng et al., 2006], is unlikely mediated by LRRC59.

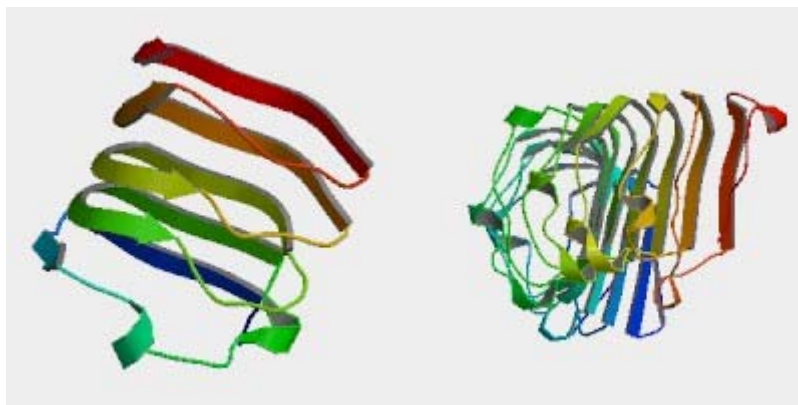


**Figure 53: 3D models of LRRC59 (left) and decorin (right)** created by ModBase (University of California, San Francisco/ CA, USA).

Although LRRC59 clearly belongs to the LRR superfamily, it may not be a SLRP. This is also supported by the fact that the transmembrane domain of LRRC59 suggests a cell membrane localization. LRRC59 has no signal peptide or potential glycoaminoglycan binding site, as confirmed with the programs SignalP 3.0 and NetNGlyc 1.0 (Center for Biological Sequence Analysis, Lyngby, Denmark). LRRC59 is therefore not posttranslational glycosylated and transported to the ECM like proteoglycans. Therefore, LRRC59 cannot be considered as a proteoglycan.

Not many other leucine-rich repeat transmembrane proteins have been described in the literature. FLRT1-3 have 10 leucine-rich repeats flanked by N-terminal and C-terminal cysteine-rich regions, a fibronectin/collagen-like domain, and an intracellular tail [Lacy et al., 1999]. They are expressed in kidney, brain, pancreas, skeletal muscle, brain, and heart, lung, liver, placenta, and heart, are glycosylated, and supposed to function in cell adhesion and/or receptor signaling. Some, like LRRTM1-4, were described in the nervous system where they are involved in the development and maintenance of the vertebrate nervous system [Lauren et al., 2003]. Fad158 (factor for adipocyte differentiation 158) contains 4 transmembrane domains and 8 leucine-rich repeats and was described as an early adipocyte differentiation regulator [Tominaga et al., 2004].

The fact, that LRRC59 is probably not a proteoglycan, makes it difficult to interpret its role in developing chondrocytes. Additionally, the co-localization with vinculin (figure 30) indicates that LRRC59 is connected to the cytoskeleton. Vinculin is a membrane-cytoskeletal protein that links integrin adhesion molecules to the actin cytoskeleton, while integrin can act as a receptor for collagen-binding SLRPs [Camper et al., 1997] or for collagen directly [White et al., 2004]. Since LRRC59 is not a SLRP and does not have the typical 3D structure of SLRPs, the hypothesis that LRRC59 might function in collagen fibrillogenesis as described for SLRP [Kalamajski et al., 2007; McEwan et al., 2006] needs to be further confirmed. Although there is no evidence yet that LRRC59 interacts directly with an ECM component, or with part of the cytoskeleton, it could be located within the cell membrane and act as an integral membrane protein. Here it might play a role in the attachment of a cell to the ECM and in signal transduction from the ECM to the cell.

Further investigation needs to address the question whether LRRC59 could interact with similar partners like the integral membrane protein integrin (figure 54). Therefore, possible interaction between talin or  $\alpha$ -actinin and LRRC59 will need to be investigated first. Talin is able to activate the  $\beta 3$  cytoplasmatic domain of integrin [Wegener et al., 2007] and doing so it links integrin to the cytoskeleton [Moes et al., 2007] via vinculin [Izard and Vonnrhein, 2004]. And  $\alpha$ -actinin has binding sites for vinculin [Kelly et al., 2006],  $\beta 1$  integrin [Kelly and Taylor, 2005], and f-actin [Hampton et al., 2007]. If an interaction of

LRRC59 with components of the ECM or the cytoskeleton can be confirmed, a knock-out model will probably help to reveal the function of LRRC59 in chondrogenesis.

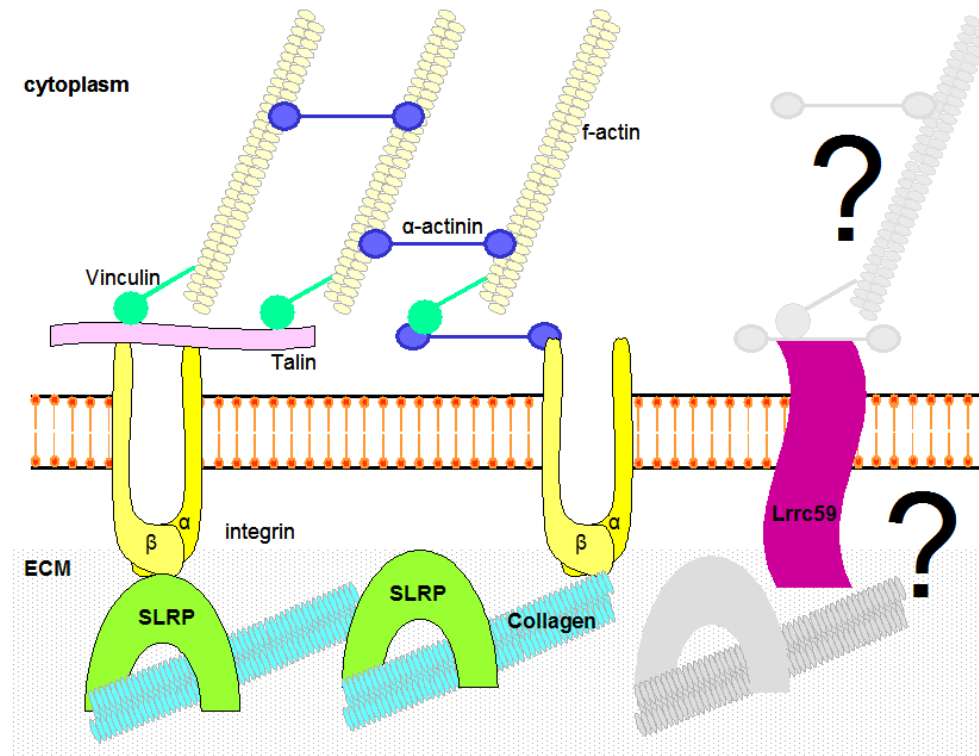


**Figure 54: Possible model for LRRC59;** SLRP: small leucine rich repeats, ECM: extracellular matrix

In summary, *LRRC59* is a member of the leucine-rich repeat (LRR) superfamily, but can not be considered as a member of the small leucine-rich repeat proteins and proteoglycans (SLRP) because of the missing cysteine-rich regions and the lack of signal peptide or potential glycoaminoglycan binding sites. Since it does not have the typical horseshoe structure of the SLRPs, an interaction with collagen fibers and therefore an involvement in their fibrillogenesis is unlikely.

Nevertheless, *LRRC59* might have a function in the cytoskeleton. It showed co-localization with vinculin that links adhesion molecules of the cell membrane to the actin cytoskeleton (figure 30). The transmembrane domain of *LRRC59* indicates that the protein is anchored in the cell membrane and could therefore have a similar function than integrin (figure 54). In the mouse, *Lrrc59* was detected in proliferating chondrocytes within a relatively small time

window (E13.5-17.5), and was neither seen in cell lines of osteoblastic origin, nor in hypertrophic chondrocytes expressing type X collagen, or fibroblasts. Expression studies in a variety of murine tissues indicated a wide expression pattern, although not ubiquitous. Further investigations including structure analysis and gene inactivation are planned and will reveal whether LRRC59 is involved in skeletogenesis.

Instead of a broad investigation of genes that might be important during skeletogenesis in general, a disease driven approach has been undertaken as well. For this purpose *LMX1B*, that has been shown to be a key DV limb determinant, has been utilized to further investigate the signalling pathways controlling DV patterning events

#### **4.2. *Lmx1b* downstream targets**

*Lmx1b* is an important transcription factor for both limb and kidney development. Mutations in *LMX1B* lead to nail-patella syndrome that is characterized by dysplastic nails, absent or hypoplastic patellae, iliac horns, abnormality of the elbows, and in some cases nephropathy and glaucoma. NPS has an incidence of approximately 1 in 50,000 [Bongers et al., 2005a; Dreyer et al., 1998; Dunston et al., 2004; Lee and Morello, 2004].

Although there are several studies elucidating the function of *Lmx1b*, only a few downstream targets of this developmentally important gene are known to date and all are in the kidney. Therefore, several approaches, both at the transcriptional and translational level, were performed to shed light on possible targets that are regulated directly by *Lmx1b*.

*Col4a4*, *Col4a3*, podocin and *Cd2ap* were previously identified as downstream *Lmx1b* targets in GBM and podocytes of the kidneys [Miner et al., 2002; Morello et al., 2001; Rohr et al., 2002]; now, in order to identify additional targets at the protein level, mouse kidneys were utilized for further analysis.

2D-gel electrophoresis with proteins isolated from newborn kidneys of *Lmx1b* knock-out compared to wild type mice were performed. Six differentially expressed proteins, including proteasome subunit p45, transforming protein

RhoA , fatty acid binding protein and histone H4, TER ATPase , stathmin , PPlase and agrin were identified by mass spectrometry (table 6). The most interesting candidate was Agrin (*Agrn*) being downregulated in kidneys of *Lmx1b* mutant mice versus WT (see 4.2.1. for further discussion).

Five potential candidate genes including Car2, HMG-1, ubiquitin-conjugating enzyme E2N, myosin light chain, ubiquitin-conjugating enzyme were also identified in a similar experiment with protein extracts from E13.5 *Lmx1b* wild type and mutant fore limbs (table 6). Here, *Car2* appeared to be the most promising candidate (see 4.2.2. for further discussion).

Most of the other putative candidate proteins function in cell signaling and metabolism and are therefore ubiquitously expressed like the two ubiquitin-conjugating enzymes, prolyl isomerase (PPlase), proteasome subunit p45, fatty acid binding protein and histone H4, TER ATPase, and high mobility group 1 (HMG-1). The remaining proteins are cytoskeletal, RhoA being involved in the formation of stress fibers of the actin cytoskeleton, myosins in actin-based motility in eukaryotic tissues, and stathmin in the dynamics of microtubules. A correlation between *Lmx1b* and these genes has not been identified yet and further investigations were ruled out. Furthermore, differential expression of these mRNAs was not seen in any of the microarrays subsequently performed.

After additional investigations failed to confirm *Lmx1b* mediated down-regulation of the two potential candidate genes of interest, a more sensitive microarray using RNA from *Lmx1b* newborn wild type versus mutant whole kidneys was performed. In such experiment, not even the known *Lmx1b* downstream targets like *Col4a4*, or *Col4a3* appeared to be down-regulated. This indicated that RNA from whole kidneys couldn't be used to find downstream targets of a gene that is expressed only in a small portion of the cells forming the kidney itself, specifically the podocytes. Therefore, laser captured glomeruli were used for RNA preparation, amplification and microarray hybridization.

Beside the known *Lmx1b* downstream targets *Col4a3* and podocin, podocalyxin-like (*Podxl*) and Vanin 1 (*Vnn1*) appeared to be downregulated and reasonable candidates. *Podxl* was thought to be a major component of the glycocalyx that covers foot processes of podocytes on their apical surface

[Takeda et al., 2001], while *Vnn1* encodes a glycosylphosphatidylinositol-linked membrane-associated pantotheinase that is expressed in a sex-specific manner in mice. It was described as co-expressed with the transcription factors *SF1* and *SOX9* and seemed to be necessary for normal Sertoli cell development [Wilson et al., 2005].

But further studies were hampered by the fact that *Lmx1b*-deficient pups die a few hours after birth, and kidney glomeruli at this stage are still immature with podocytes that do not fully express their differentiation markers.

Therefore, a third approach at the RNA level was performed, concentrating on the fact that *Lmx1b* is also highly expressed during limb development. To investigate potential *Lmx1b* downstream targets in this tissue, RNA was extracted from wild type and *Lmx1b*<sup>-/-</sup> E11.5 fore limb buds and then processed for microarray analysis. By so doing, four potential candidate genes were identified (3.2.1.1.): Neuropilin 2 (*Nrp2*), single-stranded DNA binding protein 2 (*Ssbp2*), peroxisome proliferative activated receptor, gamma, co-activator 1 alpha (*Ppargc1a*) and short stature homeobox 2 (*Shox2*). After expression studies using qRT-PCR and WISH, only *Nrp2* remained of major interest, because it was the only gene that showed specific expression in the dorsal limb buds (figure 43) and was down regulated in *Lmx1b* mutant mice (see 4.2.3. for further discussion). The other three genes showed reduced expression by microarray analysis that was confirmed by qRT-PCR. However, a specific expression in the dorsal limb bud could not be seen by WISH and this is probably due to the lower sensitivity of this assay. If these genes were only weakly expressed in a certain cell population, only a more sensitive microarray or qRT-PCR experiment could detect their expression. Moreover, we cannot exclude technical issues with the WISH procedure. *Ppargc1a* for example seemed ubiquitously expressed and can therefore not be considered a specific *Lmx1b* downstream candidate. While we cannot rule out that these genes could be potential *Lmx1b* downstream targets, a more detailed investigations on limb sections by ISH would be necessary to understand this. Since *Nrp2* showed the best results in all the described experiments, at present further investigations were only planned with this gene.



#### 4.2.1. Potential *Lmx1b* downstream target Agrin (*Agrn*)

Although a down regulation of Agrin in *Lmx1b*<sup>-/-</sup> tissues could not be proved by qRT-PCR and immunohistochemical experiments, it could still be a potential downstream target gene. *Agrn* was not detected in protein extracts from *Lmx1b*-null kidneys and hybridization of murine RNAs from wild type and mutant *Lmx1b* kidneys on human cDNA filters showed decreased *Agrn* expression in the mutant tissue (performed by Astra Zeneca, Wilmington, DE, USA with RNA prepared by Dr. Roy Morello, Baylor College of Medicine, Houston, TX, USA). Additionally, two probes for agrin were found slightly down regulated in mutant *Lmx1b* glomeruli and E11.5 limb buds by microarray.

Agrin showed tissue-specific alternative splicing at the 5' and 3' end and different isoforms were expressed in neuromuscular junctions, immunological synapses, the central nervous system, but also in lung and kidney. Agrin can induce the aggregation of acetylcholine receptors and other postsynaptic proteins on muscle fibers and is crucial for the formation of the neuromuscular junction [Bezakova and Ruegg, 2003].

In the kidneys, it was identified as a major heparan sulfate proteoglycan in the glomerular basement membrane which also contains  $\alpha 3(\text{IV})$  and  $\alpha 4(\text{IV})$  collagen and that had been shown to be down regulated by *Lmx1b* [Raats et al., 2000]. More recently, Agrin was found highly expressed in chondrocytes and required for normal growth [Hausser et al., 2007]. *Agrin*-null mice die right after birth because they do not form functional neuromuscular synapses. *Lmx1b* mutant mice also die within the first hours after birth for no obvious reason. A potential down regulation of *Agrn* caused by lack of *Lmx1b* and therefore malformations in neuromuscular junctions, could explain the poor breathing efforts of *Lmx1b* mutant pups. And since *Lmx1b* is upstream of two GBM components,  $\alpha 3(\text{IV})$  and  $\alpha 4(\text{IV})$  collagen, it could perhaps also regulate a proteoglycan whose down regulation might result in the split GBM as seen in *Lmx1b* mutant mice [Eremina and Quaggin, 2004].

#### 4.2.2. Potential *Lmx1b* downstream target carbonic anhydrase 2 (*Car2*)

As for *Agrn*, a down regulation of *Car2* by *Lmx1b* was not proved in the present analysis. However, the family of carbonic anhydrases could still be of

interest when considering potential targets of *Lmx1b*. *Car2* was far less represented in protein extracts from E13.5 *Lmx1b* mutant fore limbs versus wild type littermates. In microarray analysis, comparing RNA from whole kidneys of newborn *Lmx1b* mutant vs. wild type mice, expression of *Car2* remained unchanged, as well as in E11.5 *Lmx1b* mutant fore limbs. Instead, family member *Car3* was one of the most up-regulated genes in the same experiment.

Carbonic anhydrases are metalloenzymes that catalyze the conversion of carbon dioxide to bicarbonate and protons. Inactivation of the cytosolic *Car2* and *Car3* did not result in obvious limb phenotypes in mice [Kim et al., 2004; Pan et al., 2006]. In humans, carbonic anhydrase 2 deficiency was identified as the primary defect in osteopetrosis with renal tubular acidosis and cerebral calcification [Bolt et al., 2005; Sly, 1989]. In growth plate cartilage, *Car2* was expressed in late proliferating and hypertrophic chondrocytes as well as in extracellular matrix of the hypertrophic zone [Vaananen, 1984]. Mice exposed prenatally (E9.5) to the Car-specific inhibitor acetazolamide developed an increased frequency of limb malformations due to reduced intracellular pH within the limb [Collins et al., 1990; Scott et al., 1990].

Although the expression of carbonic anhydrases was recently investigated in osteoclasts [David et al., 2001; Riihonen et al., 2007], and *CAR2* deficiency affects the balance between osteoblasts and osteoclasts, previous publications also indicate a role for carbonic anhydrases in chondrocytes that needs to be further investigated in relation to *Lmx1b*. That *Car2* was only found reduced by 2D-gel electrophoresis in *Lmx1b* mutant fore limbs, but its expression remained unchanged in qRT-PCR and microarray experiments, suggests that it might be posttranslationally modified and that disruption of *Lmx1b* could affect this modification, without effect on RNA levels. Further investigation will therefore need to be performed on protein level.

#### **4.2.3. Potential *Lmx1b* downstream target Neuropilin 2 (*Nrp2*)**

The most promising *Lmx1b* downstream target was *Nrp2* which was found down regulated in limb buds of E11.5 *Lmx1b* knockout mice. Neuropilin-2 and its family member *Nrp1* are transmembrane binding receptors for class 3 semaphorins (Sema3, figure 55). The semaphorin group consists of more

than 20 members divided in 7 groups and functions as potent neural repellents or attractants [Fujisawa, 2004]. The first semaphorin, collapsing-1 (now referred to as Sema3A), was discovered in 1993 as an axon guidance mediator that collapsed the motile structures at the end of developing axons (growth cones) and repelled axons in dorsal root ganglia [Luo et al., 1993]. There are 7 class 3 semaphorins (Sema3A-G) and they are highly conserved between species [Klagsbrun and Eichmann, 2005; Taniguchi et al., 2005]. Binding to neuropilin receptors was mainly described for Sema3A and Sema3F. Sema3F competes with Sema3A for Nrp1 binding, while Nrp2 binds Sema3F with highest affinity [Chen et al., 1998a]. Additionally both neuropilins were described as co-receptors for vascular endothelial growth factor isoform 164 (VEGF<sub>164</sub>) which is important in vascularization, and Nrp2 can also bind the isoforms VEGF<sub>145</sub> and VEGF<sub>120</sub> [Gluzman-Poltorak et al., 2001; Neufeld et al., 2002]. Nrp1 forms a stable complex with plexin A1 [Takahashi et al., 1999] that belongs to a group of Sema3 signaling receptors, and that are referred to as plexin A1-3, and D1 [Pasterkamp and Kolodkin, 2003].

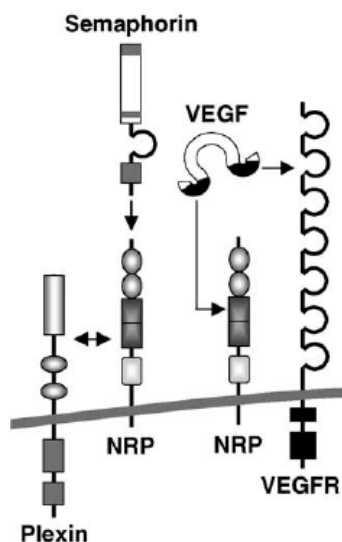


**Figure 55: Ligand/ receptor pairs that are involved in axon guidance and blood vessel development:** seven class III semaphorins were described to date, as well as two neuropilins. Neuropilin binding of semaphorins can be enhanced through a complex with the transmembrane receptor plexin and VEGF can either bind to its traditional receptor VEGFR, or with less affinity to the neuropilin receptor (adapted from Klagsbrun and Eichmann, 2005).

*Nrp2* is expressed in neurons and participates in the guidance of growing axons towards their targets. During neuronal development, *Nrp2* expression was detected in certain brain areas as early as E9.5. Signals were found in the midbrain and the hindbrain, overlapping with the expression of several semaphorins. At E11.5, *Nrp2* can mainly be seen in several regions of the

cerebral vesicle, as well as around the optic stalk [Melendez-Herrera and Varela-Echavarria, 2006]. *Nrp2* deficient mice lack the oculomotor nerve (third cranial nerve) and the trochlea nerve, the fourth cranial nerve and the only motor nerve that exits the brain dorsally to innervate the superior oblique muscle of the eye [Fujisawa, 2004]. Beside the eye defect, they do not show clear abnormalities in the projections and trajectories of the spinal nerves [Giger et al., 2000]. Beside the expression in the brain, *Nrp2* expression was found in parts of the peripheral nervous system. Sema3F-*Nrp2* signaling was found to guide axons of a medial subset of lateral motor column neurons to the ventral limb [Huber et al., 2005].

Also *Lmx1b* is required during neuronal development since it is a critical intermediate factor that couples early specification with terminal differentiation of dopaminergic and serotonergic neurons in the central nervous system (CNS) [Cheng et al., 2003; Ding et al., 2003]. Furthermore, it was implicated in a complex transcription factor cascade controlling the differentiation and migration of the superficial dorsal horn neurons [Ding et al., 2004]. Although little is known about a potential *Lmx1b* function in brain development, it is early expressed at the midbrain-hindbrain junction at E9.5 [Dunston et al., 2005]. More recently, neuronal and neurobehavioral aspects of the NPS phenotype were investigated in a study including 16 patients with different *LMX1B* mutations [Dunston et al., 2005]. The inability of afferent sensory neurons to migrate into the dorsal horn as described in *Lmx1b* mutant mice [Ding et al., 2004] was consistent with diminished pain response, numbness, hand/foot cold sensation and weakness as seen in the NPS patients.

Overall, there was no investigation about overlapping expression patterns of *Nrp2* and *Lmx1b* in neuronal tissues yet. It is still remarkable that targeted mutation of *Lmx1b* in mice result in iris and ciliary body hypoplasia, as well as cornea stromal defects [Pressman et al., 2000], and *Nrp2* mRNAs was evident in developing inner nuclear and ganglion cell layers of rat retinas at birth [de Winter et al., 2004]. Additionally, *Nrp2*-deficient mice lack two (third and fourth cranial nerve) out of three optical nerves [Giger et al., 2000] and glaucoma, an eye disease affecting the second cranial nerve, was seen with high incidence in nail patella syndrome patients [Mimiwati et al., 2006]. It could therefore be

speculated that the neuronal aspects of NPS, especially the eye defects, could involve *Nrp2* down regulation in patients.

More importantly for the present study, neuropilins and class 3 semaphorins were detected in mouse and rat kidneys. Both receptors were found several times more abundant in embryonic kidneys than in newborn or adult tissues. They were expressed in the endothelial cells that surround the S-shaped bodies of the developing podocytes, in the vascular cleft and later on in glomerular capillaries and arterioles during kidney vascularization. In later stages, their expression is restricted to peritubular and some glomerular capillaries. Interestingly, their ligands Sema3A and Sema3F co-localized with VEGF in the renal tubular epithelial cells, whereas the neuropilins co-localized with the VEGF receptors VEGFR1 and VEGFR2 in the endothelial cells [Villegas and Tufro, 2002].

*Lmx1b* is first expressed in podocytes precursor cells of the S-shaped body and continues to show this expression throughout nephrogenesis [Chen et al., 1998b; Pavenstadt et al., 2003]. Homozygous *Lmx1b* mutant mice have podocytes and GBM abnormalities at birth [Chen et al., 1998b], and Nail-Patella syndrome patients often have glomerulopathy [Dreyer et al., 1998]. *Lmx1b*-null mice have overall smaller kidneys than their wild type littermates [Rohr et al., 2002]. The kidneys contain less mature glomeruli, and the glomerular tuft area was significantly decreased. The GBM was split and fibrillar materials, as well as erythrocytes were found in the Bowman's space. No foot processes or slit diaphragms were noticed in the more mature mutant glomeruli. Additionally, the mutant glomeruli were less differentiated and therefore showed less capillary branching [Rohr et al., 2002]; this could be due to a *Nrp2* down-regulation. Therefore, the expression of *Nrp2* ligand *VEGF*, involved in the branching process [Eremina and Quaggin, 2004], was investigated by *in situ* hybridization, and was found decreased in mutant podocytes in comparison to wild type cells. In previously described conditionally immortalized mouse podocyte cell lines [Mundel et al., 1997; Schiwek et al., 2004], both neuropilins and all class 3 semaphorins were expressed in undifferentiated and differentiated cells at similar levels, indicating the first published cell line with a functional autocrine semaphorin system that is regulated by differentiation and ligand availability [Guan et al., 2006]. The second publication showed expression of nephrin and

*Lmx1b* in a stable podocyte cell culture. These two cell lines could be useful models for further characterization of the potential down regulation of *Nrp2* by *Lmx1b*.

The role of *Nrp2* in bone development is closely related to its ligand VEGF. Different isoforms of VEGF are involved in the three key stages of endochondral bone development. VEGF-mediated vascularization is important in the establishment of the primary and the secondary ossification centers, as well as during longitudinal bone growth. Furthermore, nonvascular effects of VEGF were described during chondrocyte proliferation, differentiation, and survival as well as the differentiation, apoptosis, resorption of hypertrophic chondrocytes and the development and activity of osteoblasts and osteoclasts. In addition it is required for osteoclasts recruitment [Maes and Carmeliet, 2007]. The functionality of VEGF is dependent on its receptors and both neuropilin receptors are able to bind VEGF<sub>164</sub>, the most common isoform of VEGF [Ferrara, 1999]. *Nrp1* is expressed in hypertrophic chondrocytes and was also detected *in vitro* in osteoblastic cells, while both neuropilins were found in perichondrial cells. *Nrp1* mutant mice die during the second half of gestation [Kitsukawa et al., 1997] and *Nrp1* chimeric mice develop severe limb abnormalities involving extra digits at the anterior side of the hind limb and duplication of different parts of the phalangeal cartilage [Kitsukawa et al., 1995]. *Nrp2* mutant mice do not show an obvious limb phenotype [Giger et al., 2000]. In a human study, NRP2 was found 6.5-fold stronger expressed in RNA from fetal femur cartilage than in 34 non-cartilage tissues [Funari et al., 2007], indicating its importance in cartilage development.

As described before, inactivation of *Lmx1b* in mice results in complete ventralization of the dorsal mesoderm-derived tissues at the zeugo- and autopodal level. Additionally, the patella and the distal ulna were absent, distal sesamoid bones were duplicated, and iliac anomalies were seen [Chen et al., 1998b]. Although *Wnt7a* is important to initiate *Lmx1b* activation, the dorsalization in the proximal limb bud is mainly due to proper *Lmx1b* expression in the dorsal mesoderm [Chen and Johnson, 1999]

Neuropilins were also described in blood vessel development. While *Nrp1* is preferentially expressed in arterial endothelial cells, *Nrp2* is mainly found in venous endothelial cells [Herzog et al., 2001]. *Nrp2*-deficient mice show

absence or severe reduction of small lymphatic vessels and capillaries during development, while larger, collecting lymphatic vessels developed normally [Yuan et al., 2002]. Double *Nrp1/Nrp2* knockout mice die at E8.5 due to a severe vascular phenotype including avascular yolk sacs, growth retardation and lack of vessel development, capillary formation and branching [Takashima et al., 2002]. Although the expression of *Lmx1b* during blood vessel development was not investigated yet, a potential down regulation of *Nrp2* in blood vessels of *Lmx1b* mutant mice could contribute to the overall shortening of the pups and might lead to the early death of the homozygous mutants.

In summary, *Nrp2* and *Lmx1b* showed similar expression patterns, with overlap during kidney development. *Nrp2* was first detected in the endothelial cells surrounding the S-shaped bodies and glomerular capillaries, while *Lmx1b* is first expressed in S-shaped podocytes precursor cells. The missing foot processes and the reduced capillary branching seen in *Lmx1b* mutant kidneys [Rohr et al., 2002] could be partly due to a down regulation of *Nrp2*. The overall reduced size of *Lmx1b* mutant mice [Chen et al., 1998b] could be explained with reduced blood support due to diminished *Nrp2* expression.

*Lmx1b* has a primary role in limb bud development. Although a regulation of *Nrp2* by *Lmx1b* in limbs does not seem obvious and cannot be explained at this point, the previously described clues seem sufficient to imagine a possible down regulation of *Nrp2* by *Lmx1b*. The *Nrp2* promoter has already shown to have potential *Lmx1b* binding sites and further investigation will demonstrate, whether this hypothesis is true.

### 4.3. Genitopatellar Syndrome

Six patients with clinical Genitopatellar Syndrome (GPS) were enrolled in a study to investigate the molecular mechanisms behind this rare condition. GPS is considered a distinct entity from Nail-Patella syndrome (NPS), because of the similar patella and renal anomalies. But in contrast to patients with NPS that is caused by mutations in *LMX1B*, GPS patients have additionally severe genital anomalies ranging from scrotal hypoplasia to cryptorchidism. Therefore, genes

involved in the development of the gonads were investigated in parallel to genes important in limb and renal formation [Schlaubitz et al., 2007].

A 3.07 Mb deletion on chromosome 9q33.3-q34.11 including *NR5A1*, *NR6A1*, *PBX3*, *LMX1B*, *ANGPTL2*, and *GARNL3* was identified using aCGH and FISH screening methods in patient 152-01-01, a phenotypic female with previously described features of GPS and NPS and additionally confirmed hermaphroditism with ovotestes. Microdeletions often cause complex clinical phenotypes resulting from altered gene dosage. The identification and mapping of the microdeletion in this patient suggests that this patients' phenotype including renal, genital, nail and knee anomalies, is caused by haploinsufficiency of genes including *LMX1B* and *NR5A1*, although RT-PCR failed to work for these two genes (see page).

*NR5A1* (Orphan nuclear receptor steroidogenic factor-1/ *SF-1*) cooperates with the Wilms tumor gene (*WT1*) in its regulation of the expression of anti-Müllerian hormone (AMH, also called Müllerian-inhibiting substance – MIS) in males [Nachtigal et al., 1998]. Expression of *AMH* is required for regression of the Müllerian ducts during uterus formation. *Nr5a1* null mice lack adrenal glands and gonads, and in particular, male mice have female internal genitalia due to loss of AMH during male sex differentiation [Luo et al., 1994; Sadovsky et al., 1995]. In contrast, *NR0B1* (*DAX1*) antagonizes the synergy between Wilms tumor gene *WT1* and *NR5A1*, probably through direct interaction with *NR5A1* [Nachtigal et al., 1998]. In patient # 152-01-01, haploinsufficiency of *NR5A1* likely results in misregulation of AMH, incomplete repression of the Müllerian ducts, and the appearance of ovotestes (figure 45).

Four patients have been described with dominant mutations in the *NR5A1* gene [Achermann et al., 1999; Achermann et al., 2002; Biason-Lauber and Schoenle, 2000; Correa et al., 2004] so far. A heterozygous 2-bp deletion in the P-box of the first zinc finger and a mutation in a secondary DNA binding domain of *NR5A1* were described in two phenotypic females with 46,XY sex reversal, adrenal insufficiency and male pseudohermaphroditism [Achermann et al., 1999; Achermann et al., 2002]. A third female with adrenal insufficiency, but no ovarian maturation and a 46,XX karyotype was described with a mutation affecting DNA binding affinity [Biason-Lauber and Schoenle, 2000]. More recently, a 8 bp deletion in *NR5A1* in a 46,XY female with gonadal agenesis but



normal adrenal function was described [Correa et al., 2004]. This mutation did not abolish *NR5A1* transcriptional activity, but the mutated protein seemed to inhibit the wildtype protein in most cell types used for transfection experiments. Since alterations in *NR5A1* have been described in 46,XY females, it seems that *NR5A1* is important for male gonadal differentiation. Its role in normal female gonadal development is less clear, but *NR5A1* does appear to be critical in adrenal gland formation in both sexes. However, deletion of *NR5A1* in 46,XX females probably would not lead to sex reversal, since it is primarily involved in Müllerian regression, probably through regulation of AMH in cooperation with Wilms tumor gene 1 [Nachtigal et al., 1998].

*WT1* is required for the normal formation of the genitourinary system and mesothelial tissues [Pritchard-Jones et al., 1990]. By studying Denys-Drash syndrome (DDS), which is characterized by Wilms tumor and genital anomalies caused by mutations in *WT1*, an interaction of *WT1* and testis-determining factor *SRY* was demonstrated [Matsuzawa-Watanabe et al., 2003]. Since *WT1* mutants associated with DDS do not form this complex to regulate transcription, it has been concluded that this *WT1-SRY* interaction is important in testis development [Matsuzawa-Watanabe et al., 2003; Wilhelm and Englert, 2002]. Because of the first patients' 46, XY karyotype (figure 46), FISH for *SRY* was performed, showing a typical male *SRY* pattern (figure 47). The loci for *WT1* and *SRY* were normal in aCGH screening, so interaction of *WT1* and *SRY* is probably unaffected and thus contributed to the development of the testicular tissue of this patients' ovotestes.

*WT1* directly or indirectly regulates other genes that are involved in sex reversal, like the autosomal genes *SOX9* and *WNT4* or the X-linked gene *DAX1* acting upstream of *NR5A1* [Wagner et al., 2003]. *WT1* was found unaffected and *NR5A1* deleted for patient # 152-01-01. Although we were not able to show a reduced transcriptional level of *NR5A1* in any of the patients' EBV transformed lymphoblasts using quantitative RT-PCR (3.3.5.), it has been suggested that *NR5A1*, like other genes including *SRY*, *SOX9* [Kwok et al., 1995; Wagner et al., 2003; Wagner et al., 1994], *WT1* [Wagner et al., 2003], *WNT4* [Jordan et al., 2001] and *DAX1* [McCabe, 1996; Meeks et al., 2003; Muscatelli et al., 1994], functions in a dosage-dependent manner to regulate

male sex determination with haploinsufficiency causing sex reversal [Susens and Borgmeyer, 1996; Veitia et al., 2001].

*NR6A1/GCNF*, located between *NR5A1* and *LMX1B*, encodes another orphan nuclear receptor of the nuclear hormone receptor family that is primarily expressed in testis [AgoulNIK et al., 1998; Chen et al., 1994]. It has not been associated with sex-reversal, but its restricted expression and the fact that it is deleted in our first patient, makes it an important candidate gene in this patient's disorder of sexual development.

Haploinsufficiency of *LMX1B* causes nail-patella syndrome (NPS) comprising nail dysplasia, joint stiffness, patella aplasia or hypoplasia, iliac horns, in some cases nephropathy, and glaucoma [Bongers et al., 2005a; Dreyer et al., 1998; Dunston et al., 2005; Vollrath et al., 1998]. The hypoplastic finger- and toenails of our first patient and the knee and renal anomalies in all the patients, makes *LMX1B* a candidate gene for the present phenotype. And indeed, FISH and aCGH indicated *LMX1B* is deleted in our first patient (figure 49, table 9).

Deletion of *LMX1B* and *NR5A1* was only found in the patient 152-01-01, therefore alterations in the putative common regulatory region of *LMX1B*, 100 kb upstream of the *LMX1B* start codon were investigated using FISH with overlapping Fosmids in the other patients. However, no other chromosomal anomalies were identified. Although we cannot fully exclude a more subtle mutation that dysregulates *LMX1B* and *NR5A1* expression, our findings suggest that genomic rearrangements between the two genes causing the complex phenotype in patient # 152-01-01 and GPS in the other patients can be excluded. Importantly, the index patient had additional anomalies, not previously reported in other patients. Hence, the deletion of the additional intervening genes may contribute to her complex phenotype.

A dose-dependent effect of the deleted genes was investigated with quantitative RT-PCR (3.3.5.). Blood was the only available material from all six patients and was used to generate EBV-transformed lymphoblasts. *LMX1B* is extremely GC rich (56.01% of the genomic sequence, 62,57% of exon 2) and amplification of the transcript therefore difficult. After trying amplification on cDNA from cultured lymphoblasts with nonsatisfying results, conditions were optimized to use total RNA instead. Results for *LMX1B*, *NR5A1*, and *NR6A1* were not reproducible and a dose-dependent effect on the expression of these deleted genes could

therefore not be investigated. After all, it was not clear whether EBV-transformed lymphoblasts could be used to research dosage effects, since the virus mediated transformation may have a certain impact on the copy number of each gene. To date, there is only one useful previous study stating that early passages preserve the chromosomal integrity of primary B-cells at the cytogenetic level during EBV-transformed B-cell immortalization except for a copy number variation in 1p36.33 due to increased mitochondrial DNA copy numbers [Jeon et al., 2007]. Lymphoblasts for the present study were cultured over a couple of weeks and can therefore not be considered as early passages anymore.

Beside the mentioned NPS, SPS and GPS, five more syndromes have been described with similar patellar anomalies like Meier-Gorlin syndrome, Coffin Siris syndrome, Arthrogryposis syndrome/ Kuskokwim syndrome, patella aplasia-hypoplasia, and RAPADILINO syndrome [Bongers et al., 2005b; Sweeney et al., 2003], but significant other clinical differences make them unlikely candidates. In comparison to GPS patients, patients with Meier-Gorlin syndrome are associated with unique facial characteristics like full lips, small ears and a prominent triangular shape of the face. Although Meier-Gorlin syndrome had been suggested as a human equivalent of the *short ear* mouse [Lacombe et al., 1994], a mutation in Bone morphogenetic protein 5 (*BMP5*) that is causing the murine phenotype was not identified in the human patients. The most prominent abnormalities of Coffin Siris syndrome patients were their hypoplastic to absent fifth fingernails and fifth distal phalanges, developmental delay, coarse facial appearance, and hirsutism [Fleck et al., 2001]. Although GPS patients were described with coarse facial appearance and developmental delay, hirsutism and abnormalities of specific phalanges were not reported. The Kuskokwim syndrome was only observed in the Kuskokwim Delta area, and does not include genital anomalies [Petajan et al., 1969], same for patella aplasia-hypoplasia [Bongers et al., 2002] and RAPADILINO syndrome that can be caused by mutation in the DNA helicase gene *RECQL4* [Siitonen et al., 2003].

The patient with the described deletion has features of GPS and NPS including dysmorphic features, flexion deformities, micrognathia, rudimentary/ displaced patella, prenatal oligohydramnios, hypoplastic finger- and toenails with

ovotestes and therefore confirmed hermaphroditism that might be due to the deletion of *LMX1B* and *NR5A1*. However, this patient was distinct with ovotestes, breathing problems, absence of multicystic kidneys and microcephaly, and a normal corpus callosum. While the other patients studied did not have microdeletions (>100kb), mutations within regulatory regions affecting the function of these two genes to produce a GPS phenotype without the presence of ovotestes, as seen in previous GPS patients, cannot be ruled out. These patients had a range of more severe mental retardations than the patient with the microdeletion, which suggests that genitopatellar syndrome is a genetically heterogeneous disorder that may involve mutations within regulatory elements of *LMX1B* and *NR5A1* needing to be investigated further, because identification of the genetic determinants of GPS remains elusive.

#### 4.4. Conclusions and further directions

Within the high throughput EST sequencing project from a human fetal cartilage library, 5000 cDNA clones were generated. A comparison with previously published data from other cartilage EST sequencing projects showed similar distributions of all known genes involved in skeletogenesis confirming the quality of the generated data. The pooled material from the 20<sup>th</sup> week of gestation until 2<sup>nd</sup> year of life closed the gap between the previous published data from earlier fetal time points [Krakow et al., 2003; Pogue et al., 2004; Zhang et al., 2003] and the study performed with adult material [Kumar et al., 2001]. According to their protein domains or their genomic location, several genes were selected and further characterized. After a first round of screening, by Northern blotting with human material, further investigations including *in situ* and whole mount hybridizations were performed with murine tissues. A potential expression in parts of the skeleton was verified for three selected genes (*LRRC59*, *CRELD2*, *ZNF577*). Since one of these genes, *LRRC59*, showed an interesting expression pattern in proliferating chondrocytes and the protein structure and localization of the gene indicates a potential involvement in the cytoskeleton, this screening modus appeared to be a time consuming, but still effective method to identify potential interesting genes that might be key players

in skeletal development. The generation of a murine knock-out model was already started and will hopefully help to verify the concrete function of *LRRC59* in skeletogenesis.

A faster way to identify genes with a specific function in skeletogenesis was the microarray experiment including RNA from three time points around precartilaginous mesenchymal condensation (E11.5, E12.5, E13.5). 35% of the 98 genes that showed statistically significant differences in expression over time were involved in cell structure and motility, indicating the specificity of the generated data. Since there is very little known about most of these genes, further investigations including expression studies by *in situ* hybridization will be needed to fully understand the generated data. Some recently published data, like the whole genome expression profile generated from human fetal cartilage in comparison to 34 non-cartilage tissues [Funari et al., 2007], or the profiling of murine articular and growth plate cartilage [Yamane et al., 2007], show the growing interest in and the increasing importance of this subject and do support the present analysis as well.

A disease-orientated approach was performed to find out more about the molecular mechanisms behind disorders similar to Nail-Patella syndrome (NPS) that is caused by mutations in *LMX1B*. A 3.07 Mb deletion including *LMX1B* and *NR5A1* (*SF1*) was found in a female patient with both Genitopatellar syndrome (GPS) and NPS features. The deletion of *LMX1B* explains the patients' knee anomalies while the genital conditions including true hermaphroditism with ovotestes were most likely caused by haploinsufficiency of *NR5A1*. These results underline the importance of investigating *LMX1B* in conditions with knee anomalies. The fact that both genes are affected in the presented patient and that they are in nearby genomic localizations suggests a common regulation of the two genes. But five other GPS patients did not show chromosomal rearrangements or deletions as investigated by aCGH. No potential regulatory element was found by FISH analysis with overlapping clones, but mutations within regulatory regions affecting the function of the two genes to produce a GPS phenotype without the presence of ovotestes, as seen in previous GPS patients, cannot be ruled out to date and need to be further investigated.

Additionally, investigations in the mouse model were undertaken to identify genes that are regulated by *Lmx1b*, but that are not in close genomic

localization. Microarray analysis revealed the potential *Lmx1b* downstream target neuropilin 2 (*Nrp2*) that shows an overlapping expression profile with *Lmx1b* and has putative *Lmx1b* binding sites in the promoter region. *Nrp2* deficient mice generated by others [Giger et al., 2000] were requested and are in process of being used to further investigate a potential down regulation of *Nrp2* by *Lmx1b* and the function of *Nrp2* in limb development.

The investigations for both, the EST sequencing project and the *Lmx1b* related screening for downstream targets, in the mouse will help to further identify and understand novel genes in skeletogenesis and may lead to a phenotype – genotype correlation for a human condition that is not associated with a genetic pathway yet.

## 5. Summary

372 osteochondrodysplasias and genetically determined dysostoses were reported in 2007 [Superti-Furga and Unger, 2007]. For 215 of these conditions, an association with one or more genes can be stated, while the molecular changes for the remaining syndromes remain illusive to date.

Thus, the present dissertation aims at the identification of novel genes involved in processes regarding cartilage/ bone formation, growth, differentiation and homeostasis, which may serve as candidate genes for the above mentioned conditions. Two different approaches were undertaken.

Firstly, a high throughput EST sequencing project from a human fetal cartilage library was performed to identify novel genes in early skeletal development (20<sup>th</sup> week of gestation until 2<sup>nd</sup> year of life) that could be investigated as potential candidate genes. 5000 EST sequences were generated and analyzed representing 1573 individual transcripts, corresponding to known (1400) and to novel, yet uncharacterized genes (173). About 7% of the proteins were already described in cartilage/ bone development or homeostasis, showing that the generated library is tissue specific. The remaining profile of this library was compared to previously published libraries from different time points (8<sup>th</sup>–12<sup>th</sup>, 18<sup>th</sup>–20<sup>th</sup> week and adult human cartilage) that also showed a similar distribution, reflecting the quality of the presented library analyzed. Furthermore, three potential candidate genes (*LRRC59*, *CRELD2*, *ZNF577*) were further investigated and their potential involvement in skeletogenesis was discussed.

Secondly, a disease-orientated approach was undertaken to identify downstream targets of *LMX1B*, the gene causing Nail-Patella syndrome (NPS), and to investigate similar conditions. Like NPS, Genitopatellar syndrome (GPS) is characterized by aplasia or hypoplasia of the patella and renal anomalies. Therefore, six GPS patients were enrolled in a study to investigate the molecular changes responsible for this relatively rare disease. A 3.07 Mb deletion including *LMX1B* and *NR5A1* (*SF1*) was found in one female patient that showed features of both NPS and GPS and investigations revealed a 46,XY karyotype and ovotestes indicating true hermaphroditism. The microdeletion was not seen in any of the five other patients with GPS

features only, but a potential regulatory element between the two genes cannot be ruled out yet.

Since *Lmx1b* is expressed in the dorsal limb bud and in podocytes, proteomic approaches and expression profiling were performed with murine material of the limbs and the kidneys to identify its downstream targets. After 2D-gel electrophoresis with protein extracts from E13.5 fore limb buds and newborn kidneys of *Lmx1b* wild type and knock-out mice and mass spectrometry analysis, only two proteins, agrin and carbonic anhydrase 2, remained of interest, but further analysis of the two genes did not show a transcriptional down regulation by *Lmx1b*. The focus was switched to expression profiles and RNA from newborn *Lmx1b* wild type and knock-out kidneys was compared by microarray analysis. Potential *Lmx1b* targets were almost impossible to study, because of the early death of *Lmx1b* deficient mice, when the glomeruli, containing podocytes, are still immature. Because *Lmx1b* is also expressed during limb development, RNA from wild type and knock-out *Lmx1b* E11.5 fore limb buds was investigated by microarray, revealing four potential *Lmx1b* downstream targets: neuropilin 2 (*Nrp2*), single-stranded DNA binding protein 2 (*Ssbp2*), peroxisome proliferative activated receptor, gamma, co-activator 1 alpha (*Ppargc1a*) and short stature homeobox 2 (*Shox2*). Whole mount *in situ* hybridization strengthened a potential down regulation of *Nrp2* by *Lmx1b*, but further investigations including *in situ* hybridization and protein-protein interaction studies will be needed.



## 6. References

- Abdul-Rahman OA, La TH, Kwan A, Schlaubitz S, Barsh GS, Enns GM, Hudgins L (2006). Genitopatellar syndrome: expanding the phenotype and excluding mutations in LMX1B and TBX4. *Am J Med Genet A* 140:1567-1572
- Achermann JC, Ito M, Ito M, Hindmarsh PC, Jameson JL (1999). A mutation in the gene encoding steroidogenic factor-1 causes XY sex reversal and adrenal failure in humans. *Nat Genet* 22:125-126
- Achermann JC, Ozisik G, Ito M, Orun UA, Harmanci K, Gurakan B, Jameson JL (2002). Gonadal determination and adrenal development are regulated by the orphan nuclear receptor steroidogenic factor-1, in a dose-dependent manner. *J Clin Endocrinol Metab* 87:1829-1833
- Adams DJ, Biggs PJ, Cox T, Davies R, van der Weyden L, Jonkers J, Smith J, Plumb B, Taylor R, Nishijima I, Yu Y, Rogers J, Bradley A (2004). Mutagenic insertion and chromosome engineering resource (MICER). *Nat Genet* 36:867-71
- Adams MD, Kelley JM, Gocayne JD, Dubnick M, Polymeropoulos MH, Xiao H, Merril CR, Wu A, Olde B, Moreno RF, et al. (1991). Complementary DNA sequencing: expressed sequence tags and human genome project. *Science* 252:1651-6
- Adamska M, Billi AC, Cheek S, Meisler MH (2005). Genetic interaction between Wnt7a and Lrp6 during patterning of dorsal and posterior structures of the mouse limb. *Dev Dyn* 233:368-72
- AgoulNIK IY, Cho Y, Niederberger C, Kieback DG, Cooney AJ (1998). Cloning, expression analysis and chromosomal localization of the human nuclear receptor gene GCNF. *FEBS Lett* 424:73-78
- Ahn J, Ludecke HJ, Lindow S, Horton WA, Lee B, Wagner MJ, Horsthemke B, Wells DE (1995). Cloning of the putative tumour suppressor gene for hereditary multiple exostoses (EXT1). *Nat Genet* 11:137-43
- Alford AI, Hankenson KD (2006). Matricellular proteins: Extracellular modulators of bone development, remodeling, and regeneration. *Bone* 38:749-57
- Altabef M, Clarke JD, Tickle C (1997). Dorso-ventral ectodermal compartments and origin of apical ectodermal ridge in developing chick limb. *Development* 124:4547-56
- Altschul SF, Gish W, Miller W, Myers EW, Lipman DJ (1990). Basic local alignment search tool. *J Mol Biol* 215:403-10
- Ameye L, Young MF (2002). Mice deficient in small leucine-rich proteoglycans: novel in vivo models for osteoporosis, osteoarthritis, Ehlers-Danlos syndrome, muscular dystrophy, and corneal diseases. *Glycobiology* 12:107R-16R
- Archer KJ, Dumur CI, Joel SE, Ramakrishnan V (2006). Assessing quality of hybridized RNA in Affymetrix GeneChip experiments using mixed-effects models. *Biostatistics* 7:198-212
- Aslan H, Ravid-Amir O, Clancy BM, Rezvankhah S, Pittman D, Pelled G, Turgeman G, Zilberman Y, Gazit Z, Hoffmann A, Gross G, Domany E, Gazit D (2006). Advanced molecular profiling in vivo detects novel function of dickkopf-3 in the regulation of bone formation. *J Bone Miner Res* 21:1935-45

- Beals RK, Eckhardt AL (1969). Hereditary onycho-osteodysplasia (Nail-Patella syndrome). A report of nine kindreds. *J Bone Joint Surg Am* 51:505-16
- Bennett WM, Musgrave JE, Campbell RA, Elliot D, Cox R, Brooks RE, Lovrien EW, Beals RK, Porter GA (1973). The nephropathy of the nail-patella syndrome. Clinicopathologic analysis of 11 kindred. *Am J Med* 54:304-19
- Bezakova G, Ruegg MA (2003). New insights into the roles of agrin. *Nat Rev Mol Cell Biol* 4:295-308
- Bi W, Huang W, Whitworth DJ, Deng JM, Zhang Z, Behringer RR, de Crombrughe B (2001). Haploinsufficiency of Sox9 results in defective cartilage primordia and premature skeletal mineralization. *Proc Natl Acad Sci U S A* 98:6698-703
- Bi Y, Nielsen KL, Kilts TM, Yoon A, M AK, Wimer HF, Greenfield EM, Heegaard AM, Young MF (2006). Biglycan deficiency increases osteoclast differentiation and activity due to defective osteoblasts. *Bone* 38:778-86
- Bialek P, Kern B, Yang X, Schrock M, Sasic D, Hong N, Wu H, Yu K, Ornitz DM, Olson EN, Justice MJ, Karsenty G (2004). A twist code determines the onset of osteoblast differentiation. *Dev Cell* 6:423-35
- Biason-Lauber A, Schoenle EJ (2000). Apparently normal ovarian differentiation in a prepubertal girl with transcriptionally inactive steroidogenic factor 1 (NR5A1/SF-1) and adrenocortical insufficiency. *Am J Hum Genet* 67:1563-1568
- Birnboim HC, Doly J (1979). A rapid alkaline extraction procedure for screening recombinant plasmid DNA. *Nucleic Acids Res* 7:1513-23
- Bodine PV, Zhao W, Kharode YP, Bex FJ, Lambert AJ, Goad MB, Gaur T, Stein GS, Lian JB, Komm BS (2004). The Wnt antagonist secreted frizzled-related protein-1 is a negative regulator of trabecular bone formation in adult mice. *Mol Endocrinol* 18:1222-37
- Bolt RJ, Wennink JM, Verbeke JI, Shah GN, Sly WS, Bokenkamp A (2005). Carbonic anhydrase type II deficiency. *Am J Kidney Dis* 46:A50, e71-3
- Bongers EM, Duijf PH, van Beersum SE, Schoots J, Van Kampen A, Burckhardt A, Hamel BC, Losan F, Hoefsloot LH, Yntema HG, Knoers NV, van Bokhoven H (2004). Mutations in the human TBX4 gene cause small patella syndrome. *Am J Hum Genet* 74:1239-1248
- Bongers EM, Huysmans FT, Levtchenko E, de Rooy JW, Blickman JG, Admiraal RJ, Huygen PL, Cruysberg JR, Toolens PA, Prins JB, Krabbe PF, Borm GF, Schoots J, van Bokhoven H, van Remortele AM, Hoefsloot LH, van Kampen A, Knoers NV (2005a). Genotype-phenotype studies in nail-patella syndrome show that LMX1B mutation location is involved in the risk of developing nephropathy. *Eur J Hum Genet* 13:935-946
- Bongers EM, van Bokhoven H, Knoers NV, Hamel BC, Woods CG (2002). Evidence for genetic heterogeneity in familial isolated patella aplasia-hypoplasia. *Am J Med Genet* 108:78-9
- Bongers EM, van Kampen A, van Bokhoven H, Knoers NV (2005b). Human syndromes with congenital patellar anomalies and the underlying gene defects. *Clin Genet* 68:302-19
- Bonnin MA, Laclef C, Blaise R, Eloy-Trinquet S, Relaix F, Maire P, Duprez D (2005). Six1 is not involved in limb tendon development, but is expressed in limb connective tissue under Shh regulation. *Mech Dev* 122:573-85

- Boulet AM, Moon AM, Arenkiel BR, Capecchi MR (2004). The roles of Fgf4 and Fgf8 in limb bud initiation and outgrowth. *Dev Biol* 273:361-72
- Boute N, Gribouval O, Roselli S, Benessy F, Lee H, Fuchshuber A, Dahan K, Gubler MC, Niaudet P, Antignac C (2000). NPHS2, encoding the glomerular protein podocin, is mutated in autosomal recessive steroid-resistant nephrotic syndrome. *Nat Genet* 24:349-54
- Bustin SA, Mueller R (2005). Real-time reverse transcription PCR (qRT-PCR) and its potential use in clinical diagnosis. *Clin Sci (Lond)* 109:365-79
- Byers PH, Barsh GS, Holbrook KA (1982). Molecular pathology in inherited disorders of collagen metabolism. *Hum Pathol* 13:89-95
- Cai WW, Mao JH, Chow CW, Damani S, Balmain A, Bradley A (2002). Genome-wide detection of chromosomal imbalances in tumors using BAC microarrays. *Nat Biotechnol* 20:393-6
- Camper L, Heinegard D, Lundgren-Akerlund E (1997). Integrin alpha2beta1 is a receptor for the cartilage matrix protein chondroadherin. *J Cell Biol* 138:1159-67
- Capdevila J, Izpisua Belmonte JC (2001). Patterning mechanisms controlling vertebrate limb development. *Annu Rev Cell Dev Biol* 17:87-132
- Capellini TD, Di Giacomo G, Salsi V, Brendolan A, Ferretti E, Srivastava D, Zappavigna V, Selleri L (2006). Pbx1/Pbx2 requirement for distal limb patterning is mediated by the hierarchical control of Hox gene spatial distribution and Shh expression. *Development* 133:2263-73
- Carter DR, Beaupre GS, Wong M, Smith RL, Andriacchi TP, Schurman DJ (2004). The mechanobiology of articular cartilage development and degeneration. *Clin Orthop Relat Res*:S69-77
- Chen F, Cooney AJ, Wang Y, Law SW, O'Malley BW (1994). Cloning of a novel orphan receptor (GCNF) expressed during germ cell development. *Mol Endocrinol* 8:1434-44
- Chen H, He Z, Tessier-Lavigne M (1998). Axon guidance mechanisms: semaphorins as simultaneous repellents and anti-repellents. *Nat Neurosci* 1:436-9
- Chen H, Johnson RL (1999). Dorsoventral patterning of the vertebrate limb: a process governed by multiple events. *Cell Tissue Res* 296:67-73
- Chen H, Johnson RL (2002). Interactions between dorsal-ventral patterning genes *lmx1b*, *engrailed-1* and *wnt-7a* in the vertebrate limb. *Int J Dev Biol* 46:937-41
- Chen H, Lun Y, Ovchinnikov D, Kokubo H, Oberg KC, Pepicelli CV, Gan L, Lee B, Johnson RL (1998a). Limb and kidney defects in *Lmx1b* mutant mice suggest an involvement of *LMX1B* in human nail patella syndrome. *Nat Genet* 19:51-5
- Chen H, Ovchinnikov D, Pressman CL, Aulehla A, Lun Y, Johnson RL (1998b). Multiple calvarial defects in *lmx1b* mutant mice. *Dev Genet* 22:314-20
- Chen L, Deng CX (2005). Roles of FGF signaling in skeletal development and human genetic diseases. *Front Biosci* 10:1961-76
- Cheng L, Chen CL, Luo P, Tan M, Qiu M, Johnson R, Ma Q (2003). *Lmx1b*, *Pet-1*, and *Nkx2.2* coordinately specify serotonergic neurotransmitter phenotype. *J Neurosci* 23:9961-7

- Chomczynski P (1993). A reagent for the single-step simultaneous isolation of RNA, DNA and proteins from cell and tissue samples. *Biotechniques* 15:532-4, 536-7
- Chomczynski P, Sacchi N (1987). Single-step method of RNA isolation by acid guanidinium thiocyanate-phenol-chloroform extraction. *Anal Biochem* 162:156-9
- Cobb J, Dierich A, Huss-Garcia Y, Duboule D (2006). A mouse model for human short-stature syndromes identifies Shox2 as an upstream regulator of Runx2 during long-bone development. *Proc Natl Acad Sci U S A* 103:4511-5
- Cohen MM, Jr. (2006). The new bone biology: pathologic, molecular, and clinical correlates. *Am J Med Genet A* 140:2646-706
- Cohn DH (2001). Defects in extracellular matrix structural proteins in the osteochondrodysplasias. *Novartis Found Symp* 232:195-210; discussion 210-2
- Collins MD, Fradkin R, Scott WJ, Jr. (1990). Induction of postaxial forelimb ectrodactyly with anticonvulsant agents in A/J mice. *Teratology* 41:61-70
- Colnot C (2005). Cellular and molecular interactions regulating skeletogenesis. *J Cell Biochem* 95:688-97
- Coons AH, Kaplan MH (1950). Localization of antigen in tissue cells; improvements in a method for the detection of antigen by means of fluorescent antibody. *J Exp Med* 91:1-13
- Cormier-Daire V, Chauvet ML, Lyonnet S, Briard ML, Munnich A, Le Merrer M (2000). Genitopatellar syndrome: a new condition comprising absent patellae, scrotal hypoplasia, renal anomalies, facial dysmorphism, and mental retardation. *J Med Genet* 37:520-4
- Correa RV, Domenice S, Bingham NC, Billerbeck AE, Rainey WE, Parker KL, Mendonca BB (2004). A microdeletion in the ligand binding domain of human steroidogenic factor 1 causes XY sex reversal without adrenal insufficiency. *J Clin Endocrinol Metab* 89:1767-72
- Corsi A, Xu T, Chen XD, Boyde A, Liang J, Mankani M, Sommer B, Iozzo RV, Eichstetter I, Robey PG, Bianco P, Young MF (2002). Phenotypic effects of biglycan deficiency are linked to collagen fibril abnormalities, are synergized by decorin deficiency, and mimic Ehlers-Danlos-like changes in bone and other connective tissues. *J Bone Miner Res* 17:1180-9
- Craig JE, Mackey DA (1999). Glaucoma genetics: where are we? Where will we go? *Curr Opin Ophthalmol* 10:126-34
- Cunningham NS, Jenkins NA, Gilbert DJ, Copeland NG, Reddi AH, Lee SJ (1995). Growth/differentiation factor-10: a new member of the transforming growth factor-beta superfamily related to bone morphogenetic protein-3. *Growth Factors* 12:99-109
- Curtiss J, Heilig JS (1998). DeLIMiting development. *Bioessays* 20:58-69
- Cygan JA, Johnson RL, McMahon AP (1997). Novel regulatory interactions revealed by studies of murine limb pattern in Wnt-7a and En-1 mutants. *Development* 124:5021-32
- Danielson KG, Baribault H, Holmes DF, Graham H, Kadler KE, Iozzo RV (1997). Targeted disruption of decorin leads to abnormal collagen fibril morphology and skin fragility. *J Cell Biol* 136:729-43

- David JP, Rincon M, Neff L, Horne WC, Baron R (2001). Carbonic anhydrase II is an AP-1 target gene in osteoclasts. *J Cell Physiol* 188:89-97
- Davidson D, Blanc A, Filion D, Wang H, Plut P, Pfeffer G, Buschmann MD, Henderson JE (2005). Fibroblast growth factor (FGF) 18 signals through FGF receptor 3 to promote chondrogenesis. *J Biol Chem* 280:20509-15
- Dawid IB, Breen JJ, Toyama R (1998). LIM domains: multiple roles as adapters and functional modifiers in protein interactions. *Trends Genet* 14:156-62
- Day TF, Guo X, Garrett-Beal L, Yang Y (2005). Wnt/beta-catenin signaling in mesenchymal progenitors controls osteoblast and chondrocyte differentiation during vertebrate skeletogenesis. *Dev Cell* 8:739-50
- De Seranno S, Benaud C, Assard N, Khediri S, Gerke V, Baudier J, Delphin C (2006). Identification of an AHNK binding motif specific for the Annexin2/S100A10 tetramer. *J Biol Chem* 281:35030-8
- de Vries BB, Pfundt R, Leisink M, Koolen DA, Vissers LE, Janssen IM, Reijmersdal S, Nillesen WM, Huys EH, Leeuw N, Smeets D, Sistermans EA, Feuth T, van Ravenswaaij-Arts CM, van Kessel AG, Schoenmakers EF, Brunner HG, Veltman JA (2005). Diagnostic genome profiling in mental retardation. *Am J Hum Genet* 77:606-16
- de Winter F, Cui Q, Symons N, Verhaagen J, Harvey AR (2004). Expression of class-3 semaphorins and their receptors in the neonatal and adult rat retina. *Invest Ophthalmol Vis Sci* 45:4554-62
- Devereux J, Haeberli P, Smithies O (1984). A comprehensive set of sequence analysis programs for the VAX. *Nucleic Acids Res* 12:387-95
- Dietz UH, Sandell LJ (1996). Cloning of a Retinoic Acid-sensitive mRNA Expressed in Cartilage and during Chondrogenesis. *J Biol C* 271:3311-3316
- Ding YQ, Marklund U, Yuan W, Yin J, Wegman L, Ericson J, Deneris E, Johnson RL, Chen ZF (2003). Lmx1b is essential for the development of serotonergic neurons. *Nat Neurosci* 6:933-8
- Ding YQ, Yin J, Kania A, Zhao ZQ, Johnson RL, Chen ZF (2004). Lmx1b controls the differentiation and migration of the superficial dorsal horn neurons of the spinal cord. *Development* 131:3693-703
- Douglas T, Heinemann S, Bierbaum S, Scharnweber D, Worch H (2006). Fibrillogenesis of collagen types I, II, and III with small leucine-rich proteoglycans decorin and biglycan. *Biomacromolecules* 7:2388-93
- Dreyer SD, Morello R, German MS, Zabel B, Winterpacht A, Lunstrum GP, Horton WA, Oberg KC, Lee B (2000). LMX1B transactivation and expression in nail-patella syndrome. *Hum Mol Genet* 9:1067-74
- Dreyer SD, Naruse T, Morello R, Zabel B, Winterpacht A, Johnson RL, Lee B, Oberg KC (2004). Lmx1b expression during joint and tendon formation: localization and evaluation of potential downstream targets. *Gene Expr Patterns* 4:397-405
- Dreyer SD, Zhou G, Baldini A, Winterpacht A, Zabel B, Cole W, Johnson RL, Lee B (1998). Mutations in LMX1B cause abnormal skeletal patterning and renal dysplasia in nail patella syndrome. *Nat Genet* 19:47-50
- Dudley AT, Ros MA, Tabin CJ (2002). A re-examination of proximodistal patterning during vertebrate limb development. *Nature* 418:539-44

- Dunston JA, Hamlington JD, Zaveri J, Sweeney E, Sibbring J, Tran C, Malbroux M, O'Neill JP, Mountford R, McIntosh I (2004). The human LMX1B gene: transcription unit, promoter, and pathogenic mutations. *Genomics* 84:565-76
- Dunston JA, Reimschisel T, Ding YQ, Sweeney E, Johnson RL, Chen ZF, McIntosh I (2005). A neurological phenotype in nail patella syndrome (NPS) patients illuminated by studies of murine Lmx1b expression. *Eur J Hum Genet* 13:330-5
- Ehlen HW, Buelens LA, Vortkamp A (2006). Hedgehog signaling in skeletal development. *Birth Defects Res C Embryo Today* 78:267-79
- Eleftheriou F, Ahn JD, Takeda S, Starbuck M, Yang X, Liu X, Kondo H, Richards WG, Bannon TW, Noda M, Clement K, Vaisse C, Karsenty G (2005). Leptin regulation of bone resorption by the sympathetic nervous system and CART. *Nature* 437:514-520
- Endele S, Klein S, Richter S, Molter T, Amann K, Klanke B, Witzgall R, Johnson RL, Hilgers KF, Winterpacht A (2007). Renal phenotype in heterozygous Lmx1b knockout mice (Lmx1b (+/-)) after unilateral nephrectomy. *Transgenic Res*
- Engsig MT, Chen QJ, Vu TH, Pedersen AC, Therkildsen B, Lund LR, Henriksen K, Lenhard T, Foged NT, Werb Z, Delaisse JM (2000). Matrix metalloproteinase 9 and vascular endothelial growth factor are essential for osteoclast recruitment into developing long bones. *J Cell Biol* 151:879-89
- Enomoto H, Furuichi T, Zanma A, Yamana K, Yoshida C, Sumitani S, Yamamoto H, Enomoto-Iwamoto M, Iwamoto M, Komori T (2004). Runx2 deficiency in chondrocytes causes adipogenic changes in vitro. *J Cell Sci* 117:417-25
- Eremina V, Quaggin SE (2004). The role of VEGF-A in glomerular development and function. *Curr Opin Nephrol Hypertens* 13:9-15
- Ferrara N (1999). Molecular and biological properties of vascular endothelial growth factor. *J Mol Med* 77:527-43
- Fleck BJ, Pandya A, Vanner L, Kerkerling K, Bodurtha J (2001). Coffin-Siris syndrome: review and presentation of new cases from a questionnaire study. *Am J Med Genet* 99:1-7
- Font B, Eichenberger D, Goldschmidt D, Boutillon MM, Hulmes DJ (1998). Structural requirements for fibromodulin binding to collagen and the control of type I collagen fibrillogenesis--critical roles for disulphide bonding and the C-terminal region. *Eur J Biochem* 254:580-7
- Foster JW, Dominguez-Steglich MA, Guioli S, Kowk G, Weller PA, Stevanovic M, Weissenbach J, Mansour S, Young ID, Goodfellow PN, et al. (1994). Campomelic dysplasia and autosomal sex reversal caused by mutations in an SRY-related gene. *Nature* 372:525-30
- Fu L, Patel MS, Bradley A, Wagner EF, Karsenty G (2005). The molecular clock mediates leptin-regulated bone formation. *Cell* 122:803-815
- Fujisawa H (2004). Discovery of semaphorin receptors, neuropilin and plexin, and their functions in neural development. *J Neurobiol* 59:24-33
- Funari VA, Day A, Krakow D, Cohn ZA, Chen Z, Nelson SF, Cohn DH (2007). Cartilage-selective genes identified in genome-scale analysis of non-cartilage and cartilage gene expression. *BMC Genomics* 8:165
- Ganss B, Kobayashi H (2002). The zinc finger transcription factor Zfp60 is a negative regulator of cartilage differentiation. *J Bone Miner Res* 17:2151-60

- Gendelman R, Burton-Wurster NI, MacLeod JN, Lust G (2003). The cartilage-specific fibronectin isoform has a high affinity binding site for the small proteoglycan decorin. *J Biol Chem* 278:11175-81
- Geng Y, McQuillan D, Roughley PJ (2006). SLRP interaction can protect collagen fibrils from cleavage by collagenases. *Matrix Biol* 25:484-91
- Gerard GF, Fox DK, Nathan M, D'Alessio JM (1997). Reverse transcriptase. The use of cloned Moloney murine leukemia virus reverse transcriptase to synthesize DNA from RNA. *Mol Biotechnol* 8:61-77
- German MS, Moss LG, Wang J, Rutter WJ (1992a). The insulin and islet amyloid polypeptide genes contain similar cell-specific promoter elements that bind identical beta-cell nuclear complexes. *Mol Cell Biol* 12:1777-88
- German MS, Wang J, Chadwick RB, Rutter WJ (1992b). Synergistic activation of the insulin gene by a LIM-homeo domain protein and a basic helix-loop-helix protein: building a functional insulin minienhancer complex. *Genes Dev* 6:2165-76
- German MS, Wang J, Fernald AA, Espinosa R, 3rd, Le Beau MM, Bell GI (1994). Localization of the genes encoding two transcription factors, LMX1 and CDX3, regulating insulin gene expression to human chromosomes 1 and 13. *Genomics* 24:403-4
- Gibson UE, Heid CA, Williams PM (1996). A novel method for real time quantitative RT-PCR. *Genome Res* 6:995-1001
- Giger RJ, Cloutier JF, Sahay A, Prinjha RK, Levensgood DV, Moore SE, Pickering S, Simmons D, Rastan S, Walsh FS, Kolodkin AL, Ginty DD, Geppert M (2000). Neuropilin-2 is required in vivo for selective axon guidance responses to secreted semaphorins. *Neuron* 25:29-41
- Gluzman-Poltorak Z, Cohen T, Shibuya M, Neufeld G (2001). Vascular endothelial growth factor receptor-1 and neuropilin-2 form complexes. *J Biol Chem* 276:18688-94
- Gluzman Y (1981). SV40-transformed simian cells support the replication of early SV40 mutants. *Cell* 23:175-82
- Godsave S, Dekker EJ, Holling T, Pannese M, Boncinelli E, Durston A (1994). Expression patterns of Hoxb genes in the Xenopus embryo suggest roles in anteroposterior specification of the hindbrain and in dorsoventral patterning of the mesoderm. *Dev Biol* 166:465-76
- Goldring MB, Tsuchimochi K, Ijiri K (2006). The control of chondrogenesis. *J Cell Biochem* 97:33-44
- Graham FL, Smiley J, Russell WC, Nairn R (1977). Characteristics of a human cell line transformed by DNA from human adenovirus type 5. *J Gen Virol* 36:59-74
- Guan F, Villegas G, Teichman J, Mundel P, Tufro A (2006). Autocrine class 3 semaphorin system regulates slit diaphragm proteins and podocyte survival. *Kidney Int* 69:1564-9
- Guo Q, Loomis C, Joyner AL (2003). Fate map of mouse ventral limb ectoderm and the apical ectodermal ridge. *Dev Biol* 264:166-78
- Hadjidakis DJ, Androulakis, II (2006). Bone remodeling. *Ann N Y Acad Sci* 1092:385-96
- Hall BK, Miyake T (2000). All for one and one for all: condensations and the initiation of skeletal development. *Bioessays* 22:138-47

- Hall CM (2002). International nosology and classification of constitutional disorders of bone (2001). *Am J Med Genet* 113:65-77
- Hampton CM, Taylor DW, Taylor KA (2007). Novel structures for alpha-actinin:F-actin interactions and their implications for actin-membrane attachment and tension sensing in the cytoskeleton. *J Mol Biol* 368:92-104
- Haque T, Nakada S, Hamdy RC (2007). A review of FGF18: Its expression, signaling pathways and possible functions during embryogenesis and post-natal development. *Histol Histopathol* 22:97-105
- Harland RM (1991). In situ hybridization: an improved whole-mount method for *Xenopus* embryos. *Methods Cell Biol* 36:685-95
- Harr B, Schlotterer C (2006). Comparison of algorithms for the analysis of Affymetrix microarray data as evaluated by co-expression of genes in known operons. *Nucleic Acids Res* 34:e8
- Haeusler G, Walter I, Helmreich M, Egerbacher M (2005). Localization of matrix metalloproteinases, (MMPs) their tissue inhibitors, and vascular endothelial growth factor (VEGF) in growth plates of children and adolescents indicates a role for MMPs in human postnatal growth and skeletal maturation. *Calcif Tissue Int* 76: 326-35
- Hausser HJ, Ruegg MA, Brenner RE, Ksiazek I (2007). Agrin is highly expressed by chondrocytes and is required for normal growth. *Histochem Cell Biol* 127:363-74
- Hecht J, Seitz V, Urban M, Wagner F, Robinson PN, Stiege A, Dieterich C, Kornak U, Wilkening U, Brieske N, Zwingman C, Kidess A, Stricker S, Mundlos S (2007). Detection of novel skeletogenesis target genes by comprehensive analysis of a Runx2(-/-) mouse model. *Gene Expr Patterns* 7:102-12
- Henry SP, Takanosu M, Boyd TC, Mayne PM, Eberspaecher H, Zhou W, de Crombrughe B, Hook M, Mayne R (2001). Expression pattern and gene characterization of asporin, a newly discovered member of the leucine-rich repeat protein family. *J Biol Chem* 276:12212-21
- Herschman HR, Passovoy DS, Pruss RM, Aharonov A (1978). Mitogens for murine embryo cell lines. *J Supramol Struct* 8:263-8
- Hertz GZ, Stormo GD (1999). Identifying DNA and protein patterns with statistically significant alignments of multiple sequences. *Bioinformatics* 15:563-77
- Herzog Y, Kalcheim C, Kahane N, Reshef R, Neufeld G (2001). Differential expression of neuropilin-1 and neuropilin-2 in arteries and veins. *Mech Dev* 109:115-9
- Hino J, Kangawa K, Matsuo H, Nohno T, Nishimatsu S (2004). Bone morphogenetic protein-3 family members and their biological functions. *Front Biosci* 9:1520-9
- Hobert O, Westphal H (2000). Functions of LIM-homeobox genes. *Trends Genet* 16:75-83
- Hocking AM, Shinomura T, McQuillan DJ (1998). Leucine-rich repeat glycoproteins of the extracellular matrix. *Matrix Biol* 17:1-19
- Hotz-Wagenblatt A, Hankeln T, Ernst P, Glatting KH, Schmidt ER, Suhai S (2003). ESTAnnotator: A tool for high throughput EST annotation. *Nucleic Acids Res* 31:3716-9
- Huber AB, Kania A, Tran TS, Gu C, De Marco Garcia N, Lieberam I, Johnson D, Jessell TM, Ginty DD, Kolodkin AL (2005). Distinct roles for secreted semaphorin signaling in spinal motor axon guidance. *Neuron* 48:949-64



- Irizarry RA, Hobbs B, Collin F, Beazer-Barclay YD, Antonellis KJ, Scherf U, Speed TP (2003). Exploration, normalization, and summaries of high density oligonucleotide array probe level data. *Biostatistics* 4:249-64
- Ishkanian AS, Malloff CA, Watson SK, DeLeeuw RJ, Chi B, Coe BP, Snijders A, Albertson DG, Pinkel D, Marra MA, Ling V, MacAulay C, Lam WL (2004). A tiling resolution DNA microarray with complete coverage of the human genome. *Nat Genet* 36:299-303
- Izard T, Vorrhein C (2004). Structural basis for amplifying vinculin activation by talin. *J Biol Chem* 279:27667-78
- Jainchill JL, Aaronson SA, Todaro GJ (1969). Murine sarcoma and leukemia viruses: assay using clonal lines of contact-inhibited mouse cells. *J Virol* 4:549-53
- Jeon JP, Shim SM, Nam HY, Baik SY, Kim JW, Han BG (2007). Copy number increase of 1p36.33 and mitochondrial genome amplification in Epstein-Barr virus-transformed lymphoblastoid cell lines. *Cancer Genet Cytogenet* 173:122-30
- Johnson JD, Zhang W, Rudnick A, Rutter WJ, German MS (1997). Transcriptional synergy between LIM-homeodomain proteins and basic helix-loop-helix proteins: the LIM2 domain determines specificity. *Mol Cell Biol* 17:3488-96
- Jones KL, Smith DW (1997). Nail-patella syndrome. In: Smith's Recognizable Patterns of Human Malformation. W.B. Saunders Company, Philadelphia, pp 438-439
- Jordan BK, Mohammed M, Ching ST, Delot E, Chen XN, Dewing P, Swain A, Rao PN, Elejalde BR, Vilain E (2001). Up-regulation of WNT-4 signaling and dosage-sensitive sex reversal in humans. *Am J Hum Genet* 68:1102-9
- Jung YK, Jeong JH, Ryoo HM, Kim HN, Kim YJ, Park EK, Si HJ, Kim SY, Takigawa M, Lee BH (2004). Gene expression profile of human chondrocyte HCS-2/8 cell line by EST sequencing analysis. *Gene* 330:85-92
- Kajava AV (1998). Structural diversity of leucine-rich repeat proteins. *J Mol Biol* 277:519-27
- Kalamajski S, Aspberg A, Oldberg A (2007). The decorin sequence SYIRIADTNIT binds collagen type I. *J Biol Chem* 282:16062-7
- Kamiya N, Shigemasa K, Takagi M (2001). Gene expression and immunohistochemical localization of decorin and biglycan in association with early bone formation in the developing mandible. *J Oral Sci* 43:179-88
- Kardon G, Campbell JK, Tabin CJ (2002). Local extrinsic signals determine muscle and endothelial cell fate and patterning in the vertebrate limb. *Dev Cell* 3:533-45
- Karsenty G (2003). The complexities of skeletal biology. *Nature* 423:316-8
- Karsenty G (2006). Convergence between bone and energy homeostases: leptin regulation of bone mass. *Cell Metab.* 4:341-348
- Kawakami Y, Capdevila J, Buscher D, Itoh T, Rodriguez Esteban C, Izpisua Belmonte JC (2001). WNT signals control FGF-dependent limb initiation and AER induction in the chick embryo. *Cell* 104:891-900
- Kawakami Y, Tsuda M, Takahashi S, Taniguchi N, Esteban CR, Zemmyo M, Furumatsu T, Lotz M, Belmonte JC, Asahara H (2005). Transcriptional coactivator PGC-1alpha regulates chondrogenesis via association with Sox9. *Proc Natl Acad Sci U S A* 102:2414-9

- Kelly DF, Taylor DW, Bakolitsa C, Bobkov AA, Bankston L, Liddington RC, Taylor KA (2006). Structure of the alpha-actinin-vinculin head domain complex determined by cryo-electron microscopy. *J Mol Biol* 357:562-73
- Kelly DF, Taylor KA (2005). Identification of the beta1-integrin binding site on alpha-actinin by cryoelectron microscopy. *J Struct Biol* 149:290-302
- Kevil CG, Walsh L, Laroux FS, Kalogeris T, Grisham MB, Alexander JS (1997). An improved, rapid Northern protocol. *Biochem Biophys Res Commun* 238:277-9
- Kim G, Lee TH, Wetzel P, Geers C, Robinson MA, Myers TG, Owens JW, Wehr NB, Eckhaus MW, Gros G, Wynshaw-Boris A, Levine RL (2004). Carbonic anhydrase III is not required in the mouse for normal growth, development, and life span. *Mol Cell Biol* 24:9942-7
- King M, Arnold JS, Shanske A, Morrow BE (2006). T-genes and limb bud development. *Am J Med Genet A* 140:1407-13
- Kitsukawa T, Shimizu M, Sanbo M, Hirata T, Taniguchi M, Bekku Y, Yagi T, Fujisawa H (1997). Neuropilin-semaphorin III/D-mediated chemorepulsive signals play a crucial role in peripheral nerve projection in mice. *Neuron* 19:995-1005
- Kitsukawa T, Shimon A, Kawakami A, Kondoh H, Fujisawa H (1995). Overexpression of a membrane protein, neuropilin, in chimeric mice causes anomalies in the cardiovascular system, nervous system and limbs. *Development* 121:4309-18
- Klagsbrun M, Eichmann A (2005). A role for axon guidance receptors and ligands in blood vessel development and tumor angiogenesis. *Cytokine Growth Factor Rev* 16:535-48
- Kmita M, Tarchini B, Zakany J, Logan M, Tabin CJ, Duboule D (2005). Early developmental arrest of mammalian limbs lacking HoxA/HoxD gene function. *Nature* 435:1113-6
- Koga T, Matsui Y, Asagiri M, Kodama T, de Crombrughe B, Nakashima K, Takayanagi H (2005). NFAT and Osterix cooperatively regulate bone formation. *Nat Med* 11:880-5
- Komori T, Yagi H, Nomura S, Yamaguchi A, Sasaki K, Deguchi K, Shimizu Y, Bronson RT, Gao YH, Inada M, Sato M, Okamoto R, Kitamura Y, Yoshiki S, Kishimoto T (1997). Targeted disruption of Cbfa1 results in a complete lack of bone formation owing to maturational arrest of osteoblasts. *Cell* 89:755-64
- Kornak U, Mundlos S (2003). Genetic disorders of the skeleton: a developmental approach. *Am J Hum Genet* 73:447-74
- Krakov D, Sebald ET, Pogue R, Rimoin LP, King L, Cohn DH (2003). Analysis of clones from a human cartilage cDNA library provides insight into chondrocyte gene expression and identifies novel candidate genes for the osteochondrodysplasias. *Mol Genet Metab* 79:34-42
- Kronenberg HM (2003). Developmental regulation of the growth plate. *Nature* 423:332-6
- Kronenberg HM, Chung U (2001). The parathyroid hormone-related protein and Indian hedgehog feedback loop in the growth plate. *Novartis Found Symp* 232:144-52; discussion 152-7
- Krzywinski M, Bosdet I, Smailus D, Chiu R, Mathewson C, Wye N, Barber S, Brown-John M, Chan S, Chand S, Cloutier A, Girn N, Lee D, Masson A, Mayo M, Olson T, Pandoh P, Prabhu AL, Schoenmakers E, Tsai M, Albertson D, Lam W, Choy CO, Osoegawa K, Zhao S, de Jong PJ, Schein J, Jones S, Marra MA (2004). A set of BAC clones spanning the human genome. *Nucleic Acids Res* 32:3651-60

- Kumar S, Connor JR, Dodds RA, Halsey W, Van Horn M, Mao J, Sathe G, Mui P, Agarwal P, Badger AM, Lee JC, Gowen M, Lark MW (2001). Identification and initial characterization of 5000 expressed sequenced tags (ESTs) each from adult human normal and osteoarthritic cartilage cDNA libraries. *Osteoarthritis Cartilage* 9:641-53
- Kwok C, Weller PA, Guioli S, Foster JW, Mansour S, Zuffardi O, Punnett HH, Dominguez-Steglich MA, Brook JD, Young ID, et al. (1995). Mutations in SOX9, the gene responsible for Campomelic dysplasia and autosomal sex reversal. *Am J Hum Genet* 57:1028-36
- Lacombe D, Toutain A, Gorlin RJ, Oley CA, Battin J (1994). Clinical identification of a human equivalent to the short ear (se) murine phenotype. *Ann Genet* 37:184-91
- Lacy SE, Bonnemann CG, Buzney EA, Kunkel LM (1999). Identification of FLRT1, FLRT2, and FLRT3: a novel family of transmembrane leucine-rich repeat proteins. *Genomics* 62:417-26
- Lampe AK, Bushby KM (2005). Collagen VI related muscle disorders. *J Med Genet* 42:673-85
- Laufer E, Dahn R, Orozco OE, Yeo CY, Pisenti J, Henrique D, Abbott UK, Fallon JF, Tabin C (1997). Expression of Radical fringe in limb-bud ectoderm regulates apical ectodermal ridge formation. *Nature* 386:366-73
- Lauren J, Airaksinen MS, Saarma M, Timmusk T (2003). A novel gene family encoding leucine-rich repeat transmembrane proteins differentially expressed in the nervous system. *Genomics* 81:411-21
- Lee B, Morello R (2004). LMX1B and the Nail Patella Syndrome. In: Epstein CJ, Erickson RP, Wynshaw-Boris A (eds) *Inborn Errors of Development: The Molecular Basis of Clinical Disorders of Morphogenesis*. Oxford University Press, New York, pp 615-624
- Lee LG, Connell CR, Woo SL, Cheng RD, McArdle BF, Fuller CW, Halloran ND, Wilson RK (1992). DNA sequencing with dye-labeled terminators and T7 DNA polymerase: effect of dyes and dNTPs on incorporation of dye-terminators and probability analysis of termination fragments. *Nucleic Acids Res* 20:2471-83
- Lee NK, Sowa H, Hinoi E, Ferron M, Ahn JD, confavreux C, Dacquin R, Mee PJ, McKee MD, Jung DY, Zhang Z, Kim JK, Mauvais-Jarvis F, Ducy P, Karsenty G (2007). Endocrine Regulation of Energy Metabolism by the Skeleton. *Cell* 130:456-469
- Lefebvre V, Garofalo S, de Crombrughe B (1995). Type X collagen gene expression in mouse chondrocytes immortalized by a temperature-sensitive simian virus 40 large tumor antigen. *J Cell Biol* 128:239-45
- Lefebvre V, Smits P (2005). Transcriptional control of chondrocyte fate and differentiation. *Birth Defects Res C Embryo Today* 75:200-12
- Leimeister C, Bach A, Gessler M (1998). Developmental expression patterns of mouse sFRP genes encoding members of the secreted frizzled related protein family. *Mech Dev* 75:29-42
- Lewandoski M, Sun X, Martin GR (2000). Fgf8 signalling from the AER is essential for normal limb development. *Nat Genet* 26:460-3
- Li X, Cao X (2006). BMP signaling and skeletogenesis. *Ann N Y Acad Sci* 1068:26-40
- Li X, Liu P, Liu W, Maye P, Zhang J, Zhang Y, Hurley M, Guo C, Boskey A, Sun L, Harris SE, Rowe DW, Ke HZ, Wu D (2005). Dkk2 has a role in terminal osteoblast differentiation and mineralized matrix formation. *Nat Genet* 37:945-52

- Lorenzo P, Aspberg A, Onnerfjord P, Bayliss MT, Neame PJ, Heinegard D (2001). Identification and characterization of asporin, a novel member of the leucine-rich repeat protein family closely related to decorin and biglycan. *J Biol Chem* 276:12201-11
- Luo X, Ikeda Y, Parker KL (1994). A cell-specific nuclear receptor is essential for adrenal and gonadal development and sexual differentiation. *Cell* 77:481-90
- Luo Y, Raible D, Raper JA (1993). Collapsin: a protein in brain that induces the collapse and paralysis of neuronal growth cones. *Cell* 75:217-27
- Maes C, Carmeliet G (2007). Vascular and Nonvascular Roles of VEGF in Bone Development. In: Ruhrberg C (ed) VEGF and Development. Landes Bioscience and Springer Science + Business Media, University College London
- Majeska RJ, Rodan SB, Rodan GA (1980). Parathyroid hormone-responsive clonal cell lines from rat osteosarcoma. *Endocrinology* 107:1494-503
- Mariani FV, Martin GR (2003). Deciphering skeletal patterning: clues from the limb. *Nature* 423:319-25
- Maroudas A (1980). Physicochemical properties of articular cartilage. In: Freeman MAR, Meachim G (eds) Adult Articular Cartilage. Pitman Medical Publishing, Tunbridge Wells, pp 30-54
- Martin GR (1998). The roles of FGFs in the early development of vertebrate limbs. *Genes Dev* 12:1571-86
- Maslen CL, Babcock D, Redig JK, Kapeli K, Akkari YM, Olson SB (2006a). CRELD2: gene mapping, alternate splicing, and comparative genomic identification of the promoter region. *Gene* 382:111-20
- Maslen CL, Babcock D, Robinson SW, Bean LJ, Dooley KJ, Willour VL, Sherman SL (2006b). CRELD1 mutations contribute to the occurrence of cardiac atrioventricular septal defects in Down syndrome. *Am J Med Genet A* 140:2501-5
- Matsuzawa-Watanabe Y, Inoue J, Semba K (2003). Transcriptional activity of testis-determining factor SRY is modulated by the Wilms' tumor 1 gene product, WT1. *Oncogene* 22:7900-4
- Maxam AM, Gilbert W (1977). A new method for sequencing DNA. *Proc Natl Acad Sci U S A* 74:560-4
- McCabe ER (1996). Sex and the single DAX1: too little is bad, but can we have too much? *J Clin Invest* 98:881-2
- McEwan PA, Scott PG, Bishop PN, Bella J (2006). Structural correlations in the family of small leucine-rich repeat proteins and proteoglycans. *J Struct Biol* 155:294-305
- McGinnis S, Madden TL (2004). BLAST: at the core of a powerful and diverse set of sequence analysis tools. *Nucleic Acids Res* 32:W20-5
- McIntosh I, Dunston JA, Liu L, Hoover-Fong JE, Sweeney E (2005). Nail patella syndrome revisited: 50 years after linkage. *Ann Hum Genet* 69:349-63
- McKusick VA (2007). Mendelian Inheritance in Man and its online version, OMIM. *Am J Hum Genet* 80:588-604
- McMahon AP (2000). More surprises in the Hedgehog signaling pathway. *Cell* 100:185-8

- Meeks JJ, Weiss J, Jameson JL (2003). Dax1 is required for testis determination. *Nat Genet* 34:32-3
- Melendez-Herrera E, Varela-Echavarria A (2006). Expression of secreted semaphorins and their receptors in specific neuromeres, boundaries, and neuronal groups in the developing mouse and chick brain. *Brain Res* 1067:126-37
- Michaud JL, Lapointe F, Le Douarin NM (1997). The dorsoventral polarity of the presumptive limb is determined by signals produced by the somites and by the lateral somatopleure. *Development* 124:1453-63
- Miller G, Shope T, Lisco H, Stitt D, Lipman M (1972). Epstein-Barr virus: transformation, cytopathic changes, and viral antigens in squirrel monkey and marmoset leukocytes. *Proc Natl Acad Sci U S A* 69:383-7
- Millonig JH, Millen KJ, Hatten ME (2000). The mouse Dreher gene Lmx1a controls formation of the roof plate in the vertebrate CNS. *Nature* 403:764-9
- Mimiwati Z, Mackey DA, Craig JE, Mackinnon JR, Rait JL, Liebelt JE, Ayala-Lugo R, Vollrath D, Richards JE (2006). Nail-patella syndrome and its association with glaucoma: a review of eight families. *Br J Ophthalmol* 90:1505-9
- Miner JH, Morello R, Andrews KL, Li C, Antignac C, Shaw AS, Lee B (2002). Transcriptional induction of slit diaphragm genes by Lmx1b is required in podocyte differentiation. *J Clin Invest* 109:1065-72
- Minguillon C, Del Buono J, Logan MP (2005). Tbx5 and Tbx4 are not sufficient to determine limb-specific morphologies but have common roles in initiating limb outgrowth. *Dev Cell* 8:75-84
- Minina E, Wenzel HM, Kreschel C, Karp S, Gaffield W, McMahon AP, Vortkamp A (2001). BMP and Ihh/PTHrP signaling interact to coordinate chondrocyte proliferation and differentiation. *Development* 128:4523-34
- Moes M, Rodius S, Coleman SJ, Monkley SJ, Goormaghtigh E, Tremuth L, Kox C, van der Holst PP, Critchley DR, Kieffer N (2007). The integrin binding site 2 (IBS2) in the talin rod domain is essential for linking integrin beta subunits to the cytoskeleton. *J Biol Chem* 282:17280-8
- Mohrmann G, Hengstler JG, Hofmann TG, Endeke SU, Lee B, Stelzer C, Zabel B, Brieger J, Hasenclever D, Tanner B, Sagemueller J, Sehoul J, Will H, Winterpacht A (2005). SPOC1, a novel PHD-finger protein: association with residual disease and survival in ovarian cancer. *Int J Cancer* 116:547-54
- Moon AM, Capecchi MR (2000). Fgf8 is required for outgrowth and patterning of the limbs. *Nat Genet* 26:455-9
- Moran JL, LeVorse JM, Vogt TF (1999). Limbs move beyond the radical fringe. *Nature* 399:742-3
- Morello R, Zhou G, Dreyer SD, Harvey SJ, Ninomiya Y, Thorner PS, Miner JH, Cole W, Winterpacht A, Zabel B, Oberg KC, Lee B (2001). Regulation of glomerular basement membrane collagen expression by LMX1B contributes to renal disease in nail patella syndrome. *Nat Genet* 27:205-8
- Mukhopadhyay K, Lefebvre V, Zhou G, Garofalo S, Kimura JH, de Crombrughe B (1995). Use of a new rat chondrosarcoma cell line to delineate a 119-base pair chondrocyte-specific enhancer element and to define active promoter segments in the mouse pro-alpha 1(II) collagen gene. *J Biol Chem* 270:27711-9

- Mundel P, Reiser J, Zuniga Mejia Borja A, Pavenstadt H, Davidson GR, Kriz W, Zeller R (1997). Rearrangements of the cytoskeleton and cell contacts induce process formation during differentiation of conditionally immortalized mouse podocyte cell lines. *Exp Cell Res* 236:248-58
- Mundlos S, Olsen BR (1997). Heritable diseases of the skeleton. Part II: Molecular insights into skeletal development-matrix components and their homeostasis. *Faseb J* 11:227-33
- Mundlos S, Otto F, Mundlos C, Mulliken JB, Aylsworth AS, Albright S, Lindhout D, Cole WG, Henn W, Knoll JH, Owen MJ, Mertelsmann R, Zabel BU, Olsen BR (1997). Mutations involving the transcription factor CBFA1 cause cleidocranial dysplasia. *Cell* 89:773-9
- Murakami S, Akiyama H, de Crombrughe B (2004). Development of Bone and Cartilage. In: Epstein CJ, Erickson RP, Wynshaw-Boris A (eds) *Inborn Errors of Development: The Molecular Basis of Clinical Disorders of Morphogenesis*. Oxford University Press, New York, pp 133-147
- Murakami S, Kan M, McKeehan WL, de Crombrughe B (2000). Up-regulation of the chondrogenic Sox9 gene by fibroblast growth factors is mediated by the mitogen-activated protein kinase pathway. *Proc Natl Acad Sci U S A* 97:1113-8
- Muscatelli F, Strom TM, Walker AP, Zanaria E, Recan D, Meindl A, Bardoni B, Guioli S, Zehetner G, Rabl W, et al. (1994). Mutations in the DAX-1 gene give rise to both X-linked adrenal hypoplasia congenita and hypogonadotropic hypogonadism. *Nature* 372:672-6
- Nachtigal MW, Hirokawa Y, Enyeart-VanHouten DL, Flanagan JN, Hammer GD, Ingraham HA (1998). Wilms' tumor 1 and Dax-1 modulate the orphan nuclear receptor SF-1 in sex-specific gene expression. *Cell* 93:445-54
- Nagaraj SH, Gasser RB, Ranganathan S (2007). A hitchhiker's guide to expressed sequence tag (EST) analysis. *Brief Bioinform* 8:6-21
- Nakashima K, Zhou X, Kunkel G, Zhang Z, Deng JM, Behringer RR, de Crombrughe B (2002). The novel zinc finger-containing transcription factor osterix is required for osteoblast differentiation and bone formation. *Cell* 108:17-29
- Neufeld G, Kessler O, Herzog Y (2002). The interaction of Neuropilin-1 and Neuropilin-2 with tyrosine-kinase receptors for VEGF. *Adv Exp Med Biol* 515:81-90
- Newman B, Gigout LI, Sudre L, Grant ME, Wallis GA (2001). Coordinated expression of matrix Gla protein is required during endochondral ossification for chondrocyte survival. *J Cell Biol* 154:659-66
- Niemann S, Zhao C, Pascu F, Stahl U, Aulepp U, Niswander L, Weber JL, Muller U (2004). Homozygous WNT3 mutation causes tetra-amelia in a large consanguineous family. *Am J Hum Genet* 74:558-63
- Nishimura R, Hata K, Harris SE, Ikeda F, Yoneda T (2002). Core-binding factor alpha 1 (Cbfa1) induces osteoblastic differentiation of C2C12 cells without interactions with Smad1 and Smad5. *Bone* 31:303-312
- Niswander L (2003). Pattern formation: old models out on a limb. *Nat Rev Genet* 4:133-43
- Nusse R (2003). Wnts and Hedgehogs: lipid-modified proteins and similarities in signaling mechanisms at the cell surface. *Development* 130:5297-305
- Ohbayashi N, Shibayama M, Kurotaki Y, Imanishi M, Fujimori T, Itoh N, Takada S (2002). FGF18 is required for normal cell proliferation and differentiation during osteogenesis

- and chondrogenesis. *Genes Dev* 16:870-9
- Okihana H, Yamada K (1999). Preparation of a cDNA library and preliminary assessment of 1400 genes from mouse growth cartilage. *J Bone Miner Res* 14:304-10
- Olsen BR, Reginato AM, Wang W (2000). Bone development. *Annu Rev Cell Dev Biol* 16:191-220
- Ornitz DM, Marie PJ (2002). FGF signaling pathways in endochondral and intramembranous bone development and human genetic disease. *Genes Dev* 16:1446-65
- Ortiz JA, Castillo M, del Toro ED, Mulet J, Gerber S, Valor LM, Sala S, Sala F, Gutierrez LM, Criado M (2005). The cysteine-rich with EGF-like domains 2 (CRELD2) protein interacts with the large cytoplasmic domain of human neuronal nicotinic acetylcholine receptor alpha4 and beta2 subunits. *J Neurochem* 95:1585-96
- Otto F, Thornell AP, Crompton T, Denzel A, Gilmour KC, Rosewell IR, Stamp GW, Beddington RS, Mundlos S, Olsen BR, Selby PB, Owen MJ (1997). *Cbfa1*, a candidate gene for cleidocranial dysplasia syndrome, is essential for osteoblast differentiation and bone development. *Cell* 89:765-71
- Pan P, Leppilampi M, Pastorekova S, Pastorek J, Waheed A, Sly WS, Parkkila S (2006). Carbonic anhydrase gene expression in CA II-deficient (*Car2*<sup>-/-</sup>) and CA IX-deficient (*Car9*<sup>-/-</sup>) mice. *J Physiol* 571:319-27
- Parr BA, McMahon AP (1995). Dorsalizing signal Wnt-7a required for normal polarity of D-V and A-P axes of mouse limb. *Nature* 374:350-3
- Parr BA, McMahon AP (1998). Sexually dimorphic development of the mammalian reproductive tract requires Wnt-7a. *Nature* 395:707-10
- Pasterkamp RJ, Kolodkin AL (2003). Semaphorin junction: making tracks toward neural connectivity. *Curr Opin Neurobiol* 13:79-89
- Pavenstadt H, Kriz W, Kretzler M (2003). Cell biology of the glomerular podocyte. *Physiol Rev* 83:253-307
- Peng H, Begg GE, Harper SL, Friedman JR, Speicher DW, Rauscher FJ, 3rd (2000). Biochemical analysis of the Kruppel-associated box (KRAB) transcriptional repression domain. *J Biol Chem* 275:18000-10
- Petajan JH, Momberger GL, Aase J, Wright DG (1969). Arthrogryposis syndrome (Kuskokwim disease) in the Eskimo. *Jama* 209:1481-6
- Peters J, Sechrist J, Luetolf S, Lored G, Bronner-Fraser M (2002). Spatial expression of the alternatively spliced EIIIB and EIIB segments of fibronectin in the early chicken embryo. *Cell Commun Adhes* 9:221-38
- Pheiffer BH, Zimmerman SB (1983). Polymer-stimulated ligation: enhanced blunt- or cohesive-end ligation of DNA or deoxyribooligonucleotides by T4 DNA ligase in polymer solutions. *Nucleic Acids Res* 11:7853-71
- Pinkel D, Segraves R, Sudar D, Clark S, Poole I, Kowbel D, Collins C, Kuo WL, Chen C, Zhai Y, Dairkee SH, Ljung BM, Gray JW, Albertson DG (1998). High resolution analysis of DNA copy number variation using comparative genomic hybridization to microarrays. *Nat Genet* 20:207-11
- Pogue R, Lyons K (2006). BMP signaling in the cartilage growth plate. *Curr Top Dev Biol* 76:1-48

- Pogue R, Sebald E, King L, Kronstadt E, Krakow D, Cohn DH (2004). A transcriptional profile of human fetal cartilage. *Matrix Biol* 23:299-307
- Pressman CL, Chen H, Johnson RL (2000). LMX1B, a LIM homeodomain class transcription factor, is necessary for normal development of multiple tissues in the anterior segment of the murine eye. *Genesis* 26:15-25
- Pritchard-Jones K, Fleming S, Davidson D, Bickmore W, Porteous D, Gosden C, Bard J, Buckler A, Pelletier J, Housman D, et al. (1990). The candidate Wilms' tumour gene is involved in genitourinary development. *Nature* 346:194-7
- Raats CJ, van den Born J, Bakker MA, Oppers-Walgreen B, Pisa BJ, Dijkman HB, Assmann KJ, Berden JH (2000). Expression of agrin, dystroglycan, and utrophin in normal renal tissue and in experimental glomerulopathies. *Am J Pathol* 156:1749-65
- Regl G, Neill GW, Eichberger T, Kasper M, Ikram MS, Koller J, Hintner H, Quinn AG, Frischauf AM, Aberger F (2002). Human GLI2 and GLI1 are part of a positive feedback mechanism in Basal Cell Carcinoma. *Oncogene* 21:5529-39
- Riddle RD, Ensini M, Nelson C, Tsuchida T, Jessell TM, Tabin C (1995). Induction of the LIM homeobox gene *Lmx1* by WNT7a establishes dorsoventral pattern in the vertebrate limb. *Cell* 83:631-40
- Riihonen R, Supuran CT, Parkkila S, Pastorekova S, Vaananen HK, Laitala-Leinonen T (2007). Membrane-bound carbonic anhydrases in osteoclasts. *Bone* 40:1021-31
- Robert B, Lallemand Y (2006). Anteroposterior patterning in the limb and digit specification: contribution of mouse genetics. *Dev Dyn* 235:2337-52
- Robinson SW, Morris CD, Goldmuntz E, Reller MD, Jones MA, Steiner RD, Maslen CL (2003). Missense mutations in CRELD1 are associated with cardiac atrioventricular septal defects. *Am J Hum Genet* 72:1047-52
- Rohr C, Prestel J, Heidet L, Hosser H, Kriz W, Johnson RL, Antignac C, Witzgall R (2002). The LIM-homeodomain transcription factor *Lmx1b* plays a crucial role in podocytes. *J Clin Invest* 109:1073-82
- Ross MD, Bruggeman LA, Hanss B, Sunamoto M, Marras D, Klotman ME, Klotman PE (2003). Podocan, a novel small leucine-rich repeat protein expressed in the sclerotic glomerular lesion of experimental HIV-associated nephropathy. *J Biol Chem* 278:33248-55
- Rupp PA, Fouad GT, Egelston CA, Reifsteck CA, Olson SB, Knosp WM, Glanville RW, Thornburg KL, Robinson SW, Maslen CL (2002). Identification, genomic organization and mRNA expression of CRELD1, the founding member of a unique family of matricellular proteins. *Gene* 293:47-57
- Sadovsky Y, Crawford PA, Woodson KG, Polish JA, Clements MA, Tourtellotte LM, Simburger K, Milbrandt J (1995). Mice deficient in the orphan receptor steroidogenic factor 1 lack adrenal glands and gonads but express P450 side-chain-cleavage enzyme in the placenta and have normal embryonic serum levels of corticosteroids. *Proc Natl Acad Sci U S A* 92:10939-43
- Salser WA (1974). DNA sequencing techniques. *Annu Rev Biochem* 43:923-65
- Sanchez-Garcia I, Rabbitts TH (1994). The LIM domain: a new structural motif found in zinc-finger-like proteins. *Trends Genet* 10:315-20
- Sanger F, Nicklen S, Coulson AR (1977). DNA sequencing with chain-terminating inhibitors. *Proc Natl Acad Sci U S A* 74:5463-7



- Santra M, Reed CC, Iozzo RV (2002). Decorin binds to a narrow region of the epidermal growth factor (EGF) receptor, partially overlapping but distinct from the EGF-binding epitope. *J Biol Chem* 277:35671-81
- Saunders JW, Jr. (1948). The proximo-distal sequence of origin of the parts of the chick wing and the role of the ectoderm. *J Exp Zool* 108:363-403
- Schena M, Shalon D, Davis RW, Brown PO (1995). Quantitative monitoring of gene expression patterns with a complementary DNA microarray. *Science* 270:467-70
- Schiwek D, Endlich N, Holzman L, Holthofer H, Kriz W, Endlich K (2004). Stable expression of nephrin and localization to cell-cell contacts in novel murine podocyte cell lines. *Kidney Int* 66:91-101
- Schlaubitzi S, Yatsenko SA, Smith LD, Keller KL, Vissers LE, Scott DA, Cai WW, Reardon W, Abdul-Rahman OA, Lammer EJ, Lifchez CA, Magenis E, Veltman JA, Stankiewicz P, Zabel BU, Lee B (2007). Ovotestes and XY sex reversal in a female with an interstitial 9q33.3-q34.1 deletion encompassing NR5A1 and LMX1B causing features of genitopatellar syndrome. *Am J Med Genet A* 143:1071-81
- Schonherr E, Broszat M, Brandan E, Bruckner P, Kresse H (1998). Decorin core protein fragment Leu155-Val260 interacts with TGF-beta but does not compete for decorin binding to type I collagen. *Arch Biochem Biophys* 355:241-8
- Schonherr E, Hausser H, Beavan L, Kresse H (1995). Decorin-type I collagen interaction. Presence of separate core protein-binding domains. *J Biol Chem* 270:8877-83
- Schweizer H (2003). Detailed analysis of Lmx1b expression in multiple organs and its role in dorso-ventral patterning with emphasis on myogenic precursor cells. Dissertation, University of Freiburg, Freiburg/ Germany
- Scott PG, McEwan PA, Dodd CM, Bergmann EM, Bishop PN, Bella J (2004). Crystal structure of the dimeric protein core of decorin, the archetypal small leucine-rich repeat proteoglycan. *Proc Natl Acad Sci U S A* 101:15633-8
- Scott WJ, Duggan CA, Schreiner CM, Collins MD (1990). Reduction of embryonic intracellular pH: a potential mechanism of acetazolamide-induced limb malformations. *Toxicol Appl Pharmacol* 103:238-54
- Seri M, Melchionda S, Dreyer S, Marini M, Carella M, Cusano R, Piemontese MR, Caroli F, Silengo M, Zelante L, Romeo G, Ravazzolo R, Gasparini P, Lee B (1999). Identification of LMX1B gene point mutations in Italian patients affected with Nail-Patella syndrome. *Int J Mol Med* 4:285-90
- Shaffer LG, Kennedy GM, Spikes AS, Lupski JR (1997). Diagnosis of CMT1A duplications and HNPP deletions by interphase FISH: implications for testing in the cytogenetics laboratory. *Am J Med Genet* 69:325-31
- Shankland SJ, Pippin JW, Reiser J, Mundel P (2007). Podocytes in culture: past, present, and future. *Kidney Int*
- Sheng Y, Mancino V, Birren B (1995). Transformation of Escherichia coli with large DNA molecules by electroporation. *Nucleic Acids Res* 23:1990-6
- Shih NY, Li J, Karpitskii V, Nguyen A, Dustin ML, Kanagawa O, Miner JH, Shaw AS (1999). Congenital nephrotic syndrome in mice lacking CD2-associated protein. *Science* 286:312-5
- Shimizu H, Yokoyama S, Asahara H (2007). Growth and differentiation of the developing limb bud from the perspective of chondrogenesis. *Dev Growth Differ* 49:449-54

- Shimoyama A, Wada M, Ikeda F, Hata K, Matsubara T, Nifuji A, Noda M, Amano K, Yamaguchi A, Nishimura R, Yoneda T (2007). Ihh/Gli2 Signaling Promotes Osteoblast Differentiation by Regulating Runx2 Expression and Function. *Mol Biol Cell*
- Shou S, Scott V, Reed C, Hitzemann R, Stadler HS (2005). Transcriptome analysis of the murine forelimb and hindlimb autopod. *Dev Dyn* 234:74-89
- Siitonen HA, Kopra O, Kaariainen H, Haravuori H, Winter RM, Saamanen AM, Peltonen L, Kestila M (2003). Molecular defect of RAPADILINO syndrome expands the phenotype spectrum of RECQL diseases. *Hum Mol Genet* 12:2837-44
- Sly WS (1989). The carbonic anhydrase II deficiency syndrome: osteopetrosis with renal tubular acidosis and cerebral calcification. In: *The Metabolic Basis of Inherited Disease*. McGraw-Hill, New York, pp 2857-2866
- Sly WS, Hewett-Emmett D, Whyte MP, Yu YS, Tashian RE (1983). Carbonic anhydrase II deficiency identified as the primary defect in the autosomal recessive syndrome of osteopetrosis with renal tubular acidosis and cerebral calcification. *Proc Natl Acad Sci U S A* 80:2752-6
- Smidt MP, Asbreuk CH, Cox JJ, Chen H, Johnson RL, Burbach JP (2000). A second independent pathway for development of mesencephalic dopaminergic neurons requires Lmx1b. *Nat Neurosci* 3:337-41
- St-Jacques B, Hammerschmidt M, McMahon AP (1999). Indian hedgehog signaling regulates proliferation and differentiation of chondrocytes and is essential for bone formation. *Genes Dev* 13:2072-86
- Stears RL, Martinsky T, Schena M (2003). Trends in microarray analysis. *Nat Med* 9:140-5
- Stelzer C (2000). Molekulargenetische Untersuchungen von Komponenten des Knorpel-/Knochengewebes. Johannes-Gutenberg University, Mainz
- Stephens TD, McNulty TR (1981). Evidence for a metameric pattern in the development of the chick humerus. *J Embryol Exp Morphol* 61:191-205
- Summerbell D (1974). A quantitative analysis of the effect of excision of the AER from the chick limb-bud. *J Embryol Exp Morphol* 32:651-60
- Summerbell D, Lewis JH, Wolpert L (1973). Positional information in chick limb morphogenesis. *Nature* 244:492-6
- Superti-Furga A, Unger S (2007). Nosology and classification of genetic skeletal disorders: 2006 revision. *Am J Med Genet A* 143:1-18
- Susens U, Borgmeyer U (1996). Characterization of the human germ cell nuclear factor gene. *Biochim Biophys Acta* 1309:179-82
- Sweeney E, Fryer A, Mountford R, Green A, McIntosh I (2003). Nail patella syndrome: a review of the phenotype aided by developmental biology. *J Med Genet* 40:153-62
- Tagariello A (2005). Identifizierung und Charakterisierung von Genen mit Einfluss auf Entwicklung und Erhalt des Knorpel-/Knochen-Systems. Dissertation, Friedrich-Alexander-Universitaet, Erlangen-Nuernberg
- Tagariello A, Schlaubitz S, Hankeln T, Mohrmann G, Stelzer C, Schweizer A, Hermanns P, Lee B, Schmidt ER, Winterpacht A, Zabel B (2005). Expression profiling of human fetal growth plate cartilage by EST sequencing. *Matrix Biol* 24:530-8

- Takahashi T, Fournier A, Nakamura F, Wang LH, Murakami Y, Kalb RG, Fujisawa H, Strittmatter SM (1999). Plexin-neuropilin-1 complexes form functional semaphorin-3A receptors. *Cell* 99:59-69
- Takashima S, Kitakaze M, Asakura M, Asanuma H, Sanada S, Tashiro F, Niwa H, Miyazaki Ji J, Hirota S, Kitamura Y, Kitsukawa T, Fujisawa H, Klagsbrun M, Hori M (2002). Targeting of both mouse neuropilin-1 and neuropilin-2 genes severely impairs developmental yolk sac and embryonic angiogenesis. *Proc Natl Acad Sci U S A* 99:3657-62
- Takeda T, McQuistan T, Orlando RA, Farquhar MG (2001). Loss of glomerular foot processes is associated with uncoupling of podocalyxin from the actin cytoskeleton. *J Clin Invest* 108:289-301
- Tanaka K, Tsumaki N, Kozak CA, Matsumoto Y, Nakatani F, Iwamoto Y, Yamada Y (2002). A Kruppel-associated box-zinc finger protein, NT2, represses cell-type-specific promoter activity of the alpha 2(XI) collagen gene. *Mol Cell Biol* 22:4256-67
- Taniguchi M, Masuda T, Fukaya M, Kataoka H, Mishina M, Yaginuma H, Watanabe M, Shimizu T (2005). Identification and characterization of a novel member of murine semaphorin family. *Genes Cells* 10:785-92
- Thameem F, Wolford JK, Wang J, German MS, Bogardus C, Prochazka M (2002). Cloning, expression and genomic structure of human LMX1A, and variant screening in Pima Indians. *Gene* 290:217-25
- Tickle C (2004). The contribution of chicken embryology to the understanding of vertebrate limb development. *Mech Dev* 121:1019-29
- Tickle C, Munsterberg A (2001). Vertebrate limb development--the early stages in chick and mouse. *Curr Opin Genet Dev* 11:476-81
- Tiku ML, Liesch JB, Robertson FM (1990). Production of hydrogen peroxide by rabbit articular chondrocytes. Enhancement by cytokines. *J Immunol* 145:690-6
- Tominaga K, Kondo C, Kagata T, Hishida T, Nishizuka M, Imagawa M (2004). The novel gene fad158, having a transmembrane domain and leucine-rich repeat, stimulates adipocyte differentiation. *J Biol Chem* 279:34840-8
- Ullmann A, Jacob F, Monod J (1967). Characterization by in vitro complementation of a peptide corresponding to an operator-proximal segment of the beta-galactosidase structural gene of *Escherichia coli*. *J Mol Biol* 24:339-43
- Vaananen HK (1984). Immunohistochemical localization of carbonic anhydrase isoenzymes I and II in human bone, cartilage and giant cell tumor. *Histochemistry* 81:485-7
- Vainio S, Heikkila M, Kispert A, Chin N, McMahon AP (1999). Female development in mammals is regulated by Wnt-4 signalling. *Nature* 397:405-9
- van Meyel DJ, Thomas JB, Agulnick AD (2003). Ssdp proteins bind to LIM-interacting co-factors and regulate the activity of LIM-homeodomain protein complexes in vivo. *Development* 130:1915-25
- Veitia RA, Salas-Cortes L, Ottolenghi C, Pailhoux E, Cotinot C, Fellous M (2001). Testis determination in mammals: more questions than answers. *Mol Cell Endocrinol* 179:3-16
- Velculescu VE (1999). Essay: Amersham Pharmacia Biotech & Science prize. Tantalizing transcriptomes--SAGE and its use in global gene expression analysis. *Science* 286:1491-2

- Venter JC, Adams MD, Myers EW, Li PW, Mural RJ, Sutton GG, Smith HO, Yandell M, Evans CA, Holt RA, Gocayne JD, Amanatides P, Ballew RM, Huson DH, Wortman JR, Zhang Q, Kodira CD, Zheng XH, Chen L, Skupski M, Subramanian G, Thomas PD, Zhang J, Gabor Miklos GL, Nelson C, Broder S, Clark AG, Nadeau J, McKusick VA, Zinder N, Levine AJ, Roberts RJ, Simon M, Slayman C, Hunkapiller M, Bolanos R, Delcher A, Dew I, Fasulo D, Flanigan M, Florea L, Halpern A, Hannenhalli S, Kravitz S, Levy S, Mobarry C, Reinert K, Remington K, Abu-Threideh J, Beasley E, Biddick K, Bonazzi V, Brandon R, Cargill M, Chandramouliswaran I, Charlab R, Chaturvedi K, Deng Z, Di Francesco V, Dunn P, Eilbeck K, Evangelista C, Gabrielian AE, Gan W, Ge W, Gong F, Gu Z, Guan P, Heiman TJ, Higgins ME, Ji RR, Ke Z, Ketchum KA, Lai Z, Lei Y, Li Z, Li J, Liang Y, Lin X, Lu F, Merkulov GV, Milshina N, Moore HM, Naik AK, Narayan VA, Neelam B, Nusskern D, Rusch DB, Salzberg S, Shao W, Shue B, Sun J, Wang Z, Wang A, Wang X, Wang J, Wei M, Wides R, Xiao C, Yan C, Yao A, Ye J, Zhan M, Zhang W, Zhang H, Zhao Q, Zheng L, Zhong F, Zhong W, Zhu S, Zhao S, Gilbert D, Baumhueter S, Spier G, Carter C, Cravchik A, Woodage T, Ali F, An H, Awe A, Baldwin D, Baden H, Barnstead M, Barrow I, Beeson K, Busam D, Carver A, Center A, Cheng ML, Curry L, Danaher S, Davenport L, Desilets R, Dietz S, Dodson K, Doup L, Ferreira S, Garg N, Gluecksmann A, Hart B, Haynes J, Haynes C, Heiner C, Hladun S, Hostin D, Houck J, Howland T, Ibegwam C, Johnson J, Kalush F, Kline L, Koduru S, Love A, Mann F, May D, McCawley S, McIntosh T, McMullen I, Moy M, Moy L, Murphy B, Nelson K, Pfannkoch C, Pratt E, Puri V, Qureshi H, Reardon M, Rodriguez R, Rogers YH, Romblad D, Ruhfel B, Scott R, Sitter C, Smallwood M, Stewart E, Strong R, Suh E, Thomas R, Tint NN, Tse S, Vech C, Wang G, Wetter J, Williams S, Williams M, Windsor S, Winn-Deen E, Wolfe K, Zaveri J, Zaveri K, Abril JF, Guigo R, Campbell MJ, Sjolander KV, Karlak B, Kejariwal A, Mi H, Lazareva B, Hatton T, Narechania A, Diemer K, Muruganujan A, Guo N, Sato S, Bafna V, Istrail S, Lippert R, Schwartz R, Walenz B, Yooseph S, Allen D, Basu A, Baxendale J, Blick L, Caminha M, Carnes-Stine J, Caulk P, Chiang YH, Coyne M, Dahlke C, Mays A, Dombroski M, Donnelly M, Ely D, Esparham S, Fosler C, Gire H, Glanowski S, Glasser K, Glodek A, Gorokhov M, Graham K, Gropman B, Harris M, Heil J, Henderson S, Hoover J, Jennings D, Jordan C, Jordan J, Kasha J, Kagan L, Kraft C, Levitsky A, Lewis M, Liu X, Lopez J, Ma D, Majoros W, McDaniel J, Murphy S, Newman M, Nguyen T, Nguyen N, Nodell M, Pan S, Peck J, Peterson M, Rowe W, Sanders R, Scott J, Simpson M, Smith T, Sprague A, Stockwell T, Turner R, Venter E, Wang M, Wen M, Wu D, Wu M, Xia A, Zandieh A, Zhu X (2001). The sequence of the human genome. *Science* 291:1304-51
- Villegas G, Tufro A (2002). Ontogeny of semaphorins 3A and 3F and their receptors neuropilins 1 and 2 in the kidney. *Mech Dev* 119 Suppl 1:S149-53
- Visser LE, de Vries BB, Osoegawa K, Janssen IM, Feuth T, Choy CO, Straatman H, van der Vliet W, Huys EH, van Rijk A, Smeets D, van Ravenswaaij-Arts CM, Knoers NV, van der Burgt I, de Jong PJ, Brunner HG, van Kessel AG, Schoenmakers EF, Veltman JA (2003). Array-based comparative genomic hybridization for the genomewide detection of submicroscopic chromosomal abnormalities. *Am J Hum Genet* 73:1261-70
- Vogel A, Rodriguez C, Warnken W, Izpisua Belmonte JC (1995). Dorsal cell fate specified by chick Lmx1 during vertebrate limb development. *Nature* 378:716-20
- Vollrath D, Jaramillo-Babb VL, Clough MV, McIntosh I, Scott KM, Lichter PR, Richards JE (1998). Loss-of-function mutations in the LIM-homeodomain gene, LMX1B, in nail-patella syndrome. *Hum Mol Genet* 7:1091-8
- Vortkamp A, Lee K, Lanske B, Segre GV, Kronenberg HM, Tabin CJ (1996). Regulation of rate of cartilage differentiation by Indian hedgehog and PTH-related protein. *Science* 273:613-22
- Wagner KD, Wagner N, Schedl A (2003). The complex life of WT1. *J Cell Sci* 116:1653-8

- Wagner T, Wirth J, Meyer J, Zabel B, Held M, Zimmer J, Pasantes J, Bricarelli FD, Keutel J, Hustert E, et al. (1994). Autosomal sex reversal and campomelic dysplasia are caused by mutations in and around the SRY-related gene SOX9. *Cell* 79:1111-20
- Wang SM (2007). Understanding SAGE data. *Trends Genet* 23:42-50
- Wang Y, Middleton F, Horton JA, Reichel L, Farnum CE, Damron TA (2004). Microarray analysis of proliferative and hypertrophic growth plate zones identifies differentiation markers and signal pathways. *Bone* 35:1273-93
- Watanabe H, Yamada Y (1999). Mice lacking link protein develop dwarfism and craniofacial abnormalities. *Nat Genet* 21:225-9
- Watanabe K, Harayama S (2001). [SWISS-PROT: the curated protein sequence database on Internet]. *Tanpakushitsu Kakusan Koso* 46:80-6
- Weber IT, Harrison RW, Iozzo RV (1996). Model structure of decorin and implications for collagen fibrillogenesis. *J Biol Chem* 271:31767-70
- Wegener KL, Partridge AW, Han J, Pickford AR, Liddington RC, Ginsberg MH, Campbell ID (2007). Structural basis of integrin activation by talin. *Cell* 128:171-82
- Wheeler DL, Church DM, Lash AE, Leipe DD, Madden TL, Pontius JU, Schuler GD, Schriml LM, Tatusova TA, Wagner L, Rapp BA (2001). Database resources of the National Center for Biotechnology Information. *Nucleic Acids Res* 29:11-6
- White DJ, Puranen S, Johnson MS, Heino J (2004). The collagen receptor subfamily of the integrins. *Int J Biochem Cell Biol* 36:1405-10
- Wilfinger WW, Mackey K, Chomczynski P (1997). Effect of pH and ionic strength on the spectrophotometric assessment of nucleic acid purity. *Biotechniques* 22:474-6, 478-81
- Wilhelm D, Englert C (2002). The Wilms tumor suppressor WT1 regulates early gonad development by activation of Sf1. *Genes Dev* 16:1839-51
- Wilson MJ, Jeyasuria P, Parker KL, Koopman P (2005). The transcription factors steroidogenic factor-1 and SOX9 regulate expression of Vanin-1 during mouse testis development. *J Biol Chem* 280:5917-23
- Winnemoller M, Schon P, Vischer P, Kresse H (1992). Interactions between thrombospondin and the small proteoglycan decorin: interference with cell attachment. *Eur J Cell Biol* 59:47-55
- Wittwer CT, Herrmann MG, Moss AA, Rasmussen RP (1997). Continuous fluorescence monitoring of rapid cycle DNA amplification. *Biotechniques* 22:130-1, 134-8
- Woods CG, Stricker S, Seemann P, Stern R, Cox J, Sherridan E, Roberts E, Springell K, Scott S, Karbani G, Sharif SM, Toomes C, Bond J, Kumar D, Al-Gazali L, Mundlos S (2006). Mutations in WNT7A cause a range of limb malformations, including Fuhrmann syndrome and Al-Awadi/Raas-Rothschild/Schinzel phocomelia syndrome. *Am J Hum Genet* 79:402-8
- Wozney JM, Rosen V (1998). Bone morphogenetic protein and bone morphogenetic protein gene family in bone formation and repair. *Clin Orthop Relat Res*:26-37
- Yamane S, Cheng E, You Z, Reddi AH (2007). Gene Expression Profiling of Mouse Articular and Growth Plate Cartilage. *Tissue Eng*

- Yang Y (2003). Wnts and wing: Wnt signaling in vertebrate limb development and musculoskeletal morphogenesis. *Birth Defects Res C Embryo Today* 69:305-17
- Yonei-Tamura S, Endo T, Yajima H, Ohuchi H, Ide H, Tamura K (1999). FGF7 and FGF10 directly induce the apical ectodermal ridge in chick embryos. *Dev Biol* 211:133-43
- Yoon BS, Pogue R, Ovchinnikov DA, Yoshii I, Mishina Y, Behringer RR, Lyons KM (2006). BMPs regulate multiple aspects of growth-plate chondrogenesis through opposing actions on FGF pathways. *Development* 133:4667-78
- Yoshida CA, Yamamoto H, Fujita T, Furuichi T, Ito K, Inoue K, Yamana K, Zanma A, Takada K, Ito Y, Komori T (2004). Runx2 and Runx3 are essential for chondrocyte maturation, and Runx2 regulates limb growth through induction of Indian hedgehog. *Genes Dev* 18:952-63
- Yoshioka H, Iyama K, Inoguchi K, Khaleduzzaman M, Ninomiya Y, Ramirez F (1995). Developmental pattern of expression of the mouse alpha 1 (XI) collagen gene (Col11a1). *Dev Dyn* 204:41-7
- Yu W, Ballif BC, Kashork CD, Heilstedt HA, Howard LA, Cai WW, White LD, Liu W, Beaudet AL, Bejjani BA, Shaw CA, Shaffer LG (2003). Development of a comparative genomic hybridization microarray and demonstration of its utility with 25 well-characterized 1p36 deletions. *Hum Mol Genet* 12:2145-52
- Yuan L, Moyon D, Pardanaud L, Breant C, Karkkainen MJ, Alitalo K, Eichmann A (2002). Abnormal lymphatic vessel development in neuropilin 2 mutant mice. *Development* 129:4797-806
- Zaidi M (2007). Skeletal remodeling in health and disease. *Nat Med* 13:791-801
- Zhang H, Marshall KW, Tang H, Hwang DM, Lee M, Liew CC (2003). Profiling genes expressed in human fetal cartilage using 13,155 expressed sequence tags. *Osteoarthritis Cartilage* 11:309-19
- Zhang LH, Qin LX, Ma ZC, Ye SL, Liu YK, Ye QH, Wu X, Huang W, Tang ZY (2003b). Allelic imbalance regions on chromosomes 8p, 17p and 19p related to metastasis of hepatocellular carcinoma: comparison between matched primary and metastatic lesions in 22 patients by genome-wide microsatellite analysis. *J Cancer Res Clin Oncol* 129:279-86
- Zheng B, Mills AA, Bradley A (1999). A system for rapid generation of coat color-tagged knockouts and defined chromosomal rearrangements in mice. *Nucleic Acids Res* 27:2354-60
- Zheng L, Pan H, Li S, Flesken-Nikitin A, Chen PL, Boyer TG, Lee WH (2000). Sequence-specific transcriptional corepressor function for BRCA1 through a novel zinc finger protein, ZBRK1. *Mol Cell* 6:757-68
- Zhu JD, Pan HO, Suzuki F, Takigawa M (1994). Proto-oncogene expression in a human chondrosarcoma cell line: HCS-2/8. *Jpn J Cancer Res* 85:364-71



## 8. Appendix

### 8.1. Abbreviations

#	number
3'UTR	three prime untranslated region
18S RNA	18S ribosomal RNA
28S RNA	28S ribosomal RNA
$\alpha$	alpha
aa	amino acid
A	adenin
AA-dUTP	aminoallyl-dUTP
Ab	antibody
AD	adult
<i>AGC1/ Agc1</i>	aggrecan
$\beta$	beta
bp	base pair
<i>BRCA1</i>	breast cancer 1, early onset
BSA	Bovine serum albumin
C	cytosine
°C	degree Celsius
<i>CDKN3/ KAP1</i>	cyclin-dependent kinase inhibitor 3
cDNA	complementary DNA
cpm	counts per minute
cm <sup>2</sup>	square centimeter
DAPI	4',6-diamidino-2-phenylindole
DI	deionized
DIG	digoxigenin
DMEM	MEM with high concentration of D-glucose
DMSO	Dimethylsulfoxide
DNA	deoxynucleic acid
dNTP	Deoxyribonucleotide triphosphate
dT	deoxyribose thymidine nucleotides
DTT	dithiothritol



---

dUTP	2'-Deoxyuridine 5'-Triphosphate
E	embryonic stage
EBV	Epstein Barr Virus
ECM	extracellular matrix
E.coli	<i>Escherichia coli</i>
EDTA	ethylenediamine tetracetic acid
EST	expressed sequence tag
EtOH	ethanol
<i>EXT1</i>	exostoses (multiple) 1
Fig.	Figure
g	gram
$\times g$	acceleration of gravity
G	guanine
GBM	glomerular basement membrane
h	hour/ s
IgG	Immunoglobulin G
ISH	<i>in situ</i> hybridisation
kb	kilo base pair
ko	knockout
$\mu\text{g}$	microgram
$\mu\text{l}$	micro litre
$\mu\text{m}$	micro metre
$\mu\text{M}$	micro molar
M	molar
MA	milli ampere
mCi	milli Curie
MEM	minimal essential medium
min	minute(s)
mg	milligram
ml	millilitre
mM	milli molar
MSC	mesenchymal stem cells
NB	newborn

---

ng	nanogram
nm	nanometer
NCBI	National Center of Biotechnology Information
NTES	sodium tris-EDTA buffer with SDS
OD	optical density
OMIM	Online Mendelian Inheritance in Man
ON	over night
[ $\alpha$ - <sup>32</sup> P]dCTP	Deoxycytidine 5'-alpha 32P triphosphate
PBS	phosphate buffered saline
PCR	polymerase chain reaction
PFA	paraformaldehyde
pH	potential of hydrogen
qRT-PCR	quantitative real time PCR
RNA	ribonucleic acid
rpm	rotations per minute
RT	room temperature
[ $\alpha$ - <sup>35</sup> S] dUTP	Deoxyuridine 5'-alpha 35S triphosphate
sec	second(s)
SDS	sodium dodecyl sulfate
<i>SPOC1/ PHF13</i>	PHD finger protein 13
SSC	standard-saline-citrate buffer
ssT-DNA	single stranded template DNA
T	thymine
TBE	tris-borate-EDTA buffer
TBST	tris buffered saline with Tween
TE	tris-EDTA buffer
mRNA	messenger ribonucleic acid
tRNA	transfer ribonucleic acid
U	Units
UV	<i>Ultraviolet</i>
vol.	volume
vs.	versus

WISH	whole mount <i>in situ</i> hybridization
wt	wild type
ZBRK1/ ZNF350	zinc finger protein 350
ZNF	zinc finger protein

## 8.2. Additional results

Symbol	Name	Legend (2 fold req)
Cbln1	cerebellin 1 precursor protein	•E11.5 — 12.5 ▲13.5
Chd7	chromodomain helicase DNA binding protein 7	•E11.5 — 12.5 ▲13.5
Dusp9	dual specificity phosphatase 9	•E11.5 — 12.5 ▲13.5
Mogat2	monoacylglycerol O-acyltransferase 2	•E11.5 — 12.5 ▲13.5
Slc4a1	solute carrier family 4 (anion exchanger), member 1	•E11.5 — 12.5 ▲13.5
5730507A09Rik	RIKEN cDNA 5730507A09 gene	•E11.5 — 12.5 ▼13.5
Anxa2	annexin A2	•E11.5 — 12.5 ▼13.5
BC049816	cDNA sequence BC049816	•E11.5 — 12.5 ▼13.5
Col5a2	procollagen, type V, alpha 2	•E11.5 — 12.5 ▼13.5
Cspg4	chondroitin sulfate proteoglycan 4	•E11.5 — 12.5 ▼13.5
Col6a2	procollagen, type VI, alpha 2	•E11.5 — 12.5 ▼13.5
Cryab	crystallin, alpha B	•E11.5 — 12.5 ▼13.5
Cugbp2	CUG triplet repeat, RNA binding protein 2	•E11.5 — 12.5 ▼13.5
D4Bwg0951e	DNA segment, Chr 4, Brigham & Women's Genetics	•E11.5 — 12.5 ▼13.5
Dkk3	dickkopf homolog 3 ( <i>Xenopus laevis</i> )	•E11.5 — 12.5 ▼13.5
Emp3	epithelial membrane protein 3	•E11.5 — 12.5 ▼13.5
Fmod	fibromodulin	•E11.5 — 12.5 ▼13.5
Gsn	gelsolin	•E11.5 — 12.5 ▼13.5
Hhip	Hedgehog-interacting protein	•E11.5 — 12.5 ▼13.5
Irx2	Iroquois related homeobox 2 ( <i>Drosophila</i> )	•E11.5 — 12.5 ▼13.5
Kcnk2	potassium channel, subfamily K, member 2	•E11.5 — 12.5 ▼13.5
Krt1-15	keratin complex 1, acidic, gene 15	•E11.5 — 12.5 ▼13.5
Maib	v-maf musculoaponeurotic fibrosarcoma oncogene family, protein B (avian)	•E11.5 — 12.5 ▼13.5
MGI:2149786	selenoprotein M	•E11.5 — 12.5 ▼13.5
Nr3c1	nuclear receptor subfamily 3, group C, member 1	•E11.5 — 12.5 ▼13.5
Pdlim3	PDZ and LIM domain 3	•E11.5 — 12.5 ▼13.5
Pmp22	peripheral myelin protein	•E11.5 — 12.5 ▼13.5
Rian	RNA imprinted and accumulated in nucleus	•E11.5 — 12.5 ▼13.5
S100a10	S100 calcium binding protein A10 (calpactin)	•E11.5 — 12.5 ▼13.5
Smoc2	SPARC related modular calcium binding 2	•E11.5 — 12.5 ▼13.5
Tekt2	tektin 2	•E11.5 — 12.5 ▼13.5
Tmeff2	TM pr. with EGF-like and two follistatin-like domains 2	•E11.5 — 12.5 ▼13.5
Zfhx1b	zinc finger homeobox 1b	•E11.5 — 12.5 ▼13.5
5930437A14Rik	RIKEN cDNA 5930437A14 gene	•E11.5 ▲12.5 —13.5
AL022943	expressed sequence AL022943	•E11.5 ▲12.5 —13.5
Col11a1	procollagen, type XI, alpha 1	•E11.5 ▲12.5 —13.5
Egfr	epidermal growth factor receptor	•E11.5 ▲12.5 —13.5
Gja3	gap junction membrane channel protein alpha 3	•E11.5 ▲12.5 —13.5
Gjb6	gap junction membrane channel protein beta 6	•E11.5 ▲12.5 —13.5

Il17b	interleukin 17B	•E11.5 ▲12.5 —13.5
Klf1	Kruppel-like factor 1 (erythroid)	•E11.5 ▲12.5 —13.5
Krt2-8	keratin complex 2, basic, gene 8	•E11.5 ▲12.5 —13.5
Lgals7	lectin, galactose binding, soluble 7	•E11.5 ▲12.5 —13.5
MGC107514	MGC107514	•E11.5 ▲12.5 —13.5
Punc	putative neuronal cell adhesion molecule	•E11.5 ▲12.5 —13.5
Samd4	sterile alpha motif domain containing 4	•E11.5 ▲12.5 —13.5
Slit2	slit homolog 2 (Drosophila)	•E11.5 ▲12.5 —13.5
Asb4	ankyrin repeat and SOCS box-containing protein 4	•E11.5 ▲12.5 ▲13.5
Frzb	frizzled-related protein	•E11.5 ▲12.5 ▲13.5
Pmaip1	phorbol-12-myristate-13-acetate-induced protein 1	•E11.5 ▲12.5 ▲13.5
4933425F03Rik	RIKEN cDNA 4933425F03 gene	•E11.5 ▼12.5 ▼13.5
Agc1	aggrecan 1	•E11.5 ▼12.5 ▼13.5
Angptl1	angiopoietin-like 1	•E11.5 ▼12.5 ▼13.5
Chodl	chondrolectin	•E11.5 ▼12.5 ▼13.5
Col5a1	procollagen, type V, alpha 1	•E11.5 ▼12.5 ▼13.5
Col6a1	procollagen, type VI, alpha 1	•E11.5 ▼12.5 ▼13.5
Col6a3	procollagen, type VI, alpha 3	•E11.5 ▼12.5 ▼13.5
Col8a2	procollagen, type VIII, alpha 2	•E11.5 ▼12.5 ▼13.5
Cthrc1	collagen triple helix repeat containing 1	•E11.5 ▼12.5 ▼13.5
Cyt1	cytokine like 1	•E11.5 ▼12.5 ▼13.5
Dcn	decorin	•E11.5 ▼12.5 ▼13.5
E430002G05Rik	RIKEN cDNA E430002G05 gene	•E11.5 ▼12.5 ▼13.5
Egfl6	EGF-like-domain, multiple 6	•E11.5 ▼12.5 ▼13.5
Egr1	early growth response 1	•E11.5 ▼12.5 ▼13.5
Enpp2	ectonucleotide pyrophosphatase/phosphodiesterase 2	•E11.5 ▼12.5 ▼13.5
Gdf10	growth differentiation factor 10	•E11.5 ▼12.5 ▼13.5
Htra1	HtrA serine peptidase 1	•E11.5 ▼12.5 ▼13.5
Irx5	Iroquois related homeobox 5 (Drosophila)	•E11.5 ▼12.5 ▼13.5
Itgb1bp2	integrin beta 1 binding protein 2	•E11.5 ▼12.5 ▼13.5
Kera	keratocan	•E11.5 ▼12.5 ▼13.5
Lox	lysyl oxidase	•E11.5 ▼12.5 ▼13.5
Ltbp3	latent transforming growth factor beta binding prot. 3	•E11.5 ▼12.5 ▼13.5
Lum	lumican	•E11.5 ▼12.5 ▼13.5
Matn1	matrilin 1, cartilage matrix protein 1	•E11.5 ▼12.5 ▼13.5
Matn4	matrilin 4	•E11.5 ▼12.5 ▼13.5
MGI:1932093	Jun dimerization protein 2	•E11.5 ▼12.5 ▼13.5
Mgp	matrix Gla protein	•E11.5 ▼12.5 ▼13.5
Mia1	melanoma inhibitory activity 1	•E11.5 ▼12.5 ▼13.5
Myom2	myomesin 2	•E11.5 ▼12.5 ▼13.5
Col12a1	procollagen, type XII, alpha 1	•E11.5 ▼12.5 ▼13.5
Nfib	nuclear factor I/B	•E11.5 ▼12.5 ▼13.5
Nfix	nuclear factor I/X	•E11.5 ▼12.5 ▼13.5
Ogn	osteoglycin	•E11.5 ▼12.5 ▼13.5
Pik3r1	phosphatidylinositol 3-kinase, regulatory subunit, polypeptide 1 (p85 alpha)	•E11.5 ▼12.5 ▼13.5
Polr2b	polymerase (RNA) II (DNA directed) polypeptide B	•E11.5 ▼12.5 ▼13.5
Prss35	protease, serine, 35	•E11.5 ▼12.5 ▼13.5
Rarb	retinoic acid receptor, beta	•E11.5 ▼12.5 ▼13.5
Rdh10	retinol dehydrogenase 10 (all-trans)	•E11.5 ▼12.5 ▼13.5

Slc26a7	solute carrier family 26, member 7	•E11.5 ▼ 12.5 ▼ 13.5
Sln	sarcolipin	•E11.5 ▼ 12.5 ▼ 13.5
Smpx	small muscle protein, X-linked	•E11.5 ▼ 12.5 ▼ 13.5
Tceal7	transcription elongation factor A (SII)-like 7	•E11.5 ▼ 12.5 ▼ 13.5
Tnc	tenascin C	•E11.5 ▼ 12.5 ▼ 13.5
Tnnt2	troponin T2, cardiac	•E11.5 ▼ 12.5 ▼ 13.5
Wisp1	WNT1 inducible signaling pathway protein 1	•E11.5 ▼ 12.5 ▼ 13.5
Zcchc5	zinc finger, CCHC domain containing 5	•E11.5 ▼ 12.5 ▼ 13.5

**Table 11: List of 98 individual genes that were found differentially expressed** (at least a 2-fold difference) over time by micro array. Colors encode biological function as follow: yellow: genes involved in cell division/ cycle and DNA replication; green: cell-cell signaling/ communication and transport; blue: cell structure and motility; red: cell/ organism defense and apoptosis; brown: gene/ protein expression, transcription factors, and posttranslational modification; gray: proteolysis; orange: and metabolism.

### **8.3. Curriculum vitae**

Name (last, first):

Home address:

Born:

Marital status:

PhD:

Diploma thesis:

Study:

Education:

## 8.4. Publications

Hankeln T, Schmidt ER, Winterpacht A, Zabel BU sowie Amid C, Bikar SE, Brückmann T, Cichutek A, Mujica A, Sampson N, Schlaubitz S (2000). Die vergleichende Genomanalyse in Mensch und Maus als Werkzeug zur Identifizierung von Genen *DHGP X-PRESS* 8: Mai 2000 (in German language)

Cichutek A, Brückmann T, Seipel B, Hauser H, Schlaubitz S, Prawitt D, Hankeln T, Schmidt ER, Winterpacht A, Zabel BU (2001) Comparative architectural aspects of regions of conserved synteny on human chromosome 11p15.3 and mouse chromosome 7 (including genes *WEE1* and *LMO1*). *Cytogenet. Cell Genet.* 93(3-4): 277-283.

Tagariello T, Schlaubitz S, Hankeln T, Mohrmann G, Stelzer C, Schweizer A, Hermanns P, Lee B, Schmidt ER, Winterpacht A, Zabel B (2005) Expression profiling of human fetal growth plate cartilage by EST sequencing. *Matrix Biol.* 24(8): 530-538

Abdul-Rahman OA, La TH, Kwan A, Schlaubitz S, Barsh GS, Enns GM, Hudgins L. (2006) Genitopatellar syndrome: Expanding the phenotype and excluding mutations in *LMX1B* and *TBX4*. *Am J Med Genet A.* 140(14): 1567-1572

Schlaubitz S, Yatsenko SA, Smith LD, Keller KL, Vissers LE, Scott DA, Cai WW, Reardon W, Abdul-Rahman OA, Lammer EJ, Lifchez CA, Magenis E, Veltman JA, Stankiewicz P, Zabel BU, Lee B. (2007) Ovotestes and XY Sex Reversal in a Female with an Interstitial 9q33.3-q34.1 Deletion Encompassing *NR5A1* and *LMX1B* causing features of Genitopatellar Syndrome. *Am J Med Genet A.* 143A:1071-1081

Morello R, Bertin TK, Schlaubitz S, Shaw CA, Kakuru S, Munivez E, Hermanns P, Chen Y, Zabel B, Lee B. (2007) Brachy-syndactyly caused by loss of *Sfrp2* function. *J Cell Phys* - submitted

## 8.5. Poster presentations

T. Brückmann, S. Schlaubitz, T. Hankeln, E.R. Schmidt, A. Winterpacht, B. Zabel: Comparative genomic sequencing of the TUB gene region in man and mouse - Identification of putative regulatory elements. The 12<sup>th</sup> Annual Meeting of the German Society of Human Genetics together with the Austrian Society of Human Genetics and the Swiss Society of Medical Genetics, Lübeck, Germany, March 22<sup>nd</sup>- 25<sup>th</sup> 2000

B. Zabel, C. Stelzer, P. Hermanns, S. Schlaubitz, G. Mohrmann, H. Friedl, C. Mühlbauer, B. Lee, T. Hankeln, A. Winterpacht, E.R. Schmidt ER: Molecular identification of genes and pathways involved in skeletogenesis by EST generation, full length cDNA isolation and expression profiling. German Humane Genome Meeting 2000, Heidelberg, Germany, November 30<sup>th</sup>– December 1<sup>st</sup> 2000

A. Winterpacht, G. Mohrmann, S. Schlaubitz, C. Stelzer, P. Hermanns, C. Mühlbauer, B. Lee, T. Hankeln, B. Zabel, E.R. Schmidt: Molecular identification of genes and pathways involved in skeletogenesis – potential candidates for human disorders. The 10<sup>th</sup> International Congress of Human Genetics, Vienna, Austria, May 15<sup>th</sup>–19<sup>th</sup> 2001

T. Hankeln, F. Luft, E.R. Schmidt, G. Mohrmann, A. Tagariello, A. Winterpacht, P. Hermanns, B. Lee, S. Schlaubitz, C. Stelzer, B. Zabel: Molecular identification of genes and pathways involved in skeletogenesis by EST sequence analysis and expression studies. German Human Genome Meeting 2001, Braunschweig, Germany, November 07<sup>th</sup>- 9<sup>th</sup> 2001

S. Schlaubitz, C. Stelzer, P. Hermanns, G. Mohrmann, A. Tagariello, F. Luft, B. Lee, A. Winterpacht, T. Hankeln, E. Schmidt, B. Zabel: A cartilage EST-sequencing project as source for genes involved in skeletal physiology and pathology. Frontiers of Skeletal Biology, Ninth Workshop of Cell Biology of



Bone and Cartilage in Health and Disease, Davos, Switzerland, March 16<sup>th</sup> – 19<sup>th</sup> 2002

S. Schlaubitz, C. Stelzer, P. Hermanns, A. Winterpacht, T. Hankeln, E.R. Schmidt, F. Jakob, B. Lee, B. Zabel: Molecular identification of novel genes, especially transcription factors, from a human fetal growth plate cartilage library. The 53<sup>rd</sup> Annual Meeting of The American Society of Human Genetics, Los Angeles, California, USA, November 4<sup>th</sup>-8<sup>th</sup> 2003

S. Schlaubitz, C. Stelzer, B. Zabel, B. Lee: Characterization of novel genes of a human fetal cartilage cDNA library. Annual Retreat of the Department of Molecular and Human Genetics, Galveston, Texas, USA, January 15<sup>th</sup>-16<sup>th</sup> 2004

S. Schlaubitz, C. Stelzer, B. Zabel, B. Lee: Characterization of novel genes of a human fetal cartilage cDNA library. The 31<sup>st</sup> European Symposium on Calcified Tissues, Nice, France, June 5<sup>th</sup>–9<sup>th</sup> 2004

S. Schlaubitz, C. Stelzer, B. Zabel, B. Lee: Molecular identification of genes and pathways involved in skeletogenesis by EST sequence analysis and functional studies. The 54<sup>th</sup> Annual Meeting of The American Society of Human Genetics, Toronto, Canada, October 26<sup>th</sup> –30<sup>th</sup> 2004

R. Morello, T. Bertin, S. Schlaubitz, K. Preuss, P. Hermanns, Y. Chen, B. Lee: Brachydactyly caused by loss of function of *sFRP2* signaling. Annual Retreat of the Department of Molecular and Human Genetics, Galveston, Texas, USA, January 13<sup>th</sup>-14<sup>th</sup> 2005

C. Stelzer, S. Schlaubitz, P. Hermanns, B. Lee, E. Schmidt, T. Hankeln, A. Winterpacht, B. Zabel: Gene expression profile of human fetal cartilage - at a glance. The 2<sup>nd</sup> Joint Meeting of the European Calcified Tissue Society and the International Bone and Mineral Society, Geneva, Switzerland, June 25<sup>th</sup> – 29<sup>th</sup>, 2005

S. Schlaubitz, C. Stelzer, B. Lee, B. Zabel: Characterization of a leucine-rich repeats containing protein selected from a human cartilage EST sequencing project. The 55<sup>th</sup> Annual Meeting of The American Society of Human Genetics, Salt Lake City, Utah, USA, October 25<sup>th</sup>-29<sup>th</sup>, 2005

S. Schlaubitz, S.A. Yatsenko, L.E. Vissers, L.D. Smith, K.L. Keller, D.A. Scott, W.W. Cai, W. Reardon, O.A. Abdul-Rahman, E.J. Lammer, E. Magenis, J.A. Veltman, P. Stankiewicz, B.U. Zabel, B. Lee: Ovotestes and XY sex reversal in a female with an interstitial 9q33.3-q34.1 deletion encompassing *NR5A1* and *LMX1B*. The 56<sup>th</sup> Annual Meeting of The American Society of Human Genetics, New Orleans, Louisiana, USA, October 9<sup>th</sup>-13<sup>th</sup>, 2006

## **8.6. Oral presentations**

B. Zabel, S. Schlaubitz, C. Stelzer, F. Luft, E.R. Schmidt, T. Hankeln, P. Hermanns, B. Lee, F. Jakob, U. Nöth, G. Mohrmann, A. Tagariello, A. Winterpacht: Molecular identification of genes and pathways involved in skeletogenesis by EST sequence analysis and microarray expression profiling of human mesenchymal stem cell differentiation. 13<sup>th</sup> Annual Meeting of the German Society of Human Genetics together with the Austrian Society of Human Genetics and the Swiss Society of Medical Genetics and the German Human Genome Project (DHGP), Leipzig, September 29<sup>th</sup>-October 2<sup>nd</sup> 2002

R. Morello, R. Mendoza, S. Schlaubitz, T. Bertin, Y. Chen, M.M. Jiang, B. Lee: Dysregulation of Wnt signaling during skeletogenesis in murine models of skeletal dysplasias Annual NIH grant meeting, Bethesda, Maryland, USA, June 2004

I hereby state, that I have done this work all by myself, and that I have only used the mentioned help and the literature cited in this dissertation.